Linking the Exposure to Engineered Nanoparticles Released From Nano-Enabled Products to Toxicology: a Case Study of Laser Printers

LINKING THE EXPOSURE TO ENGINEERED NANOPARTICLES RELEASED FROM NANO-ENABLED PRODUCTS TO TOXICOLOGY: A CASE STUDY OF LASER PRINTERS

SANDRA VANESSA PIRELA LEÓN

A Dissertation Submitted to the Faculty of

The Harvard T.H. Chan School of Public Health

in Partial Fulfillment of the Requirements

for the Degree of Doctor of Science

in the Department of Environmental Health

Harvard University

Boston, Massachusetts

May, 2015

Dissertation Advisor: Dr. Philip Demokritou Sandra Vanessa Pirela León

Linking The Exposure To Engineered Nanoparticles Released From Nano-Enabled Products To Toxicology: A Case Study Of Laser Printers

Abstract

A research gap in the fields of exposure assessment and toxicology that remains unaddressed is the assimilation of experimental conditions to those of the real world human exposure. Currently, there is a lack of understanding of the properties of particles released by nano-enabled products (NEPs). Thus, we designed a multi-tiered methodology to physico-chemically, morphologically and toxicologically characterize engineered nanomaterials (ENMs) released from NEPs (*i.e.*, toner powder). It is well established that printers emit nanoparticles during their operation; however, the physico-chemical and toxicological characterization of real world printer-emitted nanoparticles (PEPs) remains incomplete, hampering proper risk assessment efforts. For example, a number of studies estimating the potential adverse effects of PEPs used bulk toner particles as test particles rather than the actual particulate matter released by laser printers. Thus, the public health implications of exposure to PEPs remain largely unknown.

For this project, a printer exposure generation system suitable for the subsequent physico-chemical, morphological, and toxicological characterization of PEPs was developed and used to assess the properties of particulate matter released from the use of commercially available laser printers. The system consists of a glovebox type environmental chamber for uninterrupted printer operation, real-time and time-integrated particle sampling instrumentation

for size fractionation and sampling of PEPs and an exposure chamber for inhalation toxicological studies.

Results from our extensive analysis show that laser printers emit up to 1,300,000 particles/cm^3, most of which are nanoparticles. Further, we confirmed that a number of ENMs incorporated into toner formulations (*e.g.*, silica, alumina, titania, ceria,) become airborne during printing. Both *in vitro* and *in vivo* toxicological evaluation showed PEPs are biologically reactive and may cause significant cytotoxicity, membrane integrity damage, reactive oxygen species production, pro-inflammatory cytokine release, angiogenesis, cytoskeletal and epigenetic changes as well as lung inflammation.

This work highlights the importance of understanding life-cycle nano environmental health and safety implications of NEPs and assessing real world exposures and their associated toxicological properties rather than focusing on ‘‘raw’’ materials used in the synthesis of an NEP. Such analysis can be achieved for pollutants emitted by any NEP by employing the multi-tiered methodology described in this dissertation.

Table of Contents

List of Figures

Chapter 1: Development and characterization of an exposure platform suitable for physico-chemical, morphological and toxicological characterization of printer-emitted particles (PEPs).

d) Chemical composition of toner powder and corresponding PEPs from three representative printers (Printer A1, B1 and C1) tested, based from magnetic sector inductively coupled plasma mass spectrometry (SF-ICP-MS) and analysis. Anions and cations can explain only 0.1–1.4% of the ‘‘other’’ pie slice in airborne PEPs and 0.7–7% in toners.

- Figure 2-4. Fourier transform infrared spectroscopy results of toner powder and PEPs. (a) FTIR spectra from different size fractions of PEPs and toner powder from Printer B1 and (b) from 11 toner powders.
- Figure 2-S1. Printer exposure generation system (PEGS). This image has been adopted from Pirela et al. (2014). Flow rates for the instruments are as follows: Harvard compact cascade impactor: 30 l/min, electrostatic precipitator: 0.5 l/min, SMPS/CPC: 1 l/min, APS: 5 l/min, ozone monitor: 2.3 l/min.
- Figure 2-S2. Chemical composition of toner powder from the remaining tested printers based on a combination of techniques: magnetic sector inductively coupled plasma mass spectrometry (SF-ICP-MS) analysis for total and water-soluble elements, organic-elemental carbon, and anion and cation analysis. The sum of anions and cations can explain only 0.7-7% of the other pie section in toners.
- Figure 2-S3. Chemical composition of the $PM_{2.5}$ size fraction of PEPs from remaining two laser printers based on a combination of analytical techniques: magnetic sector inductively coupled plasma mass spectrometry (SF-ICP-MS) for total and water soluble elements, organic-elemental carbon, and anions and cations. The sum of anions and cations can explain only 0.2-1.4% of the other pie section in the airborne PEPs.

Chapter 5: Short-term exposure to engineered nanomaterials affects cellular epigenome.

analysis was determined by one-way ANOVA followed by Dunnett's test. *$p < 0.05$, **$p < 0.01$, ***$p < 0.001$. Compared with control group in each cell line.

- Figure 5-6. Analysis of expression levels of DNA methylation machinery in three cell lines after exposure to ENMs. The expression levels of *DNMT1*, *DNMT3A*, *DNMT3B*, and *UHRF1* in RAW264.7 (A), THP-1 (B), and SAEC (C). Data are presented as mean ± SD. Statistics analysis was determined by one-way ANOVA followed by Dunnett's test. *$p < 0.05$, **$p < 0.01$, ***$p < 0.001$. Compared with control group in each cell line.
- Figure 5-S1. Physico-chemical and morphological characterization of ENMs. The average primary particle diameter d_{BET} of MS-WF, TiO_2, and CuO was determined from their SSA. The morphology of these ENMs was also obtained using TEM. N/A indicates not applicable. The TEM image of PEPs was cited by a previous study of our group (Pirela et al., 2014).
- Figure 5-S2. The rate of ENMs deposition. The fraction of the administered dose of ENMs in suspension deposited over 24 h in 96-well plate.
- Figure 5-S3. The rate of ENMs deposition. The fraction of the administered dose of ENMs in suspension deposited over 24 h in 100 mm dish.
- Figure 5-S4. The levels of 10 cytokines significantly increased after 30 μg/mL MS-WF or PEPs treatment in SAEC. A. GM-CSF; B. Fractalkine; C. IFNa2; D. GRO; E. IL-6; F. IL-8; G. MCP-1; H. MIP-1a; I. MIP-1b; J. IL-10. Data are presented as mean ± SD. Statistics analysis was determined by one-way ANOVA followed by Dunnett's test. *$p < 0.05$, **$p < 0.01$, ***$p < 0.001$. Compared with control group in each cell line.
- Figure 5-S5. The levels of 9 cytokines significantly affected after 30 μg/mL MS-WF, CuO or PEPs treatment in SAEC. A. FGF-2; B. PDGF-BB; C. IL-7; D. Eotaxin-1; E.

List of Tables

- Table 2-S4. Magnetic sector inductively coupled plasma mass spectrometry (SF-ICP-MS) analysis of standard printing paper used in the study. The most abundant elements are presented on this table. T, T; WS, water soluble.
- Table 2-S5. Anions and cations analysis of PEPs, toners, and paper by ion chromatography. '-' represents values obtained from analysis that were not different than the blank samples evaluated.

Chapter 3: Laser printer-emitted engineered nanoparticles lead to cytotoxicity, inflammation and changes in DNA methylation in human cells.

- Table 3-1. Properties of laser printer emitted particle dispersions. d_H: hydrodynamic diameter, PdI: polydispersity index, ζ: zeta potential, σ: specific conductance, ρ_{agg}: effective density.
- Table 3-2. Summary of parameters used in the *in vivo* lung Multiple Path Particle Deposition model (MPPD2).
- Table 3-S1. Assays for determination of LINE-1 and Alu methylation.
- Table 3-S2. Assays for determination of gene expression.
- Table 3-S3. *In vitro* doses and the respective equivalent consumer inhalation exposure duration to PEPs. [a] *In vitro* administered- and delivered-to-cell doses are based on a 24-hour cell exposure. [b] Calculations of the corresponding consumer inhalation exposure duration (hours) to PEPs was based on the added values of deposition mass flux ($\mu g/m^2 \bullet min$) in the various human airways, excluding head airways: the conducting zone (generations 0 to 16) and the transitional and respiratory zones (generations 17 through 23).

Chapter 4: Small airway epithelial cells exposure to printer-emitted engineered nanoparticles induces cellular effects on human microvascular endothelial cells in an alveolar-capillary co-culture model.

- Table 4-1. Properties of ENMs dispersions in dIH_2O and SABM. d_H: hydrodynamic diameter; PdI: polydispersity index; ζ: zeta potential; σ: specific conductance and effective density. pH was measured of the SABM media that was used for treatment of cells as well. Values represent the mean (±SD) of a triplicate reading. The average diameters obtained from DLS characterization are derived from the intensity-weighted distributions based on the intensity of light scattered by the particle.
- Table 4-S1. Summary of parameters used in the *in vivo* lung Multiple Path Particle Deposition model (MPPD2) (Anjilvel and Asgharian 1995). The parameters for airborne nanoparticle distribution (assuming density of aerosolized particles as 2.27 g/cm^3) were derived from real-time monitoring data from Printer B1 as previously published by our group (Pirela, 2014).
- Table 4-S2. *In vitro* doses and respective equivalent consumer inhalation exposure to PEPs. Notes: [a] *In vitro* administered and delivered to cell doses are based on a 24-hour cell exposure. [b] Calculations of the corresponding consumer inhalation exposure duration (hours) to PEPs was based on the added values of deposition mass flux ($\mu g/m^2 \bullet min$) in the various human airways, excluding head airways: the conducting zone (generations 0 to 16) and the transitional and respiratory zones (generations 17 through 23).

Chapter 5: Short-term exposure to engineered nanomaterials affects cellular epigenome.

Chapter 6: A pilot study investigating the murine biological responses following acute exposure to printer-emitted particles either *via* intratracheal instillation and whole-body inhalation.

Acknowledgements

My dissertation project has been both challenging and extremely rewarding; it is one of the most significant academic feats I have accomplished. Without the support of my adviser, committee members, colleagues, friends and family, this work would not have been possible to complete.

I would like to express the deepest appreciation to my dissertation advisor Dr. Philip Demokritou. His patience, encouragement and confidence in my abilities made me step out of my comfort zone and provided me with the opportunities to develop my scientific skills and enhance my analytical thinking capabilities. Without Dr. Demokritou's guidance, this dissertation would not have been possible. I am fortunate to have had the opportunity to train under his supervision.

I would like to thank my committee members: Dr. Joseph Brain, Dr. Lester Kobzik and Dr. John Godleski. I am extremely grateful for their advice and feedback, as they were critical in strengthening my knowledge in the field of physiology and thus, improve the quality of the studies presented here. I feel lucky to have been able to count on their support and direction while working on my dissertation.

I am also indebted to the colleagues and collaborators who provided their expertise during my training and helped expand the scope of my dissertation. Thank you to Georgios Sotiriou, Christa Watson, Ramon Molina, Xiaoyan Lu and Thomas Donaghey, your help and guidance in various areas through the completion of the work presented here. To George Pyrgiotakis, thank you for taking the time to thoroughly and patiently teach me practical and theoretical knowledge in the different areas pertaining to my are of research as well as for always being there to offer advice as it related to science or life in general, I am deeply grateful

of your support since day 1. I would like to express my gratitude to the collaborators at the National Institute for Occupational Safety and Health: Vincent Castranova, Yong Qian, Nancy Gao, Jennifer Sisler; at the Consumer Protection Safety Commission: Treye Thomas; and at the University of Arkansas: Igor Koturbash and Issabelle Miousse.

Additionally, I would like to acknowledge the financial support provided by the National Institute of Environmental Health Sciences Center (# ES-000002), the National Institute for Occupational Safety and Health and Consumer Protection Safety Commission (# 212-M-51174), National Institute of Health (# HL007118) and the Initiative to Maximize Student Diversity (# 5R25GM055353).

To my friends, thank you for the support and encouragement you have provided me during the entire process, it has been invaluable. To my amazing family, I don't have the words to describe the appreciation I have for all of you. Mamá, Papá, Susi: Thank you for always supporting and encouraging me to reach my goals. Mom and Dad, thank you for giving me the opportunity to pursue my dreams and interests, none of which would have been possible if you had not sacrificed your own lives and moved from Venezuela to the United States 15 years ago. It is because of you that I have accomplished so much and I am forever indebted to you both.

Thank you all from the bottom of my heart,

Sandra Vanessa Pirela León

April 24, 2015

Introduction

Nanotechnology has exponentially grown showing approximately a 50% growth rate in the last two decades and has had a research and development investment of almost $9 billion annually (Nanotechnologies, 2015). This field has become one of the prominent science fields with an immense influence in many aspects of our every day life. Many industries ranging from consumer care products to food packaging and pharmaceutics, to mention a few have been revolutionized by modifying their products to now include engineered nanomaterials (ENMs) due to the various innovative physical, chemical, mechanical and optical properties ENMs have that are a vast improvement to their larger size counterparts (*i.e.*, micron-sized particles). For example, the automotive sector uses nano-silica (nano-SiO_2) layers onto displays and panels to improve their anti-reflection properties while maintaining the ultra-thin design (Malsch et al., 2004). Another example is the use of nano-silver (nano-Ag) as a coating of clothing (*e.g.*, sports fabrics, socks) due to the enhanced anti-microbial characteristics of this ENM (Rai et al., 2009, Morones et al., 2005). Currently, there are thousands of nano-enabled products (NEPs) in the market widely available to the consumer and since manufactures are not required to report use of ENMs, the amount of products identified as NEPs by manufacturers makes up a small percentage of the final figure mentioned above. Therefore, the exact quantity of NEPs launched annually for sale is grossly underestimated. The National Science Foundation reported that up to $70 billion worth of NEPs were being sold annually in the United States (Kessler, 2011). This extensive availability of NEPs in the market makes the exposure to ENMs in NEPs unavoidable and since the protection of the consumer is of paramount importance, efforts to evaluate the potential toxicity associated with exposures to such particles has become mandatory.

Addressing the risk of exposure to such NEPs at the consumer level requires the use of data from both the exposure scenario and the toxicological assessment. Nanotoxicology focuses on the evaluation of adverse effects following exposure to ENMs. However, there is a lack of scientific data addressing exposures at the consumer level, which has led to a lag behind the ever-increasing innovations in nanotechnology. Mainly, there has been a lack of studies evaluating exposures at all stages of the lifecycle of a NEP. Particularly, the emphasis has been on the manufacturing stage with nanotoxicology studies using raw or pristine materials used in the production of such products rather than the particulate matter released by the NEP during the use at the consumer stage or even the end of life stage of the product. This emphasis on exposures at the manufacturing stage only leads to the evaluation of unrealistic or misrepresentative scenarios. Thus, there is a critical gap as many industries include ENMs in their products and there is still no assessment linking the exposure scenario to the adverse effects on the health of consumers.

Further, both risk assessors and industry are struggling with the limited population exposure data across the various lifecycle stages of NEPs and the fact that most of the current nano-Environmental Health and Safety (nano-EHS) data focuses on pristine (raw) materials used in the synthesis of NEPs rather than impacts associated with real world exposures across their lifecycle. This important knowledge gap has also been recently emphasized in both the National Research Council report, as well as the National Nanotechnology Initiative's Strategy on Nano-EHS (NNI, 2011, NRC, 2012). In turn, this impedes public health assessors from addressing nano-related risk issues and discourages industry from exploring the multitude of nanotechnology applications. These nano-EHS uncertainties surrounding NEPs, if unaddressed, will also have implications at societal and economic levels as well as on the sustainable

development of the nanotechnology industry as a whole.

Since many industries manufacture NEPs, we aimed at investigating if the laser-based printing industry had followed the other industries to include ENMs in their toner formulation and subsequently, understand what are the implications of such shifts. This served as the motivation of this dissertation project, which focused on creating a multi-tiered approach that would serve to link the exposure condition to the toxicology associated with the use of a NEP at the consumer level. For this approach, the laser printer was used as a case study of an example of a product using toner powders that are thought to be NEPs.

During the last couple of years, there has been an interest in studying the exposure to printer-emitted particles (PEPs) since the use of printing equipment (*e.g.*, laser printers, photocopiers) has grown exponentially over the last decade. This growth has been driven primarily by the substantial increase in the number of home-based businesses in the USA and the use of personal computing (Jamieson, 2012). According to a recent report, the annual production of laser printers was estimated to be about 23 million units a year worldwide, and the number of workers in quick-printing centers in the USA is increasing, with more than 160,000 workers (Dun & Bradstreet Reports, 2011). In addition, there has been an increment in the number of home offices in the United States going from 26 to 38 million in a decade. Moreover, it's been estimated that about 50% of American households will be involved in home-based businesses (IDC, 2014). Consequently, this change in lifestyle and office settings may equate to the fact that office equipment, such as printers, will now become a common item in many homes. Thereby, increasing the risk of exposure to the pollutants released by laser printers.

Aside from exposures at printing centers, there is also the risk of occasional exposures in many other settings, such as schools, hospitals, offices and homes. Thus, it is of growing

importance to evaluate printer emissions and perform a proper science-based risk assessment on particular scenarios, such as that simulating consumer exposure.

A laser printer functions with the aid of a photosensitive drum to attract the toner powder and fuse it on the page with a set of rollers that apply high level of pressure and heat (Petterson and Fogden, 2006). The toner particles that are not fused to the paper remain on the photosensitive drum and are cleaned off by a cleaning blade inside the toner cartridge.

As far as the knowledge on emissions from laser printers, there is a number of studies associating the process of printing with emission of particles and gaseous pollutants, such as semi-volatile organic compounds (sVOCs), particulate matter (PM) and ozone, among others (Worthan and Black, 1999, Wensing M, 2006, Brown, 1999). Additionally, it has been concluded that consumer grade printers can elevate indoor particle number concentrations to values as high as 44 times the background levels, as this equipment can emit up to 760 million particles per printed page (Barthel et al. 2011, He et al., 2007). These printer emitted particles (PEPs) were identified to be released all around the printer, specifically around the board cooler, rear of printer, paper tray and toner waste bin (E.C. Kleinsorge, 2011, Morawska et al., 2009, Kagi et al., 2007, McGarry et al., 2011, He et al., 2007, Schripp et al., 2008)C-W. Lee, 2007).

Such documented high concentrations of PEPs only corroborate the lack of toxicological and epidemiological evidence regarding exposure to such emissions on human health. Moreover, the toxicological significance of PEPs is currently poorly understood, but circumstantial evidence continues to grow. A major limitation of some of the current toxicological studies is the use of toner powder particles in both *in vitro* and *in vivo* test platforms (Morimoto et al., 2013, Gminski et al., 2011).

The few *in vivo* studies performed have shown that long-term inhalation exposures using toner powders can cause chronic inflammation. Additionally, when toner powder was intratracheally instilled in rodents, they exhibited lung fibrosis and development of lung tumors (Moller et al., 2004, Mohr et al., 2006, Mohr et al., 2005). There is also evidence from certain *in vitro* studies showing that toner powders led to increased levels of reactive oxygen species (ROS), cytotoxicity and genotoxicity markers, fibrosis, reduced pulmonary clearance and cell proliferation (Furukawa et al., 2002, Mohr U, 2005, Nies et al., 2000, Slesinski and Turnbull, 2008).

The lack of agreement of results obtained from both platforms could be explained by the vast difference, physically and chemically, between toner powders and PEPs as well as a disregard for dosimetry considerations. Thus, these studies assessed a scenario that does not accurately reflect that of actual exposures, which are exclusively to nanoparticles emitted by laser printers. Thus, proper comparison and interpretation of the findings is not possible, further stressing the need for a proper study of PEPs using the correct exposure system and an appropriate physico-chemical, morphological and toxicological evaluation.

While there is evidence that laser printers release particulate matter and gaseous pollutants, their complex chemistry, morphology and potential toxicological properties remain unidentified.

In this dissertation work, the development and optimization, of a standardized integrated methodology to thoroughly assess the release of PM during the consumer stage of a laser printer is presented.

In chapter 1, the development of a printer exposure generation system (PEGS) is described in detail. The PEGS was used to generate real world PEPs exposures associated with

commonly used laser printers. The system is suitable for physico-chemical, morphological and toxicological characterization of PEPs. The PEGS consists of: (a) a glovebox type environmental chamber to house the printers for uninterrupted operation; (b) real-time and time-integrated PM particle sampling and monitoring instrumentation to quantify particle size distribution and collect size-fractionated PEPs for analysis and (c) an animal inhalation exposure system for toxicological evaluation. In this chapter, we further describe the evaluation of the emission profile (*e.g.*, size distribution, particle number concentration) of 11 printers and ranked them based on the maximum number of particles emitted during a 60-minute print job. Following the assessment, we provide evidence that PM peak emissions are brand independent and varied between 3,000 to 1,300,000 particles/cm^3, with modal diameters ranging from 49 to 208 nm, with the majority of PEPs in the nanoscale (<100 nm) size. These results were in agreement with those findings in the literature in terms of the size and the concentration of the particles emitted. However, there was no definitive study clearly identifying the source of emissions from these particles.

In chapter 2, we aimed at delving deeper into the hypothesis stated in chapter 1 that engineered nanomaterials (ENMs) are used in toners and thus, these ENMs are released during printing (consumer use). The motivation for this study was the lack of comprehensive data regarding the physico-chemical properties of PEPs and the relationship between PEPs and their precursors in toner powder. The chemical and morphological characterization of the PEPs was performed using the exposure platform described in chapter 1 in order to collect size-fractionated PM emitted by the laser printer. Subsequent to the collection of PEPs, a thorough investigation to assess the presence of nanoscale materials in the toner formulations and evaluate if such ENMs are released into the air during printing (consumer use) was performed. The analytical methods

included magnetic sector field inductively coupled plasma mass spectrometry, organic/elemental carbon analysis, Fourier transform infrared spectroscopy, scanning and transmission electron microscopy coupled with energy dispersive X-ray spectroscopy. Such an integrated methodology for the risk assessment of NEPs during consumer use will not only provide detailed characterization of exposures from such a NEP product but will also enable toxicological testing using real world emitted particles rather than the pristine toner particles. Our results serve as evidence that there is routine incorporation of ENMs in toners -classifying them as NEPs- and in turn, these ENMs become airborne during printing.

Due to the confirmation that ENMs incorporated to the toner used by laser printers are released during a print job at concentrations comparable to those in highways, the next step was to evaluate the toxicological potential of these particles to human health. Thus, we decided to utilize the emissions from a high emitting printer to evaluate the toxicological response due to exposure to PEPs using a variety of physiologically relevant cell lines and different culture methods explained in detail in chapters 3, 4 and 5. The *in vitro* toxicological characterization starts with chapter 3 using three cell lines (small airway epithelial cells, monocyte-matured macrophages and lymphoblasts) to evaluate basic toxicity responses following exposure to PEPs in a wide range of doses that are comparable to approximately 8 and more hours of inhalation exposure to PEPs. The effects observed included a significant increase in production of reactive oxygen species, cell death, inflammation and changes in epigenetic modifications. The mechanism of action of PEPs on epigenetics was further evaluated by the development of a platform to quantify modulations in DNA methylation patterns following an exposure to a stressor (*i.e.*, PEPs).

Based on these preliminary results, we decided to investigate if PEPs exposure had an effect on cell-cell interactions. Hence, the biological response exhibited by human microvascular endothelial cells co-cultured with small airway epithelial cells exposed to PEPs at low cytotoxic doses. The findings indicated that exposure of epithelial cells to PEPs can have an indirect effect on endothelial cells, possibly due to paracrine signaling. These effects included increased reactive oxygen species, gap junctions, angiogenesis and actin filament remodeling, among other responses.

Lastly, in chapter 6, the thorough toxicological assessment of exposure to PEPs is extended to the use of an *in vivo* rodent experimental model to identify the adverse effects caused by treatment with PEPs either *via* intratracheal instillation or whole-body inhalation. The doses of exposure used in this phase of the study are relevant to current real world occupational and recreational scenarios. The preliminary results obtained in this pilot animal study allowed for the recognition of key mechanisms of toxicity that must be pursued further in order to establish a clear biological response pathway.

Bibliography

brown, S. K. 1999. Assessment of pollutant emissions from dry-process photocopiers. *Indoor Air,* 9**,** 259-67.

E.C. Kleinsorge, M. E., María Gimena Galan, Caterina Barison, María Eugenia Gonsebatt, María Fernanda Simoniello 2011. Assessment of oxidative status and genotoxicity in photocopier operators: a pilot study. *Biomarkers,* 16**,** 642-648.

Furukawa, Y., Aizawa, Y., Okada, M., Watanabe, M., Niitsuya, M. & Kotani, M. 2002. Negative effect of photocopier toner on alveolar macrophages determined by in vitro magnetometric evaluation. *Ind Health,* 40**,** 214-21.

HE, C., MORAWSKA, L. & TAPlin, L. 2007. Particle emission characteristics of office printers. *Environ Sci Technol,* 41**,** 6039-45.

IDC 2014. IDC Finds Continued Growth in the Worldwide Hardcopy Peripherals Market in the Fourth Quarter of 2013 Framingham, Massachusetts.

Kagi, N., Fujii, S., Horiba, Y., Namiki, N., Ohtani, Y., Emi, H., Tamura, H. & Kim, Y. S. 2007. Indoor air quality for chemical and ultrafine particle contaminants from printers. *Building and Environment,* 42**,** 1949-1954.

Kessler, R. 2011. Engineered nanoparticles in consumer products: understanding a new ingredient. *Environ Health Perspect,* 119**,** a120-5.

Malsch, I., Gleiche, M., Hoffschulz, H., Bøgedal, M., Locatelli, S., Nicollet, C., Guibert, J. C., Denis, M., Morrison, M., GrüNwald, A., Dupuy, J.-P., Parr, D., Speller, S. & Oud, M. 2004. Benefits, Risks, Ethical, Legal and Social Aspects of Nanotechnology. *In:* MALSCH, I. (ed.). Nanoforum: Nanoforum.

Mcgarry, P., Morawska, L., He, C., Jayaratne, R., Falk, M., Tran, Q. & Wang, H. 2011. Exposure to particles from laser printers operating within office workplaces. *Environ Sci Technol,* 45**,** 6444-52.

Mohr U, E. H., Roller M, Pott F. 2005. Carcinogenicity study with nineteen granular dusts in rats. *Eur J Oncol,* 10**,** 249-281.

Mohr, U., Ernst, H., Roller, M. & Pott, F. 2005. Carcinogenicity study with nineteen granular dusts in rats. *Eur J Oncol,* 10**,** 249-281.

Mohr, U., Ernst, H., Roller, M. & Pott, F. 2006. Pulmonary tumor types induced in Wistar rats of the so-called "19-dust study". *Exp Toxicol Pathol,* 58**,** 13-20.

Moller, A., Muhle, H., Creutzenberg, O., Bruch, J., Rehn, B. & Blome, H. 2004. Biological procedures for the toxicological assessment of toner dusts. *Gefahrstoffe—Reinhaltung der Luft,* 64**,** 13-20

Morawska, L., He, C., Johnson, G., Jayaratne, R., Salthammer, T., Wang, H., Uhde, E., Bostrom, T., Modini, R., Ayoko, G., Mcgarry, P. & Wensing, M. 2009. An investigation into the characteristics and formation mechanisms of particles originating from the operation of laser printers. *Environ Sci Technol,* 43**,** 1015-22.

Morones, J. R., Elechiguerra, J. L., Camacho, A., Holt, K., Kouri, J. B., Ramirez, J. T. & Yacaman, M. J. 2005. The bactericidal effect of silver nanoparticles. *Nanotechnology,* 16**,** 2346-53.

Nanotechnologies, P. O. E. 2015. *Introduction to Nanotechnology* [Online]. NanoTechProject: PROCESSwire. Available: http://www.nanotechproject.org/topics/nano101/introduction_to_nanotechnology/ [Accessed April 10, 2015 2015].

Nies, E., Blome, H. & Bruggemann-Prieshoff, H. 2000. Characterization of coloured toner powders and emissions from colour photocopiers/colour laser printers. *Gefahrstoffe Reinhaltung Der Luft,* 60**,** 435-441.

NNI 2011. Environmental, Health, and Safety (EHS) Research Strategy.

NRC 2012. A Research Strategy for Environmental, Health, and Safety Aspects of Engineered Nanomaterials.

Rai, M., Yadav, A. & Gade, A. 2009. Silver nanoparticles as a new generation of antimicrobials. *Biotechnol Adv,* 27**,** 76-83.

Schripp, T., Wensing, M., Uhde, E., Salthammer, T., He, C. & Morawska, L. 2008. Evaluation of ultrafine particle emissions from laser printers using emission test chambers. *Environ Sci Technol,* 42**,** 4338-43.

Slesinski, R. S. & Turnbull, D. 2008. Chronic inhalation exposure of rats for up to 104 weeks to a non-carbon-based magnetite photocopying toner. *Int J Toxicol,* 27**,** 427-39.

Wensing M, P. G., Bednarek M, Schripp T, Uhde E, Salthammer T. 2006. Particle measurement of hardcopy devices. *Healthy Buildings Conference.* Lisboa.

Worthan, A. W. & Black, M. S. 1999. Emissions from office equipment. *Is&T's Nip15: International Conference on Digital Printing Technologies***,** 459-462.

Chapter 1: Development and characterization of an exposure platform suitable for physico-chemical, morphological and toxicological characterization of printer-emitted particles (PEPs)

Sandra V. Pirela[1], Georgios Pyrgiotakis[1], Dhimiter Bello[2], Treye Thomas[3], Vincent Castranova[4], and Philip Demokritou[1*]

Inhalation Toxicology. 2014. 26 (7): 400-408.

[1]Department of Environmental Health, Center for Nanotechnology and Nanotoxicology, Harvard School of Public Health, Boston, MA, USA.

[2]Department of Work Environment, University of Massachusetts Lowell, Lowell, MA, USA.

[3]U.S. Consumer Product Safety Commission, Office of Hazard Identification and Reduction, Rockville, MD, USA.

[4]National Institute for Occupational Health and Safety, Health Effects Laboratory Division (HELD), Morgantown, WV, USA.

[*]Corresponding author

Abstract

An association between laser printer use and emissions of particulate matter (PM), ozone and volatile organic compounds has been reported in recent studies. However, the detailed physico-chemical, morphological and toxicological characterization of these printer-emitted particles (PEPs) and possible incorporation of engineered nanomaterials into toner formulations

remain largely unknown. In this study, a printer exposure generation system suitable for the physico-chemical, morphological, and toxicological characterization of PEPs was developed and used to assess the properties of PEPs from the use of commercially available laser printers. The system consists of a glovebox type environmental chamber for uninterrupted printer operation, real-time and time-integrated particle sampling instrumentation for the size fractionation and sampling of PEPs and an exposure chamber for inhalation toxicological studies. Eleven commonly used laser printers were evaluated and ranked based on their PM emission profiles. Results show PM peak emissions are brand independent and varied between 3,000 to 1,300,000 particles/cm^3, with modal diameters ranging from 49 to 208 nm, with the majority of PEPs in the nanoscale (< 100 nm) size. Furthermore, it was shown that PEPs can be affected by certain operational parameters and printing conditions. The release of nanoscale particles from a nano-enabled product (printer toner) raises questions about health implications to users. The presented PEGS platform will help in assessing the toxicological profile of PEPs and the link to the physico-chemical and morphological properties of emitted PM and toner formulations.

Introduction

The use of printing equipment, such as laser printers and photocopiers, has grown exponentially over the last decade, driven primarily by the substantial increase in the number of home-based businesses in the USA and the use of personal computing (Jamieson, 2012). According to a recent report, the annual production of laser printers was estimated to be about 23 million units a year worldwide, and the number of workers in quick-printing centers in the USA is increasing, with more than 160,000 workers (Dun & Bradstreet Reports, 2011). Aside from exposures at printing centers, there is also the risk of occasional exposures in many other settings, such as schools, hospitals, offices and homes. Thus, it is of growing importance to

evaluate printer emissions and to perform a proper science-based risk assessment.

Laser printers (or other printing equipment) utilize a photosensitive drum to attract the toner powder and fuse it on the page with a set of rollers that apply high levels of pressure and heat (Pettersson & Fogden, 2006). There are numerous studies associating the process of printing with emission of particulate matter (PM) and gaseous pollutants, such as semi- volatile organic compounds (sVOCs) and ozone, among others (Barthel et al., 2011; Brown, 1999; Castellano et al., 2012; Kagi et al., 2007; Tang et al., 2012; Wang et al., 2012; Wensing et al., 2006). It was shown that consumer grade printers can increase indoor particle number concentrations from 860 to 38,000 particles/cm^3 and emit up to 7.6 x 10^9 particles per printed page (Barthel et al., 2011; He et al., 2007). These printer-emitted particles (PEPs) were identified to have an average mobility equivalent particle diameter between 50 and 244 nm and are released via the board cooler, rear of printer, paper tray and toner waste bin (Byeon & Kim, 2012; He et al., 2007; Jiang & Lu, 2010; Kagi et al., 2007; Lee & Hsu, 2007; McGarry et al., 2011; Morawska et al., 2009; Schripp et al., 2008; Wang et al., 2012; Wensing et al., 2008). It is important to note that there is limited literature on the physico-chemical properties of PEPs, and more significantly there is no evidence on the incorporation of engineered nanomaterials (ENMs) in the toner formulation and their possible emission into the air. More specifically, while it is clear that laser printers emit PM, neither their complex chemistry, nor their formation is clearly understood (Byeon & Kim, 2012; Castellano et al., 2012; Jiang & Lu, 2010; Wang et al., 2012). Furthermore, it was shown in many studies that various operational parameters, such as fuser roller temperature, page coverage, printer brand, printer speed and newness of toner cartridge may affect PM emissions (Byeon & Kim, 2012; He et al., 2007).

Undoubtedly, the high levels of PM emissions have undoubtedly raised concerns about

possible toxicity, since there is a plethora of historic epidemiological and toxicological evidence linking exposures to ambient particles with adverse health effects (Dockery et al., 1993; Dominici et al., 2006; Perrone et al., 2013; Zhao et al., 2013). The toxicological potential of PEPs is currently poorly understood, but circumstantial evidence continues to grow. A major limitation of some of the current toxicological studies is the use of toner powder particles in both *in vitro* and *in vivo* test platforms (Gminski et al., 2011; Morimoto et al., 2005). Several *in vivo* studies revealed that long-term inhalation exposures using toner powders can cause chronic inflammation and fibrosis in rats and development of lung tumors in rats after intratracheal instillation (Mohr et al., 2005, 2006; Moller et al., 2004). Furthermore, *in vitro* cellular bioassays using toner powder reported increased levels of reactive oxygen species, cyto- and genotoxicity markers, fibrosis, reduced pulmonary clearance and cell proliferation (Furukawa et al., 2002; Mohr et al., 2005; Morimoto et al., 2005; Slesinski & Turnbull, 2008). The conflicting results from the aforementioned cellular studies might be attributed to variable chemical composition of toner powders (obscured by improper characterization of the test material used in the experiments), a lack of a harmonization protocol for PM liquid suspension preparation and dosimetric considerations. Additionally, toxicological assessment of PEPs using toner particles rather than actually emitted ones does not accurately reflect the actual exposures and properties of PEPs and prohibits interpretation of the findings. Therefore, there is a need to develop exposure generation systems suitable for physico-chemical and toxicological characterization of realistic exposures from printers.

A recent study by the authors on the physico-chemical and morphological evaluation of different PM size fractions ($PM_{0.1}$, $PM_{2.5}$ and PM_{10}) sampled in photocopy centers revealed for the first time the incorporation of ENMs in the toner formulation for photocopier equipment,

which were emitted in high numbers during the photocopying process. Detailed physico-chemical characterization of the emitted aerosol revealed complex chemistry that reflected that of the toner, and contained several nanoscale metals/metal oxides, sVOCs, traces of elemental carbon and a substantial fraction of organic carbon, which comprised 50–70% of the total mass of the aerosol fraction (Bello et al., 2012). More importantly, in a series of both *in vitro* and *in vivo* toxicological studies, also performed by our group using size-fractionated PM collected from photocopy centers, revealed the potential of emitted PM to affect the physiology of the lung (Khatri et al., 2013a,b; Pirela et al., 2013), consistent with acute inflammation in upper airways and systemic oxidative stress findings in human volunteers (Khatri et al., 2012). These new toner formulations may pose potential health and safety issues given the hazard uncertainties associated with this class of nanomaterials. The unique physical and chemical properties exhibited by ENMs, which are distinct from those of their micron-sized counterparts, endow them with exceptional performance in consumer products. However, these properties may also be responsible for unique biological effects that can render them unsafe for humans and the environment (Demokritou et al., 2012; Nel et al., 2006; Sotiriou et al., 2014). The possibility that laser printer toner formulations contain ENMs and their potential to be released into the air still remain to be shown.

In this study, an integrated platform suitable for the physico-chemical, morphological and toxicological characterization of realistic PEPs was developed and tested. The developed exposure system was utilized to assess various laser printers in terms of their PM emission profiles and operational parameters. This article is the first of a trilogy of manuscripts describing the integrated exposure platform and the detailed physico-chemical, morphological and toxicological characterization of both PEPs and toner formulations for commonly used laser

printers.

Methods

A printer exposure generation system (PEGS) was developed to generate real world PEPs exposures associated with commonly used laser printers. The system is suitable for physico-chemical, morphological and toxicological characterization of PEPs. The PEGS consists of: (a) a glovebox type environmental chamber to house the printers for uninterrupted operation; (b) real-time and time-integrated PM particle sampling and monitoring instrumentation to quantify particle size distribution and collect size-fractionated PEPs for analysis and (c) an animal inhalation exposure system for toxicological evaluation. Figure 1-1 illustrates the PEGS. In more detail:

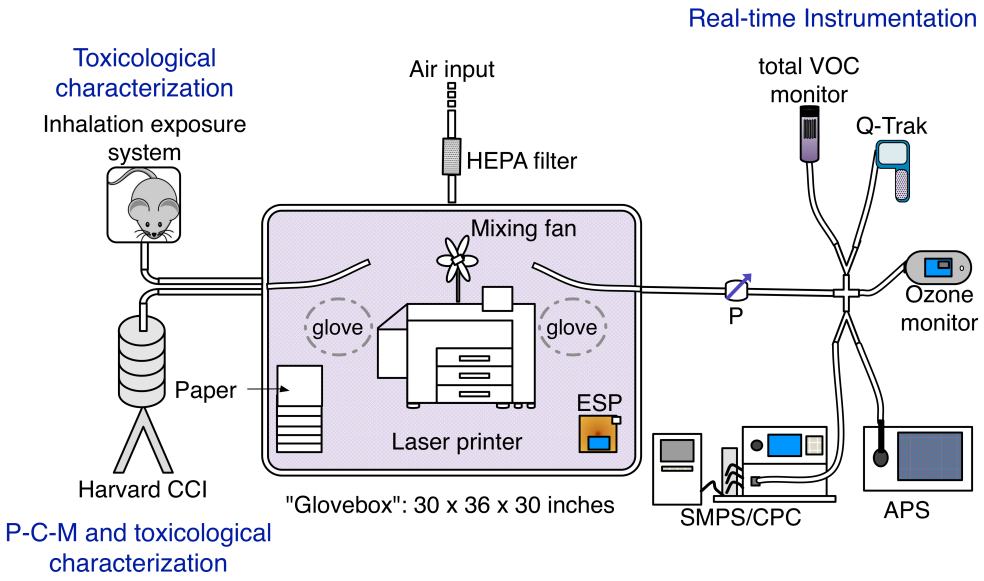

Figure 1-1. Printer exposure generation system (PEGS).

Environmental exposure chamber: An environmental exposure chamber with a volume of 0.52 m^3 was constructed to contain each printer individually during the respective print job

evaluation. The chamber was made out of aluminum frames with polyacrylic panels (MiniTec Framing Systems, LLC, Victor, NY), lined with grounded aluminum foil to minimize particle loss. The front panel of the chamber had a pair of neoprene gloves to facilitate handling of printers inside the chamber (*e.g.*, ensure change toner cartridge, add paper, clear paper jams) and ensure uninterrupted operation. The chamber was equipped with a power strip for operation of various instruments inside the chamber and a Universal Serial Bus port that allowed connectivity to a computer outside the chamber in which the monitoring software was used. A modulated-speed, small fan was placed in the back of the chamber for air mixing. Two sampling ports were placed on the center of both side panels for the real-time and time-integrated instrumentation and the sampling tube was extended in the chamber for 20 cm, to sample air from the center of the chamber.

Real-time instrumentation for PM and gaseous pollutants: A water-based condensation particle counter (WCPC Model 3785, TSI Inc., Shoreview, MN) was used to monitor the number concentration of particles sized from 5 to 1000 nm. A scanning mobility particle sizer (SMPS Model 3080, TSI Inc.) was also used to measure the particle size distribution (ranging from 2.5 to 210 nm) in the chamber. An aerodynamic particle sizer (APS Model 3321, TSI Inc.) was used to measure, the particle number concentration as a function of time for particles from 0.5 to 20 μm. In addition to PM data, real-time measurements of environmental conditions in the chamber, including temperature, relative humidity and ozone concentration, were obtained using a Q-Trak (Model 8551, TSI Inc.). Total VOC (tVOC) measurements were also obtained using a photo ionization based system (GrayWolf Sensing Solutions, Shelton, CT) equipped with a sensitive ppb probe. All the instruments were calibrated and background tests were performed at the beginning of each sampling experiment.

Size-selective integrated PM sampling: The Harvard compact cascade impactor (CCI; Demokritou et al., 2004) was used to size fractionate and collect PM samples. The CCI operates with four stages and allows for collection of moderately large amounts of particles (mg level) for the following size fractions: $PM_{2.5-10}$, $PM_{0.1-2.5}$ and $PM_{0.1}$. The main advantage of CCI is the fact that size-fractionated PM is collected on pre-cleaned adhesive-free polyurethane foam (PUF) impaction substrates from which the particles can be efficiently extracted using a water-based protocol (Chang et al., 2013; Demokritou et al., 2002; Khatri et al., 2013a,b; Lough et al., 2005; Pirela et al., 2013).

Animal inhalation exposure system: The BuxCo environmental exposure chamber system, previously described by the authors (Pyrgiotakis et al., 2014), is used to house the animals for inhalation studies. It consists of eight individual cages (PLY42211 V1.0, BuxCo Research Systems, Wilmington, NC) with attached transducers (TRD5700, BuxCo systems) that are connected to the Max II acquisition center (BuxCo systems) and enable monitoring of the breathing pattern of the animals during the aerosol exposure (Reynolds et al., 2008). Please note that the data from the *in vivo* inhalation part of the study will be included in an upcoming companion paper.

Post-sampling gravimetric analysis of impaction substrates

The PUF impaction substrates and Teflon filter (used to collect the $PM_{0.1}$ size fraction) from the CCI were weighed pre- and post-sampling following a 48-h stabilization process in a temperature- and humidity-controlled environmental chamber utilizing a Mettler Toledo XPE analytical microbalance as previously described (Bello et al., 2012). Thus, the weight difference was used to determine the collected PEPs mass and the time averaged particle mass concentration in the chamber during the printing episode. All sampling media (Teflon filters and

PUF substrates) were pre-cleaned in the laboratory to minimize background contamination following a published protocol (Bello et al., 2012).

Assessing the emission profiles from 11 commonly used laser printers using the PEGS

Printers, paper and toner: Eleven laser printers (two color and nine halftone) were assessed in terms of PEPs emissions using the PEGS platform described above. Printers were selected based on a variety of factors (*e.g.*, marketability, age, model, printer speed) to represent a broad spectrum of possibilities in a university office setting. The printers represent four of the most commercially available manufacturers (A, B, C, and D), and various models from each manufacturer were used. New toner cartridges and the standard white letter paper size (8.5 x11 in.) were used for all experiments in this study. Supplementary Table 1-S1 summarizes the information on the printer properties.

Protocol for evaluating PEP profiles: The following protocol was used in the assessment of the PEP emission profiles from each printer. Each printer was placed inside the environmental chamber. HEPA-filtered air was supplied at a flow rate of 30 l/min until the chamber background particle concentration reached approximately 200 particles/cm^3. Once this level was attained, the chamber airflow rate was reduced to 5 l/min, which is the total air flow required by the real-time instrumentation. The air change per hour was calculated to be 0.33. The printer was then set to operate continuously for 60 min, printing a single-sided monochrome document with a 5% page coverage. A standard page with a 5% coverage from the International Organization for Standardization and International Electrotechnical Commission was used (ISO.ORG, 2014). During the print job, both real-time aerosol data and size-fractionated PM samples were collected, including measurement of size distribution, particle number and mass concentration, as well as chamber air quality parameters. The size-fractionated PEPs were sampled using the

Harvard CCI, and gravimetric analysis was performed on the collected PEPs to calculate the time-integrated particle mass concentration of the PEPs. Printers were ranked based on the maximum particle number concentration during the 60-min print job.

Evaluation of the effect of operational parameters on PEPs profiles: The PEGS was also used to assess the influence of certain operational parameters on the emission characteristics of three randomly selected printers (B1, C5 and C6). Specifically, we tested various page coverages (5%, 25% and 40%), printing of a single- or double-sided page using a 5% page coverage, as well as a continuous and intermittent printing mode using a 5% page coverage. Two printing scenarios for the intermittent mode were used: (a) print 25 pages, pause for a couple of minutes and print the remaining 25 pages; (b) print 17 pages, pause for a couple of minutes and repeat twice until 51 pages were printed.

Calculation of the potential deposition of PEPs in the human lung: The multiple path particle deposition model (MPPD2, Anjilvel & Asgharian, 1995) was utilized to calculate the lung deposition fraction and deposition mass flux of the particles emitted from one of the highest emitting laser printers (Printer B1) on the human respiratory system. Supplementary Table 1-S2 summarizes the parameters used in the model. The aerosol size distribution obtained from the real-time monitoring instrumentation measurements described above was used in the model.

Statistical analysis

Raw data from the sampling instruments were imported into a spreadsheet. The database was then exported into SPSS (v17, SPSS Inc., Chicago, IL) for further data reduction and analysis. All files from the real-time instrumentation were transferred into a new worksheet and standard statistical methods were utilized to obtain the geometric mean, standard deviation and

mode of the measurements pertaining to each laser printer tested. Experiments were performed in triplicate. The distributions of the total number concentration and other continuous dependent variables from the real-time instruments were examined graphically via probability plots and histograms. The total number concentration and tVOC were found to be lognormal and subsequently they were log-transformed. All analyses were conducted on the transformed data. Summary aerosol statistics including the geometric mean (GM), geometric standard deviation (GSD) and mode were calculated.

Results

Laser printer ranking in terms of PEPs

Table 1-1 summarizes the ranking of the 11 printers in terms of the maximum particle number concentration during the 1-h printing episode. The printers with the highest particle emissions are A1 and B1, with maximum particle concentrations close to 1.3 million particles/cm^3.

Table 1-1. Ranking of the 11 laser printers evaluated based on number of particles emitted during a continuous printing episode.

Ranking	Printer	Particle number concentration (#/cm^3)			Particle diameter (nm)		
		Maximum	Geometric Mean	Geometric St. Dev.	Mean	Mode	St. Dev
1	A1	1.27×10^6	7.4×10^4	35.9	74.31	70.03	87.48
2	B1	1.26×10^6	4.0×10^5	11.2	38.99	38.16	38.64
3	B2	6.78×10^5	5.7×10^4	22.5	78.43	67.60	96.79
4	C1	2.62×10^5	3.0×10^4	18.7	59.11	54.90	65.16
5	C2	2.12×10^5	5.6×10^4	12.1	78.27	61.11	52.84
6	C3	1.70×10^5	3.0×10^4	8.0	121.99	106.73	145.09
7	C4	1.52×10^5	1.8×10^4	16.2	136.20	121.77	161.09
8	C5	1.02×10^5	1.3×10^4	11.9	137.66	148.17	1.63
9	C6	3.27×10^4	7.5×10^3	6.7	120.69	143.74	1.66
10	D1	5.27×10^3	2.4×10^3	3.0	91.39	79.20	99.05
11	A1	2.99×10^3	4.1×10^3	16.1	130.12	166.7	2.31

PEPs profiles for commercial printers

Figure 1-2 illustrates the particle number concentration of the three highest emitting printers during the 60-min print job (the data on the remaining tested printers are summarized in Supplementary Figure 1-S1). Almost all of the 11 printers showed an ‘‘initial burst’’ emission pattern, evidenced by a transient peak within the first 10–20 min of initiating the print job. For all of the printers, the particle number concentration upon completion of the print job is about 0.2–0.7 times the peak concentration and did not seem to depend on the printer model and consequently, the toner cartridge used. The highest particle number concentration observed was in the order of 1.27 million particles/cm^3 by Printers A1 and B1, while the lowest was 3,000 particles/cm^3 by Printer A2.

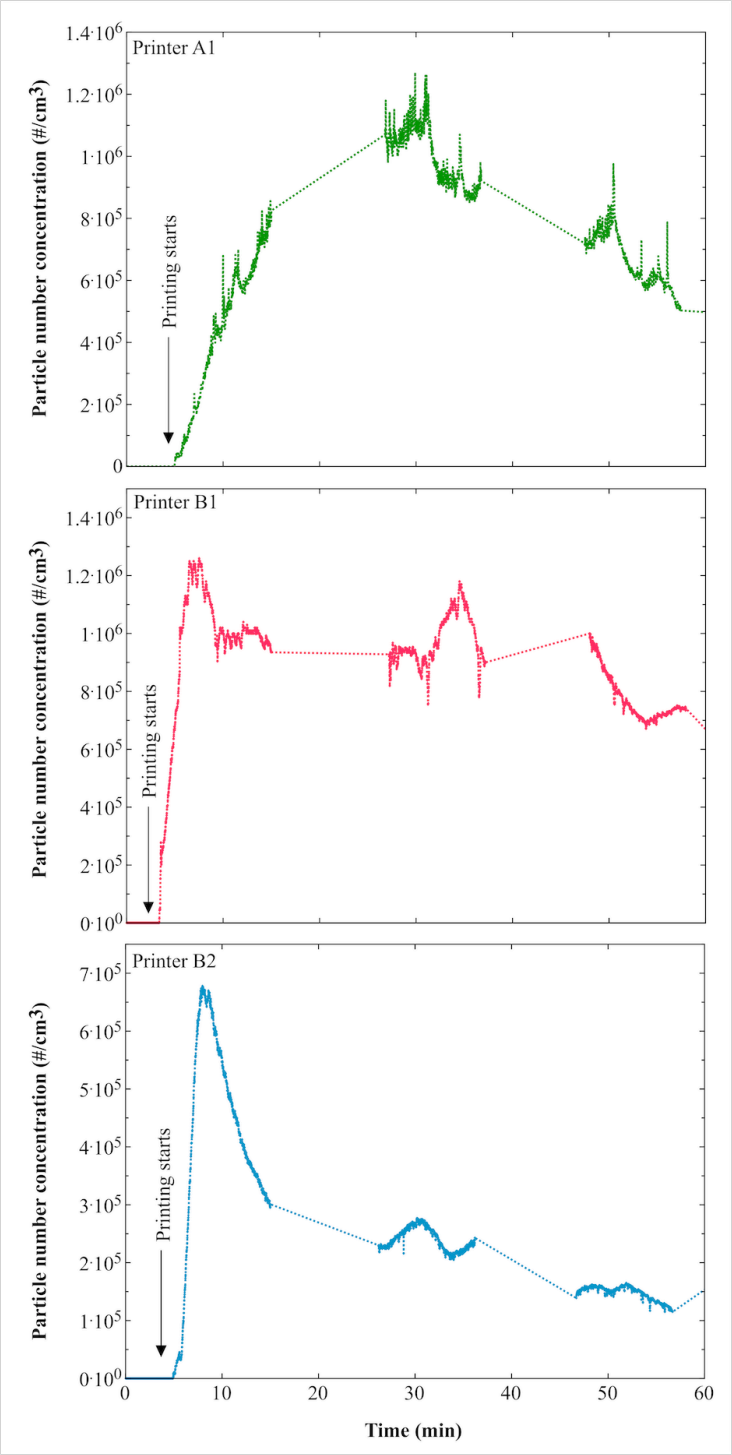

Figure 1-2. Total emitted particle number concentration from the three highest emitting printers during a 60-min print job using a 5% page coverage (dashed line represents no data for that particular time point).

Figure 1-3 shows the size distribution for emitted particles at three different 10-min intervals of the print job: early (10–20 min), middle (30–40 min) and end (50–60 min) for the three highest particle-emitting printers (please refer to Supplementary Figure 1-S2 for data on all other tested printers). A unimodal size distribution is evident throughout the printing job of the majority of printers used, with the exception of two printers (B2 and C5) that had a bimodal distribution. Mean particle diameters ranged from 39 to 138 nm for all printers tested. The majority, if not all, of the particles emitted during the 1-h print job appear to be in nanoscale (5100 nm) and only a minuscule number of particles are larger than 200 nm. However, there are a small number of emitted particles larger than 2 μm. Furthermore, there is a noticeable variation in the mobility diameter of the PEPs at the three different time points of the printing (modal diameter varies from 50 to 110 nm). In particular, Printer A1 emits approximately 2.5 times fewer particles at the middle stage rather than the early stage of the print job; and emitted particles were halved at the completion of the job. The printers from the remaining manufacturers had similar size distributions, with higher level of particles emitted early when compared to the end of printing.

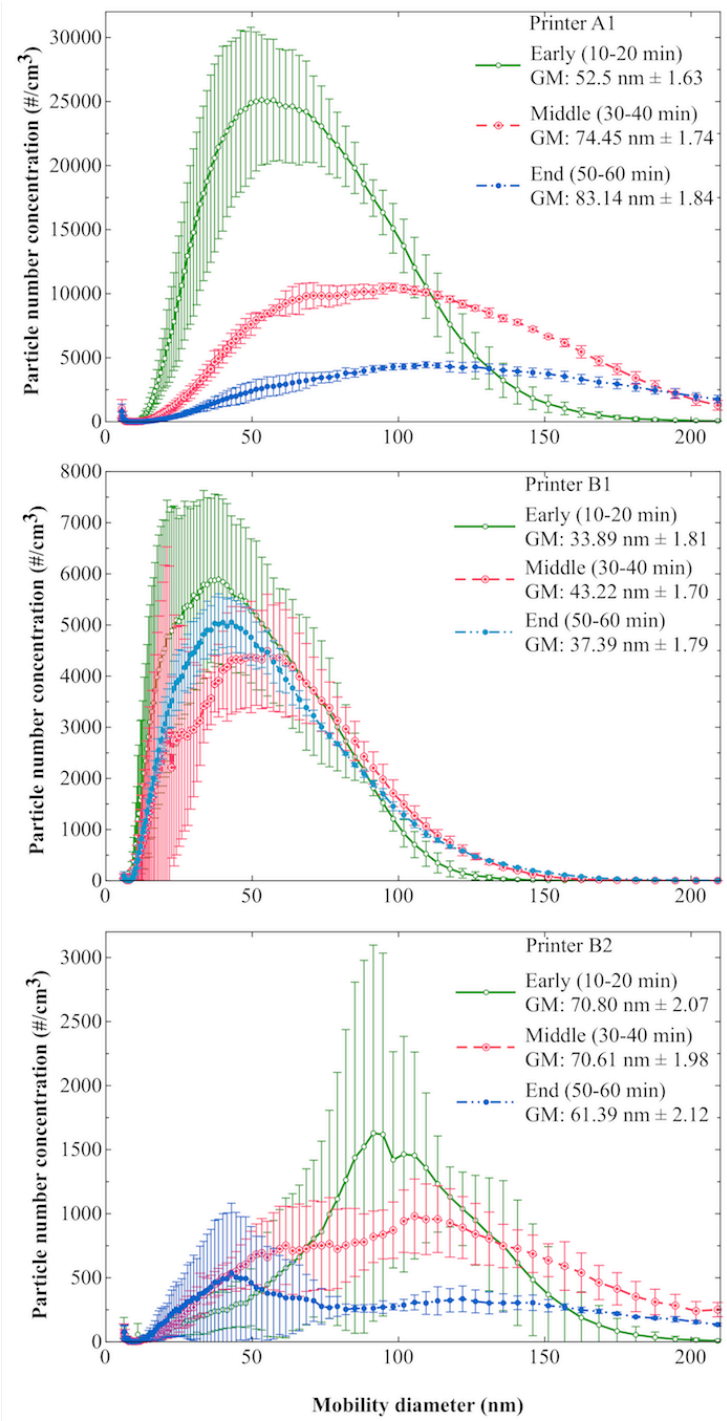

Figure 1-3. Mean PEP size distribution generated by the three highest particle-emitting laser printers at different time points of a 60-min print job using a 5% page coverage. Graph data shows the GM±GSD at different print job time points.

Figure 1-4 presents the mass concentration data of the size-fractionated PEPs of the six highest emitting printers based on the gravimetric analysis and CCI. Overall, for most printers, it can be observed that the mass concentration of particles less than 2.5 μm in size is considerably larger than the mass concentration for those particles greater than 2.5 μm in size. In particular, printers C2 and A1 released amounts of $PM_{2.5}$ as high as 94.71 and 99.81 $\mu g/m^3$, respectively, for the tested conditions. Generally, $PM_{>2.5}$ mass concentrations were lower than that of $PM_{2.5}$ and ranged from 13.18 to 49.41 $\mu g/m^3$, with the exception of Printer B2, which released the largest observed $PM_{>2.5}$ mass concentration of 49.41 $\mu g/m^3$.

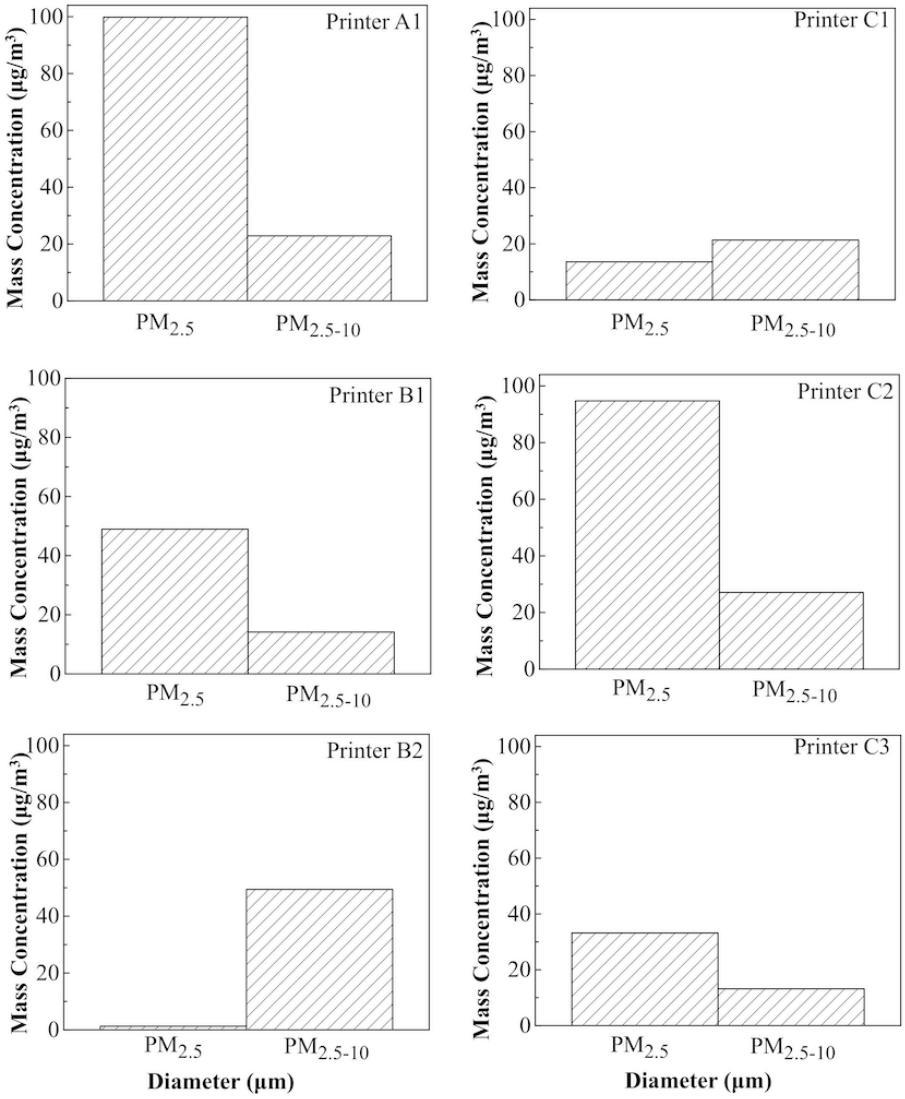

Figure 1-4. Maximum airborne mass concentration of the six highest emitting laser printers during a print job using a 5% page coverage. The printers are graphed in order of increasing number of particles emitted.

Table 1-2 shows the various indoor environmental parameters measured in the chamber during the printing process. There are no observable differences in temperature or ozone levels for all printers, which ranged from 27.83 to 34.29°C and 9.54 to 23.84 parts per billion by

volume (ppbv), respectively. The average relative humidity and temperature in the chamber was close to that of the ambient environment. Carbon monoxide (CO) levels were very low, while carbon dioxide (CO_2) levels varied from 666 to 716 ppm. The levels of tVOCs were measured only during print jobs using the six highest emitting printers, and there was a noticeable increase to mean values of up to 2,889 ppb for Printer B2, which is the third highest particle emitter. These concentrations are up to 13 times the chamber background levels and are directly proportional to the chamber temperature during the print job. This might also be attributed to VOC emissions associated not only with the printer itself but also with the stack of paper piled in the chamber and used during the printing job.

Table 1-2. Measurement of chamber air quality for the 11 laser printers evaluated during a continuous printing episode.

Printer	Temperature (°C)	RH (%)	Ozone (ppbv)	CO_2 (ppm)
Background	*22.6*	*20.1*	*15.8*	*715*
A1	28.3	55.0	13.7	685
B1	32.3	48.6	13.8	681
B2	34.3	56.8	14.5	682
C1	28.9	39.6	23.9	671
C2	29.3	70.2	20.1	666
C3	28.4	70.6	9.83	716
C4	30.1	77.8	15.0	709
C5	27.8	66.0	16.5	674
C6	77.1	34.3	Not measured	683
D1	28.6	64.0	11.5	709
A2	32.3	59.1	9.54	703

Note: CO levels remained at 0.00 ppm throughout experiments.

Effect of operational parameters on printer emission profiles

Page coverage: Figure 1-5 shows an increase in particle number concentration as a function of the page coverage. It is apparent that more particles are emitted as the coverage of the page increments. For instance, the particle emissions ranged from 25,000 to almost 60,000 particles/cm^3 for Printer C6. However, the 5% page coverage led to higher emissions than the 10% coverage.

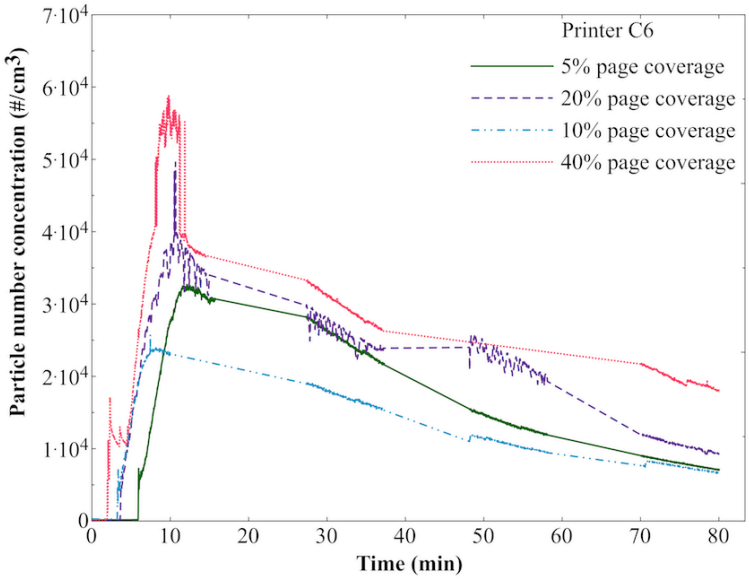

Figure 1-5. Particle number concentration while printing using different page coverages (5%, 10%, 20% or 40%) using Printer C6.

Single- and double-sided printing: There was no difference in the printer emission profile in single- and double-sided printing (data not shown).

Printing frequency mode: Compared with continuous printing, the intermittent mode led to a reduction of about half the maximum number of emitted particles in printers B1 and C5 (data not shown). As for Printer C6, a slight difference in particle concentration was barely

noticeable in the two printing scenarios. The data suggest that intermittent printing results in a different number of emitted particles as opposed to continuous printing.

Potential deposition of PEPs in the human lung

Figure 1-6 shows the modeled deposited mass fraction and mass flux for the various areas of human lung. It can be observed that the majority of the inhaled PEPs would deposit in the respiratory bronchioles and distal alveoli due to their small size. Approximately 30% of the inhaled PEPs would deposit in the lungs. Furthermore, for exposure durations of 8 h, or 60 and 15 min the total lung surface dose is equal to 831.5, 103.9 and 25.99 $\mu g/m^2$, respectively. These values were derived using the total deposition mass flux of 1.732 $\mu g/min \bullet m^2$ and the corresponding exposure time.

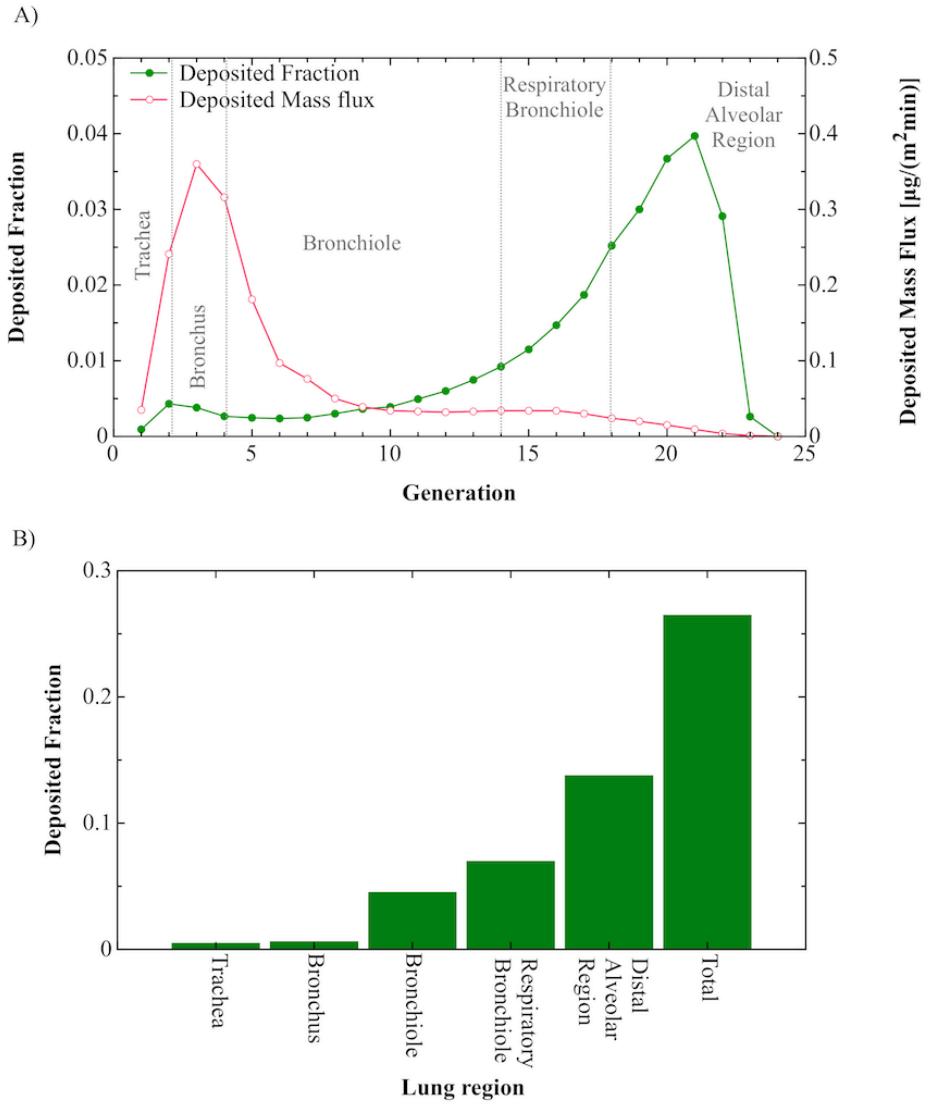

Figure 1-6. Deposition of PEPs in the human lung. (A) Deposition fraction and deposition mass flux as a function of generation number of the human respiratory tree. (B) Deposition mass fraction in the total and various sections of the human lung: trachea, bronchus, bronchiole, respiratory bronchioles and distal alveolar region.

Discussion

The data presented illustrate the versatility of the developed PEGS platform and its ability to generate realistic PEP exposures suitable for the physico-chemical and toxicological characterization of PEPs. Data also provide evidence that laser printers emit particles at substantially high levels that can reach particle number concentrations close to 1.3 million particles/cm^3 in addition to other pollutants (*e.g.*, ozone, tVOCs). Real-time PM monitoring data also showed that the majority of PEPs are in the nanoscale with very few particles greater than 200 nm. This is in accordance with a study by He et al. (2007), which concluded that approximately 73–99% of the total particles emitted by three different laser printers ranged from 40 to 76 nm. Jiang & Lu (2010) also observed PEPs formed agglomerates of 10–200 nm in size, although the majorities were approximately 80 nm. Interestingly, a study by Byeon & Kim (2012) found the mobility diameter of the emitted particles was directly proportional to the printing speed.

Moreover, the data showed consistently that most of the printers, regardless of the manufacturer and model, had an ‘‘initial burst’’ emission pattern characterized by a transient peak in particle number concentration within the first 10–20 min of printing, followed by a steady decay until completion of printing. This ‘‘initial burst’’ type of emission was also observed in other published studies, and it has been attributed to the rise in temperature of the fuser unit (Barthel et al., 2011; Schripp et al., 2008; Wensing et al., 2008). The intensity of the emission initial particle peak varies with the printer model and manufacturer.

Note that in our experiments using the PEGS platform, some printers emitted PEPs at extremely high levels with particle number concentrations in the order of a million particles/cm^3. Such levels are higher than those observed in highly polluted highways (Fuller et al., 2013;

Padro-Martinez et al., 2012). Similarly, the $PM_{2.5}$ mass concentration levels for one of the high emitters (Printer A1) was 99.81 $\mu g/m^3$, which surpasses the Environmental Protection Agency retained 24-h ambient PM standard of 35 $\mu g/m^3$ (EPA.GOV, 2014). Our findings raise concerns about potential health effects of PEPs given the historic epidemiological and toxicological evidence linking PM exposures to disease (Dockery et al., 1993; Dominici et al., 2006; Perrone et al., 2013; Zhao et al., 2013). Furthermore, the levels of tVOCs in the exposure chamber during the 1-h printing experiment were found to be in the range of 216.7–2,889 ppb. These high levels may be due to the fact that high temperatures are used in the printer (up to 225 ºC) to fuse the toner powder to the paper (Lee et al., 2001). The temperature and relative humidity in the chamber remained fairly similar amongst the 11 printers, as did the ozone levels, which remained close to background levels and similar to those observed in the literature (He et al., 2010; Lee et al., 2001; McKone et al., 2009). Notably, a modification in the printing technology employed by manufacturers in the past years in order to get rid of the ozone generating corona wire device, which produces the ion field, has led to a dramatically decrease in ozone levels.

Moreover, the data presented illustrate the effect of various operational parameters on the emission pattern. It was shown that there is an association between the number of particles emitted and the page coverage as well as the continuity of the printing. As expected, increasing the page coverage had a direct effect on the number of particles emitted. This is in agreement with another published study (He et al., 2007). Printing double-sided pages led to no real change in the number of particles emitted when compared to single-sided printing. Lastly, the data presented show that continuous versus intermittent printing also affects the number of PEPs. This is in agreement with a similar investigation by Wensing et al. (2008). Even though operational parameters may vary across manufacturers and models, these results provide an understanding of

the particle emission trends for various laser printers with different operational settings, which can be helpful in providing insight into how to reduce or prevent the risk of exposure to PEPs.

Due to their nanoscale size the PEPs would make their way deep into the lungs where they are deposited, as indicated in the presented lung deposition data. The potential high deposited doses in the lungs reported here raise concerns for adverse health effects (Bengalli et al., 2013; Michael et al., 2013) as more than 52% of those inhaled particles deposit in the alveoli and 26% in the respiratory bronchioles. Specifically, particle deposition in the lung would be approximately 4 and 16 $\mu g/m^2$ for 15- and 60-min PEPs exposures, respectively. Considering the average lung has a surface area of approximately 70 m^2, total dose of exposure now becomes 1,115 μg, for a 1-h exposure duration. A major concern when discussing adverse effects of respirable PM is the focus on susceptible populations like asthmatics and elderly, among others (Harkema et al., 2004; Murr et al., 2006). A study by Tanaka et al. (2013) showed exposure to nanoparticle-rich diesel exhaust exacerbated ovalbumin-induced eosinophilic airway inflammation, evidenced by an increase in levels of key cyto-/chemokines and myeloperoxidase release into alveolar spaces. Thus, the potential of high deposited dose of PEPs in the lungs highlights the critical need to fully understand the effects these PEPs on pulmonary response and more importantly the potential health effects on those with preexisting respiratory and cardiovascular conditions.

In summary, the developed PEGS platform described here can serve as a test platform for the uninterrupted generation, collection and characterization of physico-chemical and toxicological properties of PEPs. Moreover, this integrated platform will enable researchers to assess the possible health implications of exposures to PEPs, which can in turn aid in the

development of control technologies that may reduce or prevent emissions from laser-based printing equipment.

This paper is the first of three companion papers on this emerging health matter. The other two companion papers, which are in preparation, will include detailed information on the chemical composition and morphology of both the toner powder and PEPs from the six highest emitting printers. Lastly, the results from an *in vitro* and *in vivo* toxicological characterization of the PEPs from one of the highest emitting printers (Printer B1) will be presented in the third companion paper.

Conclusion

Overall, the presented integrated realistic exposure generation platform (*i.e.*, PEGS) is suitable for the physico-chemical, morphological and toxicological characterization of PEPs. It will enable toxicologists to link chemical composition and morphology of toners and PEPs to toxicological outcomes. This integrated approach provides a testing platform for nano-risk assessors to understand the properties of released PM from nano-enabled products and their link to toxicological outcomes and can be used for other nanomaterials. Such a methodological approach will improve our understanding of the potential impact of nano exposures on human health in both occupational and non-occupational settings and generate suitable data for science-based risk assessment.

Declaration of interest

The authors acknowledge funding for this study from NIEHS Center Grant ES-000002, NIOSH and CPSC (Grant # 212-2012-M-51174). The findings and conclusions in this manuscript have not been formally disseminated by the NIOSH or CPSC and should not be

construed to represent any agency determination or policy.

Supplemental Material

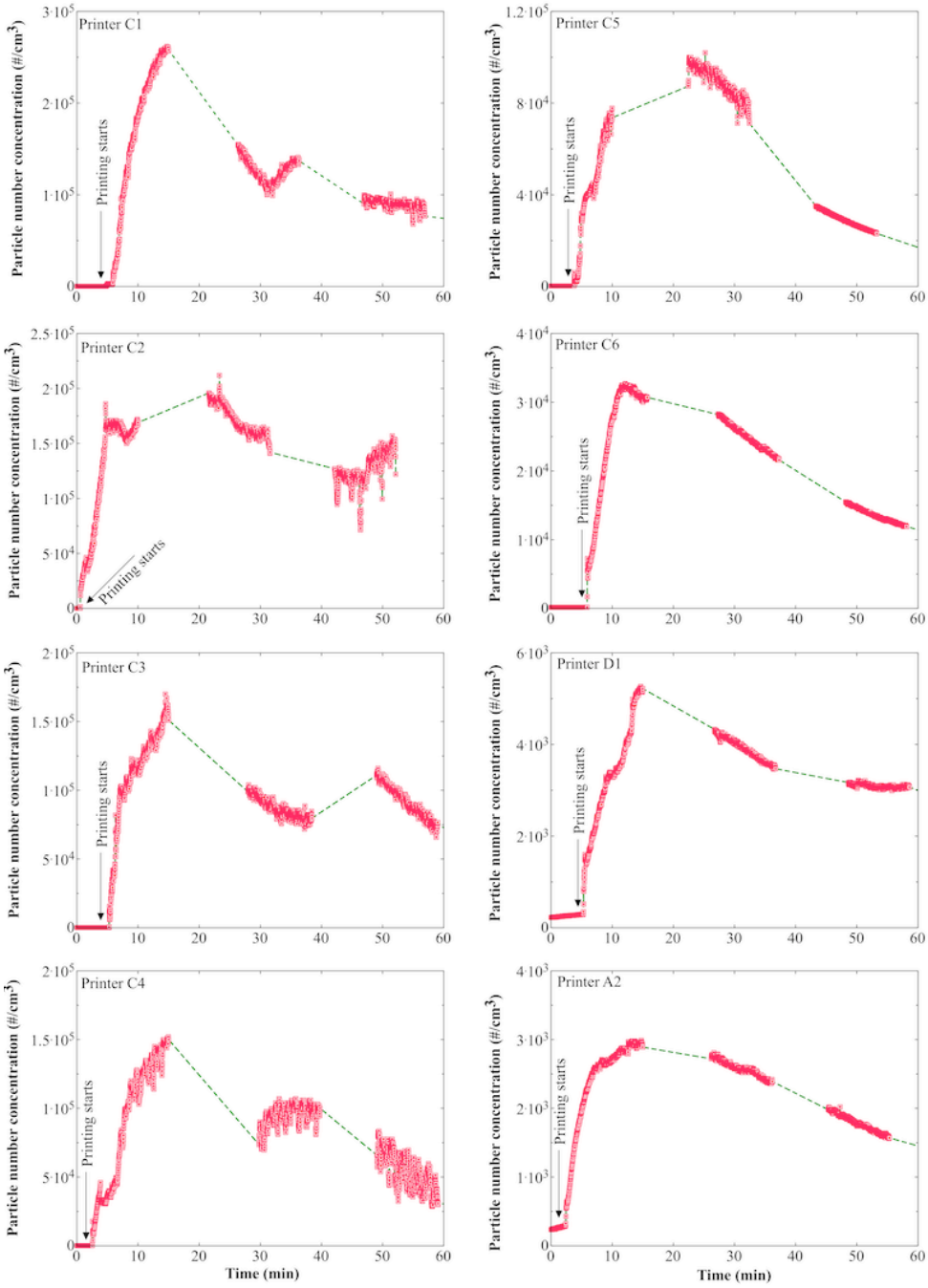

Figure 1-S1. Particle number concentration of the remaining eight tested laser printers during a 60-minute print job using a 5% page coverage. Data obtained from CPC instrument.

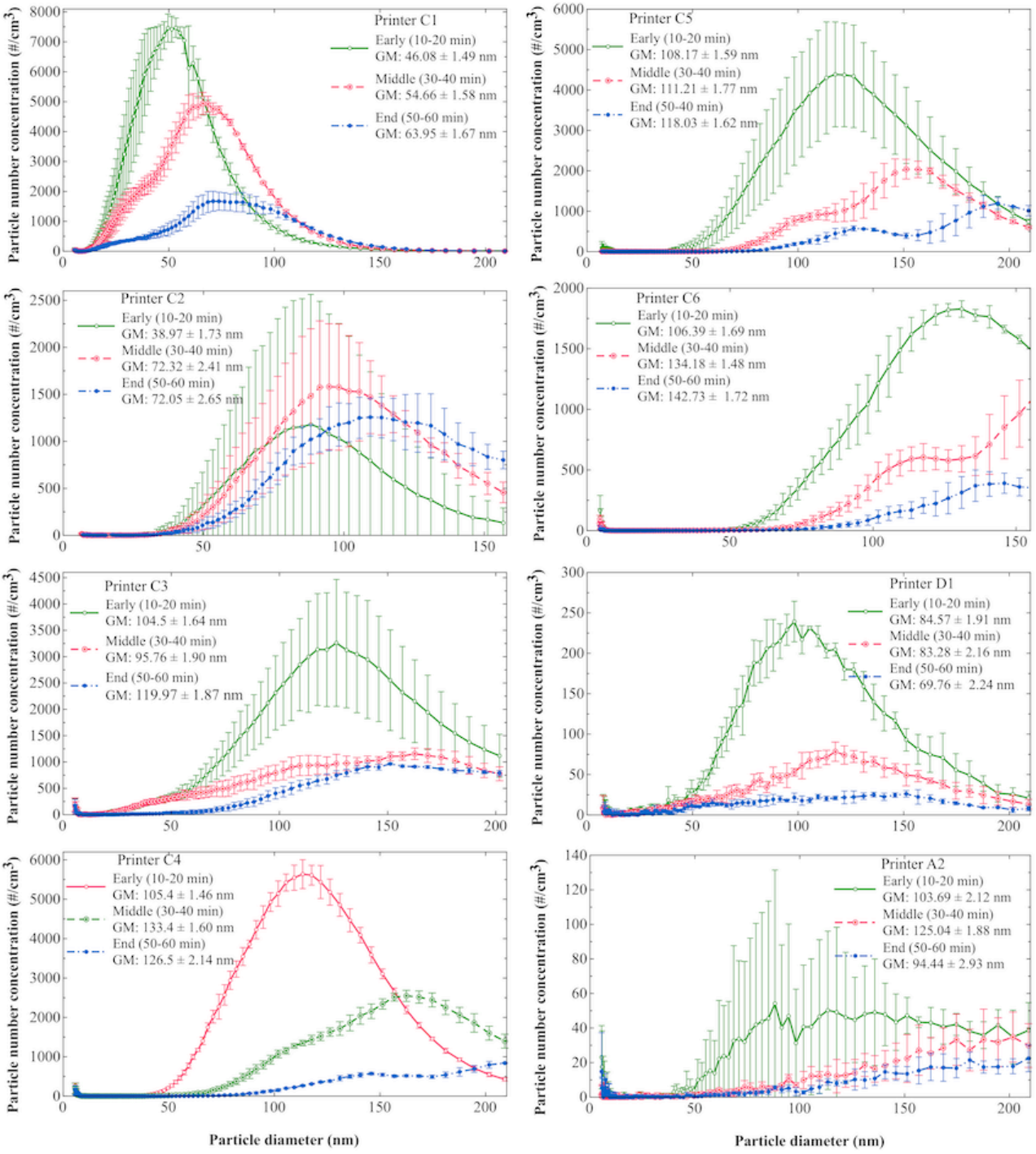

Figure 1-S2. Average PEP size distribution generated by the remaining laser printers at different time points of a 60-minute print job using a 5% page coverage. Graph data shows the geometric standard mean (GM) ± geometric standard deviation at different print job time points.

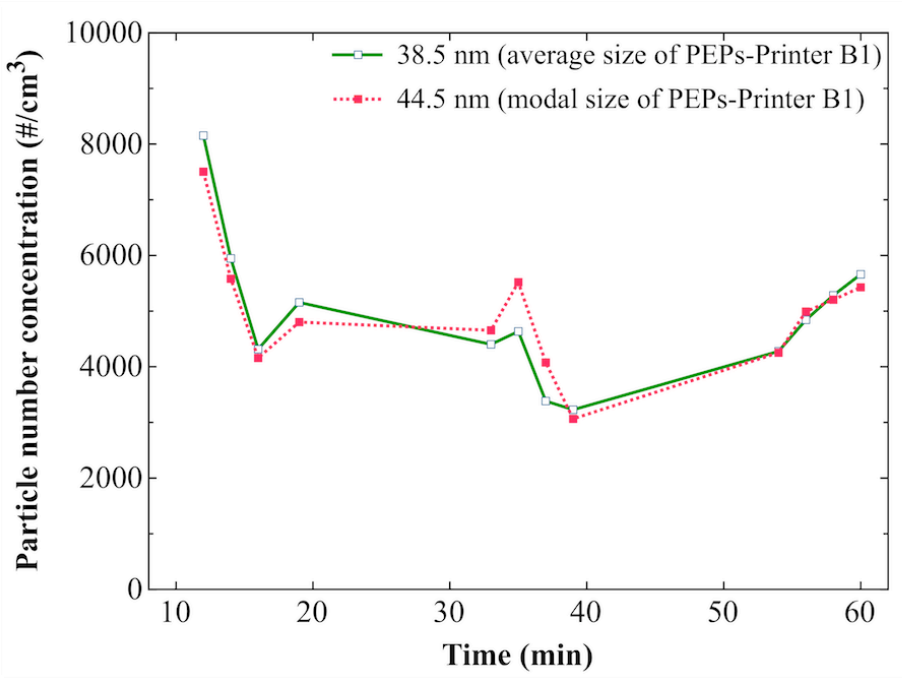

Figure 1-S3. Snapshot of number concentration of particles emitted by Printer B1, for two particle diameters, as a function of time.

Table 1-S1. Functional properties of all the eleven evaluated laser printers.

Printer	Printing speed (pages/min)	Color or halftone	Manufacture year
A1	31	Color	2011
A2	38	Halftone	2013
B1	24	Halftone	2012
B2	21	Halftone 3	2004
C1	12	Halftone	2007
C2	35	Halftone	2009
C3	30	Color	2009
C4	33	Halftone	2012
C5	27	Halftone	2007
C6	25	Halftone	2011
D1	26	Halftone	2012

Table 1-S2. Summary of parameters used in the *in vivo* lung Multiple Path Particle Deposition model (MPPD2, Anjilvel and Asgharian 1995).

Human Model	**Breathing Parameters**	***Airborne Nanoparticle Distribution****
Functional Residual Capacity: 3300 mL	*Tidal Volume*: 625 ml	*CMD:* 57.45 nm
Head Volume: 50 mL	*Breathing Frequency:* 12 breaths/ min	*Geometric Standard Deviation*: 1.67
Breathing Route: Nasal	*Inspiratory Fraction*: 0.5 *Pause Fraction*: 0.0	*Mass Concentration*: 23.86 μg/m^3

Bibliography

Anjilvel S, Asgharian B. (1995). A multiple-path model of particle deposition in the rat lung. Fundam Appl Toxicol 28:41–50.

Barthel M, Pedan V, Hahn O, et al. (2011). XRF-analysis of fine and ultrafine particles emitted from laser printing devices. Environ Sci Technol 45:7819–25.

Bello D, Martin J, Santeufemio C, et al. (2012). Physico-chemical and morphological characterisation of nanoparticles from photocopiers: implications for environmental health. Nanotoxicology 7:989–1003.

Bengalli R, Mantecca P, Camatini M, Gualtieri M. (2013). Effect of nanoparticles and environmental particles on a cocultures model of the air–blood barrier. Biomed Res Int 2013:801214. doi:10.1155/ 2013/801214.

Brown S. (1999). Pollutant emission properties of photocopiers and laser printers. In: Indoor Air 99: proceedings of the 8th International Conference on Indoor Air Quality and Climate. Vol. 5. 813 August, 1999, Edinburgh, Scotland, 123–8.

Byeon JH, Kim J-W. (2012). Particle emission from laser printers with different printing speeds. Atmos Environ 54:272–6.

Castellano P, Canepari S, Ferrante R, L'Episcopo N. (2012). Multiparametric approach for an exemplary study of laser printer emissions. J Environ Monit 14:446–54.

Chang C, Demokritou P, Shafer M, Christiani D. (2013). Physico-chemical and toxicological characteristics of welding fume derived particles generated from real time welding processes.

Environ Sci Process Impacts 15:214–24.

Demokritou P, Gass S, Pyrgiotakis G, et al. (2012). An in vivo and in vitro toxicological characterization of realistic nanoscale CeO_2 inhalation exposures. Nanotoxicology 7:1338–50.

Demokritou P, Kavouras IG, Ferguson ST, Koutrakis P. (2002). Development of a high volume cascade impactor for toxicological and chemical characterization studies. Aerosol Sci Technol 36: 925–33.

Demokritou P, Lee SJ, Ferguson ST, Koutrakis P. (2004). A compact multistage (cascade) impactor for the characterization of atmospheric' aerosols. J Aerosol Sci 35:281–99.

Dockery D, Arden C, Xu X, et al. (1993). An association between air pollution and mortality in six U.S. cities. N Engl J Med 329:1753–9. Dominici F, Peng R, Bell M, et al. (2006). Fine particulate air pollution and hospital admission for cardiovascular and respiratory diseases.

JAMA 295:1127–34. Dun & Bradstreet Reports. (2011). SIC 7334 photocopying and

duplicating services – description, market prospects, industry history [Online]. Reference for Business, Encyclopedia of Business, 2nd ed. Available from: http://www.referenceforbusiness.com/industries/Service/Photocopying-Duplicating-services.html. [Last accessed: Feb 2014].

EPA.GOV. (2014). National Ambient Air Quality Standards (NAAQS) j Air and Radiation j US EPA. Available from: http://www.epa.gov/air/ criteria.html [Last accessed: 23 Jan 2014].

Fuller CH, Brugge D, Williams PL, et al. (2013). Indoor and outdoor measurements of particle number concentration in near-highway homes. J Exp Sci Environ Epidemiol 23:506–12.

Furukawa Y, Aizawa Y, Okada M, et al. (2002). Negative effect of photocopier toner on alveolar macrophages determined by in vitro magnetrometric evaluation. Indus Health 40:214–21.

Gminski R, Decker K, Heinz C, et al. (2011). Genotoxic effects of three selected black toner powders and their dimethyl sulfoxide extracts in cultured human epithelial A549 lung cells in vitro. Environ Mol Mutagen 52:296–309.

Harkema JR, Keeler G, Wagner J, et al. (2004). Effects of concentrated ambient particles on normal and hypersecretory airways in rats. Res Rep Health Effect Inst 120:1–68.

He C, Morawska L, Taplin L. (2007). Particle emission characteristics of office printers. Environ Sci Technol 41:6039–45.

He C, Morawska L, Wang, H, et al. (2010). Quantification of the relationship between fuser roller temperature and laser printer emissions. J Aerosol Sci 41:523–30.

ISO.ORG. (2014). ISO/IEC 19752:2004 – information technology – method for the determination of toner cartridge yield for monochro- matic electrophotographic printers and multi-function devices that contain Printer Components. Available from: http://www.iso.org/iso/home/store/catalogue_tc/catalogue_detail.htm?csnumber1⁄434911. [Last accessed: 21 Jan 2014].

Jamieson L. (2012). Ink and toner cartridge use among SMBs in the United States. Photizo Group. Available from: http://photizogroup.- com/wp-content/uploads/2012/09/8.31.12-U.S.-SMB-Ink-and-Toner- Cartridge-Use.pdf [Last accessed: 17 Mar 2013].

Jiang H, Lu L. (2010). Measurement of the surface charge of ultrafine particles from laser printers and analysis of their electrostatic force. Atmos Environ 44:3347–51.

Kagi N, Fujii S, Horiba Y, et al. (2007). Indoor air quality for chemical and ultrafine particle contaminants from printers. Build Environ 42: 1949–54.

Khatri M, Bello D, Gaines P, et al. (2012). Nanoparticles from photocopiers induce oxidative stress and upper respiratory tract inflammation in healthy volunteers. Nanotoxicology 7:1014–27.

Khatri M, Bello D, Pal A, et al. (2013a). Human cell line evaluation of cytotoxic, genotoxic and inflammatory responses caused by nanoparticles from photocopiers. Particle Fiber Toxicol 10:42. doi:10.1186/1743-8977-10-42.

Khatri M, Bello D, Pal A, et al. (2013b). Toxicological effects of PM0.1- 2.5 particles collected from a photocopy center in three human cell lines. Inhal Toxicol 25:621–32.

Lee C-W, Hsu D-J. (2007). Measurements of fine and ultrafine particles formation in photocopy centers in Taiwan. Atmos Environ 41: 6598–609.

Lee SC, Lam S, Fai HK. (2001). Characterization of VOCs, ozone, and PM10 emissions from office equipment in an environmental chamber. Build Environ 36:837–42.

Lough G, Schauer J, Park J, et al. (2005). Emissions of metals associated with motor vehicle roadways. Environ Sci Technol 39:826–36.

Mcgarry P, Morawska L, He C, et al. (2011). Exposure to particles from laser printers operating within office workplaces. Environ Sci Technol 45:6444–52.

Mckone T, Maddalena R, Destaillats H, et al. (2009). Indoor pollutant emissions from electronic office equipment. California, unpublished work. Available from:

http://www.arb.ca.gov/research/seminars/ mckone/mckone.pdf. [Last accessed: Feb 2014].

Michael S, Montag M, Dott W. (2013). Pro-inflammatory effects and oxidative stress in lung macriophages and epithelial cells induced by ambient particular matter. Environ Pollut 183:19–29.

Mohr U, Ernst H, Roller M, Pott F. (2005). Carcinogenicity study with nineteen granular dusts in rats. Eur J Oncol 10:249–81.

Mohr U, Ernst H, Roller M, Pott F. (2006). Pulmonary tumor types induced in Wistar rats of the so-called ‘‘19-dust study’’. Exp Toxicol Pathol 58:13–20.

Moller A, Muhle H, Creutzenberg O, et al. (2004). Biological procedures for the toxicological assessment of toner dusts. Gefahrst Reinhalt Luft 64:13–20.

Morawska L, He C, Johnson G, et al. (2009). An investigation into the characteristics and formation mechanisms of particles originating from the operation of laser printers. Environ Sci Technol 43:1015–22.

Morimoto Y, Kim H, Oyabu T, et al. (2005). Negative effect of long- term inhalation of toner on formation of 8-hydroxydeoxyguanosine in DNA in the lungs of rats in vivo. Inhal Toxicol 17:749–53.

Murr LE, Soto KF, Garza KM, et al. (2006). Combustion-generated nanoparticles in the El Paso, TX, USA/Juarez, Mexico Metroplex: their comparative characterization and potential for adverse health effects. Int J Environ Res Public Health 1:48–66.

Nel A, Xia T, Madler L, Li N. (2006). Toxic potential of materials at the nanolevel. Science

311:622–7.

Padro-Martinez LT, Patton AP, Trull JB, et al. (2012). Mobile monitoring of particle number concentration and other traffic related air pollutants in a near-highway neighborhood over the course of a year. Atmos Environ (1994) 61:253–64.

Perrone MG, Gualtieri M, Consonni V, et al. (2013). Particle size, chemical composition, seasons of the year and urban, rural or remote site origins as determinants of biological effects of particulate matter on pulmonary cells. Environ Pollut 176C:215–27.

Pettersson T, Fogden A. (2006). Levelling during toner fusing: effects on surface roughness and gloss of printed-paper. J Imaging Sci Technol 50:202–15.

Pirela S, Molina R, Watson C, et al. (2013). Effects of copy center particles on the lungs: a toxicological characterization using a Balb/c mouse model. Inhal Toxicol 9:498–508.

Pyrgiotakis G, Mcdevitt J, Bordini A, et al. (2014). A chemical free, nanotechnology-based method for airborne bacterial inactivation using engineered water nanostructures. Environ Sci Nano 1:15–26.

Reynolds JS, Johnson VJ, Frazer DG. (2008). Unrestrained acoustic plethysmograph for measuring specific airway resistance in mice. J Appl Physiol 105:711–17.

Schripp T, Wensing M, Uhde E, et al. (2008). Evaluation of ultrafine particle emissions from laser printers using emission test chambers. Environ Sci Technol 42:4338–43.

Slesinski RS, Turnbull D. (2008). Chronic inhalation exposure of rats for up to 104 weeks to a non-carbon-based magnetite photocopying toner. Int J Toxicol 27:427–39.

Sotiriou G, Watson C, Murdaugh KM, et al. (2014). Engineering safer- by-design, transparent, silica-coated ZnO nanorods with reduced DNA damage potential. ES Nano 1:144–53.

Tanaka M, Aoki Y, Tajano H, et al. (2013). Effects of exposure to nanoparticle-rich or -depleted diesel exhaust on allergic pathophysi- ology in the murine lung. J Toxicol Sci 38:35–48.

Tang T, Hurrass J, Gminski R, Mersch-Sundermann V. (2012). Fine and ultrafine particles emitted from laser printers as indoor air contaminants in German offices. Environ Sci Pollut Res Int 19: 3840–9.

Wang H, He C, Morawska L, et al. (2012). Ozone-initiated particle formation, particle aging, and precursors in a laser printer. Environ Sci Technol 46:704–12.

Wensing M, Pinz G, Bednarek M, et al. (2006). Particle measurement of hardcopy devices. Healthy Buildings Conference. Lisboa.

Wensing M, Schripp T, Uhde E, Salthammer, T. (2008). Ultra-fine particles release from hardcopy devices: sources, real-room measure- ments and efficiency of filter accessories. Sci Total Environ 407: 418–27.

Zhao J, Gao Z, Tian Z, et al. (2013). The biological effects of individual-level PM2.5 exposure on systemic immunity and inflammatory response in traffic policemen. Occup Environ Med 70:426–31.

Chapter 2: Consumer exposures to laser printer-emitted engineered nanoparticles: A case study of life-cycle implications from nano-enabled products

Sandra V. Pirela[1], Georgios A. Sotiriou[1], Dhimiter Bello[1,2], Martin Shafer[3], Kristin Lee Bunker[4], Vincent Castranova[5], Treye Thomas[6], and Philip Demokritou[1*]

Nanotoxicology. 2014.

[1]Department of Environmental Health, Center for Nanotechnology and Nanotoxicology, School of Public Health, Harvard University, Boston, MA, USA.

[2]Department of Work Environment, College of Health Sciences, and Center for High Rate Nanomanufacturing, University of Massachusetts, Lowell, MA, USA.

[3]Wisconsin State Laboratory of Hygiene, Madison, WI, USA.

[4]R. J. Lee Group, Inc., Monroeville, PA, USA.

[5]Department of Basic Pharmaceutical Sciences, West Virginia University, Morgantown, WV, USA.

[6]U.S. Consumer Product Safety Commission, Office of Hazard Identification and Reduction, Rockville, MD, USA.

[*]Corresponding author

Abstract

It is well established that printers emit nanoparticles during their operation. To-date, however, the physico-chemical and toxicological characterization of ‘‘real world’’ printer-emitted nanoparticles (PEPs) remains incomplete, hampering proper risk assessment efforts. Here, we investigate our earlier hypothesis that engineered nanomaterials (ENMs) are used in toners and ENMs are released during printing (consumer use). Furthermore, we conduct a detailed physico-chemical and morphological characterization of PEPs in support of ongoing toxicological assessment. A comprehensive suite of state of the art analytical methods and tools was employed for the physico-chemical and morphological characterization of 11 toners widely utilized in printers from major printer manufacturers and their PEPs. We confirmed that a number of ENMs incorporated into toner formulations (*e.g.*, silica, alumina, titania, iron oxide, zinc oxide, copper oxide, cerium oxide, carbon black among others) and released into the air during printing. All evaluated toners contained large amounts of organic carbon (OC, 42–89%), metals/metal oxides (1–33%), and some elemental carbon (EC, 0.33–12%). The PEPs possess a composition similar to that of toner and contained 50–90% OC, 0.001–0.5% EC and 1–3% metals. While the chemistry of the PEPs generally reflected that of their toners, considerable differences are documented indicative of potential transformations taking place during consumer use (printing). We conclude that: (i) Routine incorporation of ENMs in toners classifies them as nano-enabled products (NEPs); (ii) These ENMs become airborne during printing; (iii) The chemistry of PEPs is complex and it reflects that of the toner and paper. This work highlights the importance of understanding life-cycle (LC) nano-EHS implications of NEPs and assessing real world exposures and associated toxicological properties rather than focusing on ‘‘raw’’ materials used in the synthesis of an NEP.

Introduction

The market for NEPs is estimated to have had an annual growth rate of approximately 50% since 2009 (Limited, 2011), rendering the possible consumer exposure to ENMs inevitable. The current ‘‘modus operandi’’ used in the nanoparticle risk assessment paradigm which focuses only on the pristine (raw) ENMs is not often appropriate to address possible adverse health effects associated with NEPs during a product’s life cycle (LC). Even though such information is crucial for risk assessment of occupational exposures during the manufacturing of NEPs, consumers typically do not get exposed to the pristine ENMs used in the synthesis of NEPs, but rather, to the nanoparticles released during the use of a product. Such emissions may have potentially altered physico-chemical and (possibly) toxicological properties that are different from those of the ‘‘raw’’ ENMs. This important knowledge gap has been emphasized recently in both the National Research Council report, as well as in the National Nanotechnology Initiative’s strategy on nano-environmental health and safety (nano-EHS) (NNI, 2011; NRC, 2012). If the nano-EHS uncertainties regarding LC implications of NEPs remain unaddressed, a proper public health risk assessment will not be possible and thus, the sustainable development of the nanotechnology industry as a whole will be affected at the social and economic levels.

Thus, new methodological approaches are urgently needed to address LC implications of NEPs (NNI, 2011; NRC, 2012). Here, such an integrated methodology for exposure assessment of NEPs during consumer use is presented for nano-enabled toners used in laser printers. This case study demonstrates the importance of studying the release of ENMs from NEPs during consumer use and characterizing their physico-chemical, morphological and, subsequently, toxicological properties.

Evaluating consumer risk of nanoparticle exposure from the use of nano-enabled toners during printing has become a necessity, since the market for this office technology has increased substantially. The laser printer market has shown positive year-over-year growth, with halftone and color laser devices accounting for 82.3 and 60%, respectively, of the total laser market in 2013 (IDC, 2014). With the wider use of the hardcopy printing technology comes the increased likelihood of consumer exposure to PEPs emanating from toner cartridges.

Prior studies on the emission of particulate matter (PM) from laser printer equipment have focused on the particle size distribution and concentration of the emitted aerosol and factors that influence these emissions (*e.g.*, printer operational parameters, printer manufacturer, age) (Barthel et al., 2011; Brown, 1999; Castellano et al., 2012; Kagi et al., 2007; Tang et al., 2012; Wang et al., 2012; Wensing et al., 2006). Recently, it was shown that laser-based printing equipment can produce up to 1.3 million particles/cm3 and these PEPs have average mobility particle diameters ranging from 49 to 208nm (Pirela et al., 2014). However, to-date there is no comprehensive data regarding the incorporation of ENMs in toners and detailed physico-chemical properties of released PEPs and the relationship between PEPs and their precursors in toner powder.

In addition, published studies focusing on the toxicological properties of PEPs primarily used pristine toner particles rather than the actual released particles (Bai et al., 2010; Gminski et al., 2011; Konczol et al., 2013; Morimoto et al., 2013). These are both unrealistic exposure scenarios and their findings are contradictory; thus, they cannot be used towards a proper risk assessment at the consumer level. Additionally, epidemiological studies on emissions from laser printers are inconclusive since there is no clear differentiation between symptoms resulting solely from PEPs or from allergic reactions due to previous sensitization events (Ewers &

Nowak, 2006). As a result, it is difficult to determine the inherent public health implications derived from this widely used NEP.

Here, an exposure platform recently developed by the authors (Pirela et al., 2014) was used to generate PEPs from 11 widely used laser printers. A thorough investigation to assess the presence of nanoscale materials in the toner formulations and study the release of such ENMs in the air during printing (consumer use) was performed. A detailed physico-chemical and morphological characterization on both PEPs and toner formulations was completed using state of the art analytical methods, such as magnetic sector field (SF) inductively coupled plasma mass spectrometry (ICP-MS), ion chromatography, organic/elemental carbon analysis, Fourier transform infrared (FTIR) spectroscopy, and scanning and transmission electron microscopy (STEM) coupled with energy dispersive X-ray (EDX) spectroscopy. Such an integrated methodology for the risk assessment of NEPs during consumer use will not only provide detailed characterization of exposures from such a NEP product, but will also enable toxicological testing using collected real world emitted particles rather than the pristine toner particles.

Methods

Collection of size fractionated PEPs and toner powder from commonly used laser printers

The recently developed Printer Exposure Generation System (PEGS, Supplemental Figure 2-S1), which is suitable to generate real world exposures to PEPs, was used in this study (Pirela et al., 2014). In summary, each laser printer was placed inside an environmental chamber and set to print a single-sided monochrome document. The selected 11 printers are from the four most commercially available manufacturers (A, B, C and D) and models. Manufacturing date varied for this particular ‘‘printer sample’’ to simulate that of a representative office environment. All printers here have been manufactured within the last 9 years (2004–2013), with

some of them being brand new (see Supplementary Table 2-S1 for printer specifications including manufacturing year). It is worth noting that the effect of the wear and tear and age of the printer as a modifier of the PM emission profile was not investigated here. The reproducibility of the PM emissions from two new laser printers of the same model was verified, as well as that of the different toner cartridges used and no differences were found (data not shown). The size-fractionated PEPs were sampled using the Harvard Compact Cascade Impactor (CCI), which has a flow rate of 30 l/min (Demokritou et al., 2004) onto polyurethane foam (PUF) impaction substrates ($PM_{>2.5}$), and Teflon ($PM_{2.5}$, chemical analysis) or quartz ($PM_{2.5}$, OC/EC analysis) filters. The collection of $PM_{2.5}$ instead of two separate size fractions, $PM_{0.1}$ and $PM_{0.1–2.5}$, was done conscientiously to enable collection of sufficient mass and to keep the number of samples manageable. These were weighed pre- and post- sampling following a 48-h stabilization process in a temperature- (22 ºC ± 1) and humidity- (43% ± 2) controlled environmental chamber utilizing a Mettler Toledo XPE analytical microbalance (Columbus, OH). Thus, the weight difference was used to determine the collected PEPs mass and to calculate the time averaged particle mass concentration in the chamber during the printing episode. Subsequently, the size selective fractions were analyzed for various analytes based on a previously published methodology (Bello et al., 2013; Chang et al., 2013). For each sampling episode, field blanks were also collected. Toner powder was also collected directly from each cartridge and transferred to clean scintillation vials for subsequent chemical and morphological analysis.

Chemical analysis of PEPs and toner powder

Detailed chemical characterization of size fractionated PEPs and toner powders, as well as the paper used during the study, included testing for total and water-soluble fraction of

multiple metals (50 elements), and for organic and elemental carbon per previously published methods (Bello et al., 2013). The analyses are described briefly below for clarity:

Magnetic sector field inductively coupled plasma mass spectrometry

Evaluation of elemental composition of the collected material (airborne PM and toner powder) was performed following a protocol previously described by Herner et al. (2006). The extracted mass from the PUF substrate and the Teflon/Quartz filter was digested using an acidic solution and diluted to different volumes with high purity water (Millipore, Bedford, MA). The dilutions were then placed in low-density polyethylene bottles that were pre-cleaned using an acid solution consisting of 2.4N hydrochloric acid for two days, then 3.2 N HNO_3 for two more days and lastly, rinsed with high purity water. The water-soluble elements in the airborne PM sample were extracted using high purity water and filtered via the use of acid-leached polypropylene syringe filters. Finally, the digested sample and extracts under- went ICP-MS analysis (Thermo-Finnigan Element 2). In addition to the collected samples, sample spikes, sample duplicates, blanks, standards and certified reference materials (NIST 2709, NIST 1648a, NIST 2556, NIST 2702) were used in the chemical testing.

Organic carbon/elemental carbon analysis (OC/EC)

The PEPs were collected on pre-baked Quartz fiber filters. A one-cm^2 filter punch was used to measure OC-EC following the protocols standardized for the ACE-Asia intercomparison study. This method is adapted from the NIOSH 5040 method, which utilizes Sunset Laboratory Inc. (Forest Grove, OR), laboratory- based thermal optical analyzer. This analysis proved informative in the case of toners and PEPs because toners contain large amounts of organic carbon (in the polymer matrix), some elemental carbon (5–20%), and other metal oxide additives (Bello et al., 2013). We decided not to employ the semi-volatile organic compound (sVOC)

analysis because in our earlier work we found that these species accounted for only a minor fraction of the total PEPs mass (Bello et al., 2013).

Fourier transform infrared spectroscopy

Attenuated total reflection Fourier transform infrared (ATR-FTIR) spectroscopy was performed on the dry toner powders and the collected PEPs using a Perkin Elmer Spectrum One spectrometer (Waltham, MA). For the analysis of the collected PEPs, the aqueous solution containing the particles was evaporated to obtain the dried powder of the sample that was then redispersed in ultra-pure ethanol (Sigma Aldrich >99.9%, St. Louis, MO). One drop of this suspension was deposited on the ATR crystal and allowed to evaporate. The data acquisition was carried out with a resolution of $4cm^{-1}$ and the spectra were averaged at least 10 times.

Ion chromatography analysis for anions and cations

The water-soluble fraction of toners and PEPs were additionally analyzed for the following anions and cations by ion chromatography (ammonium, chloride, nitrate and sulfate), which were extracted from the filter samples with milliQ water (15.0 mL, for 6h, with continuous agitation, in the dark, in pre-cleaned polypropylene tubes) and quantified using an established low- level ion chromatographic (IC) technique (Thermo Scientific Dionex, Sunnyvale, CA). QA/QC samples included sample and milli-Q spikes, replicates, method and filter blanks, and primary and secondary standard checks.

Morphological analysis of PEPs and toner powder

The airborne PM from the six highest emitting printers as ranked based on real time monitoring particle number concentration data (Pirela et al., 2014) was collected onto a 100 mesh copper grid with a carbon film (EM Sciences, Hatfield, PA) using an electrostatic

precipitator (ESP, NIOSH Spokane Research Laboratory, Spokane, WA) operating at 100ml/min, typically for a duration of 3–10 min. The ESP flow rate was checked before sampling. Morphological analysis of PEPs collected onto the transmission electron microscopy (TEM) grids was conducted with TEM on a JEOL 2100 microscope (Peabody, MA) operated at 200 kV. The toner powder was attached on carbon tape that was mounted on the scanning electron microscopy (SEM) holder imaged with a scanning and transmission electron microscope (STEM) with a Carl Zeiss Supra55 microscope (Peabody, MA). For the SEM, gun voltage ranged from 2 to 10 kV. Furthermore, energy dispersive spectroscopy (EDX) was also used to evaluate the chemical composition of both the toner powders and the PEPs (EDX, JEOL 2010, Peabody, MA).

Total volatile organic compounds

Although the focus of the investigation was on the PEPs, the real-time release of total volatile organic compounds (tVOC) was also monitored using a tVOC monitor (Graywolf Sensing Solutions, Shelton, CT) equipped with a sensitive probe (parts per billion range). The instrument was factory calibrated within the past year and laboratory calibrated, as per the manufacturer's instructions, with isobutylene and zero air in the laboratory prior to the sampling. The instrument has a photoionization potential of 9.6 eV.

Mass balance calculations

Mass balance calculations were performed according to the procedure described by Bello et al. (2013). The total $PM_{2.5}$ mass from gravimetric analysis was partitioned between organic and elemental carbon, as well as overall inorganic content (from OC/EC analysis). The inorganic fraction was then further subdivided into different elements based on the ICP-MS analysis. More prominent elements were reported individually on the pie charts (*e.g.*, Si, Fe, Al and Ti) with the

remaining metals summed into a ‘‘metals category’’ and the difference was expressed as ‘‘other’’. This difference, always greater than zero, includes anions (*e.g.*, chlorides, sulfates, carbonates) and cations not included in the initial list of measured elements.

It should be noted that in this study, we sampled for $PM_{2.5}$ primarily due to cost considerations and to obtain sufficient mass for gravimetric analysis. Although the real-time data shows almost exclusively nanoparticle emissions (Pirela et al., 2014), which is consistent with published work, the total mass of $PM_{2.5}$ is influenced disproportionally more by a few much larger particles. In separate experiments with one high emitting printer (B1), sampling was done for both $PM_{0.1}$ and $PM_{0.1–2.5}$.

Results

Hypothesis #1: Inclusion of nanoscale materials in toner formulations?

In this study, we examined 11 toners used in 11 laser printer models made by four different market-leading manufacturers (A, B, C and D). Based on the information provided by the toner manufacturers' Material Safety Data Sheets (MSDS), the 11 toners typically consisted of a mixture of polymers (55–85% by mass) and a small fraction of fillers, such as ferrite and silicon dioxide (55%) and carbon black (510%) (see Table 2-S1 for full toner composition). No information was provided by the manufacturers in terms of the use of nanoscale materials in the toner formulation.

Figure 2-1 shows representative SEM images and the respective EDX spectra of dry toner powders from three of the eleven printers (A1, A2 and C6), which have different morphology: regular spheres (*e.g.*, Printer C6) versus irregular spheres (*e.g.*, Printer A1, A2) of a size range of ~10–15 mm. In one printer toner (A2), we found fibers (~2–10 mm in length) on the toner particle surface, which were identified to be titania by EDX analysis. The rest of the

examined toners exhibit similar morphological characteristics (Figure 2-S4). This is in agreement with toner particles used in photocopier equipment (Bello et al., 2013).

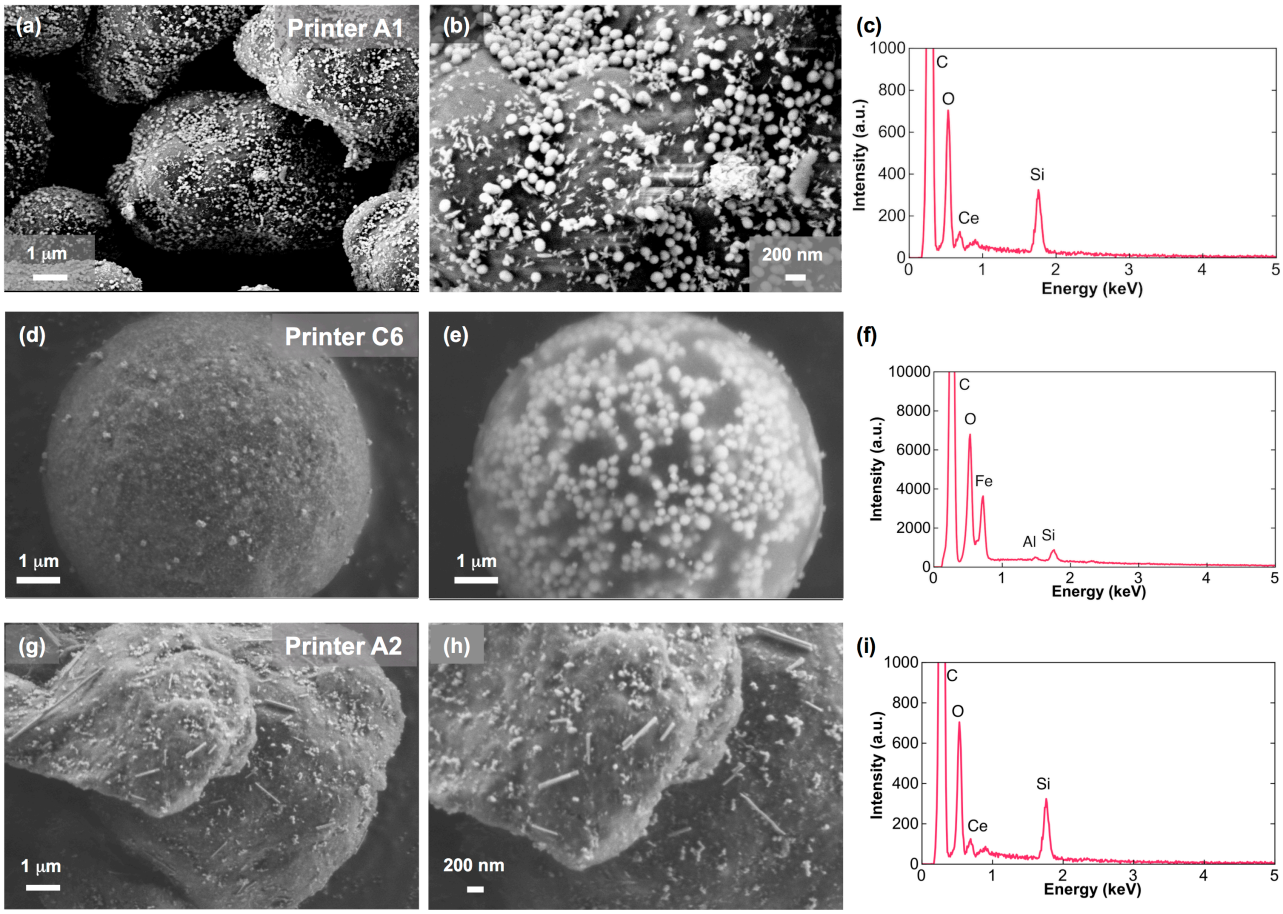

Figure 2-1. Representative scanning electron microscopy images of three toner powders from Printer A1 (a,b), Printer C6 (d,e), Printer A2 (g,h) and their respective EDX spectrum (c,f,i). Nanoparticles on the toner surface are commonly amorphous silica, illustrated by the EDX spectra.

Furthermore, the presence of nanoscale particles on the toner particle surface was clearly documented for all 11 toners examined as can be seen in the magnified SEM images in Figures 1b, e and h for three representative printers. It should be noted that nanoparticles are found not only on the surface of the toner particles, but also incorporated inside them. When the SEM

operational voltage is increased from 2 to 10 kV, the electron beam penetrates further inside the toner particle, revealing the presence of spherical, non-agglomerated inorganic nanoparticles (Figure 2-1e). However, detailed imaging of nano- particles encapsulated inside each toner particle is more challenging and requires more specialized techniques and was not performed as part of this study.

The elemental composition of toner particles was also qualitatively determined by EDX spectroscopy. Figures 2-1c,f,i show the EDX spectra for the corresponding toners that include signals from oxygen (O), silicon (Si), aluminum (Al) and magnesium (Mg), verifying their presence in the toner composition, most probably as metal/metal oxides. Often these surface nanoparticles are amorphous silica, as documented by closer investigation of their EDX spectra, which may be used as dispersants. The presence of other engineered nanometals and metal oxides, such as CeO_2, Al_2O_3, TiO_2 and Fe_2O_3, ZnO was also identified in the EDX analysis of some the other toners (data not shown). Of note, in one case, toner particles were covered on their surface with numerous respirable fibers (51 to 10mm long) made of TiO_2 (Figure 2-1g,h,i).

Hypothesis #2: Are nanoparticles released during consumer use (printing) from NEP? Sources and physico-chemical properties of PEPs

Figure 2-2a shows real-time representative particle number concentration profiles of the PEPs from three of the 11 tested printers (A1, B1 and C2) after 10min of continuous printing. Corresponding average mobility particle size distributions over the printing duration from the same printers (A1, B1 and C2) are shown in Figure 2-2b and are in agreement with the literature (Pirela et al., 2014). It is also worth pointing out that detailed investigation of the real-time PM emissions of the 11 printers reveals that the number concentrations differ for each printer and reach high values within 12 min after initiating the print job (Pirela et al., 2014).

Figure 2-2 also shows STEM images (c,d,e) and the corresponding EDX spectra (f,g,h) of PEPs that were collected using an electrostatic precipitator *in situ* (inside the chamber) during the printing process. The size of these PEPs, as obtained from electron microscopy images seems to correspond well to the real-time particle size distributions represented in Figure 2-2a, which confirms that emitted PM is predominantly in the nanoscale. The EDX analysis (Figures 2-2f,g,h) of the PEPs reveals the presence of inorganic elements, such as zinc (Zn), copper (Cu), titanium (Ti), cerium (Ce), silicon (Si), calcium (Ca) and sulfur (S), in their composition.

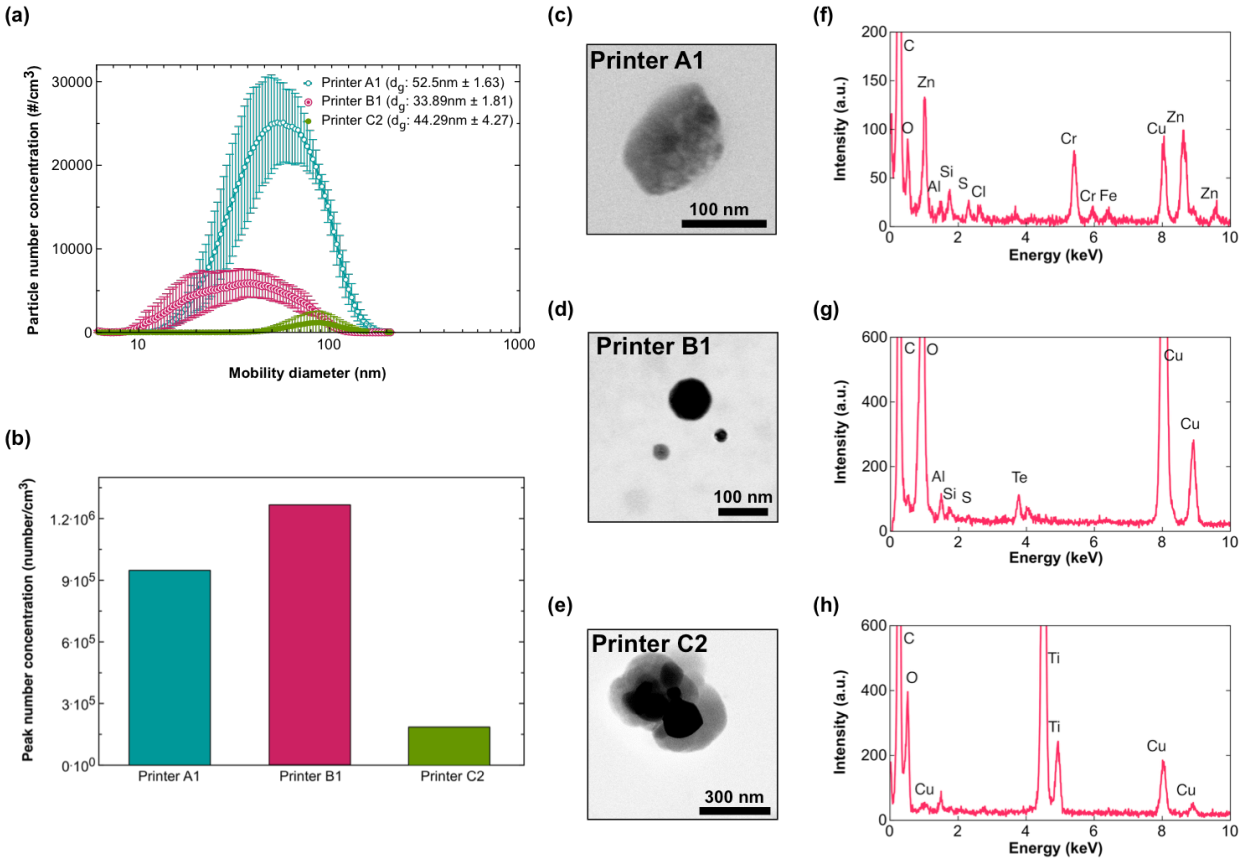

Figure 2-2. Characterization of PEPs from three printers of different manufacturers: Printer A1, B1 and C2. (a) Size distribution (mean ± SE) of airborne PM emitted during the first 10 min after printing started. (b) Peak particle number concentration achieved in the first 10 min after printing

started. (c,d,e) Transmission electron microscopy images of PEPs from three printers and their respective EDX spectrum (f,g,h). Cu signal for the most part comes from the TEM grid.

After confirming the presence and determining the physico-chemical and morphological properties of ENMs in both the toner formulations and emitted PEPs, we aimed to investigate the sources of these emitted particles.

The chemical composition of both toner and PEPs was assessed using state of the art analytical methods, such as ICP-MS for inorganic elements and EC/OC for carbonaceous compounds. ICP-MS analysis on both the toners and PEPs is illustrated in Figure 2-3b,c,d and Supplemental material Figures 2-S2 and 2-S3. In summary, the 11 evaluated toner powders possess complex chemistries and contained large amounts of organic carbon (42 to 89%), metals/metal oxides (1 to 33%), and some elemental carbon (0.33 to 12%). Elemental carbon is almost negligible for the majority of the printers from manufacturer C (*i.e.*, C2, C4, C5 and C6). The inorganic components of the toner powders were similar across the different brands, but the amount of each element varied significantly among the manufacturers. The main elements found in all 11 toner powders were Ca, Si, S, sodium (Na) and phosphorus (P). Interestingly, only the printers from a specific manufacturer (A1 and A2) had Zn in their powder (13.5 and 2.6%, respectively). Other metals found in the chemical analysis included, but were not limited to, nickel (Ni), chromium (Cr), Cu, Ce and Mg, among others (Table 2-S2).

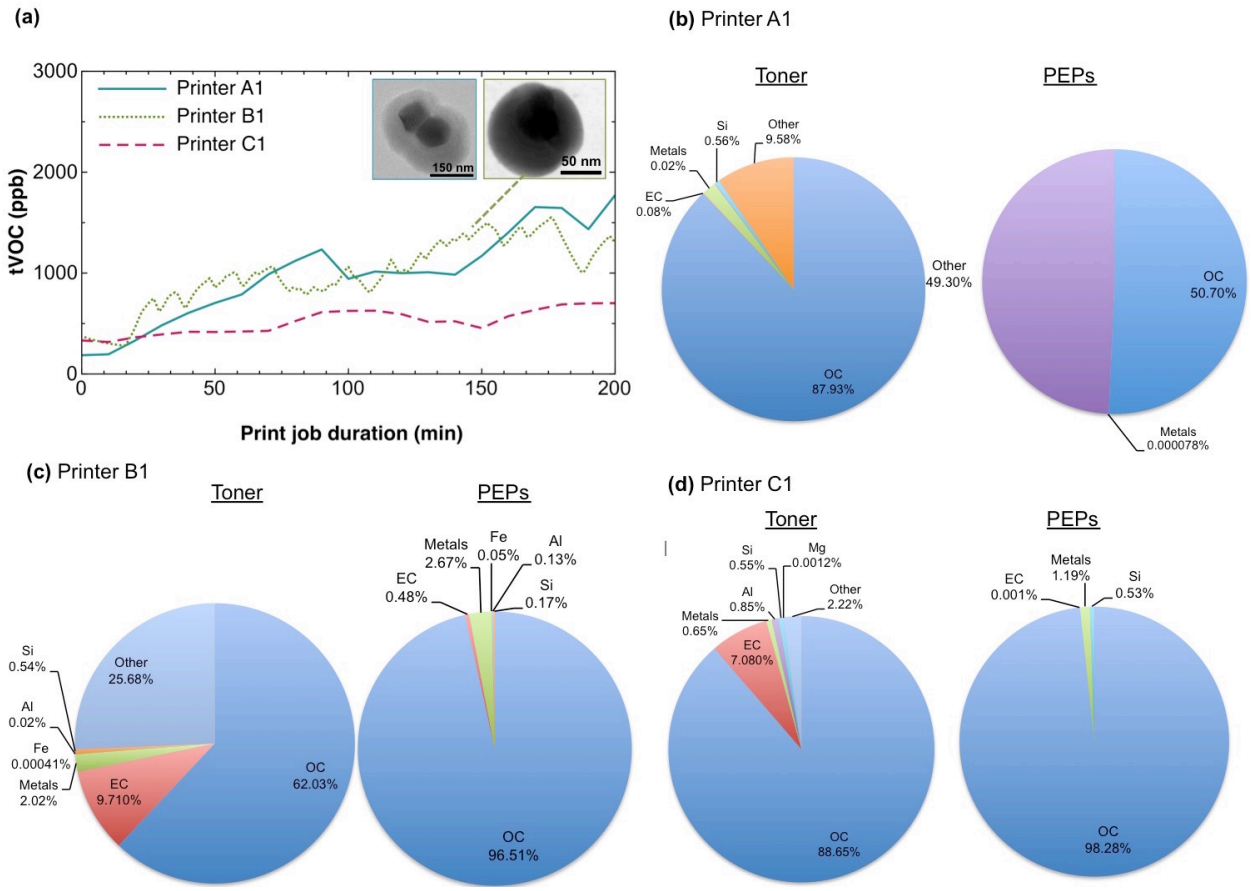

Figure 2-3. Chemistry of toners and PEPs resulting from ICP-MS, OC/EC, gravimetric, and cations and anions analysis. (a) Total VOC concentration throughout a continuous print job. Inset: electron microscopy images of PEPs from Printers A1 and B1 showing the organic layer covering the metal- rich core particle, common for airborne PEPs. (b-d) Chemical composition of toner powder and corresponding PEPs from three representative printers (Printer A1, B1 and C1) tested, based from magnetic sector inductively coupled plasma mass spectrometry (SF-ICP-MS) and analysis. Anions and cations can explain only 0.1–1.4% of the ‘‘other’’ pie slice in airborne PEPs and 0.7–7% in toners.

Table 2-S3 summarizes the elemental composition data of the water-soluble elemental examination PEPs from the high-emitting printers previously characterized by the authors (Pirela et al., 2014). The emitted PEPs were composed of a variety of elements that could be traced back to those found in the toner powder (*e.g.*, Si, Zn, Na, P, S). Additional chemical analysis of the PEPs indicated the presence of a variety of elements mostly identified on ICP-MS analysis, such as Cu, Ce, Cr, Ni, Fe, Ti and Cl.

Additionally, Figure 2-4a, b shows the ATR-FTIR spectra of all the 11 toner powders and the PEPs ($PM_{0.1}$, $PM_{0.1–2.5}$, $PM_{2.5}$) from the (high emitting) Printer B1. The toner and the collected emitted PM belonging to Printer B1 were evaluated to determine if the same chemical fingerprint is shared by the two samples (Figure 2-4a). The CH_x methyl groups around 3000 cm^{-1} and the carbon and oxygen double bond at ~1700 cm^{-1} are present in the toner, as well as the collected PEPs. Figure 2-4b shows the spectra for the 11 analyzed toners, which exhibit similar chemistry; this hints to a comparable toner composition (also confirmed by their reported chemistry, Table 2-S1) despite the brand. Important to note is the presence of carbonyl reach region in the airborne PEPs. Taken together with the EDX data on both toner and PEPs, this data set provides clear evidence that there is a release of particles from the toner to the air.

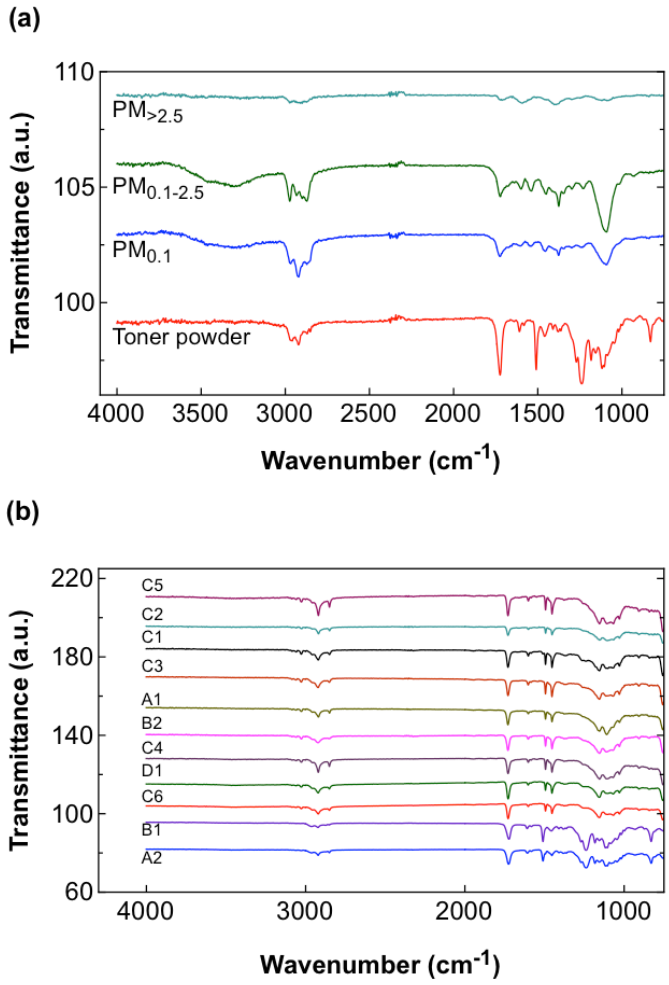

Figure 2-4. Fourier transform infrared spectroscopy results of toner powder and PEPs. (a) FTIR spectra from different size fractions of PEPs and toner powder from Printer B1 and (b) from 11 toner powders.

Another possible source of emitted particles investigated is the paper used during printing. The paper was analyzed to obtain its chemical composition and evaluate whether particles from the paper could also be found in the emitted PM (Supporting Information, Table 2-S4). As expected, calcium made up of more than 70% of the elemental content of the paper, and can be traced back to the paper pulp (*i.e.*, calcium carbonate). Additionally, certain brightening and whitening elements, such as aluminum oxides, titanium dioxide and silicon dioxide, were

also found in the paper. By comparing the ratio of the above-mentioned signature elements on the paper, toner and emitted PEPs, it can be postulated that paper, in addition to the toner powder, the paper itself may be another emission source of some of these airborne inorganic nanoparticles (Supporting Information, Tables 2-S2, 2-S3 and 2-S4).

Emission of VOC during printing

As shown in Figure 2-3a, the tVOC concentration increases with time during a continuous print job. Some of these VOC and sVOC can condense on the surface of solid inorganic particles surrounding them (confirmed by EDX analysis – data not shown), as shown in the inset of Figure 2-3a.

Discussion

ENMs in toner formulations

As illustrated in Figure 2-1, toner powder particles have a size of approximately 10mm and their morphology depends on the formulation technique that is utilized during their production (Xerox, 2013). For example, mechanical milling leads to toner particles with irregular shape (Figures 2-1a and b), while particles made by emulsion aggregation have a rather spherical shape (Figures 2-1d and e). In addition, it was clearly demonstrated here that a variety of nanoscale particles have been incorporated into toner formulations in order to improve the functional properties of the toner, such as charging and heat-resistance and enhance the sharpness of the image and text quality (Xerox, 2013). Both electron microscopy and EDX analysis provided confirmation that toners contain a variety of ENMs and constitute broadly a NEP. The ENMs found in toners included ceria, silica, titania, alumina, zinc oxide, iron oxide, magnesium oxide and carbon black. These findings are consistent with our recently published

work, which provided evidence of the incorporation of several types of ENMs (*e.g.*, silica, alumina, titania and iron oxide among others) in toners from photocopiers (Bello et al., 2013). This previous study gathered sufficient evidence to postulate that the copier toner manufacturing industry has shifted towards using nano-enabled toners and called for an industry-wide investigation on the chemical and possible toxicological outcomes of ENMs released from laser-based printing equipment in general. Our findings here establish that toner manufacturing, in general, has shifted mainstream to nanotechnology.

Laser printers release ENMs into the air

It has been well established in the literature that laser printers emit airborne nanoparticles during printing (Morawska et al., 2009; Pirela et al., 2014; Schripp et al., 2008). Here, it is demonstrated that PM peak emissions were brand-independent and varied between 3,000 to 1.3 million particles/cm^3 with modal diameters ranging from 49 to 208 nm, with the majority of the PEPs in the nanoscale (< 100 nm). Of note, size of the PEPs observed in the STEM analysis is in agreement with the real time aerosol data shown in Figure 2-2, and presented in greater detail in our recently published companion paper (Pirela et al., 2014).

It is worth noting that the highest emitting laser printers A1 and B1 (Figure 2-2), emitted over one million particles/cm^3, a substantially high particle number concentration compared to the approximate value of 2,000 particles/cm^3 typically found in an urban indoor environment (Quang et al., 2012). In fact, such high particle exposure levels are similar to those of highly polluted highways (Padro-Martinez et al., 2012), for which a range of human health effects, from increased morbidity to stroke attacks to low birth weight and changes in global gene expression patterns of human bronchial epithelial cells (Ding et al., 2014, Vinikoor- Imler et al., 2014, Yu et al., 2014), has been documented. It is not only the potentially high exposure levels encountered

during printing but also the chemistry of such emissions that require more thorough toxicological and epidemiological investigations. As Khatri et al. (2013) showed, a few hours of exposure to 20,000 to 30,000 copier-emitted particles/cm^3 is sufficient to induce clear inflammatory responses in healthy human volunteers.

The composition of inorganic constituents in airborne PEPs and especially the presence of ENMs in them, are an emerging area of research. Here, we establish that such a NEP (toner) releases particles including nanoscale particles used in its synthesis. An important contribution of this study is, therefore, not only the incorporation of nanoscale materials in the toner formulation and their release to the air during consumer use, but also the detailed physico-chemical and morphological characterization of both toner and released particles. More importantly, it was demonstrated that realistic exposure properties should be used in the toxicological characterization studies rather than the current use of toner particles.

Sources of airborne PM emitted by laser printers: toner powder and paper

It is evident based on the EDX spectra of Printers A1, B1 and C2 that emitted ENMs during consumer use (printing) (Figure 2-2f,g,h) are of metal origin. Specifically, the presence of these exact elements was also identified by ICP-MS in the respective toner powder used by the printers (Tables 2-S1 and 2-S2). The nearly identical chemical fingerprinting of the toner and PEPs serves as evidence that the ENMs currently being incorporated into the toner powder are indeed making their way into the emitted PM during printing. These findings are in agreement with a published analysis performed by the authors on photocopier-emitted particles, which found Cr, Fe and Ni in the chemical composition of the copier toner and the copier-emitted PM (Bello et al., 2013). Even though elemental carbon occupies a rather large fraction of up to 12% in the toner formulations presumably as pigment, it is present only in minor quantities of less

than 0.5% by mass in the PEPs. Of note, the total inorganic fraction in the airborne PEPs was printer dependent and varied from ~50% for Printer A to less than 2% for Printer C1. This remarkable variation in the chemistry of airborne PEPs supports our earlier recommendation for an industry-wide assessment of the chemistry of such exposures. New in the chemical characterization is analysis of anions and cations (Table 2-S4). Of the species analyzed, the more abundant ions were chlorides, sulfates and sodium, which originated primarily from the paper. These species account for only a small fraction of the total PEPs mass, from 0.2 to 1.4% (and 0.4 to 7% in toners and 5 to 10% in the paper). Therefore, only a negligible mass of the ‘‘other’’ component in the pie charts could be accounted for these ions.

A significant portion of the PEPs from all evaluated printers is organic in nature. Yet their chemistry is not well characterized. Using ATR-FTIR to analyze the toners and PEPs, similar fingerprint features were identified (Figure 2-4a). In particular, the toner powder exhibits the distinctive spectrum for a polyester resin mixture (Merrill et al., 2003), as also stated in the corresponding MSDS. Additionally, there were CHx methyl groups (3,000 cm^{-1}) and carbon and oxygen double bonds (1,700 cm^{-1}) in both the toner and the collected PM. At lower frequencies, however, there are some differences in the spectra. Significantly, the peak that is present in the toner powder corresponding to the aromatic ring (1,600 cm^{-1}) is absent in the PEPs. This is in agreement with a previous study characterizing resin and epoxy resin composites, the main components of toner powder (Liao et al., 2012). The current data indicate that the organic composition of the PEPs is similar to the original toner powder to a certain extent, possibly explained by the chemical transformation the toner undergoes, due to the high temperatures (~225ºC) and pressures required to melt and fuse the toner to the paper during printing.

Furthermore, additional research is needed to better characterize this substantial organic fraction of airborne PEPs.

Another important finding in this study is the fact that the data obtained *via* ICP-MS (Table 2-S2) and the general information reported in the Material Safety Data Sheets (MSDS, Table 2-S1) for the toner powders are generally in good agreement with results from various chemical analyses (OC-EC, ICP-MS, EDX and FTIR spectra), especially as it relates to its main ingredients: the polymer content (assessed *via* OC analysis), elemental carbon (EC analysis), individual elements (*via* ICP-MS) and ENM (*via* morphological TEM/EDX analysis and limited XRD analysis not presented herein). For example, Manufacturer A toner cartridges were composed of polyester resin, iron oxide, carbon black, polymer wax, titanium dioxide and blue pigment. Manufacturer B toners composition contained styrene acrylate copolymer, carbon black, fatty acid ester, silica, PMMA and polyester resin. Manufacturer C toner cartridges included styrene acrylate copolymer, iron oxide, wax, carbon black, amorphous silica, titanium dioxide and zinc. Lastly, manufacturer D toner cartridges list styrene acrylate copolymer, iron oxide and wax as their main components. However, it is also worth mentioning that the MSDS sheets do not provide any information about the size of its ingredients, which highlights the importance of a nano-labeling system for NEPs (Kessler, 2011), or presence of large amounts of metals of up to 34% by mass (*e.g.*, toners of Printers C2, C4-6, D1), of which appreciable amounts of transition metals of toxicological relevance, such as Mn, Cr, Co and Ni (Table 2-S2), or the presence of respirable TiO_2 fibers on one toner.

Consumer exposure to PEPs: possible health implications?

The presence of metal/metal oxide nanoparticles in the PEPs and the complex chemistry of PM, even at minute concentrations, is concerning because metals/metal oxides have the

potential to trigger a toxic response in the lungs and translocate to other organs (Bondarenko et al., 2013; Cohen et al., 2014; Demokritou et al., 2013; Kumar & Nagesha, 2013; Moschini et al., 2013; Zhou et al., 2014). Specifically, metal oxides, such as silica, ceria, iron oxide and zinc oxide have been shown to produce DNA damage to cells exposed at doses as low as 5 μg/ml for 4 hours (Watson et al., 2014). Moreover, an integrative study by Sotiriou et al. (2012) and Demokritou et al. (2013) using the Harvard VENGES showed significant toxicity (*e.g.*, lung injury and inflammation, decreased cell viability) by exposure to nanoscale iron oxide and ceria using both an *in vitro* and *in vivo* experimental design. Other recently published studies assessing the toxicological potential of ceria, titania, zinc oxide, copper oxide and iron oxide have confirmed increased inflammation, reactive oxygen species generation, neutrophilia and neurotoxicity in exposed rodents and human cell lines (Kumar & Nagesha, 2013; Landsiedel et al., 2014; Shrivastava et al., 2013). It is also worth noting that particle size and dose-dependent pulmonary effects were found in mice instilled with two size fractions of copier-emitted PM ($PM_{0.1}$ and $PM_{0.1–2.5}$) (Pirela et al., 2013). These copier emissions have a similar chemical fingerprint as those from PEPs; thus, it may be possible that this complex chemical makeup may render the PEPs deleterious to the lung to those who are exposed to them.

The release of volatile organic compounds (VOCs) is also a concern when assessing consumer exposure to laser printer emissions. The presence of such gaseous compounds can influence the biological response to inhaled aerosols (Ebersviller et al., 2012; Wang et al., 2013; Wang et al., 2014). In particular, exposure to VOCs is associated with adverse changes in the pulmonary and cardiovascular system, including inflammation and heart rate variability, as well as changes in gene expression (Song et al., 2013; Weichenthal et al., 2012). Although we did not speciate tVOCs in this study, these substances have been extensively studied and summarized in

past studies (Destaillats et al., 2008). The presence of carbonyl compounds (*i.e.*, formaldehyde, acetaldehyde, and benzaldehyde) and aromatic hydrocarbons (*e.g.*, styrene and xylenes) are of particular interest. Unfortunately, the absorption of VOCs onto the surface of inorganic nanoparticles and the interactions of the organic and the metal components of PEPs remains poorly understood in the context of this particular exposure scenario.

All of the above results point out that the recent toner formulations contain ENMs and should be categorized as NEPs. More importantly, ENMs become airborne during printer use and exposure levels can reach extremely high levels up to of 1.3 million particles/cm^3. The chemistry of both toner particles and PEPs is highly complex and includes organic and elemental components, such as Mg, Al, P, S, Si, Ca, Ti, Ni, Cu and Zn, among others. The PEPs have similar chemical composition to the toner particles and their overall nanoscale size may present health risks to consumers. These results highlight the need to perform appropriate exposure and toxicological assessments using the ‘‘real-world’’ emitted PM, rather than the toner particles, which were used in past efforts to assess health risks related to printing processes (Konczol et al., 2013; Morimoto et al., 2013). In the coming companion papers, we will present evidence of the toxicological potential of PEPs from the high-emitting Printer B1 using both mono- and co-culture *in vitro* as well as *in vivo* study designs (Sisler et al., 2014). Results from such toxicological investigation will help assess the potential consumer risks from the use such NEPs.

Conclusion

In summary, the thorough evaluation of the toner powder and PM emitted from printing equipment provided ample evidence that a variety of ENMs (at least eight different types) are embedded in current toner formulations and are released in the air during printing. The complex chemical fingerprint of the PEPs matches to a significant extent that of toner powders and paper,

which identifies them as source of ENMs in PM emissions. This study will help identify potential hazards from the consumer interaction with NEPs and assist in developing future guidelines for such investigations. Furthermore, it is worth noting that a number of companion manuscripts are currently under preparation on the assessment of biological properties of PEPs and possible adverse health effects using both *in vitro* and *in vivo* approaches.

Declaration of interest

The authors report no competing financial interests. The findings and conclusions in this manuscript have not been formally disseminated by the NIOSH or CPSC and should not be construed to represent any agency determination or policy. The authors acknowledge funding for this study from NIEHS Center Grant ES-000002, NIOSH and CPSC (Grant # 212-2012-M-51174). This work was performed in part at the Harvard Center for Nanoscale Systems (CNS), a member of the National Nanotechnology Infrastructure Network (NNIN), which is supported by the National Science Foundation under NSF award number ECS-0335765. G. Sotiriou gratefully acknowledges the Swiss National Science Foundation for the Advanced Researcher fellowship (Grant # 145392).

Supplemental Material

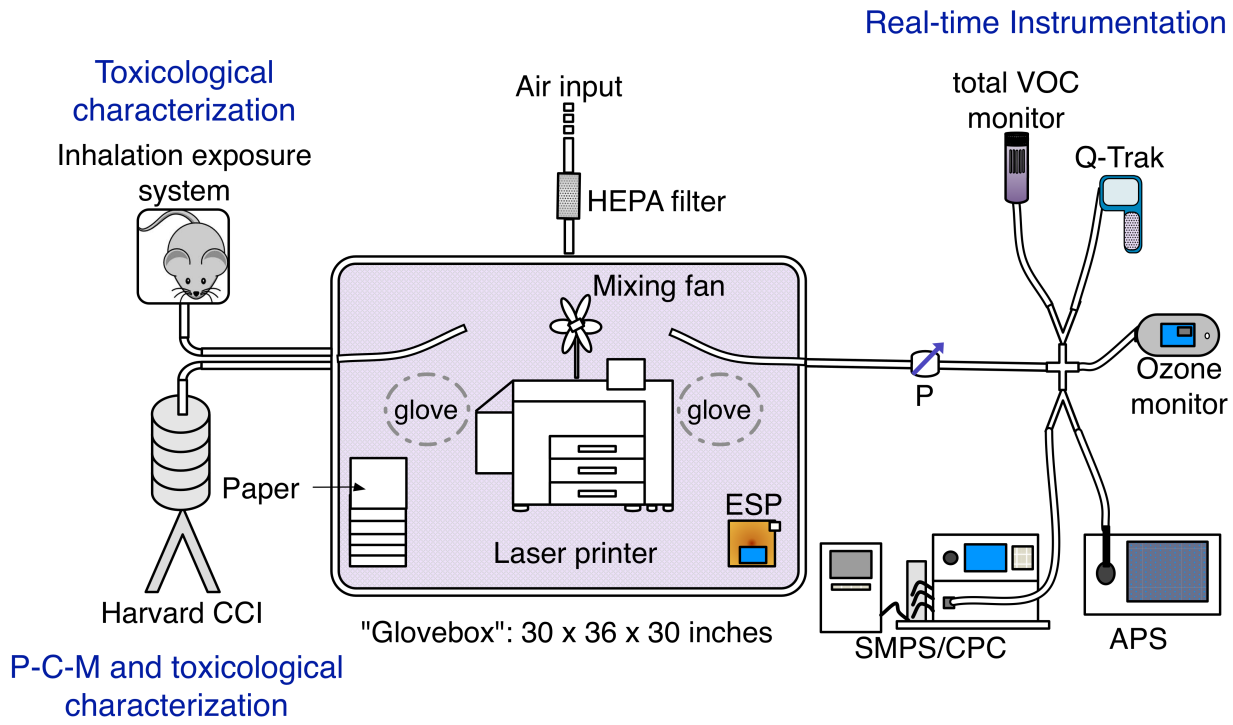

Figure 2-S1. Printer exposure generation system (PEGS). This image has been adopted from Pirela et al. (2014). Flow rates for the instruments are as follows: Harvard compact cascade impactor: 30 l/min, electrostatic precipitator: 0.5 l/min, SMPS/CPC: 1 l/min, APS: 5 l/min, ozone monitor: 2.3 l/min.

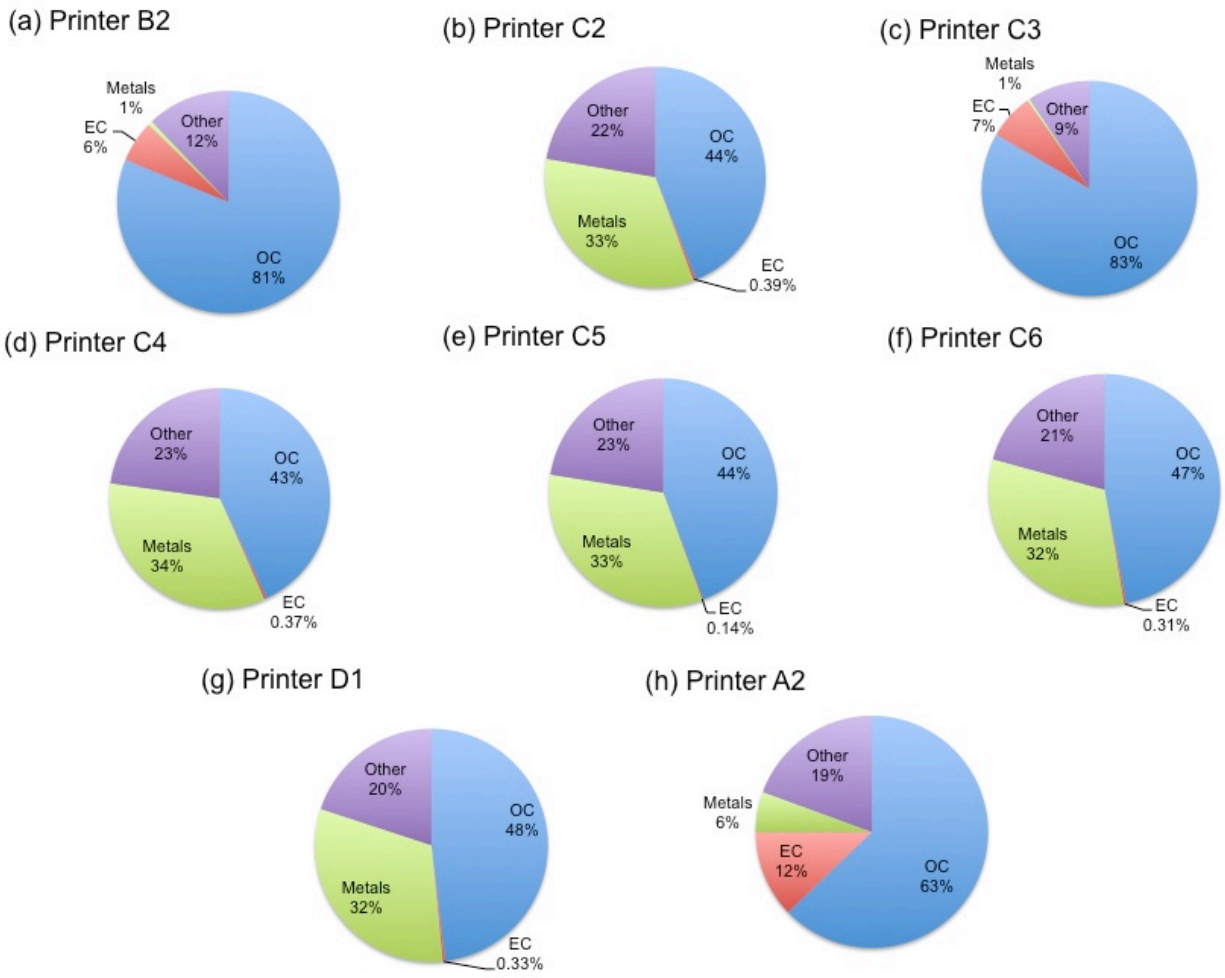

Figure 2-S2. Chemical composition of toner powder from the remaining tested printers based on a combination of techniques: magnetic sector inductively coupled plasma mass spectrometry (SF-ICP-MS) analysis for total and water-soluble elements, organic- elemental carbon, and anion and cation analysis. The sum of anions and cations can explain only 0.7-7% of the other pie section in toners.

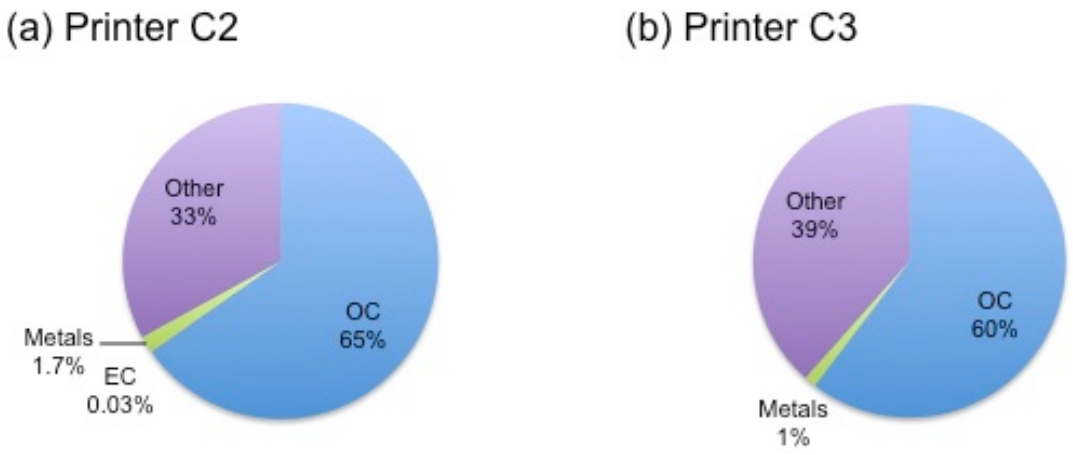

Figure 2-S3. Chemical composition of the $PM_{2.5}$ size fraction of PEPs from remaining two laser printers based on a combination of analytical techniques: magnetic sector inductively coupled plasma mass spectrometry (SF-ICP-MS) for total and water soluble elements, organic-elemental carbon, and anions and cations. The sum of anions and cations can explain only 0.2-1.4% of the other pie section in the airborne PEPs.

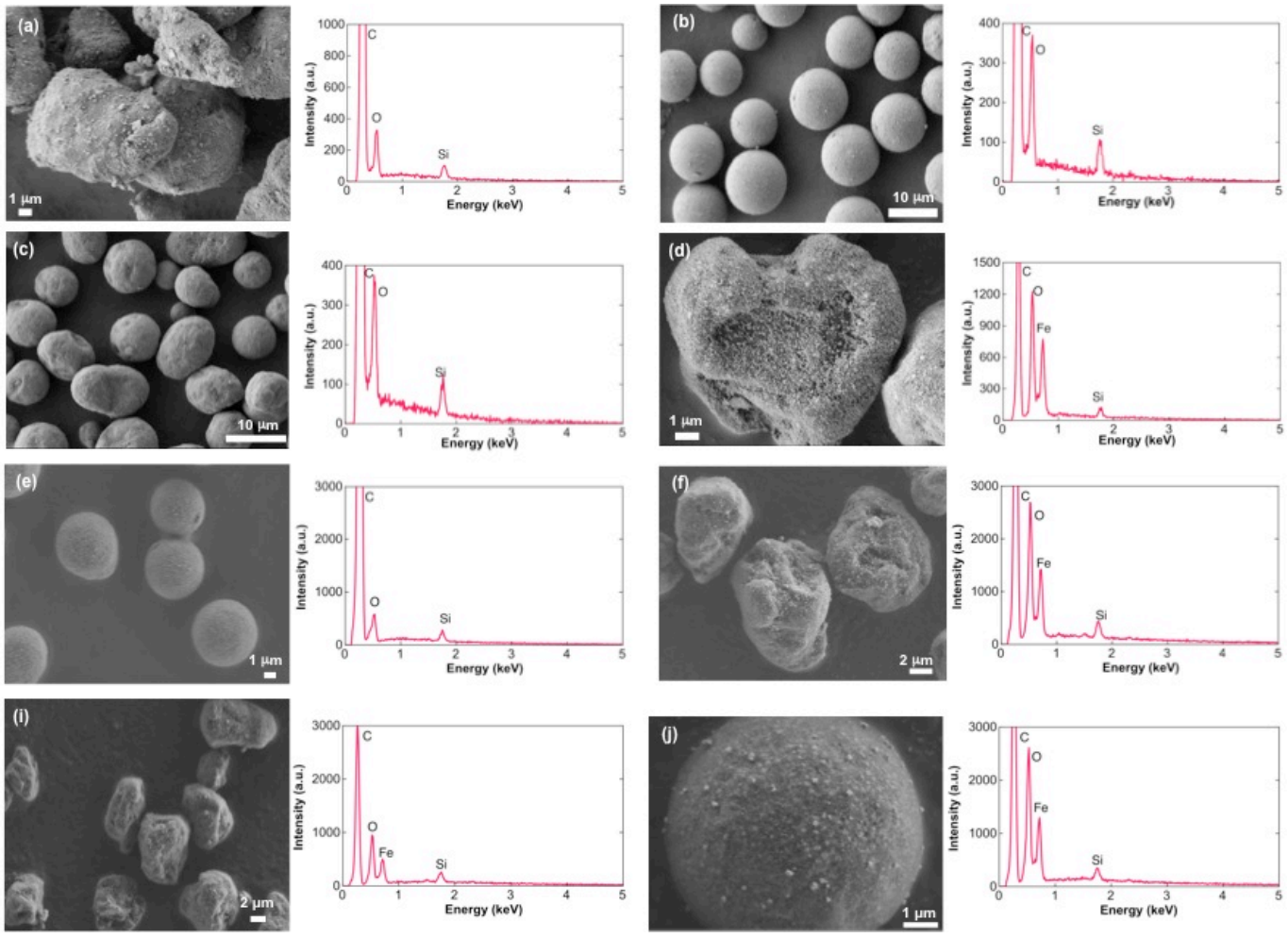

Figure 2-S4. Representative morphological images and respective EDX spectrum of the remaining 8 toner powders evaluated in this study.

Table 2-S1. Printer specifications and the respective toner powder composition**.** [a]Information obtained from material safety data sheet (MSDS) of each toner manufacturer.

Printer	Speed (pages/min)	Year of manufacture	Toner composition information (% weight) [a]
A1	31	2011	Styrene/acrylate copolymer (70-80%), polyolefin wax (<10%), carbon black (<10%), amorphous silica (<10%), blue pigment (<10%), titanium dioxide (<1%).
A2	38	2013	Polyester resin (65-85%), iron oxide (7-13%), carbon black (5-10%), polymer wax (1-5%), amorphous silica modified (1-5%), titanium dioxide (0.1-1%).
B1	24	2012	Polymer (5-10%), carbon black (2-5%), resin, polyester resin (1-2.5%).
B2	21	2004	Styrene acrylate copolymer (<84%), carbon black (5-7%), fatty acid ester (4-6%), silicon dioxide (1-3%), PMMA (<1%).
C1	12	2007	Styrene acrylate copolymer (<85%), wax (<15%), carbon black (<6%), amorphous silica (<2%).
C2	35	2009	Styrene acrylate copolymer (<55%), ferrite including zinc (<50%), amorphous silica (<2%).
C3	30	2009	Styrene acrylate copolymer (<85%), carbon black (<10%), wax (<10%), amorphous silica (<3%), titanium dioxide (<1%).
C4	33	2012	Styrene acrylate copolymer (<55%), ferrite including zinc (<50%), amorphous silica (<3%).
C5	27	2007	Styrene acrylate copolymer (<55%), ferrite including zinc (<50%), amorphous silica (<3%).
C6	25	2011	Styrene acrylate copolymer (<55%), ferrite (45%), wax (<10%).
D1	26	2012	Styrene acrylate copolymer (45-55%), ferrite (35-45%), wax (5-10%).

Table 2-S2. Magnetic sector inductively coupled plasma mass spectrometry (SF-ICP-MS) analysis of toner powders used in the study. The most abundant elements are presented on this table. T, T; WS, water soluble.

Printer		Mg	Al	P	S	Si	Ca	Ti	Cr	Mn	Fe	Co	Ni	Cu	Zn	Sr	Mo	Sn	Sb
A1	T (SD) (ng/g)	24 (1.3)	4.9E5 (4310)	1329 (247)	3.16 (8.2E4)	5.6E6 (1.2E5)	2.8E4 (4488)	4.2E6 (2.6E4)	613 (25)	1.4E5 (1.7E4)	3.9E5 (3.8E4)	1001 (34)	458 (116)	1.2E6 (1.2E4)	2E5 (3.6E3)	3833 (771)	551 (9)	1060 (282)	46 (10)
	WS (SD) (ng/g)	81.6 (53)	23.5 (14)	869 (198)	961 (1311)	1933 (184)	1814 (2117)	0.978 (2.35)	0.96 (1.1)	2.0 (0.72)	63 (7)	0.12 (0.30)	5.0 (1.0)	2.1 (7.6)	978 (38)	31 (3)	0.66 (0.09)	8.3 (0.63)	0.06 (0.07)
	WS (%)	0.33	0.00	65.37	3.10	0.03	6.40	0.00	0.16	0.00	0.02	0.01	1.09	0.00	4.94	0.81	0.12	0.78	0.13
B1	T (SD) (ng/g)	1.2E4 (3.1E3)	8.5E6 (5.9E5)	1.2E4 (1304)	1.2E6 (7.1E4)	5.5E6 (1.3E6)	1.8E7 (2E5)	1.4E4 (8.2E3)	1457 (138)	1.1E4 (6.1E3)	2.1E6 (1.1E6)	522 (156)	2872 (46)	3823 (862)	1.3E4 (7131)	2.5E4 (8514)	51.3 (13.9)	8.7E5 (3.6E4)	236 (18.6)
	WS (SD) (ng/g)	202 (45)	107 (17)	1100 (297)	3438 (1651)	4381 (248)	4.4E4 (3.3E3)	2.77 (3.24)	0.4 (1.4)	7.0 (2.4)	49 (9.4)	0.76 (0.48)	12 (3.1)	3.31 (9.7)	68 (16)	253 (5)	4.19 (0.05)	7.56 (0.77)	2.18 (0.10)
	WS (%)	1.64	0.00	9.31	0.26	0.08	0.27	0.02	0.03	0.06	0.00	0.14	0.42	0.87	0.50	1.02	8.17	0.00	0.92
B2	T (SD) (ng/g)	2.1E4 (3.4E3)	339 (3165)	1015 (582)	2.1E6 (1.2E5)	3.1E6 (1.1E6)	1.9E5 (2.9E4)	5.3E5 (4.4E4)	2654 (195)	443 (176)	1.6E5 (1.4E4)	9.37 (16.6)	31 (39)	595 (808)	1399 (1762)	913 (287)	7.1 (10.7)	5.5E5 (2.6E4)	9.2E4 (5176)
	WS (SD) (ng/g)	109 (53)	9.18 (15)	359 (168)	1466 (1483)	6022 (238)	6752 (2370)	2.44 (4.83)	0.21 (1.38)	0.13 (0.58)	6.64 (6.76)	0.21 (0.26)	18.9 (4.9)	2.06 (8.6)	30.27 (11.7)	29.41 (4.0)	0.29 (0.02)	12.26 (4.63)	14.07 (0.69)
	WS (%)	0.51	2.71	35.33	0.07	0.20	3.64	0.00	0.01	0.03	0.00	2.24	60.65	0.35	2.16	3.22	4.12	0.00	0.02
C1	T (SD) (ng/g)	9.5E4 (1E3)	2.2E5 (1.3E3)	1.6E4 (77)	7.7E4 (1.4E3)	5.4E6 (5.4E4)	7E4 (2E3)	5.2E5 (4E3)	972 (9.8)	29.8 (15)	4089 (1040)	0.76 (0.8)	203 (152)	132 (510)	1.8E4 (655)	39.6 (42)	53.5 (10.6)	3.2E4 (352)	14.57 (11.6)
	WS (SD) (ng/g)	430 (53.6)	102 (15.5)	674 (219)	3037 (1475)	2596 (207)	3753 (2358)	7.01 (6.01)	6.64 (1.2)	2.76 (1.2)	98 (7.35)	0.39 (0.14)	7.24 (1.4)	13.7 (8.7)	552 (37.4)	2.7 (3)	2.05 (0.73)	27.7 (1.02)	0.63 (0.14)
	WS (%)	0.45	0.05	4.31	3.94	0.05	5.34	0.00	0.68	9.27	2.39	51.61	3.57	10.37	3.08	6.85	3.83	0.09	4.34
C2	T (SD) (ng/g)	6.3E5 (3.6E3)	1.1E6 (3969)	4882 (139)	1.9E6 (2.1E4)	2.1E6 (2.6E6)	1.6E6 (1.7E4)	2.9E6 (5.4E4)	5400 (213)	1.8E6 (1.3E4)	3.1E8 (4.1E6)	4.5E4 (347)	1.7E4 (96)	6628 (112)	2.5E6 (2E5)	2.6E6 (1.8E4)	222 (6.5)	914 (183)	114 (78.5)
	WS (SD) (ng/g)	208 (108)	11.4 (19.6)	676 (223)	5493 (1884)	6835 (266)	2042 (3027)	3.19 (3.73)	3.27 (1.72)	39.3 (3.09)	18.78 (8.66)	0.459 (0.36)	21.1 (3.8)	11.07 (11)	27.9 (8.8)	2706 (52)	0.376 (0.04)	-0.11 (0.84)	0.049 (0.09)
	WS (%)	0.03	0.00	13.85	0.29	0.32	0.13	0.00	0.06	0.00	0.00	0.00	0.12	0.17	0.00	0.10	0.17	0.00	0.04

Table 2-S2 (Continued).

Printer		Mg	Al	P	S	Si	Ca	Ti	Cr	Mn	Fe	Co	Ni	Cu	Zn	Sr	Mo	Sn	Sb
C3	T (SD) (ng/g)	4767 (2498)	8.2E4 (6609)	3951 (655)	9.3E4 (1.3E4)	2E6 (1.2E6)	5.1E4 (1.8E4)	1.4E6 (1.1E5)	543 (103)	72 (166)	10542 (4726)	4.59 (17.6)	726 (409)	1764 (842)	1.0E5 (5.6E3)	179 (290)	14.13 (11.1)	1009 (204)	630 (41.5)
	WS (SD) (ng/g)	65.9 (42)	86.8 (18)	733 (198)	2747 (1493)	9581 (382)	1246 (2407)	20.4 (9.14)	0.51 (1.44)	0.51 (0.68)	5.51 (6.86)	0.087 (0.15)	7.87 (4.3)	7.71 (9.0)	912 (61)	2.28 (3)	1.33 (0.18)	1.02 (0.68)	0.724 (0.09)
	WS (%)	1.38	0.11	18.56	2.97	0.47	2.43	0.00	0.09	0.70	0.05	1.56	1.08	0.44	0.89	1.27	9.41	0.10	0.11
C4	T (SD) (ng/g)	6.6E5 (5.7E4)	1.1E6 (7.9E4)	8064 (1601)	1.9E6 (1E5)	3.9E6 (1.3E6)	1.7E6 (1.9E5)	3.2E6 (2.5E5)	6799 (407)	1.9E6 (9.9E4)	3.2E8 (1.8E7)	4.3E4 (2.7E3)	1.9E4 (991)	1.9E5 (1.7E3)	2.4E6 (1.2E5)	2.8E6 (1.8E5)	417 (59)	1049 (75)	70.0 (12)
	WS (SD) (ng/g)	19.4 (30.1)	147 (18.6)	97.9 (199)	1963 (1668)	4506 (307)	1243 (2741)	4.4 (5.81)	1.33 (1.43)	29.1 (2.81)	44.5 (8.21)	0.445 (0.27)	8.91 (5.3)	8.91 (9.8)	30.7 (14.5)	1821 (78)	1.06 (0.10)	12.7 (0.76)	0.099 (0.08)
	WS (%)	0.00	0.01	1.21	0.10	0.12	0.07	0.00	0.02	0.00	0.00	0.00	0.05	0.05	0.00	0.06	0.25	1.21	0.14
C5	T (SD) (ng/g)	5.4E5 (4.7E4)	1.1E6 (7.9E4)	5889 (1194)	1.9E6 (1.1E5)	8.9E5 (1.6E6)	1.8E6 (2.0E5)	3.2E6 (2.5E5)	1.3E4 (877)	2.6E6 (1.6E5)	3.1E8 (1.8E7)	4.2E4 (2.7E3)	2.9E4 (1.6E3)	3644 (1208)	2.7E6 (1.4E5)	2.8E6 (2E5)	510 (70)	3552 (717)	657 (68)
	WS (SD) (ng/g)	234 (53)	72.6 (15.8)	1276 (199)	3145 (1603)	1762 (211)	1.1E4 (2.6E3)	6.30 (7.82)	1.20 (1.4)	13.54 (1.75)	11.81 (7.35)	0.17 (0.18)	30.9 (7.1)	8.87 (9.4)	74.7 (19.2)	616 (12)	0.54 (0.21)	3.67 (0.73)	5.04 (0.22)
	WS (%)	0.04	0.01	21.7	0.17	0.20	0.60	0.00	0.01	0.00	0.00	0.00	0.11	0.24	0.00	0.02	0.11	0.10	0.77
C6	T (SD) (ng/g)	2.7E4 (3.7E3)	4.9E4 (4.9E3)	5.6E5 (5E4)	1.9E6 (1E5)	4.7E6 (1.3E6)	1.1E6 (1.2E5)	9.6E5 (7.6E4)	1.4E4 (870)	1.4E6 (7.5E4)	3.1E8 (1.8E7)	2.9E4 (1.9E3)	2.9E4 (1.6E3)	4575 (941)	7.5E4 (4.4E3)	1.6E6 (1E5)	102 (18.9)	402 (69)	15.5 (10.1)
	WS (SD) (ng/g)	131 (49)	29.8 (19)	104 (265)	4275 (1825)	1941 (233)	4069 (2913)	16.1 (10.13)	0.91 (1.56)	2.28 (1.61)	60 (8.5)	0.11 (0.18)	8.89 (1.8)	9.9 (11.2)	232 (46)	615 (10)	0.44 (0.09)	4.8 (1.0)	0.11 (0.09)
	WS (%)	0.48	0.06	0.02	0.23	0.04	0.39	0.00	0.01	0.00	0.00	0.00	0.03	0.22	0.31	0.04	0.43	1.19	0.68
D1	T (SD) (ng/g)	2.6E4 (3.8E3)	6.7E4 (7.4E3)	5.6E5 (4.9E4)	1.8E6 (9.8E4)	6.3E6 (1.6E6)	8.5E5 (1E5)	7.5E5 (5.9E4)	6932 (420)	1.3E6 (7.2E4)	3.0E8 (1.7E7)	2.6E4 (1.7E3)	2.7E4 (1.3E3)	1774 (1027)	8.9E4 (5.2E3)	1.2E6 (7.9E4)	80.8 (17.7)	350 (62)	0.78 (11.8)
	WS (SD) (ng/g)	128 (32.8)	32.7 (13.5)	440 (158)	2080 (1381)	2887 (198)	1804 (2206)	3.29 (4.3)	4.68 (1.26)	5.64 (1.34)	78.6 (6.49)	0.322 (0.23)	0.042 (0.04)	0.03 (0.01)	0.08 (0.02)	0.42 (0.02)	0.001 (0.00)	0.005 (0.001)	0.001 (0.00)
	WS (%)	0.50	0.05	0.08	0.11	0.05	0.21	0.00	0.07	0.00	0.00	0.00	0.15	1.51	0.09	0.03	0.76	1.55	58.9
A2	T (SD) (ng/g)	4.1E4 (4.7E3)	4.8E4 (4.8E3)	1.1E4 (2E3)	4.8E5 (2.9E4)	5.9E6 (1.4E6)	1.8E5 (2.7E4)	3.1E6 (2.5E5)	4360 (276)	5.1E5 (2.8E4)	4.2E7 (2.5E6)	5325 (335)	1.8E4 (1E3)	1502 (908)	1.6E6 (8.1E4)	7209 (1118)	253 (38)	1.9E6 (8.9E4)	1.9E5 (1E4)
	WS (SD) (ng/g)	99.2 (73)	0.34 (17)	809 (218)	4841 (1755)	1568 (225)	2674 (2796)	1.36 (3.24)	0.84 (1.5)	4.1 (1.4)	7.17 (7.97)	0.67 (0.48)	37.6 (5.1)	26.6 (11.6)	332 (15)	48.7 (6)	25.2 (0.47)	19.9 (6.85)	101 (1.8)
	WS (%)	0.24	0.00	7.18	1.01	0.03	1.51	0.00	0.02	0.00	0.00	0.01	0.21	1.77	0.02	0.68	9.98	0.00	0.05

Table 2-S3. Magnetic sector inductively coupled plasma mass spectrometry (SF-ICP-MS) analysis of PEPs of five high emitting printers used in the study. The most abundant elements are presented on this table.

Printer		Mg	Al	P	S	Si	Ca	Ti	Cr	Mn	Fe	Co	Ni	Cu	Zn	Sr	Mo	Pb	Sb
A1	T (SD) (ng/g)	5.30 (1.74)	3.71 (1.02)	12.6 (12.2)	18.4 (101)	4.49 (12.9)	526 (167)	0 (0.1)	0.23 (0.1)	0.51 (0.09)	3.01 (0.52)	0.023 (0.02)	2.61 (0.22)	2.24 (0.63)	19.2 (3.15)	1.91 (0.40)	0.058 (0.01)	0.246 (0.06)	0.033 (0.01)
	WS (SD) (ng/g)	64.9 (64.4)	91.05 (95.4)	43.1 (13.8)	820 (77.7)	4660 (14087)	2026 (230)	7.33 (6.1)	11.9 (2.16)	1.28 (1.52)	44.3 (43.2)	0.209 (0.26)	13.2 (8.62)	13.05 (9.04)	80.8 (5.92)	10.9 (1.90)	0.869 (0.24)	20.4 (2.72)	0.037 (0.29)
	WS (%)	8.16	4.08	29.10	2.24	0.10	26.00	0.00	1.90	39.70	6.81	11.20	19.80	17.10	23.70	17.50	6.71	1.21	90.50
B1	T (SD) (ng/g)	4.57 (0.97)	2.06 (0.26)	75.5 (5.50)	173 (26.1)	13.4 (3.67)	483 (50)	0.02 (0.6)	0.087 (0.02)	0.16 (0.02)	0.15 (0.12)	0.006 (0.00)	0.34 (0.07)	1.57 (0.16)	33.5 (1.54)	2.19 (0.11)	0.254 (0.01)	1.131 (0.01)	0.069 (0.00)
	WS (SD) (ng/g)	79.7 (17.2)	549 (45.7)	724 (67.6)	2999 (167)	2242 (3595)	6527 (733)	21.4 (2.5)	9.12 (0.69)	4.06 (0.49)	222 (16.6)	0.037 (0.05)	7.60 (1.83)	104 (8.34)	605 (32.2)	29.8 (2.05)	3.60 (0.55)	159 (6.33)	1.44 (0.11)
	WS (%)	5.73	0.37	10.43	5.78	0.60	7.39	0.10	0.96	3.95	0.07	17.26	4.47	1.51	5.54	7.37	7.06	0.71	4.81
C1	T (SD) (ng/g)	16.7 (4.25)	2.77 (0.99)	85.8 (12.0)	269 (89.2)	7.52 (11.2)	738 (142)	0.07 (0.2)	0.40 (0.09)	0.37 (0.12)	3.78 (0.42)	0.04 (0.04)	5.15 (0.22)	2.25 (0.57)	19.2 (3.91)	2.76 (0.35)	0.05 (0.00)	0.71 (0.05)	0.03 (0.01)
	WS (SD) (ng/g)	67.2 (5.86)	28.1 (11.3)	69.3 (11.7)	846 (175)	10542 (1081)	2110 (264)	62.3 (7.1)	6.24 (0.39)	2.78 (0.21)	1443 (17.3)	0.16 (0.10)	39.6 (4.25)	129 (10.8)	190 (13.7)	12.60 (0.85)	0.41 (0.09)	58.2 (2.64)	0.4 (0.04)
	WS (%)	24.86	9.86	123.	31.77	0.07	34.95	0.11	6.38	13.23	2.65	26.22	12.99	1.75	10.11	21.95	13.06	1.21	8.45
C2	T (SD) (ng/g)	2.17 (0.59)	0.146 (0.22)	-0.48 (2.70)	13.8 (21.5)	0.130 (2.76)	326 (37.6)	0.02 (0.0)	0.024 (0.02)	0.06 (0.02)	0.007 (0.1)	0.006 (0.00)	-0.001 (0.01)	0.479 (0.13)	3.70 (0.64)	1.67 (0.15)	0.01 (0.00)	0.049 (0.01)	0.01 (0.00)
	WS (SD) (ng/g)	95.7 (14.0)	160 (23.3)	70.5 (8.44)	391 (26.8)	1304 (2988)	8728 (1022)	50.5 (5.1)	5.78 (0.95)	29.01 (1.68)	4580 (272)	0.724 (0.13)	3.57 (2.56)	23.1 (2.91)	120 (6.92)	77.9 (5.37)	0.297 (0.06)	37.1 (1.68)	0.309 (0.06)
	WS (%)	2.26	0.09	-0.68	3.52	0.01	3.73	0.03	0.42	0.21	0.00	0.76	-0.02	2.07	3.08	2.14	3.25	0.13	2.99
C3	T (SD) (ng/g)	6.58 (2.47)	1.84 (1.00)	17.35 (11.7)	28.0 (101.0)	44.4 (13.08)	654 (167)	0.08 (0.2)	0.23 (0.10)	0.23 (0.05)	0.55 (0.47)	0.02 (0.01)	2.43 (0.39)	4.26 (0.60)	190 (9.13)	2.46 (0.29)	0.1 (0.03)	0.17 (0.05)	0.03 (0.01)
	WS (SD) (ng/g)	73.0 (56.0)	95.6 (95.5)	16.3 (14.6)	41.7 (58.1)	8822 (13962)	1515 (175)	1.5 (5.3)	5.9 (1.97)	0.92 (1.51)	15.6 (42.4)	0.16 (0.18)	11.5 (10.4)	20.2 (9.22)	163 (9.24)	6.66 (1.86)	1.16 (0.20)	25.3 (2.83)	n/a
	WS (%)	9.01	1.93	100	67.10	0.50	43.16	5.40	3.95	24.60	3.50	11.20	21.10	21.10	100.0	37.00	8.93	0.66	27.00

Table 2-S4. Magnetic sector inductively coupled plasma mass spectrometry (SF-ICP-MS) analysis of standard printing paper used in the study. The most abundant elements are presented on this table. T, T; WS, water soluble.

	Ca	Mg	Al	S	Sr	Si	P	Fe	Ti	Mn	Cr	Ni	Zn	Sn	Ce	La	Cu	Co	Mo	Sb
T (SD) (ng/g)	2.1E6 (2.4E5)	1.7E4 (1.4E3)	1E4 (752)	1E4 (576)	1E4 (710)	5494 (586)	1837 (169)	1124 (64)	186 (15)	155 (8.6)	24.1 (1.6)	17.44 (2.5)	14.48 (4.31)	8.41 (9.33)	4.53 (0.28)	2.15 (0.16)	1.41 (1.17)	0.80 (0.08)	0.218 (0.05)	0.15 (0.05)
WS (SD) (ng/g)	3E5 (8.4E3)	7136 (176)	1.8E4 (605)	1.5E4 (785)	3979 (120)	5478 (150)	828 (94)	36.36 (2.87)	1.09 (1.44)	17.02 (1.38)	2.51 (0.55)	24.33 (3.86)	77.1 (10.7)	1.85 (0.26)	5.73 (0.13)	0.38 (0.02)	10.46 (3.56)	0.42 (0.18)	0.757 (0.07)	0.20 (0.04)
WS (%)	14.1	43.13	169	141	39.05	99.7	45.07	3.23	0.59	11.00	10.43	140	532	21.93	126.6	17.79	740	52.47	348	131

Table 2-S5. Anions and cations analysis of PEPs, toners, and paper by ion chromatography. '-' represents values obtained from analysis that were not different than the blank samples evaluated.

Matrix	Printer	Chloride (µg/g)	Nitrate (µg/g)	Phosphate (µg/g)	Sulfate (µg/g)	Sodium (µg/g)	Ammonium (µg/g)	Potassium (µg/g)	Anions (µg/g)	Cations (µg/g)	Sum (% of total)
PEPs	A1	0.225	0.758		-	0.291	0.116	0.664	0.221	1.07	0.400
	B1	0.081	1.14		1.03	0.063	0.114	0.045	2.25	0.223	0.200
	C1	0.118	1.62		0.810	7.46	0.804	2.68	2.55	10.9	
	C2	1.08	3.16		0.522	0.689	-	0.518	4.77	1.19	0.400
	C3	0.838	0.788		-	2.06	0.129	2.02	0.915	4.20	1.40
Toners	A1	2.43	22.3			11.0	58.6	2.19	24.8	71.8	0.700
	B1	46.2	599		1.10	10.2	15.3	18.6	646	44.1	6.30
	B2	85.9	397		268	50.1	11.7	44.6	751	107	7.00
	C1	37.3	359		-	6.50	0.06	-	393	4.99	3.20
	C2	28.6	243		-	23.4	25.1	9.26	254	57.7	3.20
	C3	10.4	35.0		-	5.73	0.17	7.20	30.2	13.1	0.400
	C4	12.9	164			23.9	38.7	54.8	177	117	2.70
	C5	7.89	55.6		15.5	37.9	11.1	13.9	79.0	62.9	1.30
	C6	58.7	112	356	34.1	115	55.1	183	560	353	9.10
	D1	39.1	0.7		-	36.18	23.3	21.9	29.8	81.4	0.800
	A2	24.4	93.6	28.8		28.68	3.44	39.0	131	71.1	1.90
Paper	152	28834	1274		514	4451	2.00	148	30622	4601	5.40
	158	29700	658		909	5176	-	147	31267	5321	5.80
	156	28846	759		513	4678	-	64.0	30118	4719	5.40
	208	39510	229		1472	6407	-	388	41211	6770	10.0
	213	40343	-		816	6556	-	202	41081	6719	10.2

Bibliography

Bai R, Zhang L, Liu Y, Meng L, Wang L, Wu Y, et al. 2010. Pulmonary responses to printer toner particles in mice after intratracheal instillation. Toxicol Lett 199:288–300.

Barthel M, Pedan V, Hahn O, Rothhardt M, Bresch H, Jann O, Seeger S. 2011. XRF-analysis of fine and ultrafine particles emitted from laser printing devices. Environ Sci Technol 45:7819–25.

Bello D, Martin J, Santeufemio C, Sun QW, Bunker KL, Shafer M, Demokritou P. 2013. Physico-chemical and morphological character- isation of nanoparticles from photocopiers: implications for environ- mental health. Nanotoxicology 7:989–1003.

Bondarenko O, Juganson K, Ivask A, Kasemets K, Mortimer M, Kahru A. 2013. Toxicity of Ag, CuO and ZnO nanoparticles to selected environmentally relevant test organisms and mammalian cells in vitro: a critical review. Arch Toxicol 87:1181–200.

Brown SK. 1999. Assessment of pollutant emissions from dry-process photocopiers. Indoor Air 9:259–67.

Castellano P, Canepari S, Ferrante R, L'Episcopo N. 2012. Multiparametric approach for an exemplary study of laser printer emissions. J Environ Monit 14:446–54.

Chang CL, Demokritou P, Shafer M, Christiani D. 2013. Physico-chemical and toxicological characteristics of welding fume derived particles generated from real time welding processes. Environ Sci-Proc Imp 15: 214–24.

Cohen JM, Derk R, Wang L, Godleski J, Kobzik L, Brain J, Demokritou P. 2014. Tracking translocation of industrially relevant engineered nanomaterials (ENMs) across alveolar epithelial monolayers in vitro. Nanotoxicology 1:216–25.

Demokritou P, Gass S, Pyrgiotakis G, Cohen JM, Goldsmith W, McKinney W, et al. 2013. An in vivo and in vitro toxicological characterisation of realistic nanoscale CeO(2) inhalation exposures. Nanotoxicology 7:1338–50.

Demokritou P, Lee SJ, Ferguson ST, Koutrakis P. 2004. A compact multistage (cascade) impactor for the characterization of atmospheric' aerosols. J Aerosol Sci 35:281–99.

Destaillats H, Maddalena R, Singer B, Hodgson A, McKone T. 2008. Indoor pollutants emitted by office equipment: a review of reported data and information needs. Atmos Environ 42:1371–88.

Ding X, Wang M, Chu H, Chu M, Na T, Wen Y, et al. 2014. Global gene expression profiling of human bronchial epithelial cells exposed to airborne fine particulate matter collected from Wuhan, China. Toxicol Lett 228:25–33.

Ebersviller S, Lichtveld K, Sexton KG, Zavala J, Lin YH, Jaspers I, Jeffries HE. 2012. Gaseous VOCs rapidly modify particulate matter and its biological effects - Part 1: simple VOCs and model PM. Atmos Chem Phys Discuss 12:5065–105.

Ewers U, Nowak D. 2006. Health hazards caused by emissions of laser printers and copiers? Gefahrstoffe Reinhaltung Der Luft 66:203–10. Gminski R, Decker K, Heinz C, Seidel A, Konczol M, Goldenberg E,

et al. 2011. Genotoxic effects of three selected black toner powders and their dimethyl sulfoxide extracts in cultured human epithelial A549 lung cells in vitro. Environ Molec Mutagenesis 52:296–309.

Herner JD, Green PG, Kleeman MJ. 2006. Measuring the trace elemental composition of size-resolved airborne particles. Environ Sci Technol 40:1925–33.

IDC. 2014. IDC finds continued growth in the worldwide hardcopy peripherals market in the fourth quarter of 2013 Framingham, Massachusetts.

Kagi N, Fujii S, Horiba Y, Namiki N, Ohtani Y, Emi H, et al. 2007. Indoor air quality for chemical and ultrafine particle contaminants from printers. Build Environ 42:1949–54.

Kessler R. 2011. Engineered nanoparticles in consumer products: understanding a new ingredient. Environ Health Perspect 119:a120–5. Khatri M, Bello D, Gaines P, Martin J, Pal AK, Gore R, Woskie S. 2013. Nanoparticles from photocopiers induce oxidative stress and upper respiratory tract inflammation in healthy volunteers. Nanotoxicology 7:

1014–27. Konczol M, Weiss A, Gminski R, Merfort I, Mersch-Sundermann V.

2013. Oxidative stress and inflammatory response to printer toner particles in human epithelial A549 lung cells. Toxicol Lett 216:171–80.

Kumar R, Nagesha DK. 2013. Size-dependent study of pulmonary responses to nano-sized iron and copper oxide nanoparticles. Methods Mol Biol 1028:247–64.

Landsiedel R, Ma-Hock L, Hofmann T, Wiemann M, Strauss V, Treumann S, et al. 2014. Application of short-term inhalation studies to assess the inhalation toxicity of nanomaterials. Part Fibre Toxicol 11:16.

Liao Z, Xu D, Zhang F, Li C, Xiao W. 2012. Thermal and FTIR characterization of unsaturated polyester resin/epoxy resin composites. In: Zhang Hx, Han Y, Chen F, Wen J, eds. Materials and Computational Mechanics, Pts 1–3. Switzerland: Trans Tech Publications Ltd, 117–19.

Limited R. E.-S. P. 2011. Nanotechnology Market Forecast to 2013. Plunkett Research Ltd. [Online] Available at: http://www.reportlin- ker.com/p0118193/Nanotechnology-Market-Forecast-to.html. Accessed on February 2014.

Merrill RA, Bartick EG, Taylor JH. 2003. Forensic discrimination of photocopy and printer toners. I. The development of an infrared spectral library. Analyt Bioanalyt Chem 376:1272–8.

Morawska L, He Cr, Johnson G, Jayaratne R, Salthammer T, Wang H, et al. 2009. An investigation into the characteristics and formation mechanisms of particles originating from the operation of laser printers. Environ Sci Technol 43:1015–22.

Morimoto Y, Oyabu T, Horie M, Kambara T, Izumi H, Kuroda E, et al. 2013. Pulmonary toxicity of printer toner following inhalation and intratracheal instillation. Inhal Toxicol 25:679–90.

Moschini E, Gualtieri M, Colombo M, Fascio U, Camatini M, Mantecca P. 2013. The modality of cell-particle interactions drives the toxicity of nanosized CuO and TiO2 in human alveolar epithelial cells. Toxicol Lett 222:102–16.

NNI. 2011. Environmental, Health, and Safety (EHS) Research Strategy. Available at http://www.nano.gov.

NRC. 2012. A Research Strategy for Environmental, Health, and Safety Aspects of Engineered Nanomaterials. Washington, DC: The National Academies Press.

Padro-Martinez LT, Patton AP, Trull JB, Zamore W, Brugge D, Durant JL. 2012. Mobile monitoring of particle number concentration and other traffic-related air pollutants in a near-highway neighborhood over the course of a year. Atmospheric Environment 61:253–64.

Pirela S, Molina R, Watson C, Cohen Jm, Bello D, Demokritou P, Brain J. 2013. Effects of copy center particles on the lungs: a toxicological characterization using a Balb/c mouse model. Inhal Toxicol 25: 498–508.

Pirela SV, Pyrgiotakis G, Bello D, Thomas T, Castranova V, Demokritou P. 2014. Development and characterization of an exposure platform suitable for physico-chemical, morphological and toxico- logical characterization of printer-emitted particles (PEPS). Inhal Toxicol 26:400–8.

Quang TN, He C, Morawska L, Knibbs LD, Falk M. 2012. Vertical particle concentration profiles around urban office buildings. Atmos Chem Phys 12:5017–30.

Schripp T, Wensing M, Uhde E, Salthammer T, He C, Morawska L. 2008. Evaluation of ultrafine particle emissions from laser printers using emission test chambers. Environ Science & Technology 42:4338–43.

Shrivastava R, Raza S, Yadav A, Kushwaha P, Flora SJ. 2013. Effects of sub-acute exposure to TiO, ZnO and AlO nanoparticles on oxidative stress and histological changes in mouse liver and brain. Drug Chem Toxicol 37:336–47.

Sisler JD, Pirela SV, Friend S, Farcas M, Schwegler-Berry D, Shvedova A, et al. 2014. Small Airway Epithelial Cells Exposure to Printer- Emitted Engineered Nanoparticles Induces Cellular Effects on Human Microvascular Endothelial Cells in an Alveolar-Capillary Co-Culture Model. Nanotoxicology doi: 10.1186/1743-8977-11-16.

Song MK, Song M, Choi HS, Park YK, Ryu JC. 2013. Discovery of a characteristic molecular signature by microarray analysis of whole- blood gene expression in workers exposed to volatile organic compounds. Biochip Journal 7:112–35.

Sotiriou GA, Diaz E, Long MS, Godleski J, Brain J, Pratsinis SE, Demokritou P. 2012. A novel platform for pulmonary and cardiovas- cular toxicological characterization of inhaled engineered nanomater- ials. Nanotoxicology 6:680–90.

Tang T, Hurras J, Gminski R, Mersch-Sundermann V. 2012. Fine and ultrafine particles emitted from laser printers as indoor air contamin- ants in German offices. Environ Sci Pollut Res Int 19:3840–9.

Vinikoor-Imler LC, Davis JA, Meyer RE, Messer LC, Luben TJ. 2014. Associations between prenatal exposure to air pollution, small for gestational age, and term low birthweight in a state-wide birth cohort. Environ Res 132C:132–9.

Wang F, Li C, Liu W, Jin Y, Guo L. 2014. Effects of subchronic exposure to low-dose volatile organic compounds on lung inflammation in mice. Environ Toxicol 29:1089–97.

Wang F, Li C, Liu W, Jin Y. 2013. Oxidative damage and genotoxic effect in mice caused by sub-chronic exposure to low-dose volatile organic compounds. Inhal Toxicol 25:235–42.

Wang H, He C, Morawska L, McGarry P, Johnson G. 2012. Ozone- initiated particle formation, particle aging, and precursors in a laser printer. Environ Sci Technol 46:704–12.

Watson C, Ge J, Cohen J, Pyrgiotakis G, Engelward BP, Demokritou P. 2014. High-throughput screening platform for engineered nanoparticle- mediated genotoxicity using cometchip technology. ACS Nano 8: 2118–33.

Weichenthal S, Kulka R, Belisle P, Joseph L, Dubeau A, Martin C, et al. 2012. Personal exposure to specific volatile organic compounds and acute changes in lung function and heart rate variability among urban cyclists. Environ Res 118:118–23.

Wensing MPG, Bednarek M, Schripp T, Uhde E, Salthammer T. 2006. Particle measurement of hardcopy devices. Healthy Buildings Conference, Lisboa 2:479–82.

Xerox. 2013. XeroxÕ Emulsion Aggregation (EA) Toner [Online]. Available at: http://www.office.xerox.com/latest/SUPWP-01.pdf. Accessed on 19 February 2014.

Yu XB, Su JW, Li XY, Chen G. 2014. Short-term effects of particulate matter on stroke attack: meta-regression and meta-analyses. PLoS One 9:e95682.

Zhou EH, Watson C, Pizzo R, Cohen J, Dang Q, De Barros PM, et al. 2014. Assessing the impact of engineered nanoparticles on wound healing using a novel in vitro bioassay. Nanomedicine (Lond) [Epub ahead of print].

Chapter 3: Laser printer-emitted engineered nanoparticles lead to cytotoxicity, inflammation and changes in DNA methylation in human cells

Sandra V. Pirela[1], Isabelle R. Miousse[2], Xiaoyan Lu[1], Vincent Castranova[3], Treye Thomas[4], Yong Qian[5], Dhimiter Bello[1,6], Lester Kobzik[1], Igor Koturbash[2], Philip Demokritou[1*].

[1] Department of Environmental Health, Center for Nanotechnology and Nanotoxicology, School of Public Health, Harvard University, 665 Huntington Ave., Boston, MA, USA.

[2] Department of Environmental and Occupational Health, University of Arkansas for Medical Sciences, Little Rock, AR, USA.

[3] Department of Pharmaceutical Sciences, West Virginia University, Morgantown, WV, USA.

[4] U.S. Consumer Product Safety Commission, Office of Hazard Identification and Reduction, Rockville, MD, USA.

[5] Pathology and Physiology Research Branch, Health Effects Laboratory Division, National Institute for Occupational Safety and Health, Morgantown, WV 26505, USA.

[6] Department of Work Environment, University of Massachusetts, Lowell, MA, USA.

[*]Corresponding author

Abstract

Background: Engineered nanomaterials (ENMs) incorporated into toner formulations of printing equipment become airborne during their consumer use. Although information on the complex physico-chemical and toxicological properties of both toner powders and printer-

emitted particles (PEPs) continues to grow, most toxicological studies have primarily used raw toner powders rather than the actual PEPs, which are not representative of current exposures experienced at the consumer level during printing.

Objectives: To assess the biological responses of a panel of human cell lines to PEPs.

Methods: Three physiologically relevant cell lines -small airway epithelial cells, macrophages and lymphoblasts- were exposed to PEPs at a wide range of doses (0.5-100 μg/mL) that correspond to human inhalation exposure durations at the consumer level of ~ 8 hours and higher. Following treatment, toxicological parameters reflecting distinct mechanisms were evaluated.

Results: PEPs caused significant cytotoxicity, membrane integrity damage, reactive oxygen species (ROS) production, cytokine release, and epigenetic changes in cells at doses comparable to those from real world exposure scenarios.

Conclusions: Laser printer-emitted engineered nanoparticles can be deleterious to lung cells and may cause persistent genetic modifications that could translate to pulmonary disorders.

Introduction

The recent incorporation of ENMs into toner formulations has possible health implications based on consumer exposure to released particulate matter (PM) from laser-based printing equipment. Laser printers are widely used in office and home environments with an exponential increase of market sales in recent years (IDC 2014). Recent studies have shown that emissions from this growing technology comprise a variety of pollutants including PM, semi-volatile organic compounds (sVOCs) and other gaseous pollutants (He et al. 2007; Morawska et al. 2009; Wang et al. 2012)

Recently, our group developed a lab based Printer Exposure Generation System (PEGS) that allows the generation and sampling of airborne PEPs for subsequent physico-chemical, morphological and toxicological analysis (Pirela et al. 2014a). This platform was used to evaluate emission profiles from 11 laser printers currently on the market (Pirela et al. 2014b). The study showed the particle number concentration of PEPs varied across different printer /manufacturers reaching up to 1.3 million particles/cm^3 with diameters <200 nm (Pirela et al. 2014a). The detailed assessment of both toners and PEPs confirmed presence of nanoscale materials in the airborne state and a complex chemistries, which included elemental/organic carbon and inorganic compounds (*e.g.*, metals, metal oxides). It has been confirmed that toners are classified as nano-enabled products (NEPs) (Pirela et al. 2014b).

Both *in vitro* and *in vivo* toxicological assays may help characterize the effects of laser printer emissions and toners on the respiratory system. However, the results to date are contradictory. Notably, the toxicity of PEPs remains poorly characterized primarily because most studies used toner powders rather than PEPs. For example, Gminski et al. (2011) reported toner powders exhibited genotoxic potential on epithelial lung cells. Additionally, similar *in vitro* assays using an air/liquid interphase system, showed significant cyto- and genotoxicity (Tang et al. 2012). In contrast, exposure of alveolar macrophages to toner powder revealed no effect using cell magnetometry analysis (Furukawa et al. 2002). An even smaller number of *in vivo* toxicological studies have been evaluated effects of PEPs exposures. Bai et al. (2010) reported that mice exposed to printer toner particles shown significant pulmonary inflammation, damage to the epithelial-capillary barrier and enhanced cell permeability. Comparable inflammatory and fibrotic responses were also observed in rats exposed to toner powders (Morimoto et al. 2013).

Concerns continue to be raised in terms of possible epigenetic effects associated with PEPs inhalation exposures. In general, the ability of ENMs to affect cellular epigenome remains largely unexplored. One important epigenetic mechanism, DNA methylation, can regulate proper expression of genetic information in a sex-, tissue-, and cell type-dependent manner (Jones 2012). Additionally, DNA methylation plays a central role in regulating the expression of transposable elements (TEs) that comprise a large part of the eukaryote genome (Smith et al. 2012). TEs are essential regulators of stability and proper function of the genome, including expression of genetic information and chromatin structure. Numerous studies indicate that exposure to various environmental stressors, including PM, may compromise the methylome and TEs (Baccarelli et al. 2009; Madrigano et al. 2011). A study by Gong et al. (2010) concluded that short-term exposure to nanomaterials might result in alterations in both global DNA methylation patterns and the DNA methylation machinery. However, the epigenetic effects of ENMs contained in PEPs remain largely unknown, and, to our knowledge, epigenetic effects as a result of exposure to PEPs using *in vitro* systems have yet to be characterized.

In the present *in vitro* toxicological study, the biological responses due to exposure to PEPs on physiologically relevant human small airway epithelial cells, macrophages and lymphoblasts were evaluated using a wide range of exposure doses. Several endpoints (*e.g.,* cell membrane integrity and viability, ROS production, DNA methylation) important for the understanding of mechanisms of toxicity were assessed in this study taking into consideration *in vitro* and *in vivo* dosimetry. Such thorough physico-chemical, morphological and cellular toxicological characterization body studies based on the "real world" exposure conditions adds to the body of scientific evidence required to understand and quantify the exposure risk to PEPs

from the use of printing equipment. More importantly, the proposed methodology can be used to assess risks associated to ENMs released across life cycle of any other nano-enabled product.

Methods

Generation and collection of size-fractionated PEPs

The PEPs were generated using the recently developed PEGS as described in our recent publication (Pirela et al. 2014a). In summary, the PEGS was used to generate, collect and sample size-fractionated PEPs from a high emitting printer (referred to as Printer B1 in companion papers) emitting up to 1.26 million particles/cm^3 (Pirela et al. 2014a).

Post sampling physico-chemical and morphological characterization of PEPs

Detailed chemical and morphological characterization of the PEPs and toner from the test printer, as well as the paper utilized in this study, are presented in detailed in a recently published companion publication (Pirela et al. 2014b). In summary, toner powder and PEPs share a similar chemical fingerprint, with PEPs containing 62 and 97% organic, 10 and 0.5% elemental carbon, ~3% metal/metal oxides (*e.g.*, aluminum, titanium) and ~25% other (*e.g.*, phosphorus, sulfur) (Pirela et al. 2014b).

Extraction of size fractionated PEPs, preparation and characterization of particle liquid suspensions for cellular studies

After sampling size-fractionated PEPs, the particles were extracted from collection filter media using an aqueous suspension methodology (Demokritou et al. 2002; Pirela et al. 2014b). Subsequently, particle dispersions in culture media were prepared using a protocol developed by the authors (Cohen et al. 2013), in which the particle critical delivered sonication energy (DSE_{cr}), hydrodynamic diameter (d_H), formed agglomerate size distribution, polydispersity index (PdI),

zeta potential (ζ), specific conductance (σ), pH, colloidal stability and effective density of formed agglomerates (DeLoid et al. 2014) are measured. For more details, please refer to Supplemental Material, Part A. It is worth noting that the effective density of the formed agglomerates, which plays an important role in the settling and dosimetry *in vitro*, was measured using the recently developed Volumetric Centrifugation Method (VCM) (DeLoid et al. 2014).

In vitro and *in vivo* dosimetric considerations

To express *in vivo* and *in vitro* doses on the same scale, the dosimetric approach recently developed by the authors was followed (Demokritou et al. 2013). In summary, the Multiple-Path Particle Dosimetry model (MPPD2) (Anjilvel and Asgharian 1995) is used to calculate the deposition mass flux in the human lung ($\mu g/m^2 \bullet min$) and the deposited PEPs mass per area ($\mu g/m^2$) following an inhalation exposure to PEPs for a determined amount of time. Table 3-1 summarizes the parameters used for the MPPD2 simulations, which includes both the airborne nanoparticle size distribution values (count median diameter, geometric standard deviation, particle mass concentration) and the human breathing parameters of a resting individual (tidal volume, breathing frequency, inspiratory fraction, pause fraction, functional residual capacity, head volume, breathing route). The calculated mass per area deposited in the lung obtained from the model is the equivalent mass per area ($\mu g/m^2$) that needs to be delivered to cells in the *in vitro* experiment (mass deposited *in vitro*).

Subsequently, because of the particokinetics of the PEPs-media suspension that define their settling rate, the delivered to cell *in vitro* mass is not necessarily equal to the administered *in vitro* mass. Therefore, the fraction of administered particle mass that is deposited on the cells as a function of *in vitro* exposure time (f_D) needs to be calculated in order to match the *in vivo* lung deposited dose estimated by the MPPD2 model. The f_D as a function of *in vitro* exposure

time is calculated using the hybrid Volumetric Centrifugation Method-*In Vivo* Sedimentation, Diffusion and Dosimetry (VCM-ISDD) methodology (Cohen et al. 2014b; DeLoid et al. 2014; Pal et al. 2014), recently developed by the authors. The mean media-formed agglomerate d_H and the VCM-measured effective density of formed agglomerates (DeLoid et al. 2014) were used as input to the VCM-ISDD fate and transport numerical model in order to estimate the f_D as a function of time.

Table 3-1. Summary of parameters used in the *in vivo* lung Multiple Path Particle Deposition model (MPPD2)[1].

Human Model	**Breathing Parameters**	**Airborne Nanoparticle Distribution**
Functional Residual Capacity: 3300 mL	*Tidal Volume*: 625 ml	*Count Mean Diameter:* 57.45 nm
Head Volume: 50 mL	*Breathing Frequency:* 12 breaths/ min	*Geometric Standard Deviation*: 1.67
Breathing Route: Nasal	*Inspiratory Fraction*: 0.5	*Mass Concentration*: 23.86 μg/m^3
	Pause Fraction: 0.0	

Source and characterization of comparative particles (controls) used in the study

The gas metal arc-mild steel welding fumes (MS-WF) were used as comparative material for the study and were provided by Dr. J. Antonini from the National Institute for Occupational Health (NIOSH). The sample was generated as described in Antonini et al. (1999), and has a count mean diameter of 1.22 μm and has been shown to induce toxicity in the lungs of rodents (Antonini et al. 2012; Sriram et al. 2012; Zeidler-Erdely et al. 2011). Its Brunau er-Emmett-Teller (BET, Quantachrome, Boynton Beach, FL) specific surface area was found to be 48.2

m^2/g and its equivalent primary particle diameter was estimated to be 23.8 nm. The amorphous silicon dioxide (SiO_2) was generated in-house using the Harvard Versatile Engineered Nanomaterial Generation System (VENGES), as previously described (Demokritou et al. 2010; Sotiriou et al. 2012) and had a BET measured primary particle diameter of 14.7 nm. Both materials were used as comparative materials due to the extensive toxicological data in the current body of literature.

Cell culture

The human monocytic immortalized cells (THP-1, American Type Culture Collection, USA) were cultured in Roswell Park Memorial Institute Medium (RPMI) 1640 supplemented with 10% fetal bovine serum (FBS). The small airway epithelial cells (SAEC) were obtained from NIOSH and cultured in serum-free small airway epithelial cell growth medium (SAGM) with the addition of multiple supplemental growth factors provided by the manufacturer (Lonza, Inc., NJ). The TK6 human lymphoblastoid cell lines were maintained in RPMI 1640 with L-glutamine supplemented with 10% horse serum (HS). It is worth noting that the TK6 lymphoblast cell line used here may not be directly physiologically relevant to lung toxicology. However, this cell line has been used historically for genotoxicity evaluations due to its increased sensitivity for DNA damage assessments, in particular when performing the comet assay (Bajpayee et al. 2013; Kimura et al. 2013). Here, TK6 cells were used to rank PEPs in terms of DNA damage potential based on this past record of utility. All media were supplemented with 1% penicillin-streptomycin. Generic cell culture protocol consisted of growing cells in an incubator (37°C/5% CO_2) in 25- or 150-cm^2 flasks, replacing media every 2–3 days and passaging before confluence. Before exposure, THP-1 cells were differentiated into macrophages (Daigneault et al. 2010).

Cellular assays

Various cellular assays were used to assess biological mechanisms. All experiments were performed in triplicate. In more detail:

Cellular membrane integrity. Following exposure to the test particles, cells were evaluated for viability using the CytoTox-One Homogenous Membrane Integrity Assay (Promega, USA). This assay estimated the number of non-viable cells present after exposure by measuring the activity of lactate dehydrogenase (LDH) leaked from the cell.

ROS production. At 23.5 hours of particle exposure, 5-μM dihydroethidium (DHE) was added to each treatment well and incubated for 30 minutes. Fluorescent measurements were taken immediately using a fluorescence microplate reader (Molecular Devices, Sunnyvale, CA, USA) at an excitation of 518 nm and emission detection of 605 nm. Hydrogen peroxide was used as a positive control in this assay and while these measurements were not shown in the figure, they were used in the calculations to normalize the data.

Autofluorescence of ENMs pertaining to both the cellular membrane integrity and ROS assays. The autofluorescence of ENMs and media can cause interference with fluoroscopic bioassays (Doak et al. 2009; Holder et al. 2012; Monteiro-Riviere et al. 2009) and control experiments for both particle- and media-only need to be included in the measurement to consider particle/media interference. We have performed such experiments in this study in order to estimate potential nanoparticle interference/absorption in the LDH and ROS assay and measured the fluorescence intensity of the particles suspended in media. The intensity was found minimal and similar to that of the media-alone control for both bioassays and this was included in the calculations.

DNA damage. To assess the potential genotoxic properties of PEPs, the high throughput Nano-CometChip assay, recently developed by our group, was used to measure DNA double stranded breaks on TK6 cells following a four-hour exposure to particles as described in Watson et al. (2014).

Epigenetic analysis. A number of assays were performed to evaluate DNA methylation patterns on SAEC exposed to PEPs (0.5 and 30 μg/mL administered doses) for 24 hours. For more information on the specific analysis, refer to Supplemental Material, Part A.

Cytokine and chemokine analysis

Supernates from treated SAECs were assayed by Eve Technologies Corporation (Calgary, Alberta, Canada) using a Human Primary Cytokine Array/Chemokine Array 41-Plex Panel (Millipore, St. Charles, MO) according to the manufacturer's protocol.

Statistical analysis

Statistical analyses were performed using GraphPad Prism 6.0 (La Jolla, CA). Comparisons between all cellular parameters after exposure were evaluated using one-way analysis of variance and Tukey correction for multiple comparison statistical significance. A *p*-value < 0.05 was considered significant. Experiments were conducted in triplicate.

Results

PEPs dispersion and characterization

Supplemental Material, Figure 3-S1 shows the hydrodynamic diameters for both PEPs and MS-WF plotted as a function of Delivered Sonication Energy (DSE). It can be observed that as the DSE increases, the DLS-measured d_H decreases towards a marginal state of minimal agglomeration. The DSE_{cr} for PEPs was 514.29 J/mL for $PM_{0.1}$. Similarly, MS-WF had a DSE_{cr}

of 400 J/mL. The DSE_{cr} for the SiO_2 was obtained from a previous publication and was found to be 242 J/mL (Cohen et al. 2013).

Table 3-2 summarizes the particle colloidal properties in both DI H_2O and different types of biological media used, including the DLS-measured hydrodynamic diameter (d_H), zeta potential (ζ), polydispersity index (PdI), specific conductance (σ) and pH. The suspension of PEPs ($PM_{0.1}$) demonstrated a lower d_H in DI H_2O when compared to that in cellular media. PEPs ($PM_{0.1}$) had a d_H of 178.3 nm, which increased to > 200 nm when dispersed in media. This is in agreement with literature (Cohen et al. 2013) as it is anticipated that presence of proteins will induce formation of a thicker protein corona on particle agglomerates. MS-WF in suspension had a d_H of 2197 nm in DI H_2O, which decreased when dispersed in media to values ranging from 1502-1878 nm. Lastly, the d_H of silica was 142.5 nm in DI H_2O and 114.6 to 207.7 nm in various media. Observed values of zeta potential were strongly negative for the PEPs in DI H_2O (-20.6 mV) and became less negative in various media. MS-WF and SiO_2 had positive zeta potentials in DI H_2O or media. In addition to d_H measurements, colloidal size stability of particle suspensions was subsequently evaluated for 24 hours. It was observed that d_H of PEPs, SiO_2 and MS-WF suspended in SAGM remained fairly stable up to 24 hours. It is worth noting that colloidal stability is important for dosimetric calculations (see section below).

Additionally, the VCM-measured effective density of PEPs ranged from 1.19-2.39 g/cm^3 in different cellular media used, while those of the comparator materials used in the study were approximately 1.2 g/cm^3 for SiO_2 and 1.37-1.56 g/cm^3 for MS-WF (Table 3-2). It is worth noting that effective density and size of formed agglomerates are important determinants of fate and transport in the *in vitro* system and define settling rates and dosimetry *in vitro*.

Table 3-2. Properties of laser printer emitted particle dispersions. d_H: hydrodynamic diameter, PdI: polydispersity index, ζ: zeta potential, σ: specific conductance, ρ_{agg}: effective density.

Material	Media	d_H (nm)	PdI	ζ (mV)	σ (mS/cm)	ρ_{agg} (g/cm^3)
PEPs ($PM_{0.1}$)	DI H_2O	178.3 ± 3.459	0.403 ± 0.050	-20.6 ± 1.87	0.185 ± 5.8x10^{-4}	-
	RPMI/ 10%HS	272.5 ± 22.27	0.688 ± 0.178	-9.80 ± 1.31	3.61 ± 0.246	1.19
	RPMI/ 10% FBS	227.3 ± 105.0	0.485 ± 0.247	9.55 ± 2.89	7.01 ± 0.960	1.56
	SAGM	381.7 ± 40.23	0.586 ± 0.048	9.97 ± 2.77	2.52 ± 0.0721	2.39
Mild steel welding fumes (MS-WF)	DI H_2O	2197 ± 118.4	0.561 ± 0.325	8.52 ± 1.24	0.028 ± 0.93x10^{-4}	-
	RPMI/ 10%HS	1878.3 ± 395.89	0.236 ± 0.080	10.5 ± 0.757	11.9 ± 0.289	1.48
	RPMI/ 10% FBS	1502 ± 96.26	0.236 ± 0.080	12.1 ± 2.66	11.5 ± 1.10	1.56
	SAGM	1526.7 ± 259.63	0.198 ± 0.041	18.8 ± 0.9	10.5 ± 0.462	1.37
SiO_2	DI H_2O	142.5 ± 2.364	0.207 ± 0.013	33.6 ± 1.70	0.008 ± 4.4x10^{-5}	-
	RPMI/ 10%HS	173.4 ± 13.36	0.541 ± 0.027	11.4 ± 3.60	11.2 ± 0.874	1.3
	RPMI/ 10% FBS	114.6 ± 0.100	0.324 ± 0.009	9.33 ± 0.841	11.6 ± 0.833	1.2
	SAGM	207.7 ± 6.029	0.583 ± 0.078	12.7 ± 1.39	11.1 ± 0.436	1.12

Notes: Values represent the mean (± SD) of a triplicate reading. '-' data not available.

Dosimetric considerations for *in vitro* testing

The delivered to cell dose at a given exposure time point may not always be the same as the dose administered (Cohen et al. 2013). The settling rate of the formed agglomerates *in vitro* is defined by two fundamental parameters, namely the hydrodynamic diameter of the formed agglomerate and their effective density (Cohen et al. 2013; DeLoid et al. 2014). Using the recently developed Harvard *in vitro* dosimetry methodology (Cohen et al. 2014b), the fraction of

the administered particles that deposited on the cells located at the bottom of the treatment well as a function of time was calculated and presented in Supplemental Material, Figure 3-S2. As expected, some of the materials used in the study settled faster than other. For instance, it will take less than two hours for all of the administered MS-WF mass, suspended in either RPMI/10%FBS or SAGM, to deposit on the cells. For silica, only approximately 35% and 100% of the administered dose will actually reach the bottom of the well in the 24-hour exposure when suspended in RPMI/10%FBS and SAGM, respectively. Interestingly, for the same exposure duration, 100% and 51.8% of the administered dose of PEPs will be deposited to the cells when suspended in SAGM or RPMI/10%FBS, respectively. This translated to a respective f_D of 1.00 and 0.518. The estimated deposited mass of administered particle mass for all treatment particles and exposure times is summarized in Supplemental Material, Table 3-S3.

Additionally, in order to bring *in vitro* and *in vivo* doses to the same scale, the deposition mass flux of PEPs in a human lung was determined to be 1.732 $\mu g/m^2 \bullet min$ using the MPPD2 model. This calculated mass flux was then used to back calculate the inhalation exposure durations to PEPs corresponding to the range of cell-administered doses used in this study (summarized in Supplemental Material, Table 3-S3). Results show that *in vitro* PEPs doses used in this study are comparable to inhalation exposures lasting for 7.8 or more hours of printing. The wide range of corresponding human exposures to laser printer emissions evaluated here, makes the doses relevant for individuals in both occupational and consumer settings. The majority of the inhaled PEPs would deposit in the respiratory bronchioles and distal alveoli (Supplemental Material, Figure 3-S3). Approximately 31% of inhaled PEPs would deposit in the tracheobronchial region and 18.4% would be deposited in the head region. Although the

selection of cell lines in this study reflects those located in the lower respiratory area, it should be noted that the upper airways are an equally interesting target.

Cell viability is negatively affected by exposure to PEPs

Cellular membrane integrity of all three human cell lines studied was decreased following exposure to PEPs. Figure 3-1 illustrates results from the lactate dehydrogenase assay, showing percent cytotoxicity of each treatment at various administered doses. In particular, SAEC experienced >40% cell death after exposure to PEPs ($PM_{0.1}$, 100 μg/mL administered dose) when compared to untreated cells. Macrophages exposed to PEPs ($PM_{0.1}$) exhibited a significant increase cell death in a dose-response manner, which was greater than MS-WF or SiO_2 treatment, where MS-WF is known to be cytotoxic (Antonini et al. 1999; Antonini et al. 2012; Zeidler-Erdely et al. 2011). Lastly, human lymphoblasts had a reverse dose-response relationship when exposed to PEPs ($PM_{0.1}$).

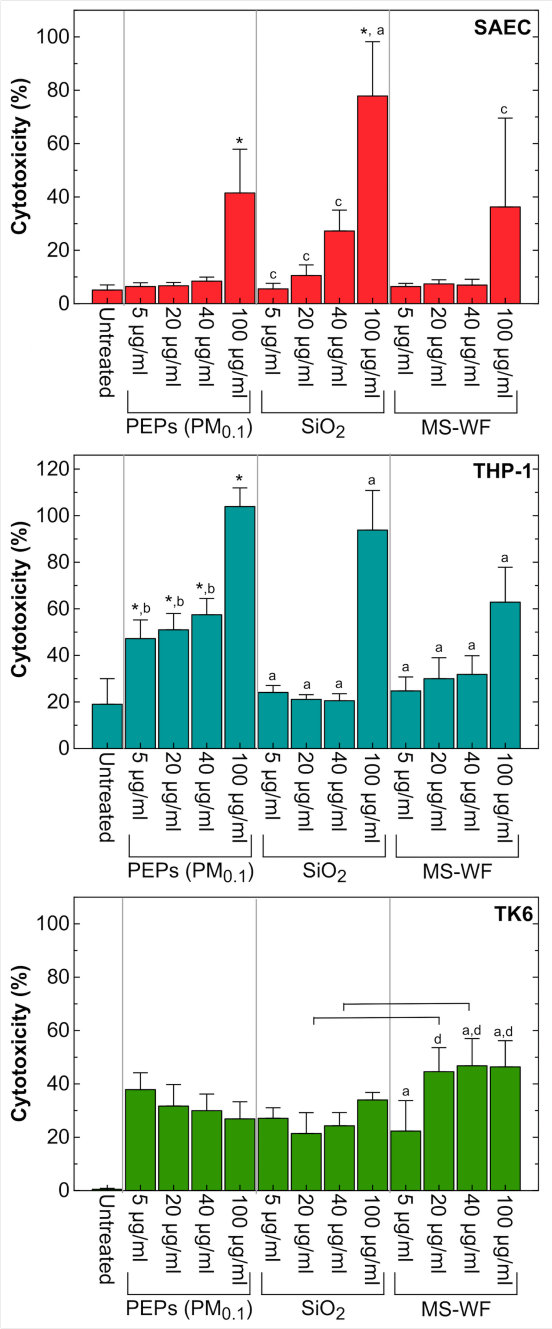

Figure 3-1. Percent cytotoxicity of cells determined using LDH assay following exposure to PEPs ($PM_{0.1}$), SiO_2 and MS-WF on three human cell lines. All values are represented as mean ± SE. Values significantly different from the [*]untreated, [a]$PM_{0.1}$ dose-matched, [b] $PM_{0.1}$ 100 µg/mL, [c]SiO_2 100 µg/mL, [d]MS-WF 5 µg/mL treatment groups. Bar represents a significant difference in measurements across the treatment groups with a p level < 0.05.

ROS production elevated after exposure to PEPs

To evaluate the potential of PEPs to induce ROS production in epithelial cells and macrophages, two cell lines that are in direct contact with inhaled foreign material, the levels of superoxide ions were measured. Figure 3-2 illustrates the results from the DHE fluorescence on each of the treatments at the various exposure doses showing contrasting responses in both cell lines. A clear dose-response relationship was observed in SAECs treated with PEPs. While MS-WF and SiO_2 also enhanced ROS production in SAECs, a dose dependence was not observed. The level of ROS production with PEPs (100 μg/mL, administered dose) was similar to that with 100 μg/mL MS-WF or SiO_2 in SAECs. Macrophages displayed elevated superoxide levels following PEPs (5 μg/mL, administered dose). Higher doses did not induce ROS production. Conversely, there was no statistically significant effect of SiO_2 on macrophages production of ROS. Treatment with PEPs (5 μg/mL) was more potent in stimulating ROS release than SiO_2 or MS-WF at the same administered dose.

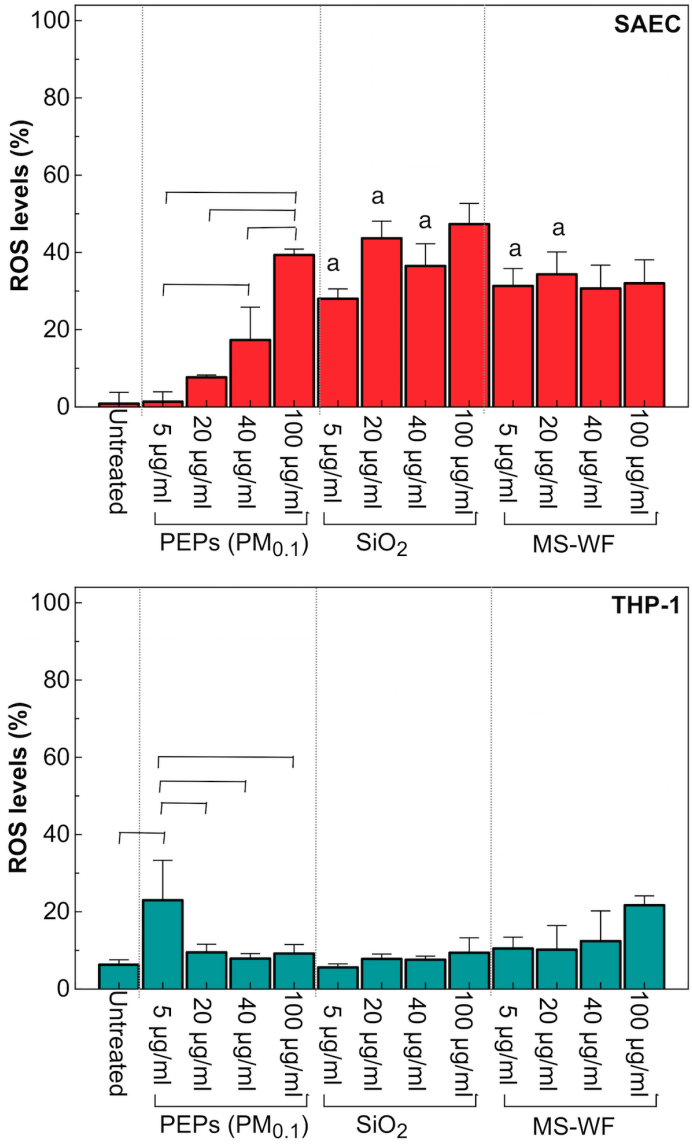

Figure 3-2. Percentage increase of reactive oxygen species compared to control measured in supernatant from SAEC and THP-1 following a 24-hour exposure to PEPs ($PM_{0.1}$), SiO_2 and MS-WF. All values are represented as mean ± SE. [a] Significantly different from $PM_{0.1}$ dose-matched treatment group. Bar represents a significant difference in measurements across the treatment groups with a p level < 0.05.

Inflammatory mediator secretion escalates following exposure to PEPs

Cytokine/chemokine release plays an important role in the regulation of an immune response towards pathogens or injury (Lacy and Stow 2011). In order to evaluate the effect of PEPs on such biological reactions, levels of a wide range of these mediators were measured in SAECs following 24-hour exposure to PEPs (5 and 40 μg/mL administered doses). Of 41 measured cytokines/chemokines, six of them, namely monocyte chemotactic protein (MCP)-1, macrophage inflammatory protein (MIP)-1b, platelet-derived growth factor (PDGF)-AA, interleukin (IL)-1ra, IL-6 and RANTES were significantly increased in SAECs exposed to PEPs ($PM_{0.1}$) (Figure 3-3). Levels of MCP-1 and RANTES were significantly higher in the PEPs (40 μg/mL, administered dose) than in the control group. Similarly, elevated MIP-1b release was observed in cells exposed to PEPs (40 μg/mL) when compared to both the untreated and the PEPs (5 μg/mL, administered dose) treatment groups. Exposure to PEPs (5 μg/mL, administered dose) led to considerable rise in IL-1ra secretion when compared to untreated cells. Both doses of PEPs exposure triggered elevated release of PDGF-AA and IL-6 as opposed to administered dose-matched SiO_2 and MS-WF treatments. Additionally, significant differences in IL-6 were observed between the two PEPs exposure groups and the untreated cells.

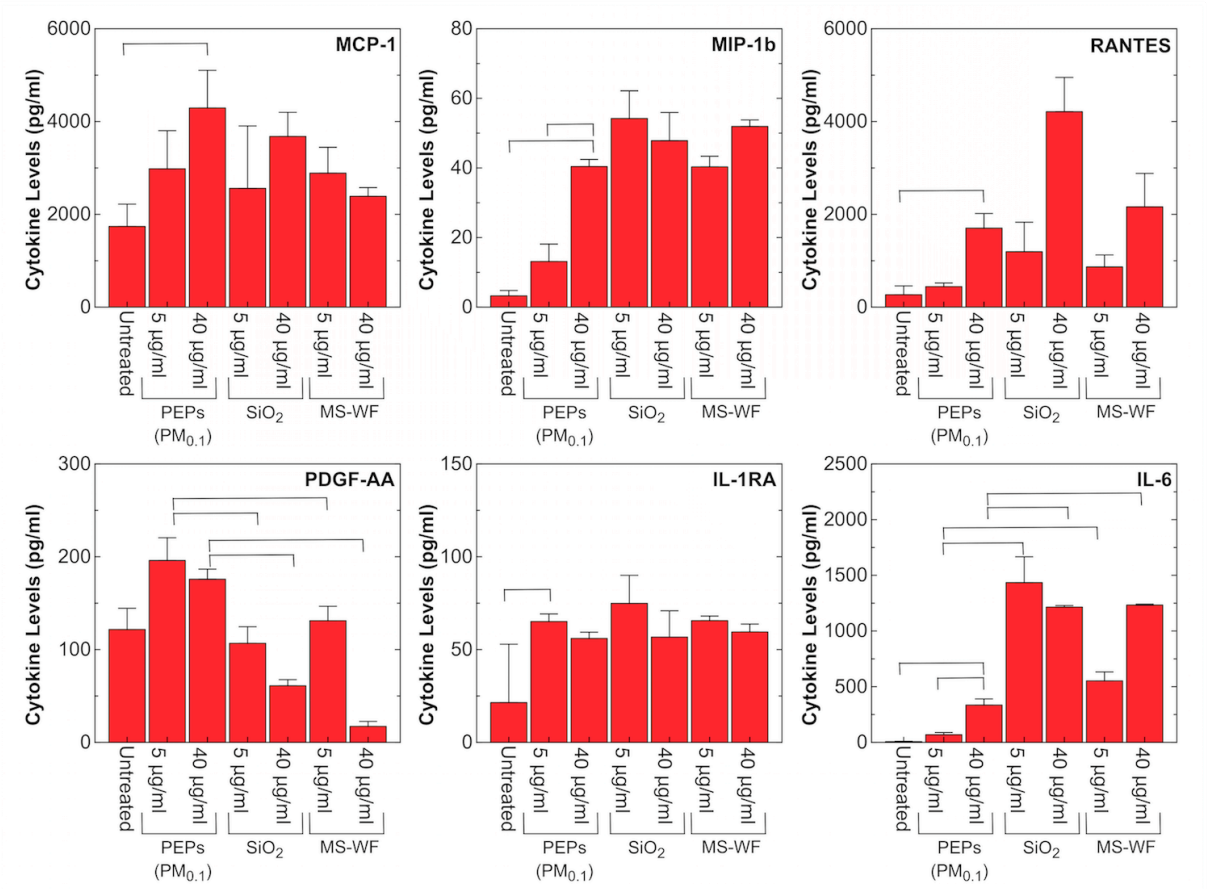

Figure 3-3. Measured levels of cytokines and chemokines in supernatant of SAECs exposed to PEPs, SiO_2 and MS-WF for 24 hours. All values are represented as mean ± SE. Bar represents a significant difference in measurements across the treatment groups with a p level < 0.05.

Exposure to PEPs does not cause genotoxicity in TK6

To evaluate the genotoxicity potential of PEPs, a DNA damage assessment was performed on human lymphoblasts, which are genetically sensitive to chemical exposures (Ayres et al. 2006; Kimura et al.). Results from the Nano-CometChip assay show PEPs did not inflict significant DNA damage on the lymphoblasts (Figure 3-S4). Likewise, neither of the

comparative testing particles (SiO_2, MS-WF) produced induction of single-stranded DNA damage when compared to untreated cells.

Exposure to PEPs results in loss of global and TEs-associated DNA methylation

L1 repetitive element comprises ~17% of the human genome, is heavily methylated, and therefore its methylation status is generally accepted as a surrogate biomarker for global DNA methylation. Therefore, to investigate whether or not short-term exposure to PEPs can affect the global DNA methylation, we evaluated methylation patterns of both L1 open reading frames (ORF1, ORF2). We report a 2.9-fold and 3.6-fold loss of DNA methylation in ORF1 and ORF2, respectively, although not statistically significant because of the high variability in L1 methylation in control samples (*p*-value 0.09, in both cases) after exposure to PEPs (0.5 μg/mL). Weak response was observed after exposure to the higher PEPs dose (Figure 3-4A).

Alu elements are another group of TEs that are highly abundant in the human genome (comprising ~10%), correspond to SINE elements in mice and can be affected by exogenous stressors (Rudin and Thompson 2001). Thus, we addressed whether the methylation of Alu elements is also affected by PEPs by examining the AluYb11 subfamily belonging to SINE1/7SL family of evolutionary-recent Alu elements. Similar to L1 ORF1 and ORF2, exposure to PEPs (0.5 μg/mL) resulted in more pronounced Alu hypomethylation than higher PEPs concentration (Figure 3-4B).

Exposure to PEPs leads to aberrant TEs expression

TEs methylation is a key mechanism in preventing their aberrant expression and their hypomethylation is often associated with TEs reactivation due to various environmental stressors (Koturbash et al. 2011; Rudin and Thompson 2001). Therefore, expression of L1 ORF2 was measured, as it is critical for activation and retrotransposition of L1. A significant and dose-

dependent reactivation of L1 ORF2 was observed post-PEPs exposure (1.5 and 1.7-fold, after treatment with 0.5 and 30 μg/mL, respectively) (Figure 3-4C). Transcriptional activation of L1 ORF2 may result in retrotransposition on the "copy-paste" based mechanism, thus increasing the L1 copy numbers in the genome. Therefore, the L1 copy numbers were analyzed; however, no significant differences were identified (Figure 3-4D). Similar to L1, congruent reactivation of Alu elements was detected, which is dependent on L1-associated Pol III. Although not statistically significant, a 1.15- and 1.32-fold increase was observed after exposure to 0.5 and 30 μg/mL of PEPs, respectively) (Figure 3-4C).

Alterations in DNA methylation are associated with decreased expression of DNA methylation machinery

To investigate further the mechanisms of observed global and TE-associated DNA hypomethylation, expression of DNA methyltransferases, key enzymes needed for establishment and maintenance of normal methylation patterns, was addressed. A significant and dose-dependent loss of expression of all three DNA methyltransferases (*DNMT1*, *DNMT3A*, *DNMT3B*) was detected after PEPs exposure (Figure 3-4E). Additionally, expression of *UHRF1*, the protein that recruits *DNMT1* to the hemimethylated DNA sites, was significantly reduced after PEPs exposure in a dose-dependent manner. A significant and dose-dependent decreased expression of all three methylcytosine dioxygenases (*TET1-TET3*) was observed (Figure 3-4E).

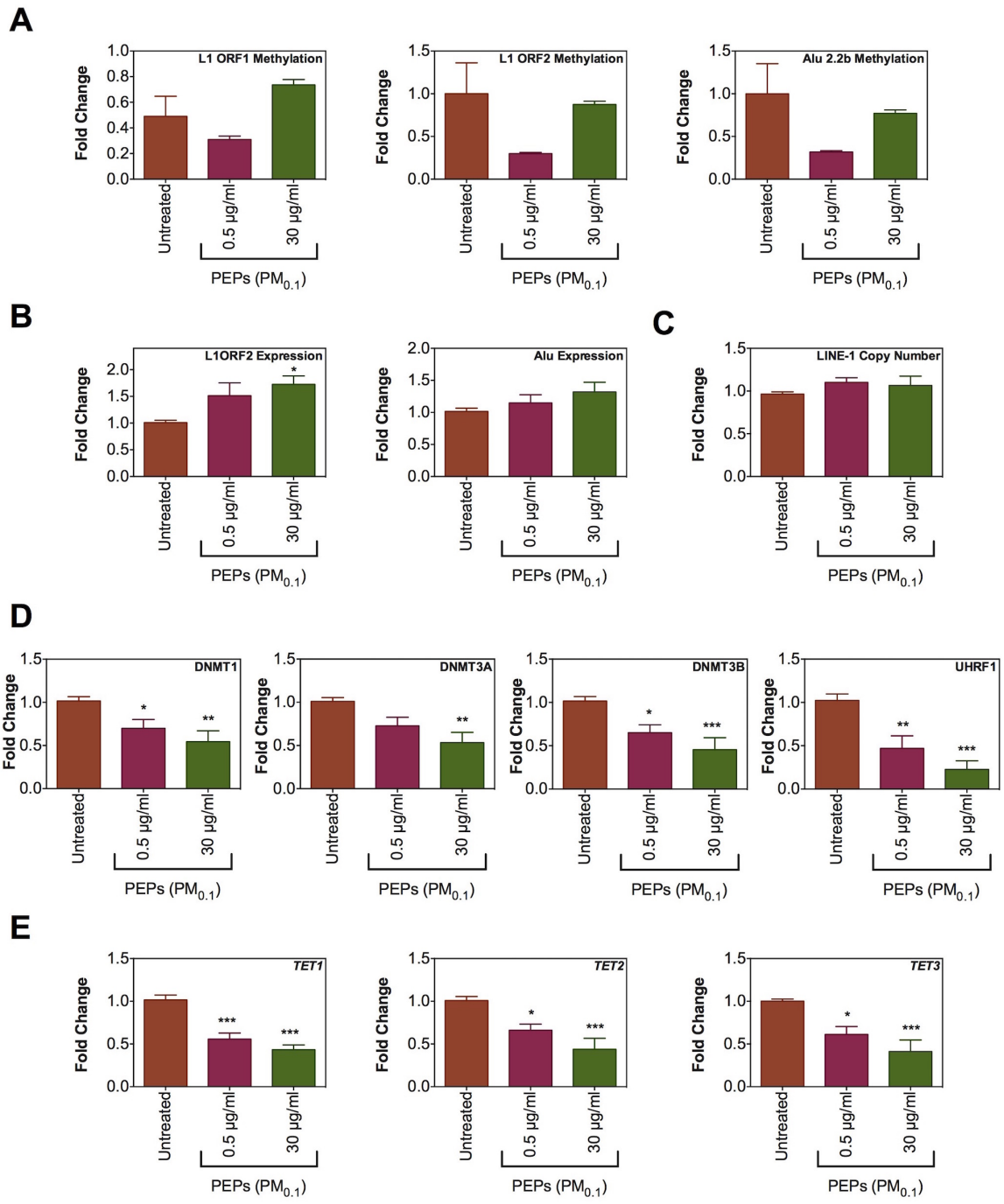

Figure 3-4. DNA methylation observed in SAECs exposed to PEPs for 24 hours. (A) fold change in 5-meC in TEs (B) mRNA expression of TEs (C) copy number (D) gene expression of DNMTs and accessory protein UHRF1. (E) Expression of methylcytosine dioxygenases (TET1-TET3) in SAECs exposed to PEPs for 24 hours. All values are represented as mean ± SE.

Discussion

We sought to evaluate the potential toxicity of varying doses of PEPs on three physiologically relevant cell lines. Using doses that approximate those associated with inhalation exposures, we measured cell viability, ROS production, inflammatory responses, DNA integrity and epigenetic changes. Since the aim of the study was to understand the biological response of cells following exposure to PEPs, doses on both the low end (0.5 μg/mL) and high end (100 μg/mL) of the spectrum were used. The low-end doses relate to real world exposure durations at the consumer level (*e.g.*, 8 hours of exposure to PEPs) while the high-end doses relate to accumulated exposures of hundreds of hours of exposure at consumer level. It must be noted that this dosimetric approach presented here may only be appropriate for short-term human exposures in the order of few days. Equating lifetime or multi-year exposure doses of accumulated PEPs mass in the alveolar region with bolus *in vitro* delivered doses ignores the differences in dose and rate of exposure. These differences may span many orders of magnitude, which can then affect clearance mechanisms and thus, the results may be highly misleading. Doses on the high end of the spectrum should only be considered as the high-end limit of an *in vitro* investigation and only when a wide range of doses, including low doses, is used (Oberdorster et al. 2012). Therefore the high end *in vitro* doses used here (100 μg/mL) were included in order to get the full spectrum of dose-dependent relationships.

This publication is part of a series of companion papers evaluating the toxicological profile of PEPs. In our first paper, eleven commonly used printers were evaluated and ranked based on their PM emission profiles using our developed PEGS platform (Pirela et al. 2014a). In the second companion paper, the complete physico-chemical and morphological properties of a number of toner powders and PEPs were thoroughly assessed (Pirela et al. 2014b). These two

publications established that toner particles constitute NEPs, whose ENMs become airborne during printing (consumer use). A third publication provided evidence that low level exposures to PEPs ($PM_{0.1}$, $PM_{2.5}$) led to changes in cellular morphology, ROS production and inflammation, among other biological outcomes using an *in vitro* alveolar-capillary co-culture model (Sisler et al. 2014). Investigating paracrine signaling by epithelial and endothelial cells is of utmost significance, since cellular communication between these two critical cell lines may play a major role in the pathogenesis of various pulmonary disorders.

Here, we investigated the toxicological potential of the smallest size fraction ($PM_{0.1}$) of PEPs from a high emitting laser printer (Printer B1 in our previous publications), which was found to emit more than one million particles/cm^3 using a mono-cell culture experimental design. Since the alveolar epithelium has direct contact with inhaled nanoparticles (Don Porto Carero et al. 2001) and the alveolar macrophages are the first responders to foreign particles in the lung, we exposed these cells to various concentrations of PEPs and observed the biological responses to these particles. Results showed that both the epithelial and the macrophage cell lines were negatively affected by treatment with PEPs and experienced >50% cell death, and with alveolar macrophages even at a cell delivered dose of 2.59 μg/mL (cell administered dose: 5 μg/mL). Of note, macrophages seem to be particularly sensitive to exposure to PEPs, which proved to be more toxic than a known pulmonary irritant (MS-WF). This is in agreement with a study by Khatri et al. (2013b), which showed subtle dose-response changes in viability of macrophages and small airway epithelial cells following a 24-hour exposure to photocopier-emitted particles that have similar chemical composition to PEPs. In addition to toxicity of PEPs ($PM_{0.1}$), we showed SAEC cell viability following exposure to PEPs ($PM_{0.1}$) was lower than that to PEPs ($PM_{2.5}$) at a dose of 2.5 μg/mL, indicative of greater potency of PEPs ($PM_{0.1}$) (Sisler et al. 2014).

In summary, these results point to significant cytotoxicity, which could lead to defects in the normal functioning of these cells, particularly on macrophages since one of their main functions is to engulf foreign materials. Cytotoxicity by PEPs to macrophages could impair their clearance mechanism, remodel cellular cross talking between different cell types as well as influence innate immune responses. The levels of cytotoxicity observed in the tested cell lines at doses comparable to current inhalation exposures, further intensifies recent concerns that PM emitted from laser printing equipment can trigger a toxicological response in the distal alveolar region, where the majority of the inhaled particles will deposit. Perhaps the toxicity of the emissions from printers can be attributed to their complex chemical composition, which includes various nano-sized metals/metal oxides that have already been shown to produce detrimental toxicological effects on various *in vitro* and *in vivo* studies. Such toxicological outcomes include decreased cell viability, increased production of reactive oxygen species and agglomeration of internalized nanoparticles due to exposure to various nanoparticles, including titania, silica, ceria, iron oxide, and silver, among others (Cohen et al. 2014a; Demokritou et al. 2013a; L'Azou et al. 2008; Watson et al. 2014). In summary, the vulnerability of alveoli and respiratory bronchioles to foreign particles highlights the necessity to understand the level of damage PEPs can have on the consumers' respiratory system and other organ systems (*i.e.*, cardiovascular and immunological) without disregarding susceptible individuals. It is also worth noting that similar to PEPs, our recent studies with photocopier-emitted particles illustrate that those particles may produce adverse responses in the lung physiology of those individuals exposed to them at relatively low doses (Khatri et al. 2013a; Khatri et al. 2013b; Pirela et al. 2013).

Another relevant parameter used to evaluate adverse effects of exposures to PM in general is secretion of cytokines. Expression of these chemical messengers in SAECs was

evaluated here to quantify the cellular inflammatory response to PEPs. Results showed that exposure to PEPs ($PM_{0.1}$) caused significant up-regulation of MCP-1, MIP-1b, PDGF-AA, IL-1ra, IL-6 and RANTES. These secreted mediators are critical in the innate immune responses to foreign particles, leading to recruitment of various leukocytes to the site of injury/inflammation (Hayden et al. 2009; Ritter et al. 2005). An increase in IL-6 and MCP-1 was also observed in our companion paper following a low level exposure to PEPs ($PM_{0.1}$, $PM_{2.5}$) using an epithelial-endothelial cell co-culture system (Sisler et al. 2014). These results were similar to those observed in a study by Setyawati et al. (2013), in which endothelial cells treated with titania nanoparticles reacted in a new non-receptor-mediated mechanism triggering a leakiness in the endothelial cell (Setyawati et al. 2013). Similarly, macrophages, primary nasal and small airway epithelial cells exposed to various doses of copier-emitted particles exhibited elevated secretion of various cytokines, including GM-CSF, IL-1b, IL-6, IL-8, TNF-a and VEGF (Khatri et al. 2013b). Furthermore, these similar cytokines were overexpressed in the nasal lavage of human volunteers (Khatri et al. 2013a). Particularly, MCP-1 is known to be a monocyte chemoattractant produced by a number of cells (*e.g.*, monocytes, macrophages) due to several stressors, such as oxidative damage, cytokine and growth factors. This chemokine regulates the migration and the infiltration of monocytes, memory T cells and natural killer cells to the site of injury, mainly leading to a differentiation of a Th2 response. Therefore, a modification in the levels of MCP-1 may hint that exposure to PEPs can affect the recruitment of monocytes/macrophages in the lung in order to eliminate invading these foreign particles *via* phagocytosis (Deshmane et al. 2009). Moreover, expression of MCP-1, can in turn contribute to an increase in the levels of IL-6, which blocks apoptosis. A study by Liu et al. (2007) found that MCP-1 mediated survival of fibroblasts by elevating IL-6 levels *via* the IL-6/STAT3 signaling pathway. Consequently, apoptosis of

fibroblasts was inhibited and resulted in maintenance of lung fibrosis. Additionally, the RANTES chemokine has been found to be strongly upregulated due to asbestos exposure, which causes malignant mesothelioma (Comar et al. 2014). Other cytokines that were significantly affected in pleural fibrosis as well as in malignant mesotheliomas include IL-6, IL-1B and IL-8, possibly through inflammasome activation (Hillegass et al. 2013). These cytokines were observed to be affected both in a mono- and co-culture model following exposure to PEPs (Sisler et al. 2014). Comparable changes in cytokine expression were also observed in a study by Dong et al. (2015), which evaluated the murine pulmonary response to multi-walled carbon nanotubes. A significant elevation in levels of TNFa, IL-1a and b, IL6, MCP-1 and PDGF was observed following exposure to the carbon nanotubes, which led to the conclusion that such exposure was associated to both an inflammatory and fibrotic response in the lung. However, more mechanistic studies looking at upstream effectors for a better understanding of the common process underlying the changes in cytokine expression, such as activation of NF-κB, are needed to enhance our understanding on inflammatory responses due to PEPs exposures. The authors plan to perform both *in vitro* and *in vivo* toxicological assessments to better understand the observed inflammatory responses in great detail and report findings in a future companion paper. In summary, the regulatory effect PEPs can have on cytokine release demonstrates that paracrine signaling can be influenced by PM emitted from printing processes, and this could trigger a biological response of the immune system to these exogenous materials.

Aside from inflammatory responses, an increase in superoxide levels was also evident in epithelial cells post-treatment with PEPs. Similar to our results, Sisler et al. (2014) observed an increment of ROS in endothelial cells after epithelial cells were exposed to low doses of PEPs using a co-culture platform. The same was not observed for the macrophages treated with PEPs,

whose cytotoxicity is almost 100% for the high dose of 100 μg/mL. However, the THP-1 cells produced very little ROS for same dose, suggesting that observed cytotoxicity of these cells might be mediated *via* an ROS-independent mechanism. Potential mechanisms other than ROS for ENMs may include direct activation of caspase-mediated apoptosis as observed by Wilhelmi et al. (2013) when macrophages were treated with zinc oxide nanoparticles, or less well defined surface reactivity effects (Frohlich et al. 2009), as well as through the HIF pathway (Nyga et al. 2015). More detailed mechanistic studies are needed in order to better understand the observed cytotoxicity. Overall, our data here is consistent with studies showing an increase in extracellular levels of reactive oxygen species and concomitant down-regulation of antioxidant levels following treatment with various doses of ENMs currently available in the market, such as ceria, titania and cobalt (Mittal and Pandey 2014; Wan et al. 2012; Zarogiannis et al. 2013). The excess cellular production of ROS in the respiratory system may cause detrimental effects to the distal areas of the lung.

Furthermore, the observed elevated levels of oxidation and inflammation prompted the assessment of DNA damage following exposure to PEPs using the newly developed high-throughput Nano-CometChip assay (Watson et al. 2014). The human lymphoblasts exposed to various doses of PEPs did not exhibit DNA damage and interestingly, our results are in disagreement with previous *in vitro* genotoxicity evaluations performed on human epithelial lung cells that displayed micronuclei formation and other characteristic injuries pertaining to DNA damage post-exposure to printer emissions and toner powder and toner powder (Gminski et al. 2011; Tang et al. 2012). Similar to our results, a study by Khatri et al. (2013b) using the comet assay concluded that treatment of macrophages with copier-emitted particles did not cause significant DNA damage. Lack of single-stranded DNA damage observed post-PEP exposure

could point to the possibility of double-stranded DNA damage or another type of toxicity mechanism responsible for the elevated cell death observed. It is important to note that heterogeneity in the PEPs chemical composition, well-documented in our earlier study (Pirela et al. 2014b), may explain differences in PEPs genotoxicity. This issue of variability in chemical makeup of PEPs and genotoxicity deserves further research.

In this study, the ability of PEPs to affect the cellular epigenome was demonstrated. Specifically, we demonstrate that short-term exposure to PEPs results in loss of global DNA methylation in SAECs and was exhibited as the hypomethylation of two most abundant TEs in the human genome – L1 and Alu that together comprise almost 30% of the genome.

DNA methylation is one of the key mechanisms that prevents aberrant transcriptional activity of TEs (Smith et al. 2012). Loss of DNA methylation within the TEs often results in their transcriptional activation (Koturbash et al. 2011; Rudin and Thompson 2001). Further, TEs reactivation, in turn, can result in retrotransposition events and lead to genomic instability and development of diseases, including cancer. In this study, we demonstrated that hypomethylation of TEs was strongly associated with their transcriptional activation. The expression of L1 ORF2 was found elevated after exposure to both concentrations of PEPs, with a significant increase observed after exposure to higher concentration. Similar trends were also observed in Alu elements. This transcriptional activation, however, did not result in potential retrotransposition events since no significant increase in L1 copies number after exposure to PEPs was identified. It is possible that the time of exposure used in our study was not sufficient for detectable L1 retrotransposition. Indeed, a recent study on chemical exposure and L1 retrotransposition report L1 mobilization after 120 hours of exposure in cell culture (Terasaki et al. 2013). Further studies

that will utilize longer exposures are clearly needed to determine the L1 retrotransposition abilities of PEPs.

DNA hypomethylation caused by exposure to PEPs was clearly associated with the loss of expression of DNA methyltransferases. These enzymes are essential for proper maintenance of DNA methylation. Loss of DNA methyltransferases *in vitro* was previously reported after short-term exposure to particulate matter (Miousse et al. 2014) and nano-SiO_2 particles (Gong et al. 2010) and was also associated with alterations in global and TEs DNA methylation. The observed profound down-regulation of DNA methyltransferases after exposure to PEPs may have detrimental effects on the levels of DNA methylation beyond the 24-hour time point that was used for the assessment in this study. Importantly, we provide evidence that hypomethylation of TEs and loss of expression of DNA methyltransferases may occur after exposure to low, environmentally relevant doses (0.5 μg/mL) of PEPs. The mechanisms of such alterations may be associated with metals present in PEPs. In their vast majority, metals are weak mutagens, but can negatively affect the DNA methyltransferases enzymatic activity (Fragou et al. 2011), leading to DNA hypomethylation. Furthermore, generation of reactive oxygen species, associated with metals present in PEPs, may compromise the normal redox status, alter glutathione content and affect one-carbon metabolism pathway (Koturbash et al. 2012). Hypomethylation may be also mediated by decreased levels of *UHRF1* gene, which specifically interacts with DNA methyltransferases and hemimethylated sites on DNA (Ehrlich and Lacey 2013). The exact mechanisms of PEPs-associated epigenotoxicity, however, still need to be determined. Additionally, an interesting potential of ROS-mediated mechanisms for the changes in DNA methylation could be up for debate as DNMT activity and modulation of DNMT-containing complexes have been observed in previous studies. For example, O'Hagan et al.

(2011) associated ROS-induced hypermethylation for promoter-specific regions and other sites of hypomethylation. Another study led by Campos et al. (2007) showed upregulation of the expression of genes for DNMTs by treatment with the superoxide ion. Interestingly, the loss of TEs methylation was not associated with increased function of methylcytosine deoxygenases, that navigate hydroxymethylation, the pathway that has been recently recognized in active DNA demethylation (He et al. 2011; Ito et al. 2011). Further studies will be needed to delineate the exact effects of exposure to PEPs on the levels of 5-hmC and TET expression, especially with regards to studies indicating loss of 5-hmC TET in numerous diseases, including cancer (Jin et al. 2011; Li et al. 2011).

In summary, exposure to PEPs may have the potential to trigger an unfavorable biological response in several physiologically relevant cell lines. A rise in cell death, oxidative stress, inflammation and altered methylation are some of the negative effects PEPs may have on the lung and may lead to increased risk of respiratory disorders in individuals who are exposed to emissions from laser printers.

Conclusion

The data indicate that PEPs emitted by laser printers can elicit unfavorable biological responses *in vitro*. Realistic exposures to PEPs led to significant changes in cell viability, hereditary genetic material changes, ROS and inflammatory mediators, among others. Moreover, the observed dysfunction of DNA methylation and demethylation machinery associated with the loss of DNA methylation and reactivation of TEs suggest that PEPs can cause a significant effect on the cellular epigenome. The results from such a comprehensive battery of toxicological assessments on PEPs are indicative of the cyto- and genotoxic potential of laser printer emissions at relevant doses comparable to current consumer and occupational settings. In order to further

investigate the mechanism of toxicity in more detail, a study on the murine responses of exposures to PEPs *via* intratracheal instillation and whole-body inhalation is currently in progress. Taken together, our mechanistically oriented toxicological studies could reveal the biological interaction of PEPs following exposures comparable to those experienced by a consumer when using laser printers.

Acknowledgements

The authors acknowledge funding for this study from NIEHS Center Grant ES-000002, NIOSH and CPSC (Grant # 212-2012-M-51174), NIH HL007118, UAMS/NIH Clinical and Translational Science Award UL1TR000039 and KL2TR000063 (IK), and the Arkansas Biosciences Institute, the major research component of the Arkansas Tobacco Settlement Proceeds Act of 2000 (IK).

Declaration of interests

The authors declare they have no competing financial interests.

Supplemental Material

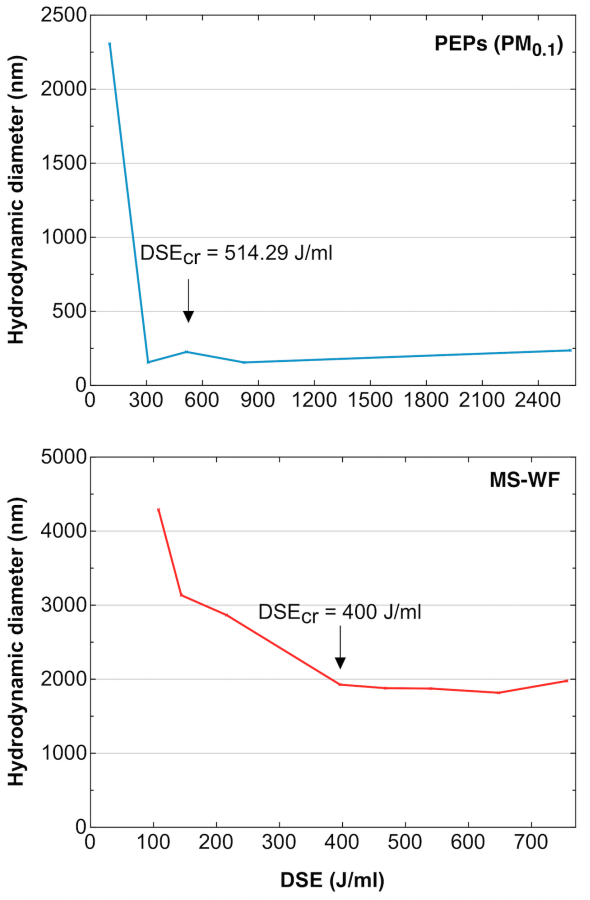

Supplemental Material, Figure 3-S1. Hydrodynamic diameter as a function of DSE for PEPs ($PM_{0.1}$) and MS-WF. DSE_{cr}: critical delivered sonication energy, energy required for minimal agglomeration.

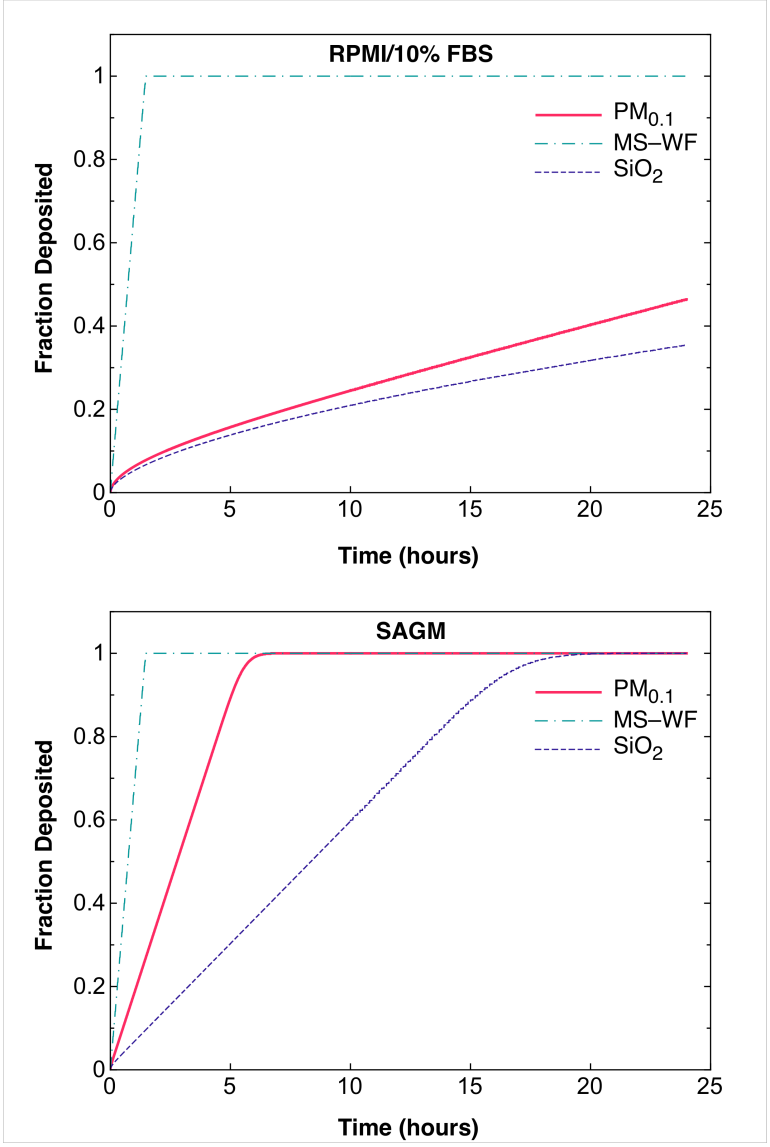

Supplemental Material, Figure 3-S2. Fraction of administered dose deposited, f_D, as a function of *in vitro* exposure time for PEPs ($PM_{0.1}$), SiO_2 and MS-WF calculated using the agglomeration diameter and estimated effective density. Plots are presented for the tested materials in the two media formulations (RPMI/10% FBS and SAGM).

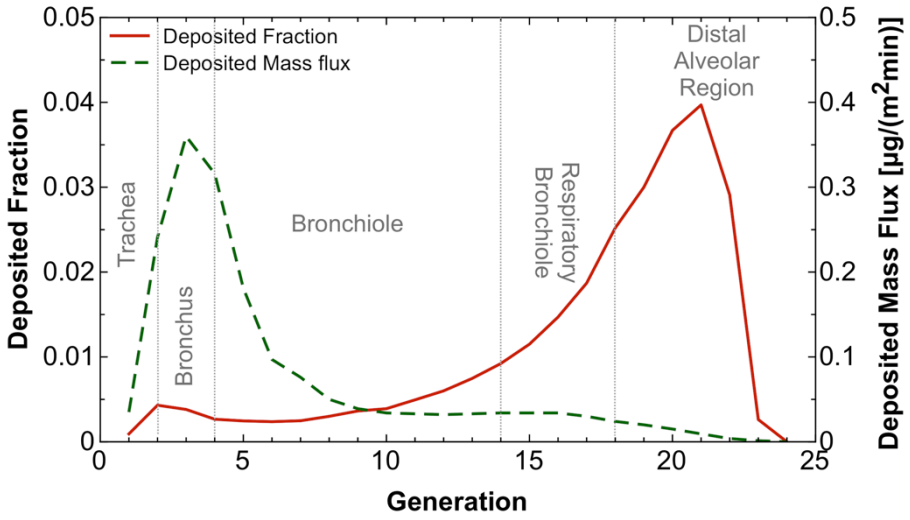

Supplemental Material, Figure 3-S3. Deposition mass flux (left axis) and deposition fraction (right axis) as a function of airway generation number.

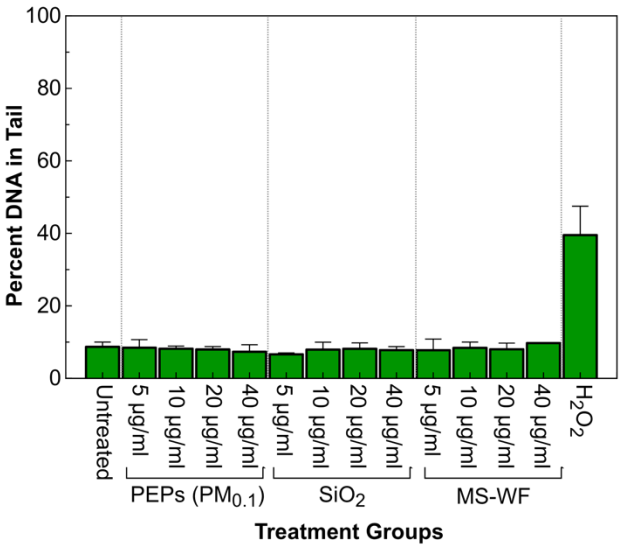

Supplemental Material, Figure 3-S4. Quantitative DNA damage assessment (Comet assay) of TK6 cells exposed for 4 hours to PEPs at various doses. All values are represented as mean ± SE.

Supplemental Material, Table 3-S1. Assays for determination of LINE-1 and Alu methylation.

	Forward Primer	**Reverse Primer**
Methylation		
LINE1 5'UTR (L1P1)	AAAGAAAGGGGTGACGGACG	TACCTAAGCAAGCCTGGGCAA
LINE1 ORF2	TGGAACCCTTGTGCACTGTT	CCAGAAGTGGAATTGCTGGA
Alu	GCCTGTAATCCCAGCACTTT	TCTCCTGCCTCAGCCTCC
Expression		
LINE1 ORF2	AAATGGTGCTGGGAAAACTG	GCCATTGCTTTTGGTGTTTT
Alu	CATGGTGAAACCCCGTCTCTA	GCCTCAGCCTCCCGAGTAG

Supplemental Material, Table 3-S2. Assays for determination of gene expression.

Gene Symbol	Assay Name	RefSeq #	Source
DNMT1	Hs.PT.56.28037916	NM_001130823	Integrated DNA Technologies
DNMT3A	Hs01027166_m1	NM_022552.4	Life Technologies
DNMT3B	Hs00171876_m1	NM_001207055.1	Life Technologies
GAPDH	Hs.PT.56.589810.g	NM_001256799	Integrated DNA Technologies
HMOX1	Hs01110250_m1	NM_002133.2	Life Technologies
TET1	Hs00286756_m1	NM_030625.2	Life Technologies
TET2	Hs00325999_m1	NM_001127208.2	Life Technologies
TET3	Hs00379125_m1	NM_144993.1	Life Technologies
UHRF1	Hs01086727_m1	NM_001048201.1	Life Technologies

Supplemental Material, Table 3-S3. *In vitro* doses and the respective consumer inhalation exposure duration to PEPs.

Particle	Cell administered dose[a] (µg/mL)	SAECs		THP-1	
		Cell delivered dose[a] (µg/mL)	Corresponding consumer inhalation exposure duration (hours) to PEPs [b]	Cell delivered dose[a] (µg/mL)	Corresponding consumer inhalation exposure duration (hours) to PEPs [b]
PEPs ($PM_{0.1}$)	0.5	0.5	15.0	0.26	7.8
	5	5	75.2	2.6	39.0
	10	10	150.4	5.2	77.9
	20	20	300.7	10.4	155.8
	30	30	451.1	15.6	233.7
	40	40	601.4	20.8	311.5
	100	100	1503.6	52.0	778.9
SiO_2	0.5	0.5	-	0.177	-
	5	5	-	1.77	-
	10	10	-	3.54	-
	20	20	-	7.08	-
	30	30	-	10.62	-
	40	40	-	14.16	-
	100	100	-	35.4	-
Mild steel welding fumes (MS-WF)	0.5	0.5	-	0.5	-
	5	5	-	5	-
	10	10	-	10	-
	20	20	-	20	-
	30	30	-	30	-
	40	40	-	40	-
	100	100	-	100	-

Notes:
[a] *In vitro* administered- and delivered-to-cell doses are based on a 24-hour *in vitro* exposure.
[b] Calculations of the corresponding consumer inhalation exposure duration (hours) to PEPs was based on the added values of deposition mass flux (µg/m^2•min) in the various human airways, excluding head airways: the conducting zone (generations 0 to 16) and the transitional and respiratory zones (generations 17 through 23).

Supplemental Material, Part A

Dosimetric considerations for in vitro testing – Example of calculations. The following example shows the step-by-step calculations performed to arrive at the number of hours of PEPs

inhalation that match the delivered-to-cell doses (*e.g.*, 0.5 μg/mL) used for the two cell lines (SAECs, THP-1) in the study.

1. **Choose the administered dose of interest used in the experiment to determine the corresponding inhalation exposure to PEPs.**
   For this example, we chose the administered dose of 0.5 μg/mL.

2. **Calculate the mass administered (μg) per well in a 96-well plate**
   Mass administered-to-cell in one well (μg) = administered dose * administered volume
   Mass administered-to-cell in one well (μg) = (0.5 μg/mL) * (0.1 mL) = 0.05 μg

3. **Converting the administered mass to delivered to cell dose as a function of the *in vitro* exposure time (t = 24 hrs) using the *in vitro* dosimetric methodology (Cohen et al. 2014):**

   The fraction of administered particle mass that is deposited on the cells in a standard 96-well plate as a function of *in vitro* exposure time (f_D) is calculated. For a 24-hour *in vitro* exposure, the f_D was found to be 1.0 for particles suspended in SAGM (SAECs) and 0.518 for particles suspended in RPMI/10%FBS (THP-1). Therefore, the delivered to cell *in vitro* mass is as follows:

   SAECs
   Delivered to cell mass (μg) = f_D*administered to cell mass (μg)=(1.00 * 0.05 μg) = 0.05 μg

   THP-1
   Delivered to cell mass (μg) = f_D*administered to cell mass (μg)=(0.518 * 0.05 μg) = 0.0259 μg

4. **Calculate the mass delivered-to-cells per well surface area (μg/m^2).**
   Dose delivered-to-cells per area (μg/m^2) = Mass delivered-to-cells (μg) / Surface area of one well in a 96-well plate (m^2)

   SAECs
   Dose delivered-to-cells per well area (μg/m^2) = (0.05 μg) / (0.000032 m^2) = 1,562.5 μg/m^2

   THP-1
   Dose delivered-to-cells per well area (μg/m^2) = (0.0259 μg) / (0.000032 m^2) = 809.4 μg/m^2

5. **Obtain deposited mass flux from MPPD2 model using the airborne nanoparticle size distribution values (*i.e.*, count median diameter, geometric standard deviation, particle mass concentration) and the human breathing parameters of a resting individual (*i.e.*, tidal volume, breathing frequency, inspiratory fraction, pause fraction, functional residual capacity, head volume, breathing route). These values can be found on Table 3-2.**

$$deposition\ mass\ flux = 1.732\ \mu g/m^2 \bullet min$$

6. **Calculate the human inhalation PEPs exposure duration (min) that matches the previously calculated *in vitro* dose delivered to cells by area (μg/m^2).**

SAECs

$T_{inhalation\ exposure}$ (min) = ?
Deposition mass flux (μg/m^2•min) = 1.732 μg/m^2•min
Dose delivered-to-cells by area (μg/m^2) = 1,562.5 μg/m^2

$T_{inhalation\ exposure}$ (min) = Mass delivered-to-cells per area (μg/m^2) / Deposition mass flux (μg/m^2•min)

$T_{inhalation\ exposure}$ = 902.14 min = 15.04 hours

THP-1

$T_{inhalation\ exposure}$ (min) = ?
Deposition mass flux (μg/m^2•min) = 1.732 μg/m^2•min
Dose delivered-to-cells by area (μg/m^2) = 809.4 μg/m^2

$T_{inhalation\ exposure}$ (min) = Mass delivered-to-cells per area (μg/m^2) / Deposition mass flux (μg/m^2•min)

$T_{inhalation\ exposure}$ = 467.32 min = 7.78 hours

Extraction of size fractionated PEPs and preparation of particle liquid suspensions

Prior to use in experiments, particle suspensions were prepared with sterile deionized water (DI H_2O), sonicating at DSE_{cr} and diluting to desired final test concentrations in the respective media. Measurements of d_H, PdI, ζ and σ of the particles suspended in cellular media were repeated to evaluate the properties of the formed particle agglomerates as described in Cohen et

al. (2012). Furthermore, colloidal stability of the suspensions, in DI H_2O and in media, was evaluated over various timepoints following sonication at DSE_{cr}. The effective density of the particle agglomerates in culture media was also measured using the volumetric centrifugation method (VCM), as described by DeLoid et al. (2014). Effective density is an important determinant of the fate and transport of the agglomerates and *in vitro* dosimetry (see below) (Cohen et al. 2014; DeLoid et al. 2014).

Cellular assays - Epigenetics

Nucleic Acids Extraction. RNA and DNA were extracted simultaneously from flash-frozen SAEC using AllPrep Mini Kit (Qiagen, Valencia, CA) according to manufacturer's protocol. DNA concentrations and integrity were analyzed by the Nanodrop 2000 (Thermo Scientific, Waltham, MA). Only DNA samples with 260/280 ratios between 1.8 and 1.9 (DNA) and 1.95 and 2.05 (RNA), and 260/230 ratios above 1.5 (DNA, RNA) were considered for further molecular analyses.

Analysis of 5-methylcytosine (5-mC) and 5-hydroxymethylcytosine (5-hmC). 0.02 mg/mL of RNase A (Sigma, St. Louis, MO) was added to 1 μg of genomic DNA and incubated (37°C, 15 minutes). The purified DNA was digested into component nucleotides using Nuclease P1, snake venom phosphodieasterase, and alkaline phosphatase as previously described (James, 2010). The digested nucleotides were stored at −20°C until LC/MS/MS analysis. Base separation was performed with a Dionex HPLC system coupled to an electrospray ionization (ESI) tandem mass spectrometer (Thermo-Finnigan LCQ) using a Phenomenex Gemini column (C18, 150x2.0 mm, 3μm particle size) and established methodology.

Analysis of transposable elements methylation status. Methylation status of LINE-1 (L1) and Alu transposable elements was determined by the methylation-sensitive quantitative real-time

PCR. One μg of genomic DNA was digested with 0.5 U of SmaI enzyme in 1X CutSmart buffer (25°C, 2 hours). This was followed by 16-hours digestion (37°C) in presence of 0.5 U of enzymes HpaII, HhaI and AciI in 1X CutSmart buffer. Digestion finalized by adding 0.5 U of BstUI enzyme in 1X CutSmart buffer (60°C, 4 hours). All enzymes were purchased from New England Biolabs (Biolabs, Ipswich, MA). Digested DNA was analyzed by qPCR on a ViiA 7 Real-Time PCR System (Applied Biosystems, Forrest City, CA). DNA samples not digested with restriction enzyme mix served as positive control, while samples lacking specific primers for DNA amplification and/or DNA template and SAEC-derived DNA pre-treated with 5-azacytidine served as negative controls. The threshold cycle (Ct) was defined as fractional cycle number passing the fixed threshold. Ct values were converted into absolute amount of input DNA using the absolute standard curve method and further normalized towards rDNA readings. Assays for determination of LINE-1 and Alu methylation are provided in Supplemental Material, Table 3-S1.

Quantitative reverse transcription polymerase chain reaction (qRT-PCR). Complementary DNA (cDNA) was synthesized from one μg RNA using random primers and a High Capacity cDNA Reverse Transcription Kit (Applied Biosystems, Foster City, CA) according to the manufacturer's protocol. Quantitative real-time PCR (qRT-PCR) to determine the levels of gene transcripts was performed using ten ng of cDNA/reaction and the TaqMan Universal PCR Master Mix, no AmpErase® UNG (Life Technologies) on a ViiA 7 instrument (Life Technologies, Carlsbad, CA). Assay IDs used in the study are provided in Supplemental Material, Tables S1-S2. The ΔΔCt were calculated as previously described (Schmittgen and Livak, 2008). Fold change data were calculated from ΔΔCt values. All qRT-PCR reactions were conducted in triplicate and repeated twice.

L1 copy numbers analysis. L1 copy numbers were assessed as following: L1 ORF1 was amplified by qRT-PCR from 10 ng of gDNA. Relative abundance of the target in gDNA was normalized to 5S ribosomal DNA using the ΔΔCt method. The FAM/ZEN-conjugated primers with probe sequence are shown in Supplemental Material, Table S2. Amplification was performed for 40 cycles using conditions for the 2X Taqman Universal Master Mix following manufacturer's recommendation (Life Technologies, Carlsbad, CA).

Bibliography

Anjilvel S, Asgharian B. 1995. A multiple-path model of particle deposition in the rat lung. Fundam Appl Toxicol 28:41-50.

Antonini J, Lawryk N, Murthy G, Brain J. 1999. Effect of welding fume solubility on lung macrophage viability and function in vitro. J Toxicol Environ Health A 58:343-363.

Antonini J, Zeidler-Erdely P, Young S, Roberts J, Erdely A. 2012. Systemic immune cell response in rats after pulmonary exposure to manganese-containing particles collected from welding aerosols. Journal of immunotoxicology 9:184-192.

Ayres FM, Cruz ADd, Steele P, Glickman BW. 2006. Low doses of gamma ionizing radiation increase hprt mutant frequencies of TK6 cells without triggering the mutator phenotype pathway. Genetics and molecular biology 29:558-561.

Baccarelli A, Wright RO, Bollati V, Tarantini L, Litonjua AA, Suh HH, et al. 2009. Rapid DNA methylation changes after exposure to traffic particles. American journal of respiratory and critical care medicine 179:572-578.

Bai R, Zhang L, Liu Y, Meng L, Wang L, Wu Y, et al. 2010. Pulmonary responses to printer toner particles in mice after intratracheal instillation. Toxicol Lett 199:288-300.

Bajpayee M, Kumar A, Dhawan A. 2013. The comet assay: Assessment of in vitro and in vivo DNA damage. Methods in molecular biology 1044:325-345.

Campos AC, Molognoni F, Melo FH, Galdieri LC, Carneiro CR, D'Almeida V, et al. 2007. Oxidative stress modulates DNA methylation during melanocyte anchorage blockade associated with malignant transformation. Neoplasia 9:1111-1121.

Cohen J, Deloid G, Pyrgiotakis G, Demokritou P. 2013. Interactions of engineered nanomaterials in physiological media and implications for in vitro dosimetry. Nanotoxicology 7:417-431.

Cohen JM, Derk R, Wang L, Godleski J, Kobzik L, Brain J, et al. 2014a. Tracking translocation of industrially relevant engineered nanomaterials (ENMs) across alveolar epithelial monolayers in vitro. Nanotoxicology 8 Suppl 1:216-225.

Cohen JM, Teeguarden JG, Demokritou P. 2014b. An integrated approach for the in vitro dosimetry of engineered nanomaterials. Part Fibre Toxicol 11:20.

Comar M, Zanotta N, Bonotti A, Tognon M, Negro C, Cristaudo A, Bovenzi M. 2014. Increased Levels of C-C Chemokine RANTES in Asbestos Exposed Workers and in Malignant Mesothelioma Patients from an Hyperendemic Area. PLoS One 9(8): e104848.

Daigneault M, Preston JA, Marriott HM, Whyte MK, Dockrell DH. 2010. The identification of markers of macrophage differentiation in PMA-stimulated THP-1 cells and monocyte-derived macrophages. PloS one 5:e8668.

DeLoid G, Cohen JM, Darrah T, Derk R, Rojanasakul L, Pyrgiotakis G, et al. 2014. Estimating the effective density of engineered nanomaterials for in vitro dosimetry. Nature communications 5:3514.

Demokritou P, Kavouras IG, Ferguson ST, Koutrakis P. 2002. Development of a high volume cascade impactor for toxicological and chemical characterization studies. Aerosol Science and Technology 36:925-933.

Demokritou P, Buchel R, Molina RM, Deloid GM, Brain JD, Pratsinis SE. 2010. Development and characterization of a versatile engineered nanomaterial generation system (VENGES) suitable for toxicological studies. Inhal Toxicol 22 Suppl 2:107-116.

Demokritou P, Gass S, Pyrgiotakis G, Cohen JM, Goldsmith W, McKinney W, et al. 2013. An in vivo and in vitro toxicological characterisation of realistic nanoscale CeO2 inhalation exposures. Nanotoxicology 7:1338-1350.

Doak SH, Griffiths SM, Manshian B, Singh N, Williams PM, Brown AP, et al. 2009. Confounding experimental considerations in nanogenotoxicology. Mutagenesis 24:285-293.

Don Porto Carero A, Hoet PH, Verschaeve L, Schoeters G, Nemery B. 2001. Genotoxic effects of carbon black particles, diesel exhaust particles, and urban air particulates and their extracts on a human alveolar epithelial cell line (A549) and a human monocytic cell line (THP-1). Environmental and molecular mutagenesis 37:155-163.

Dong J, Porter DW, Battelli LA, Wolfarth MG, Richardson DL, Ma Q. 2015. Pathologic and molecular profiling of rapid-onset fibrosis and inflammation induced by multi-walled carbon nanotubes. Arch Toxicol 89(4):621-633.

Ehrlich M, Lacey M. 2013. DNA hypomethylation and hemimethylation in cancer. Advances in experimental medicine and biology 754:31-56.

Fragou D, Fragou A, Kouidou S, Njau S, Kovatsi L. 2011. Epigenetic mechanisms in metal toxicity. Toxicology mechanisms and methods 21:343-352.

Frohlich E, Samberger C, Kueznik T, Absenger M, Roblegg E, Zimmer A, et al. 2009. Cytotoxicity of nanoparticles independent from oxidative stress. The Journal of toxicological sciences 34:363-375.

Furukawa Y, Aizawa Y, Okada M, Watanabe M, Niitsuya M, Kotani M. 2002. Negative effect of photocopier toner on alveolar macrophages determined by in vitro magnetometric evaluation. Industrial health 40:214-221.

Gminski R, Decker K, Heinz C, Seidel A, Konczol M, Goldenberg E, et al. 2011. Genotoxic effects of three selected black toner powders and their dimethyl sulfoxide extracts in cultured human epithelial A549 lung cells in vitro. Environ Mol Mutagen 52:296-309.

Gong C, Tao G, Yang L, Liu J, Liu Q, Zhuang Z. 2010. Sio(2) nanoparticles induce global genomic hypomethylation in HaCaT cells. Biochemical and biophysical research communications 397:397-400.

Hayden PJ, Bolmarcich J, Armento A, Jackson J, G.R. H, T.L. K, et al. 2009. Role of toll-like receptor (TLR) activation in asthma exacerbation: Experiments with in vitro models of human airway epithelial cells (epiairway) and epithelial cell/fibroblast co-cultures (epiairway-ft). In: American Thoracic Society Annual Meeting. San Diego, CA.

He C, Morawska L, Taplin L. 2007. Particle emission characteristics of office printers. Environmental science & technology 41:6039-6045.

He YF, Li BZ, Li Z, Liu P, Wang Y, Tang Q, et al. 2011. TET-mediated formation of 5-carboxylcytosine and its excision by TDG in mammalian DNA. Science 333:1303-1307.

Hillegass M, Miller JM, MacPherson MB, Westbom CM, Sayan M, Thompson JK, Macura SL, Perkins TN, Beuschel SL, Alexeeva V, Pass HI, Steele C, Mossman BT, Shukla A. 2013.

Asbestos and erionite prime and activate the NLRP3 inflammasome that stimulates autocrine cytokine release in human mesothelial cells. Part Fibre Toxicol 10:39.

Holder AL, Goth-Goldstein R, Lucas D, Koshland CP. 2012. Particle-induced artifacts in the MTT and LDH viability assays. Chemical research in toxicology 25:1885-1892.

IDC. 2014. Idc finds continued growth in the worldwide hardcopy peripherals market in the fourth quarter of 2013 Framingham, Massachusetts.

Ito S, Shen L, Dai Q, Wu SC, Collins LB, Swenberg JA, et al. 2011. TET proteins can convert 5-methylcytosine to 5-formylcytosine and 5-carboxylcytosine. Science 333:1300-1303.

Iwamoto T, Okamoto H, Toyama Y, Momohara S. 2008. Molecular aspects of rheumatoid arthritis: Chemokines in the joints of patients. The FEBS journal 275:4448-4455.

Jin SG, Jiang Y, Qiu R, Rauch TA, Wang Y, Schackert G, et al. 2011. 5-hydroxymethylcytosine is strongly depleted in human cancers but its levels do not correlate with IDH1 mutations. Cancer research 71:7360-7365.

Jones PA. 2012. Functions of DNA methylation: Islands, start sites, gene bodies and beyond. Nature reviews Genetics 13:484-492.

Khatri M, Bello D, Gaines P, Martin J, Pal AK, Gore R, et al. 2013a. Nanoparticles from photocopiers induce oxidative stress and upper respiratory tract inflammation in healthy volunteers. Nanotoxicology 7:1014-1027.

Khatri M, Bello D, Pal AK, Cohen JM, Woskie S, Gassert T, et al. 2013b. Evaluation of cytotoxic, genotoxic and inflammatory responses of nanoparticles from photocopiers in three human cell lines. Part Fibre Toxicol 10:42.

Kimura A, Miyata A, Honma M. 2013. A combination of in vitro comet assay and micronucleus test using human lymphoblastoid TK6 cells. Mutagenesis 28:583-590.

Koturbash I, Scherhag A, Sorrentino J, Sexton K, Bodnar W, Tryndyak V, et al. 2011. Epigenetic alterations in liver of C57Bl/6J mice after short-term inhalational exposure to 1,3-butadiene. Environmental health perspectives 119:635-640.

Koturbash I, Simpson NE, Beland FA, Pogribny IP. 2012. Alterations in histone H4 lysine 20 methylation: Implications for cancer detection and prevention. Antioxidants & redox signaling 17:365-374.

L'Azou B, Jorly J, On D, Sellier E, Moisan F, Fleury-Feith J, et al. 2008. In vitro effects of nanoparticles on renal cells. Part Fibre Toxicol 5:22.

Lacy P, Stow JL. 2011. Cytokine release from innate immune cells: Association with diverse membrane trafficking pathways. Blood 118:9-18.

Li Z, Cai X, Cai CL, Wang J, Zhang W, Petersen BE, et al. 2011. Deletion of TET2 in mice leads to dysregulated hematopoietic stem cells and subsequent development of myeloid malignancies. Blood 118:4509-4518.

Liu X, Das AM, Seideman J, Griswold D, Afuh CN, Kobayashi T, Abe S, Fang Q, Hashimoto M, Kim H, Wang X, Shen L, Kawasaki S, Rennard SI. 2007. The CC chemokine ligand 1 (CCL2) mediates fibroblast survival through IL-6. Am J of Resp Cell and Mol Bio 37(1):121-128.

Madrigano J, Baccarelli A, Mittleman MA, Wright RO, Sparrow D, Vokonas PS, et al. 2011. Prolonged exposure to particulate pollution, genes associated with glutathione pathways, and DNA methylation in a cohort of older men. Environmental Health Perspectives 119:977-982.

Miousse IR, Chalbot MC, Aykin-Burns N, Wang X, Basnakian A, Kavouras IG, et al. 2014. Epigenetic alterations induced by ambient particulate matter in mouse macrophages. Environ Mol Mutagen 55:428-435.

Mittal S, Pandey AK. 2014. Cerium oxide nanoparticles induced toxicity in human lung cells: Role of ROS mediated DNA damage and apoptosis. BioMed research international 2014:891934.

Monteiro-Riviere NA, Inman AO, Zhang LW. 2009. Limitations and relative utility of screening assays to assess engineered nanoparticle toxicity in a human cell line. Toxicology and applied pharmacology 234:222-235.

Morawska L, He C, Johnson G, Jayaratne R, Salthammer T, Wang H, et al. 2009. An investigation into the characteristics and formation mechanisms of particles originating from the operation of laser printers. Environmental science & technology 43:1015-1022.

Morimoto Y, Oyabu T, Horie M, Kambara T, Izumi H, Kuroda E, et al. 2013. Pulmonary toxicity of printer toner following inhalation and intratracheal instillation. Inhal Toxicol 25:679-690.

Nyga A, Hart A, Tetley TD. 2015. Importance of the HIF pathway in cobalt nanoparticle-induced cytotoxicity and inflammation in human macrophages. Nanotoxicology:1-13.

Oberdorster, G. 2012. Nanotoxicology: in Vitro–in Vivo Dosimetry. Environmental Health Perspectives 120(1):a13.

O'Hagan HM, Wang W, Sen S, Destefano Shields C, Lee SS, Zhang YW, et al. 2011. Oxidative damage targets complexes containing DNA methyltransferases, SIRT1, and polycomb members to promoter CpG islands. Cancer cell 20:606-619.

Pal AK, Cohen J, Bello D, Demokritou P. 2014. Implications of in-vitro dosimetry on toxicological ranking of low aspect ratio engineered nanomaterials. Nanotoxicology.

Pirela S, Molina R, Watson C, Cohen JM, Bello D, Demokritou P, et al. 2013. Effects of copy center particles on the lungs: A toxicological characterization using a Balb/c mouse model. Inhal Toxicol 25:498-508.

Pirela SV, Pyrgiotakis G, Bello D, Thomas T, Castranova V, Demokritou P. 2014a. Development and characterization of an exposure platform suitable for physico-chemical, morphological and toxicological characterization of printer-emitted particles (PEPs). Inhal Toxicol 26:400-408.

Pirela SV, Sotiriou GA, Bello D, Shafer M, Bunker KL, Castranova V, et al. 2014b. Consumer exposures to laser printer-emitted engineered nanoparticles: A case study of life-cycle implications from nano-enabled products. Nanotoxicology:1-9.

Ritter M, Mennerich D, Weith A, Seither P. 2005. Characterization of toll-like receptors in primary lung epithelial cells: Strong impact of the TLR3 ligand poly(i:C) on the regulation of toll-like receptors, adaptor proteins and inflammatory response. J Inflamm (Lond) 2:16.

Rudin CM, Thompson CB. 2001. Transcriptional activation of short interspersed elements by DNA-damaging agents. Genes, chromosomes & cancer 30:64-71.

Deshmane SL, Kremlev S, Amini S, Sawaya BE. 2009. Monocyte Chemoattractant Protein-1 (MCP-1): An Overview. J Interferon Cytokine Res 29(6): 313-326.

Setyawati MI, Tay CY, Chia SL, Goh SL, Fang W, Neo MJ, et al. 2013. Titanium dioxide nanomaterials cause endothelial cell leakiness by disrupting the homophilic interaction of VE-cadherin. Nature communications 4:1673.

Sisler JD, Pirela SV, Friend S, Farcas M, Schwegler-Berry D, Shvedova A, et al. 2014. Small airway epithelial cells exposure to printer-emitted engineered nanoparticles induces cellular

effects on human microvascular endothelial cells in an alveolar-capillary co-culture model. Nanotoxicology:1-11.

Smith ZD, Chan MM, Mikkelsen TS, Gu H, Gnirke A, Regev A, et al. 2012. A unique regulatory phase of DNA methylation in the early mammalian embryo. Nature 484:339-344.

Sotiriou GA, Diaz E, Long MS, Godleski J, Brain J, Pratsinis SE, et al. 2012. A novel platform for pulmonary and cardiovascular toxicological characterization of inhaled engineered nanomaterials. Nanotoxicology 6:680-690.

Sriram K, Lin GX, Jefferson AM, Roberts JR, Andrews RN, Kashon ML, et al. 2012. Manganese accumulation in nail clippings as a biomarker of welding fume exposure and neurotoxicity. Toxicology 291:73-82.

Tang T, Gminski R, Konczol M, Modest C, Armbruster B, Mersch-Sundermann V. 2012. Investigations on cytotoxic and genotoxic effects of laser printer emissions in human epithelial A549 lung cells using an air/liquid exposure system. Environ Mol Mutagen 53:125-135.

Terasaki N, Goodier JL, Cheung LE, Wang YJ, Kajikawa M, Kazazian HH, Jr., et al. 2013. In vitro screening for compounds that enhance human l1 mobilization. PloS one 8:e74629.

Wan R, Mo Y, Feng L, Chien S, Tollerud DJ, Zhang Q. 2012. DNA damage caused by metal nanoparticles: Involvement of oxidative stress and activation of ATM. Chemical research in toxicology 25:1402-1411.

Wang H, He C, Morawska L, McGarry P, Johnson G. 2012. Ozone-initiated particle formation, particle aging, and precursors in a laser printer. Environmental science & technology 46:704-712.

Watson C, Ge J, Cohen J, Pyrgiotakis G, Engelward BP, Demokritou P. 2014. High-throughput screening platform for engineered nanoparticle-mediated genotoxicity using CometChip technology. ACS nano 8:2118-2133.

Wilhelmi V, Fischer U, Weighardt H, Schulze-Osthoff K, Nickel C, Stahlmecke B, et al. 2013. Zinc oxide nanoparticles induce necrosis and apoptosis in macrophages in a p47phox- and NRF2-independent manner. PloS one 8:e65704.

Zarogiannis SG, Filippidis AS, Fernandez S, Jurkuvenaite A, Ambalavanan N, Stanishevsky A, et al. 2013. Nano-TiO(2) particles impair adhesion of airway epithelial cells to fibronectin. Respiratory physiology & neurobiology 185:454-460.

Zeidler-Erdely P, Battelli L, Salmen-Muniz R, Li Z, Erdely A, Kashon M, et al. 2011. Lung tumor production and tissue metal distribution after exposure to manual metal arc-stainless steel welding fume in A/J and C57Bl/6J mice. Journal of toxicology and environmental health Part A 74:728-736.

Chapter 4: Small airway epithelial cells exposure to printer-emitted engineered nanoparticles induces cellular effects on human microvascular endothelial cells in an alveolar-capillary co-culture model

Jennifer D. Sisler[1], Sandra V. Pirela[2], Sherri Friend[1], Mariana Farcas[1], Diane Schwegler-Berry[1], Anna Shvedova[1], Vincent Castranova[3], Philip Demokritou[2*], and Yong Qian[1*]

Nanotoxicology. 2014.

[1]Pathology and Physiology Research Branch, Health Effects Laboratory Division, National Institute for Occupational Safety and Health, Morgantown, WV, USA,

[2]Department of Environmental Health, Harvard School of Public Health, Harvard University, Boston, MA, USA,

[3]Department of Basic Pharmaceutical Sciences, West Virginia University, Morgantown, WV, USA

[*]Corresponding author

For the contents of this chapter, please refer to Appendix A.

Chapter 5: Short-term exposure to engineered nanomaterials affects cellular epigenome

Xiaoyan Lu[1], Isabelle R.Miousse[2], Sandra V. Pirela[1], Stepan Melnyk[3], Igor Koturbash[2*], Philip Demokritou[1*]

Nanotoxicology. 2014.

[1]Center for Nanotechnology and Nanotoxicology, Department of Environmental Health, Harvard School of Public Health, Boston, MA, USA

[2]Department of Environmental and Occupational Health, College of Public Health, University of Arkansas for Medical Sciences, Little Rock, AR, USA

[3]Department of Pediatrics, University of Arkansas for Medical Sciences, Little Rock, AR, USA

[*]Corresponding authors:

For the contents of this chapter, please refer to Appendix B.

Chapter 6: A pilot study investigating the murine biological responses following acute exposure to printer-emitted particles either *via* intratracheal instillation and whole-body inhalation

Sandra V. Pirela[1], Xiaoyan Lu[1], Jennifer Sisler[2], Nancy Gao[2], Vincent Castranova[3], Treye Thomas[4], Philip Demokritou[1*]

[1] Department of Environmental Health, Center for Nanotechnology and Nanotoxicology, School of Public Health, Harvard University, 665 Huntington Ave., Boston, MA, USA.

[2] Pathology and Physiology Research Branch, Health Effects Laboratory Division, National Institute for Occupational Safety and Health, Morgantown, WV, USA.

[3] Department of Basic Pharmaceutical Sciences, West Virginia University, Morgantown, WV, USA.

[4] U.S. Consumer Product Safety Commission, Office of Hazard Identification and Reduction, Rockville, MD, USA.

*Corresponding author.

Keywords: nanoparticles, printers, photocopiers, inflammation, lung injury.

Running title: pulmonary toxicity of nanoparticles emitted by laser printers.

Abstract

Incorporation of engineered nanomaterials (ENMs) into toners used in laser printers has led to countless quality and performance improvements. However, the release of ENMs during printing (consumer use) raises concerns about their potential adverse health effects. The aim of this study was to use "real world" printer-emitted particles (PEPs), rather than raw toner powder, to assess the pulmonary responses following exposure using an animal model. Nine-week old male *Balb/c* mice were exposed to PEPs at various doses either *via* intratracheal instillation (0.5, 2.5 and 5 mg/kg bw) or whole-body inhalation (6 and 30 hours). Toxicological parameters reflecting distinct mechanisms of action were performed. Results from this preliminary toxicological analysis showed that while exposure to PEPs does not cause immediate lung injury as indicated by unaffected levels of lactate dehydrogenase, there were increases in white blood cell differentials and neutrophil degranulation as well as upregulation in expression of the CCL5 (RANTES), NOS1, BCL2, UCP2 and AKT1 genes. Based on the results, we can conclude that PEPs may cause inflammatory responses in addition to modifications in gene expression at doses that can be comparable to consumer exposure scenarios.

Introduction

The use of laser printers leads to exposure to various pollutants, including ozone, volatile organic compounds and particulate matter (PM), among others pollutants (He et al. 2007; Morawska et al. 2009; H Wang et al. 2012). In particular, the release of a significant number of particles –the majority of which are in the nano scale- during the use of this growing technology has become a reason of concern. In order to assess the complex chemistry of printer emitted particles (PEPs) and potential health hazards of these emissions, a Printer Exposure Generation

System (PEGS) was recently developed that allows the generation and sampling of airborne PEPs for subsequent physico-chemical, morphological and toxicological analyses (Pirela et al. 2014a). The PM emission profiles from 11 laser printers were evaluated and further characterization, on both raw toner powder and PEPs, was performed. The detailed analysis showed that during a print job, the evaluated laser printers emit up to 1.3 million particles/cm^3, of which the majority of such particles has modal diameters of <200 nm (Pirela et al. 2014a). Moreover, a study by Pirela et al. (2014b) confirmed not only the presence of nanoscale materials in the airborne state but also their complex chemistry, which include elemental and organic carbon, as well as inorganic compounds such as metals and metal oxides. It has been now confirmed that toners are classified as nano-enabled products (NEPs).

Toxicological evidence on the PEPs continues to rise. In a series of recently published papers, several physiologically relevant cell lines such as small airway epithelial cells, human microvascular endothelial cells, macrophages and lymphoblasts were treated with various doses of PEPs ($PM_{0.1}$, $PM_{2.5}$) using both mono- and co-culture exposure systems (Pirela et al. 2015; Sisler et al. 2014). In both studies, it was shown that PEPs triggered an unfavorable series of biological responses in macrophages, small airway epithelial cells and microvascular endothelial cells at doses comparable to approximately 8 hours or more of consumer inhalation to PEPs. Specifically, the PEPs led to significant changes in cell viability, hereditary genetic material changes, reactive oxygen species (ROS) and inflammatory mediators, among others.

Moreover, dysfunction of DNA methylation and demethylation machinery associated with the loss of DNA methylation and reactivation of TEs shown in recently published studies (Lu et al. 2015; Pirela et al. 2015) suggest that PEPs can cause a significant effect on the cellular epigenome. Additionally, a more detailed analysis of the changes in epigenetics in small airway

epithelial cells due to exposure to PEPs found a substantial upregulation of heme oxygenease 1 and a decrease in the methylation status of repetitive elements (*i.e.*, transposable elements, LINE-1, Alu elements) due to the 24-hour treatment with PEPs (Lu et al. 2015).

Notably, the toxicity of PEPs remains poorly characterized *in vitro*, and the few *in vivo* studies in the published domain used toner powders rather than emitted PEPs. For example, Bai et al. (2010) reported that mice exposed to printer toner particles showed significant pulmonary inflammation, damage to the epithelial-capillary barrier and enhanced cell permeability. Comparable inflammatory and fibrotic responses were also observed in rats exposed to toner powders (Morimoto et al. 2013). A historic rodent chronic inhalation exposure concluded that toner led to substantial lung weight, chronic inflammatory response, incidence of primary lung tumors, as well as lung fibrosis in exposed rats (Muhle et al. 1991). However, as extensive as these studies were in identifying the biological response in the rodent lung following exposure to toner, they are limited by addressing only the toxicity of toner powder which might be relevant for occupational settings and workers handling toner powders but not relevant to consumers using laser printers.

In this study, we sought to further expand on the recently published cellular toxicology studies performed by our group on PEPs (Lu et al. 2015; Pirela et al. 2015; Sisler et al. 2014). Here, we present findings on the murine responses of exposures to various doses and size fractions of PEPs either *via* intratracheal instillation or whole-body inhalation. The endpoints evaluated included levels of lactate dehydrogenase, myeloperoxidase, white blood cell differentials, expression of a number of genes involved in immune responses and cell survival and signaling, among other important biological processes.

Methods

Experimental design

Figure 6-1 shows the exposure platform used for the study, which includes: the Harvard Compact Cascade Impactor (CCI) (Demokritou et al. 2002) for collection of PEPs used for the intratracheal instillation exposure and the BUXCO system for the inhalation exposure scenario.

A group of mice were exposed to various exposure doses and durations of PEPs either *via* intratracheal instillation or whole-body inhalation. Following the exposure, animals were sacrificed and bronchoalveolar lavage (BAL) was performed. The BAL fluid (BALF), blood and lung tissue were subsequently used to measure biochemical markers of inflammation, albumin and hemoglobin levels, white blood cell differentials and expression of a number of genes.

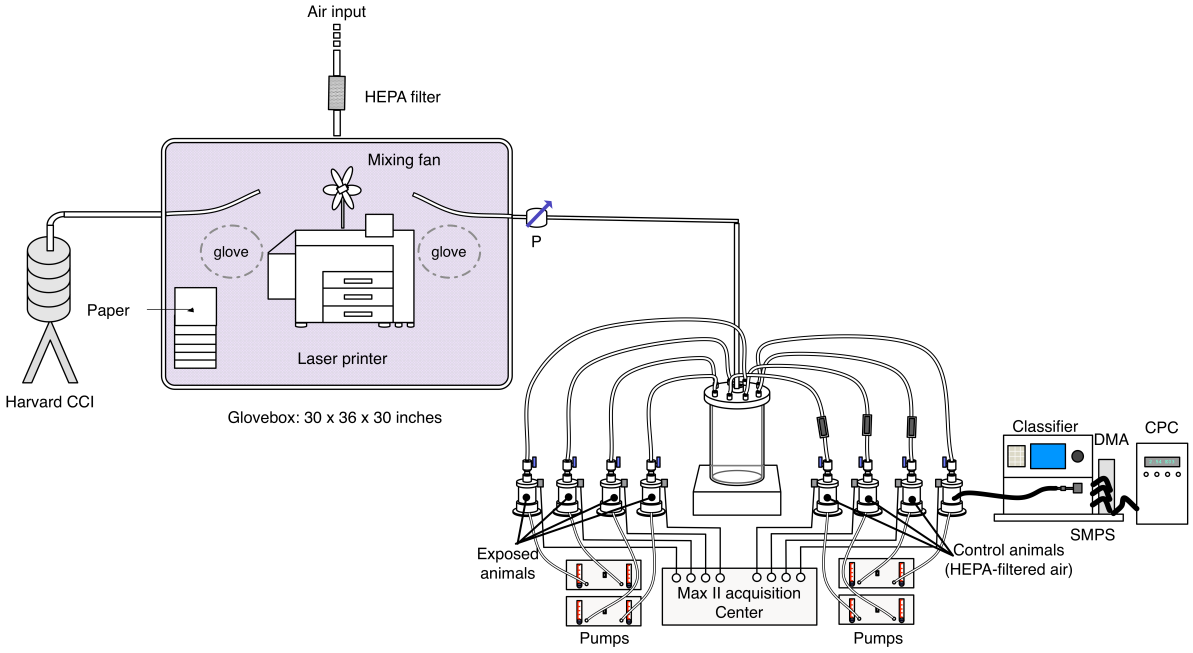

Figure 6-1. Printer Generation Exposure System (PEGS) used in the murine exposure to PEPs.

Animals

Eight-week-old *Balb/c* male mice weighing an average of 24.25 grams (SD = 1.92) were purchased from Taconic Farms Inc. (Hudson, NY). Mice were housed in groups of 4 in

polypropylene cages and allowed to acclimate for 1 week before the studies were initiated. Mice were maintained on a 12-hour light/dark cycle. Food and water were provided *ad libitum*. Animal protocols used in this study were approved by the Harvard Medical Area Institutional Animal Care and Use Committee (IACUC).

Methodology for *in vivo* exposure to PEPs

Generation of airborne PM for whole-body inhalation exposures. The PEGS platform (Pirela et al. 2014a) was used to perform the inhalation experiment with the BUXCO system. The Printer B1 was initiated to start a 5%-page coverage print job continuously throughout the whole exposure duration. HEPA-filtered air was circulated at a flow rate of 60 liters/minute until the chamber background particle concentration reaches approximately 200 particles/cm^3. Once this level was attained, the chamber airflow rate was reduced to ~3 L/min, which is the total airflow required by the real-time and time-integrated instrumentation. The generated PEPs were directed to 4 of the BUXCO chambers, while the remaining 4 other mouse chambers received HEPA-filtered air (control exposure). The animals were exposed to PEPs for 6 hours/day for either one day or 5 consecutive days. At the end of exposures, the mice were sacrificed and bronchoalveolar lavage was performed. The bronchoalveolar lavage fluid was then analyzed for biochemical markers for damage and white blood cell differentials.

Sampling and preparation of size-fractionated airborne PM for intratracheal instillation exposures. The size-fractionated PEPs were sampled using the Harvard Compact Cascade Impactor (CCI) (Demokritou et al. 2004) onto polyurethane foam (PUF) impaction substrates ($PM_{2.5}$) and Teflon filters ($PM_{0.1}$). These were weighed pre- and post-sampling following a 48-hour stabilization process in a temperature (22ºC ± 1) and humidity (43% ± 2) controlled environmental chamber using a Mettler Toledo XPE analytical microbalance. Thus,

the weight difference was used to determine the collected PEPs mass during the printing episode. After sampling size-fractionated PEPs, the particles were extracted from collection filter media using an aqueous suspension methodology as previously described (Pirela et al. 2014b). Subsequently, particle dispersions in deionized water (DI H_2O) were prepared using a protocol developed by the authors (Cohen et al. 2012), in which the particle critical delivered sonication energy (DSE_{cr}), hydrodynamic diameter (d_H), formed agglomerate size distribution, polydispersity index (PdI), zeta potential (ζ), specific conductance (σ), colloidal stability and effective density of formed agglomerates (DeLoid et al. 2014) were measured for all particle suspensions used in the study. Results from the characterization of PEPs have been extensively described (Pirela et al. 2014b; Sisler et al. 2014). Once the particle suspensions were prepared for intratracheal instillation of PEPs, each mouse was weighed and the dose calculated at 2.5 mL/kg bw. The dosing solution was measured in a sterile syringe with an attached blunt-tipped 21-gauge gavage needle. The mice were anesthetized with vaporized isoflurane, quickly restrained on a slanted board and held upright by their upper incisor teeth resting on a rubber band. As the animals were under anesthesia, the tip of the needle was gently inserted into the trachea between the vocal cords, with the tip just above the tracheal bifurcation, and the dosing suspension was delivered in one bolus. After instillation, the animal was allowed to recover from anesthesia in a slanted position while the thorax was gently massaged to facilitate distribution of the instillate throughout the lungs. The mice received an intratracheal instillation of PEPs ($PM_{0.1}$) at 0.5, 2.5 and 5.0 mg/kg bw and vehicle control (DI H_2O).

In vivo dosimetry considerations

The Multiple Path Particle Deposition model (MPPD2, Anjilvel and Asgharian, 1995) was used to calculate the lung deposition fraction and deposition mass flux of the particles

emitted from a high emitting laser printer (Printer B1 in our previous publications) on the rodent respiratory system. Table 6-1 summarizes the parameters used for the MPPD2 simulations, which include both the rodent breathing parameters (tidal volume, breathing frequency, inspiratory fraction, pause fraction, functional residual capacity, head volume, breathing route) and the airborne nanoparticle size distribution values (count median diameter, geometric standard deviation, particle mass concentration).

Table 6-1. Summary of parameters used in the *in vivo* lung Multiple Path Particle Deposition model (MPPD2)[1].

Rodent Model	**Breathing Parameters**	**Airborne Nanoparticle Distribution**
Functional Residual Capacity: 4.0 mL	*Tidal Volume*: 2.1 mL	*Count Mean Diameter:* 57.45 nm
Head Volume: 0.42 mL	*Breathing Frequency:* 102 breaths/min	*Geometric Standard Deviation*: 1.67
Breathing Route: Nasal	*Inspiratory Fraction*: 0.5	*Mass Concentration*: 23.86 $\mu g/m^3$
	Pause Fraction: 0.0	

Bronchoalveolar lavage and analyses performed post exposure to PEPs

Twenty-four hours after intratracheal instillations and immediately following whole-body inhalation exposure to PEPs, mice were anaesthetized with an intraperitoneal injection of FatalPlus (0.1-0.2 mL), and sacrificed by exsanguination, followed by bronchoalveolar lavage (BAL). The lungs were lavaged *in situ* with 12 washes of 0.75 mL of sterile 0.9% saline. The first two washes were pooled for biochemical assays. Cells were separated from the supernatant in all washes (400 x g at 40 °C for 10 minutes). Total and differential cell counts, as well as

hemoglobin measurements were made from the cell pellets. Total cell counts were performed manually using a hemocytometer. Cell smears were made with a cytocentrifuge (Shandon Southern Instruments, Inc., Sewickley, PA) and stained with Diff-Quick (American Scientific Products, McGaw Park, IL). Differential cell counts were performed by counting 200 cells per mouse. The supernatant fraction of the first two washes was clarified by sedimentation at 15 000 x g for 30 minutes and used for measurement of enzyme activity, albumin and cytokine measurements. Standard spectrophotometric assays were used for lactate dehydrogenase (LDH), myeloperoxidase (MPO), albumin, and hemoglobin (Hb) to identify damage to the lungs as described in Beck et al. (1982).

Multiplex cytokine analysis

Cytokine levels in BAL fluid were measured by Eve Technologies Corporation (Calgary, Alberta, Canada) using a MILLIPLEX Mouse Cytokine/Chemokine 32-plex kit (Millipore, St. Charles, MO) according to the manufacturer's protocol. The 32-plex consisted of eotaxin, G-CSF, GM-CSF, IFN-gamma, IL-1alpha, IL-1beta, IL-2, IL-3, IL-4, IL-5, IL- 6, IL-7, IL-9, IL-10, IL-12 (p40), IL-12 (p70), IL-13, IL-15, IL-17, IP-10, KC, LIF, LIX, MCP-1, M-CSF, MIG, MIP-1alpha, MIP-1beta, MIP-2, RANTES, TNF-alpha, and VEGF. The sensitivities of the assay to these markers ranged from 0.3 to 63.6 pg/mL.

Genetic expression

The RNA from the lungs of mice instilled with PEPs (2.5 mg/kg) and vehicle control (DI H_2O) was isolated. cDNA was amplified following the manufacturer protocol of the High Capacity cDNA Reverse Transcription kit. The cDNA was used to analyze the following genes: EGFr, GPX1, PPARg, STAT3, VEGFa, Riiad1, AOX1, SOD1, TGFB1, NOS1, CCL5, BCL2, UCP2 and AKT1 using TaqMan Universal PCR Master Mix and TaqMan primers according to

manufacturer guidelines. Relative gene expression was analyzed using the $2^{-\Delta\Delta CT}$ method with POLR2a as the internal control.

Statistical analysis

Statistical analyses were performed using GraphPad Prism 6.0 (La Jolla, CA). Comparisons between all bronchoalveolar lavage fluid parameters after exposure to PEPs and control were evaluated using one-way analysis of variance (ANOVA) and Tukey correction for multiple comparison statistical significance. A p-value of 0.05 was considered significant.

Results

In vivo dosimetry considerations

The inhaled mass deposited across rodent lung as well as the deposition mass flux were calculated using the MPPD2 model (Figure 6-2). The PEPs deposited mass per murine body weight following 6 and 30 hours of inhalation exposure was calculated to be 0.4 and 1.9 mg/kg, respectively and fall within the range of doses (*i.e.*, 0.5, 2.5, 5.0 mg/kg) chosen for the intratracheal instillation experiments. Table 6-2 shows the doses of exposure to PEPs across the two treatment experiments performed in this study, as well as the equivalent inhalation time for a consumer would have to be exposed to PEPs to obtain the same mass deposition.

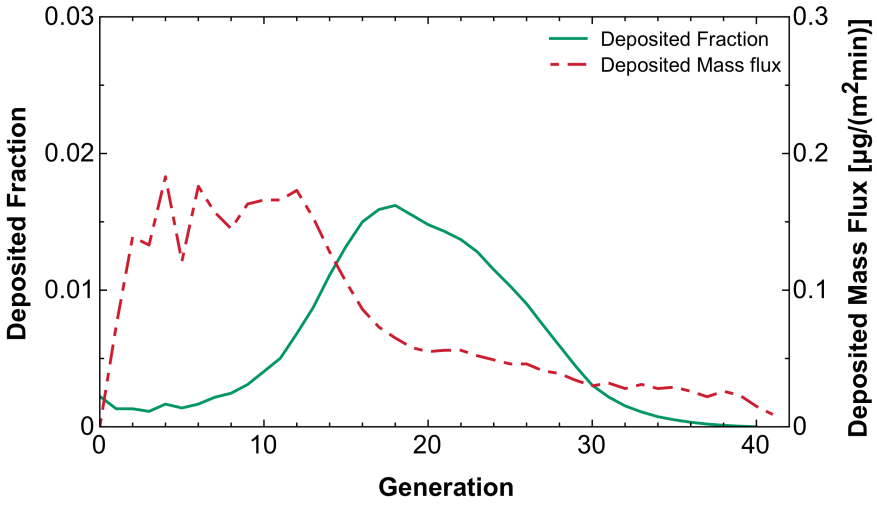

Figure 6-2. Deposition mass flux and deposition fraction of the mass of PEPs inhaled as a function of generation number.

Table 6-2. Comparison of doses of murine PEPs exposures used in the study *via* intratracheal instillation and whole-body inhalation with comparable human inhalation exposures to PEPs.

PEPs exposure *via* IT (mg/kg bw)	**PEPs exposure *via* whole-body inhalation (hours)**	**Duration of inhalation exposure of PEPs (hours)**
0.38	6	13.9
0.5	8	18.5
1.9	30	69.2
2.5	40	92.3
5.0	80	185

Characterization of PEPs exposure

Whole-body inhalation. The representative exposure scenario for the PEPs inhalation experiment is shown in Figure 6-3. The particle concentration in the exposure chamber from the PEGS averaged at 479,513 particles/cm^3 for 6 hours; however, levels as high as close to 1

million particles/cm^3 were measured (Figure 6-3A). The size distribution of the printer emissions did not vary in size throughout the 6-hour exposure window. Particularly, the geometric mean of the particle diameter ranged from 33.26 to 44.82 nm (Figure 6-3B).

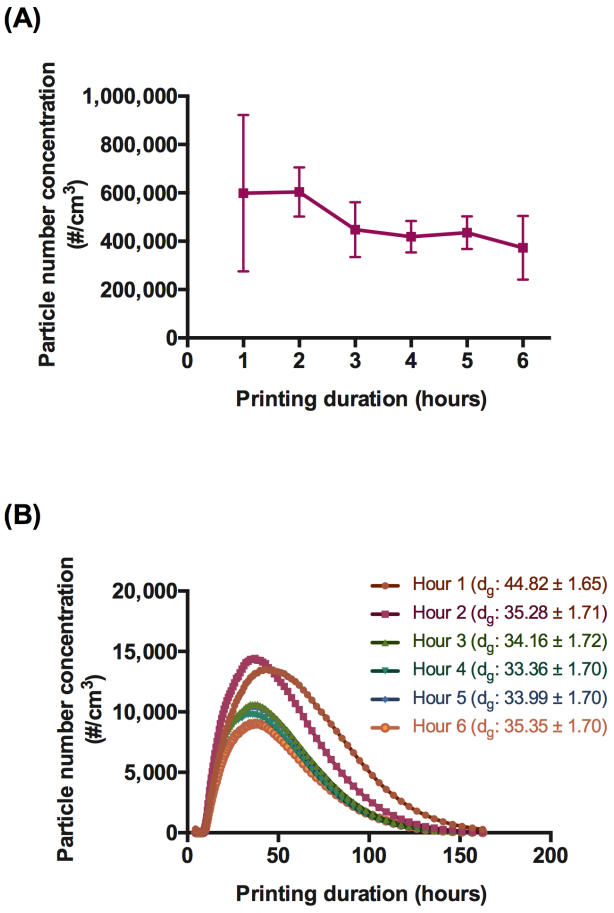

Figure 6-3. Representative average PEPs (A) size distribution and (B) total emitted particle number concentration generated by laser Printer B1 during a 6-hour exposure duration using the BUXCO system. Error bars represent standard deviation for the average total particle number concentration.

Intratracheal instillation. Particle dispersions were prepared for one size fraction of PEPs ($PM_{0.1}$) by suspending them in DI H_2O. Table 6-3 summarizes the particle behavior in

suspension as described by diameter (d_H), zeta potential (ζ), polydispersity index (PdI) and specific conductance (σ). These properties have been explained in studies previously published by our group (Pirela et al. 2015; Sisler et al. 2014). Briefly, the smallest size fraction of PEPs ($PM_{0.1}$) when suspended in DI H_2O was monodispersed and had an average hydrodynamic diameter of approximately 180 nm.

Table 6-3. Properties of laser printer emitted particle dispersions. d_H: hydrodynamic diameter, PdI: polydispersity index, ζ: zeta potential, σ: specific conductance.

Material	Media	d_H (nm)	PdI	ζ (mV)	σ (mS/cm)
PEPs ($PM_{0.1}$)	DI H_2O	178.3 ± 3.459	0.403 ± 0.050	-20.6 ± 1.87	0.185 ± $5.8x10^{-4}$

Notes: Values represent the mean (± SD) of a triplicate reading.

Biological murine response following exposure to PEPs *via* whole-body inhalation

To test the possibility of a transient effect due to PEPs treatment, animals were exposed to freshly generated PEPs for either 6 or 30 hours and their bronchoalveolar lavage fluid was subsequently analyzed.

Pulmonary membrane integrity and neutrophil degranulation. Levels of lactate dehydrogenase were substantially elevated in both the gaseous pollutant and the PEPs/gaseous pollutant exposed mice after 6 hours when compared to the longer exposure. Concentration of myeloperoxidase was significantly elevated following only in the PEPs/gaseous pollutant exposed group (6 hours) to both the dose-matched control and the 30-hour counterpart exposure (Figure 6-4A). No change was observed in the amount of hemoglobin and albumin in the bronchoalveolar lavage fluid of the exposed animals (data not shown).

Inflammatory cellular response. The murine white blood cell population exhibited slight

differences in the neutrophil and lymphocyte percent lavaged, albeit not statistically significant, between the PEPs exposure of 6 and 30 hours. (Figure 6-4B). No differences in the percent population of macrophages were exhibited by PEPs-exposed mice (data not shown).

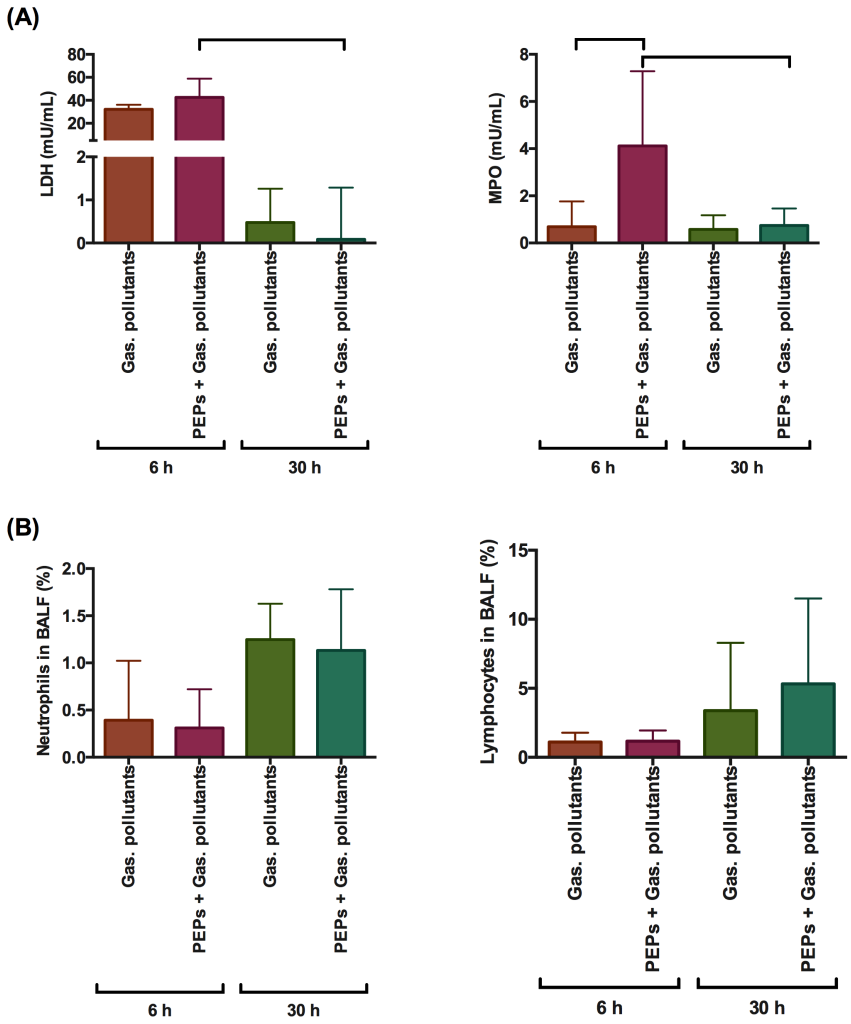

Figure 6-4. BALF markers of lung injury following exposure to PEPs *via* whole-body inhalation. (A) Expression of extracellular Lactate Dehydrogenase (LDH), Myeloperoxidase (MPO). (B) Percentage of lavageable neutrophils and lymphocytes. Values are expressed as means (±SD). Bar represents a significant difference between the two groups.

Biological murine response following exposure to PEPs *via* intratracheal instillation

In order to assess the potential toxicity of PEPs exposure *via* intratracheal instillation, mice treated with 0.5, 2.5 and 5.0 mg/kg of PEPs, as well as DI H_2O (vehicle control) were sacrificed 24-hours post exposure for the following analysis:

Pulmonary membrane integrity and neutrophil degranulation. The bronchoalveolar lavage fluid from mice exposed to 0.5, 2.5 and 5.0 mg/kg of PEPs ($PM_{0.1}$) was evaluated and compared to that of the vehicle control group (DI H_2O) (Figure 6-5). No significant differences in lactate dehydrogenase or myeloperoxidase were observed between the PEPs and the control treatment groups (Figure 6-5A). No differences were observed in the levels of hemoglobin or albumin across the different treatment groups (data not shown).

Inflammatory cellular response. Significant differences in white blood cell population were visible in the percent of neutrophils present in the bronchoalveolar lavage fluid of mice exposed to PEPs at the highest dose (5 mg/kg) compared to the vehicle control and the lowest dose of PEPs (Figure 6-5B). A dose dependent elevation in the neutrophil population is visible across the three doses of PEPs instilled. A minor increase in lymphocytes was observed in the 0.5 and 2.5 mg/kg PEPs exposure group only. Conversely, there was a marked decrease exhibited after exposure to 5 mg/kg of PEPs. The macrophage population remained unchanged across the exposure groups (data not shown).

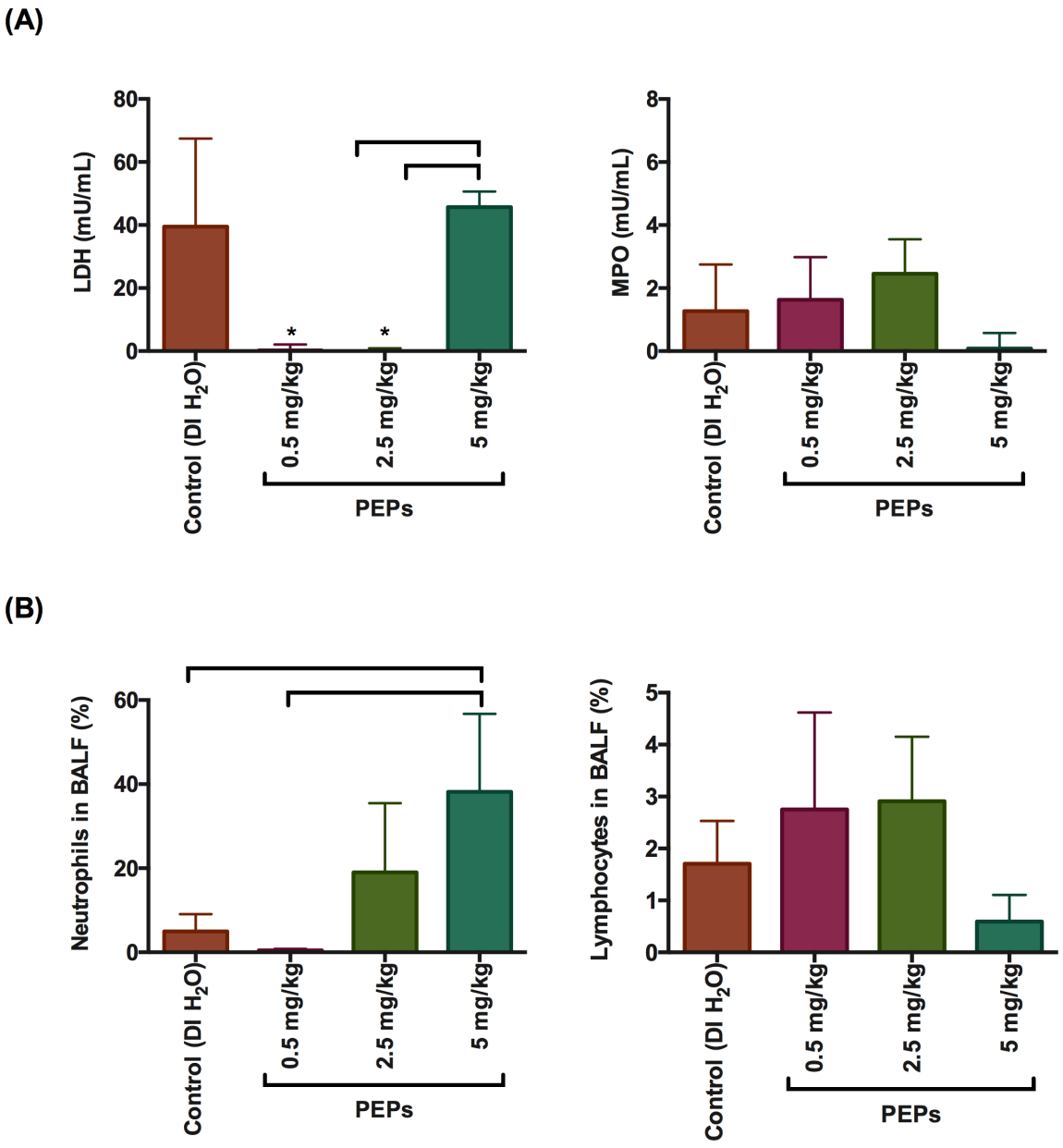

Figure 6-5. BALF markers of lung injury following exposure to PEPs *via* intratracheal instillation. (A) Expression of extracellular Lactate Dehydrogenase (LDH), Myeloperoxidase (MPO). (B) Percentage of lavaged neutrophils and lymphocytes. Values are expressed as means (±SD). Bar represents a significant difference between the two groups.

Genetic expression. The lung tissue was used to analyze the RNA and quantify the expression of a number of genes in both the PEPs-treated and the vehicle control group. The genes evaluated included EGFr, GPX1, PPARg, STAT3, VEGFa, Riiad1, AOX1, SOD1, TGFB1, NOS1, CCL5, BCL2, UCP2 and AKT1. In the PEPs exposure group, there was an evident elevation in the fold induction of NOS1, CCL5, BCL2, UCP2 and AKT1 in comparison to the control group (Figure 6-6).

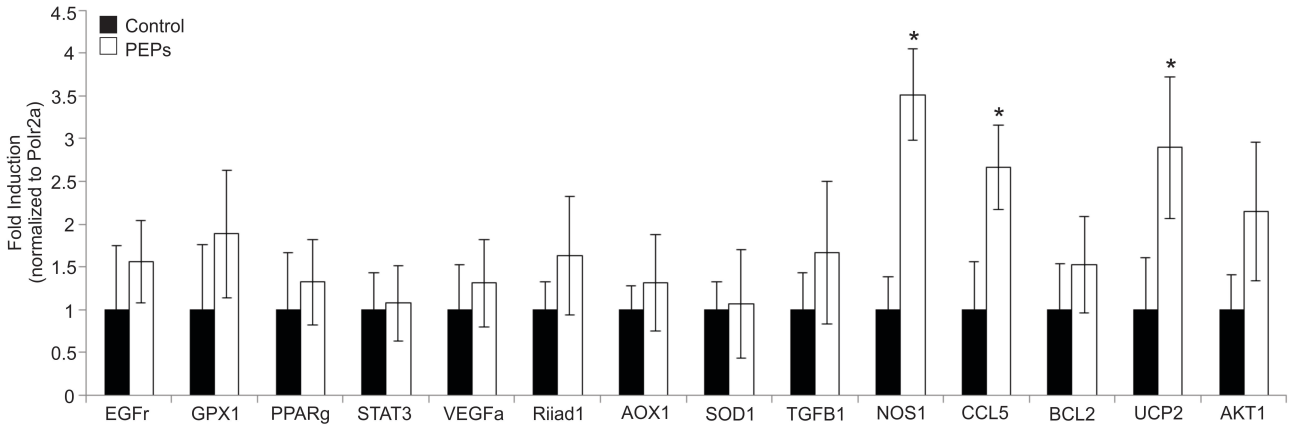

Figure 6-6. Gene expression in mice instilled with PEPs (2.5 mg/kg). n = 3. * indicates significant difference when compared to the control exposure ($p < 0.05$).

Cytokine expression. To assess if exposure to PEPs could lead to modifications in cytokine/chemokine expression involved in the inflammatory response. Out of 32 cytokines, only the leukemia inhibitory factor (LIF) was considerably upregulated by PEPs when compared to the vehicle control exposure group (Figure 6-7).

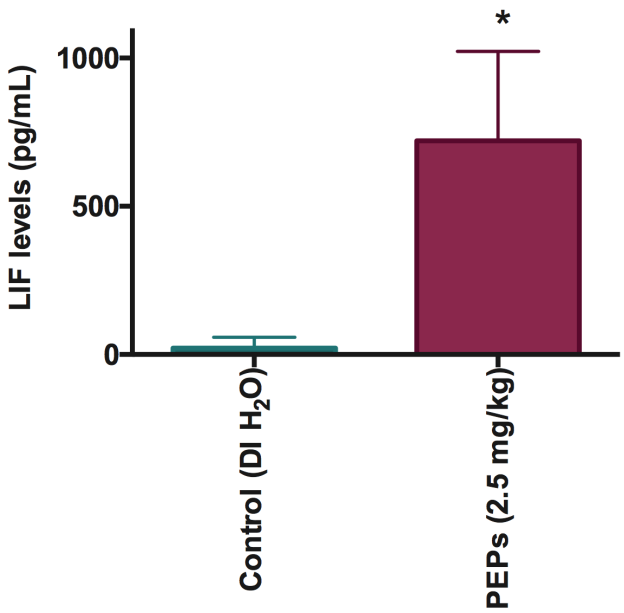

Figure 6-7. Expression levels of the Leukemia Inhibitory Factor (LIF) chemokine in the bronchoalveolar lavage fluid of mice exposed to PEPs. * indicates significant difference when compared to the control exposure ($p < 0.05$).

Discussion

The aim of this study was to assess the effects of inhaled and instilled PEPs using a mouse experimental model. This investigation is a part of a series of studies performed by our group to thoroughly evaluate the physico-chemical, morphological and toxicological properties of PM emitted from laser printers (Lu et al. 2015; Pirela et al. 2014a; Pirela et al. 2014b; Pirela et al. 2015; Sisler et al. 2014). In particular, in this research study we focused on the effect of dose and the inherent rodent biological response, if any, to PEPs.

Here, we present preliminary data on the outcome of exposure of mice to PEPs either *via* whole-body inhalation or intratracheal instillation as it pertains to several endpoints of interest: lung injury and inflammation, cytokine expression, gene expression.

In the acute inhalation exposure of PEPs, the particle concentration had a 6-hour average

of 479,513 particles/cm^3 with mean aerodynamic diameters of 40 nm. These particle distributions are in agreement with ranges previously published by our group (Pirela et al. 2014a). The properties of the airborne PEPs were used to decide our doses of exposure in both the intratracheal instillation and inhalation route. The material instilled in mice at 0.5, 2.5 and 5.0 mg/kg is equivalent to approximately 8, 40 and 80 hours of rodent inhalation exposure to PEPs. These levels were chosen to be comparable, to some extent, in both of our murine exposure experiments. Table 6-1 shows the dose comparison across the murine exposure doses used in our study to the equivalent human inhalation exposure durations that would occur in a real world scenario.

Exposure to PEPs, regardless of the route of exposure, did not seem to have an effect on the levels of lactate dehydrogenase (LDH). However, an interesting result occurred in LDH levels of mice exposed for 6 hours when compared to those exposed for 30 hours. The massive increase in lung injury observed in the BALF of mice exposed to both the gaseous pollutant only control group and the PEPs/gaseous pollutant group at 6 hours of exposure may be attributed to the total volatile organic compounds (tVOCs) emitted by the printer, which reached concentrations as high as 1,900 ppb as previously reported (Pirela et al. 2014b). Since the animals instilled with just the PEPs showed no differences in released LDH when compared to the control group, we may conclude that PEPs do not compromise the integrity of the cellular membrane.

Furthermore, the results showing lung injury are in agreement with previous work stating the irritant and inflammatory properties of VOCs in the lung. For example, mice exposed for 20 hours to a variety of VOCs displayed marked increases in oxidative stress, leukocyte infiltration, and pro-inflammatory cytokine expression (F Wang et al. 2012). Furthermore, a study by Jung et

al. (2007) in which mice exposed to formaldehyde exhibited significant airway inflammation. The authors claimed the response was due to the extensive oxidative damage and eosinophil infiltration at the site of injury.

While there was no membrane integrity damage following exposure to PEPs alone, there was extensive release of myeloperoxidase (MPO), a marker for neutrophil degranulation, in BALF of mice exposed to a 6-hour inhalation of PEPs when compared to the 30-hour exposure group. A similar upregulation of MPO in the sputum supernatant was observed in healthy volunteers post a 2-hour exposure to diesel exhaust particles (Nightingale et al. 2000). Interestingly, while there was substantial neutrophil degranulation, no evidence of neutrophilic inflammation was observed post-PEPs inhalation exposure (6 hours), which is in agreement with results from a study evaluating the response of individuals exposed to diesel exhaust (Larsson et al. 2013). Moreover, a dose-dependent increase in the percent of lavageable neutrophils was evident in mice exposed to PEPs; with the highest instilled dose (5 mg/kg) having the strongest effect compared to the PEPs (0.5 mg/kg) and the vehicle control group. The inflammatory response reported here was observed in the study by Pirela et al. (2013), in which the number of neutrophils was upregulated following instillation of $PM_{0.1}$ and $PM_{0.1\text{-}2.5}$ of copier-emitted particles.

After observing a substantial rise in expression of a variety of chemokines and cytokines in the *in vitro* toxicological assessments of PEPs (Pirela et al. 2015; Sisler et al. 2014), it was expected to have similar results of inflammation following *in vivo* exposure to PEPs. However, out of 41 cytokines evaluated, only the expression of the Leukemia Inhibitory Factor (LIF) was significantly upregulated in mice instilled with PEPs (2.5 mg/kg) compared to the vehicle control. LIF is part of the IL-6 family of cytokines that is prominently elevated in pneumonia

(Quinton et al. 2008). Principally, LIF has been associated with a protective role during pneumonia as well as having a central anti-inflammatory role during the early stages of an immune response (Banner et al. 1998; Quinton et al. 2012). Perhaps, the distinct increase in LIF post-instillation to PEPs provides protection against PEPs-induced lung injury. However, more analyses have to be performed to evaluate the signaling pathway occurring after exposure to PEPs. Additionally, LIF was found to suppress cytokine production, cell death, airway hyperresponsiveness, epithelial membrane integrity and consequently, lung injury and inflammation. Particularly, though, the suppression of LIF signaling led to enhanced gene expression of CCL5 (RANTES) in small airway epithelial cells infected with the respiratory syncytial virus (Foronjy et al. 2014).

Interestingly, instillation of PEPs (2.5 mg/kg) caused a substantial rise in the gene expression levels of five genes, namely CCL5 (RANTES), NOS1, BCL2, UCP2 and AKT1. Particularly, CCL5 (RANTES) is a pro-inflammatory chemokine that plays an important role in the trafficking of natural killer, dendritic cells, macrophages and the activation of leukocytes (Aldinucci and Colombatti 2014; Appay and Rowland-Jones 2001). Interestingly, CCL5 (RANTES) was one of the cytokines whose expression was also upregulated in both *in vitro* toxicology assessments of PEPs previously published by our group (Pirela et al. 2015; Sisler et al. 2014). More information is required to understand the association between gene expression and cytokine levels of LIF and CCL5 (RANTES) and discern regulation mechanisms of this cytokine network affected by exposure to PEPs.

Conclusion

The study described here was meant to evaluate the toxicological potential of PEPs in an *in vivo* experimental model. Our data shows that despite of uncompromised pulmonary

membrane integrity, there may be the initiation of an immune response following the exposure to PEPs. In more detail, mice exposed to PEPs exhibited a variety of responses that translate into hallmarks of the initiation of an immune reaction due to the stress induced by PEPs.

In addition to understanding the immediate effect of PEPs on the murine lung, we aimed to discern whether the method of exposure would affect the responses observed in the treated mice, even when the exposure doses were comparable. By focusing on a few endpoints in this study: lung injury, inflammation and changes in gene expression, we were able to create new hypotheses pertaining to a detailed mechanism of toxicity of PEPs.

For instance, the focus of future studies may be to better understand the major steps leading to an adverse health outcome in both the direct site of injury (*i.e.*, lungs) and indirect sites such as the cardiovascular and nervous system, since these particles can be translocated into the circulatory system. Additionally, it is critical to investigate the response *in vivo* following exposures to PEPs at both different doses and durations in relation to alterations in gene expression and mechanisms of DNA modification (*e.g.*, epigenetics). Of particular interest would be testing if there are changes in the regulation of the epigenome and modulation in expression of genes that play important roles in lung function and/or respiratory diseases. Such studies would open be useful to identify if individuals exposed to PEPs may have a predisposition to developing pulmonary disorders. Besides further examining the effect of PEPs alone, it would be valuable to assess the toxicological potential of the PEPs along with gaseous pollutants as well as just the gaseous pollutants alone and understand if there is toxicological synergy with particulate matter and gaseous pollutants.

Taken together, our mechanistically oriented toxicological studies could reveal the biological interaction of PEPs following exposures comparable to those experienced by a

consumer and worker when using laser printers. Most importantly, this experimental toxicological approach can be used to study other occupational and non-occupational exposures to the particles released by any NEP, which allows for a more realistic risk assessment and management evaluation.

Bibliography

Aldinucci D, Colombatti A. 2014. The inflammatory chemokine ccl5 and cancer progression. Mediators of inflammation 2014:292376.

Appay V, Rowland-Jones SL. 2001. Rantes: A versatile and controversial chemokine. Trends in immunology 22:83-87.

Bai R, Zhang L, Liu Y, Meng L, Wang L, Wu Y, et al. 2010. Pulmonary responses to printer toner particles in mice after intratracheal instillation. Toxicol Lett 199:288-300.

Banner LR, Patterson PH, Allchorne A, Poole S, Woolf CJ. 1998. Leukemia inhibitory factor is an anti-inflammatory and analgesic cytokine. The Journal of neuroscience : the official journal of the Society for Neuroscience 18:5456-5462.

Beck B, Brain J, Bohannon D. 1982. An in vivo hamster bioassay to assess the toxicity of particulates for the lungs. Toxicology and Applied Pharmacology 66:9-29.

Cohen J, Deloid G, Pyrgiotakis G, Demokritou P. 2012. Interactions of engineered nanomaterials in physiological media and implications for in vitro dosimetry. Nanotoxicology.

DeLoid G, Cohen JM, Darrah T, Derk R, Rojanasakul L, Pyrgiotakis G, et al. 2014. Estimating the effective density of engineered nanomaterials for in vitro dosimetry. Nature communications 5:3514.

Demokritou P, Kavouras IG, Ferguson ST, Koutrakis P. 2002. Development of a high volume cascade impactor for toxicological and chemical characterization studies. Aerosol Science and Technology 36:925-933.

Demokritou P, Lee SJ, Ferguson ST, Koutrakis P. 2004. A compact multistage (cascade) impactor for the characterization of atmospheric aerosols. Journal of Aerosol Science 35:281-299.

Foronjy RF, Dabo AJ, Cummins N, Geraghty P. 2014. Leukemia inhibitory factor protects the lung during respiratory syncytial viral infection. BMC immunology 15:41.

He C, Morawska L, Taplin L. 2007. Particle emission characteristics of office printers. Environmental science & technology 41:6039-6045.

Jung WW, Kim EM, Lee EH, Yun HJ, Ju HR, Jeong MJ, et al. 2007. Formaldehyde exposure induces airway inflammation by increasing eosinophil infiltrations through the regulation of reactive oxygen species production. Environmental toxicology and pharmacology 24:174-182.

Larsson N, Brown J, Stenfors N, Wilson S, Mudway IS, Pourazar J, et al. 2013. Airway inflammatory responses to diesel exhaust in allergic rhinitics. Inhal Toxicol 25:160-167.

Lu X, Miousse IR, Pirela SV, Melnik S, Koturbash I, Demokritou P. 2015. Short-term exposure to engineered nanomaterials affects cellular epigenome. Nanotoxicology.

Morawska L, He C, Johnson G, Jayaratne R, Salthammer T, Wang H, et al. 2009. An investigation into the characteristics and formation mechanisms of particles originating from the operation of laser printers. Environmental science & technology 43:1015-1022.

Morimoto Y, Oyabu T, Horie M, Kambara T, Izumi H, Kuroda E, et al. 2013. Pulmonary toxicity of printer toner following inhalation and intratracheal instillation. Inhal Toxicol 25:679-690.

Muhle H, Bellmann B Fau - Creutzenberg O, Creutzenberg O Fau - Dasenbrock C, Dasenbrock C Fau - Ernst H, Ernst H Fau - Kilpper R, Kilpper R Fau - MacKenzie JC, et al. 1991. Pulmonary response to toner upon chronic inhalation exposure in rats. Fundamental and Applied Toxicology 17:280-299.

Nightingale JA, Maggs R, Cullinan P, Donnelly LE, Rogers DF, Kinnersley R, et al. 2000. Airway inflammation after controlled exposure to diesel exhaust particulates. American journal of respiratory and critical care medicine 162:161-166.

Pirela S, Molina R, Watson C, Cohen JM, Bello D, Demokritou P, et al. 2013. Effects of copy center particles on the lungs: A toxicological characterization using a balb/c mouse model. Inhal Toxicol 25:498-508.

Pirela SV, Pyrgiotakis G, Bello D, Thomas T, Castranova V, Demokritou P. 2014a. Development and characterization of an exposure platform suitable for physico-chemical, morphological and toxicological characterization of printer-emitted particles (peps). Inhal Toxicol 26:400-408.

Pirela SV, Sotiriou GA, Bello D, Shafer M, Bunker KL, Castranova V, et al. 2014b. Consumer exposures to laser printer-emitted engineered nanoparticles: A case study of life-cycle implications from nano-enabled products. Nanotoxicology:1-9.

Pirela SV, Miousse IR, Lu X, Castranova V, Thomas T, Qian Y, et al. 2015. Laser printer-emitted engineered nanoparticles lead to cytotoxicity, inflammation and changes in dna methylation in human cells. Environmental health perspectives.

Quinton LJ, Jones MR, Robson BE, Simms BT, Whitsett JA, Mizgerd JP. 2008. Alveolar epithelial stat3, il-6 family cytokines, and host defense during escherichia coli pneumonia. American journal of respiratory cell and molecular biology 38:699-706.

Quinton LJ, Mizgerd JP, Hilliard KL, Jones MR, Kwon CY, Allen E. 2012. Leukemia inhibitory factor signaling is required for lung protection during pneumonia. Journal of immunology 188:6300-6308.

Sisler JD, Pirela SV, Friend S, Farcas M, Schwegler-Berry D, Shvedova A, et al. 2014. Small airway epithelial cells exposure to printer-emitted engineered nanoparticles induces cellular effects on human microvascular endothelial cells in an alveolar-capillary co-culture model. Nanotoxicology:1-11.

Wang F, Li C, Liu W, Jin Y. 2012. Effect of exposure to volatile organic compounds (vocs) on airway inflammatory response in mice. The Journal of toxicological sciences 37:739-748.

Wang H, He C, Morawska L, McGarry P, Johnson G. 2012. Ozone-initiated particle formation, particle aging, and precursors in a laser printer. Environmental science & technology 46:704-712.

Appendix A - Chapter 4: Small airway epithelial cells exposure to printer-emitted engineered nanoparticles induces cellular effects on human microvascular endothelial cells in an alveolar-capillary co-culture model

Jennifer D. Sisler[1], Sandra V. Pirela[2], Sherri Friend[1], Mariana Farcas[1], Diane Schwegler-Berry[1], Anna Shvedova[1], Vincent Castranova[3], Philip Demokritou[2*], and Yong Qian[1*]

Nanotoxicology. 2014.

[1]Pathology and Physiology Research Branch, Health Effects Laboratory Division, National Institute for Occupational Safety and Health, Morgantown, WV, USA,

[2]Department of Environmental Health, Harvard School of Public Health, Harvard University, Boston, MA, USA,

[3]Department of Basic Pharmaceutical Sciences, West Virginia University, Morgantown, WV, USA

[*]Corresponding author

Abstract

The printer is one of the most common office equipment. Recently, it was reported that toner formulations for printing equipment constitute nano-enabled products (NEPs) and contain engineered nanomaterials (ENMs) that become airborne during printing. To date, insufficient research has been performed to understand the potential toxicological properties of printer-emitted particles (PEPs) with several studies using bulk toner particles as test particles. These

studies demonstrated the ability of toner particles to cause chronic inflammation and fibrosis in animal models. However, the toxicological implications of inhalation exposures to ENMs emitted from laser printing equipment remain largely unknown. The present study investigates the toxicological effects of PEPs using an *in vitro* alveolar-capillary co-culture model with Human Small Airway Epithelial Cells (SAEC) and Human Microvascular Endothelial Cells (HMVEC). Our data demonstrate that direct exposure of SAEC to low concentrations of PEPs (0.5 and 1.0 μg/mL) caused morphological changes of actin remodeling and gap formations within the endothelial monolayer. Furthermore, increased production of reactive oxygen species (ROS) and angiogenesis were observed in the HMVEC. Analysis of cytokine and chemokine levels demonstrates that interleukin (IL)-6 and MCP-1 may play a major role in the cellular communication observed between SAEC and HMVEC and the resultant responses in HMVEC. These data indicate that PEPs at low, non-cytotoxic exposure levels are bioactive and affect cellular responses in an alveolar-capillary co-culture model, which raises concerns for potential adverse health effects.

Introduction

The printer is one of the most common pieces of equipment within an office space. The use of printers has increased exponentially in the United States over the past few years due to the increase of home offices (Jamieson, 2012). It has been shown in several studies that a laser printer has the ability to increase indoor air particle levels from 860 to 38000 particles/cm^3 (Barthel et al., 2011; He et al., 2007), with the emitted particles being spherical in shape and having a particle diameter in the range of 50–244 nanometers (nm). The majority of the particles are released from various parts of the laser printer, such as the board cooler, rear of the printer, paper tray and toner waste bin (Byeon & Kim, 2012; Chia-Wei Lee, 2007; He et al., 2007; Jiang,

2010; Kagi et al., 2007; McGarry et al., 2011; Morawska et al., 2009; Schripp et al., 2008; Wang et al., 2012; Wensing et al., 2008). The *in vitro* studies performed have used bulk toner particles and concluded that exposures caused delayed pulmonary clearance which led to increased super oxide radicals, cell growth, and cyto and genotoxicity (Furukawa et al., 2002; Mohr et al., 2006; Slesinski & Turnbull, 2008). Moreover, long-term exposure to the toner material resulted in chronic inflammation, fibrosis and tumor growth in rat lungs (Mohr et al., 2006; Morimoto et al., 2005). These studies suggest toxicity of toner powder; however, these results cannot be correlated to exposures at consumer level since the test particles used are not representative of the ‘‘real world’’ exposure to PEPs (Pirela et al., 2014a,b).

The authors recently developed and utilized a Printer Exposure Generation System (PEGS) to generate, characterize *in situ*, and collect size-fractionated PEPs from 11 commonly used laser printers and ranked them based on their emission profiles. Results show particulate matter (PM) peak emissions from laser printers can reach up to 1.27 million particles/cm^3 with geometric mean diameters ranging from 49 to 208 nm (Pirela et al., 2014a). In a companion paper, the authors confirmed the hypothesis that toner formulations contained engineered nanomaterials (ENMs), which are released during printing. A detailed physico-chemical and morphological analysis of both the PEPs and their respective toners, using state of the art technologies, revealed a complex chemistry of organic and inorganic carbon, as well as, several metal/metal oxides (*e.g.*, silica, copper oxide, titanium, nickel, chromium), which correlated with the ENMs present in the toner formulation (Pirela et al., 2014b).

This current manuscript is the first in a series of papers assessing the toxicological properties of the PEPs and possible biological mechanisms of toxicity. Herein, a human alveolar capillary co-culture model using SAEC and HMVEC was used to determine if different size

fractions of PEPs are capable of producing adverse cellular effects on the latter cell line. This co-culture system mimics the alveolar-capillary interaction in the small airways of the lower respiratory tract, reflecting a more physiologically relevant cellular communication. In this study, SAEC were directly treated with non-cytotoxic, low concentrations of 0.5 and 1.0 μg/mL of PEPs ($PM_{0.1}$ and $PM_{2.5}$) for 24 h and then HMVEC were analyzed to determine SAEC-HMVEC communication and the resultant biological responses.

Methods

Generation and collection of size-fractionated PEPs

The PEPs were generated using the PEGS (Pirela et al., 2014a), a platform recently developed by the authors suitable for the generation and sampling of real world exposures to PEPs. One of the highest emitting printers (referred to as Printer B1 in companion papers), found to emit up to 1.26 million particles/cm^3, was used in this study. Size-selective PM sampling was performed using the Harvard Compact Cascade Impactor (CCI), which collects particles onto impaction substrates in three stages corresponding to $PM_{0.1}$, $PM_{0.1–2.5}$ and $PM_{2.5–10}$ size fractions (Demokritou et al., 2004). After collecting the size-fractionated PM samples, the impaction substrates were removed from the CCI and the particles were extracted using an aqueous suspension methodology (Bello et al., 2013; Chang et al., 2013; Pirela et al., 2013).

Post-sampling characterization of PEPs

Detailed chemical and morphological characterization of PEPs and toner powder for this particular printer, as well as the paper utilized during the study, included testing for total and water- soluble fraction of multiple metals (50 elements), organic and elemental carbon, as well as scanning and transmission electron microscopy (STEM) analysis. Detailed results from the

physico-chemical characterization of PEPs from this high-emitting printer are presented in more detail in the companion paper (Pirela et al., 2014b).

Preparation and characterization of particle liquid suspensions for *in vitro* study

Following extraction of PEPs from the CCI impaction substrates, particle dispersions in water were prepared using a protocol developed by the authors (Cohen et al., 2013), which includes the calibration of sonication equipment and standardized reporting of sonication energy. In summary, the critical delivered sonication energy (DSE_{cr}) for each particle used in the study was identified for subsequent sonication and characterization by dynamic light scattering (DLS) to measure hydrodynamic diameter (d_H), polydispersity index (PdI), zeta potential (ζ) and specific conductance (σ). Preparation of all of the particle suspensions was performed just prior to use in the experiments by creating a 1 mg/mL nanoparticle suspension with sterile deionized water (dIH_2O), sonicating at DSE_{cr} and diluting to desired final test concentrations in the respective media. DLS characterization was then repeated to evaluate the properties of the particle in cellular media. Furthermore, colloidal stability of the suspensions, in dIH_2O and in cellular media, was evaluated over various time points following sonication at DSE_{cr}. Subsequently, the effective density of each particle suspension was measured using the volumetric centrifugation method (VCM), recently developed by the authors, as described by Cohen et al. (2013). Effective density is an important determinant of the fate and transport of the agglomerates and *in vitro* dosimetry (see below) (Cohen et al., 2014; DeLoid et al., 2014).

***In vitro* and *in vivo* dosimetric considerations**

It is important to bring *in vivo* and *in vitro* doses on the same scale. Therefore, the dosimetric approach recently developed by the authors was followed (Demokritou et al., 2013; Khatri et al., 2013b). In summary, the Multiple-Path Particle Dosimetry 2 (MPPD2) (Anjilvel &

Asgharian, 1995) model was used to calculate the dose deposited in the head region, conducting zone, the transitional and respiratory zones of human respiratory system. The airborne nanoparticle distribution values (count median diameter, geometric standard deviation and mass concentration), as well as the human breathing parameters (tidal volume, breathing frequency, inspiratory fraction, pause fraction, functional residual capacity, head volume and breathing route) listed in Supplemental Table 4-S1 were used in the simulations. It is worth mentioning that the breathing frequency used in the MPPD2 simulation was that of a resting individual (12 breaths/min). Please note that the MPPD2 model provides the deposition mass flux for all the generations of the human respiratory tree (not including head region).

Thus, the total deposition mass flux of the entire human airway comprised of the conducting zone and the transitional and respiratory zones (excluding the head airway region) was used in the computation of the *in vitro* equivalent volumetric dose, $dose_{in\ vitro,eq}$ (μg/mL), which represents dose delivered to cells. It was calculated as follows:

$$dose_{in\ vitro,\ eq} = m_{model} \times T_{exp} \times \frac{A_{well}}{V_{admin}}$$

where, $dose_{in\ vitro,eq}$ is the equivalent *in vitro* dose (μg/mL), T_{exp} is the total exposure time (min), m_{model} is the sum of each of the MPPD2 model-derived values for mass flux in the conducting, transitional and respiratory zones of the human lung (μg/m^2•min), A_{well} is the surface area of treatment well (m^2) and V_{admin} is the volume of the media in one well (mL).

Subsequently, the hybrid Volumetric Centrifugation Method-*In Vivo* Sedimentation, Diffusion and Dosimetry (VCM-ISDD) methodology recently developed by the authors (Cohen et al., 2014; DeLoid et al., 2014) was used to calculate the fraction of administered *in vitro* particles that deposited to the bottom of the well in a standard 96-well plate as a function of time. For the estimation of the dose delivered to the cell, the agglomerate hydrodynamic diameter,

measured by DLS, and the VCM-measured effective density were used as input to the VCM-ISDD model.

Comparative materials

The mild steel welding fumes (WF) were used as a comparative material in this study based upon their complex makeup of metal oxide similar to that of the PEPs. Furthermore, their toxicity in several *in vitro* and *in vivo* studies has been well documented (Antonini et al., 1999, 2012; Sriram et al., 2012; Zeidler-Erdely et al., 2011). Amorphous silica (SiO_2), which was previously characterized, was also used as a comparative nanomaterial (Cohen et al., 2013; Gass et al., 2013).

Cell culture

SAEC were a gift from Dr Tom K. Hei (Columbia University, New York, NY) and were cultured as previously described (Piao et al., 2005). Briefly, the SAEC were cultured in serum-free Small Airway Epithelial Cell growth medium (SABM) with an addition of multiple supplemental growth factors (Bovine Pituitary Extract, Hydrocortisone, Human Epidermal Growth Factor, Epinephrine, Transferrin, Insulin, Retinoic, Triiodothyronine, Gentimicin Amphoteracin-B and Bovine serum Albumin-fatty acid free (BSA-FAF)) provided by the manufacturer (Lonza, Inc., Allendale, NJ). The HMVEC were gifted by Dr Rong Shao (BioMedical Research Institute, Baystate Medical Center, University of Massachusetts, Amherst, MA) and have been described previously (Shao & Guo, 2004). HMVEC were cultured in endothelial basal medium-2 (EBM-2) (Lonza, Inc., Allendale, NJ) with the addition of 10% fetal bovine serum (FBS) (Atlanta Biological, Lawrencville, GA), 100 U/mL penicillin and 10 mg/ mL streptomycin (Lonza, Inc., Allendale, NJ), 0.01 mg/mL epidermal growth factors (EGF)

(Sigma, St. Louis, MO), and 1 mg/mL hydrocortisone (Sigma, St. Louis, MO). Cells were maintained at 37°C with 5% carbon dioxide.

Details of the *in vitro* alveolar-capillary co-culture model, summarized in Supplemental Figure 4-1, were previously published (Snyder-Talkington et al., 2013b). Briefly, 6-well polyester 0.4-mm pore size transwells (Corning Inc., Corning, NY) were hydrated with SABM for at least 1 h in a secondary 6-well plate. HMVEC (2.25 x 10^5cells per well) were plated with or without a coverslip. HMVEC were fully attached before the addition of the transwell insert. Then SAEC were plated at 1.5 x 10^5 cells per well and allowed to fully attach for 24 h, followed by media changes to remove any dead cells in both chambers. At 48 h, each of the chambers was serum starved for an additional 24h then treated with PEPs for 24 h and then assayed.

Cytotoxicity of SAEC

SAEC were plated at 1.5 x 10^4 cells per well in a 96-well plate (BD Biosciences, San Jose, CA). The Cell Titer 96® Aqueous One Solution Cell Proliferation Assay Kit (Promega, Madison, WI) was used to determine the changes in cell proliferation according to the manufacturer's protocol. The following concentrations were used to determine cytotoxicity in the MTS Assay: 0.0, 0.5, 1.0 and 2.5 μg/mL.

Transmission electron microscopy

Following treatment with PEPs $PM_{0.1}$ for 24 h, SAEC were fixed in Karnovsky's fixative (2.5% glutaldehyde, 2.5% paraformaldehyde in 0.1 M Sodium Cacodylic buffer). HMVEC on the bottom chamber of the transwells were trypsinized and centrifuged at 1000g for 5min at room temperature and then fixed with Karnovsky's fixative. SAEC and HMVEC samples were post-fixed in osmium tetroxide, mordanted in 1% tannic acid and stained in bloc in 0.5% uranyl acetate. The samples were embedded in epon, sectioned and stained with Reynold's lead citrate

and uranyl acetate. The sections were imaged on a JEOL 1220 transmission electron microscope (JEOL, Tokyo, Japan).

Cytokine and chemokine analysis

The SAEC and HMVEC cellular lysates were collected following the protocol from the Bio-Plex™ Cell Lysis Kit (Bio Rad, Hercules, CA). Both the condition media and cellular lysates were analyzed for 27 cytokines and chemokines using the Bio-Plex Pro Human Cytokine 27-Plex Assay (Bio-Rad, Hercules, CA) after the co-cultured SAEC were treated with dIH_2O, PEPs $PM_{0.1}$ 1.0 μg/mL, SiO_2 1.0 μg/mL, or WF 1.0 μg/mL for 24 h. The samples were run on the Bio-Plex®200 System and analyzed using Bio-Plex Manager® 6.0 software (Bio-Rad, Hercules, CA). Cytokines and chemokines that were elevated within the PEPs $PM_{0.1}$ are shown in Figure 4-6; however, the following cytokines and chemokines were included in the Bio-Plex: IL-1b, IL-ra, IL-2, IL-4, IL-5, IL-6, IL-7, IL-8, IL-9, IL-10, IL-12p70, IL-13, IL-15, IL-17A, Ecotaxin, Basic FGF, G-CSF, GM-CSF, IFN-g, IP-10, MCP-1, MIP-1a, MIP- 1b, PDGF-BB, RANTES, TNF-a and VEGF.

Confocal microscopy

To measure the amount of ROS, 5mM final concentration of dihydroethidium (DHE) (Invitrogen, Grand Island, NY) was added to the HMVEC media during the last 30 min of the PEPs treatment. To confirm the production of ROS, the HMVEC were pre-treated with 2000 U/mL catalase (Sigma, St. Louis, MO) for 1 h to scavenge the ROS. The cells on the coverslips were fixed with 3.6% paraformaldehyde and washed three times with 1 x PBS. The cells were mounted and imaged with a LSM510 confocal microscope (Zeiss, Heidelberg, Germany).

Changes in actin filaments and gap formation were measured in the HMVEC monolayer. The HMVEC on the coverslips were fixed with 3.6% paraformaldehyde and permeabilized with

0.1% triton x-100/PBS. Samples were blocked in 3% BSA (Fisher Scientific, Pittsburgh, PA) and washed three times with 1 x PBS. HMVEC were stained with phalloidin (AlexaFluor 546, Invitrogen, NY) for actin filaments and rabbit anti-VE cadherin (Alexis Biochemicals, San Diego, CA). Samples were incubated with secondary anti-rabbit Alexa Fluor 647 (Invitrogen, Grand Island, NY) mounted with ProLong Gold anti-fad (Invitrogen, NY) and imaged using a Zeiss LSM510 microscope (Zeiss, Heidelberg, Germany). Scale bars were generated and inserted using LSM software (Zeiss, Heidelberg, Germany).

Angiogenesis assay

SAEC and HMVEC were grown in the co-culture system to 90–100% confluence and were exposed to PEPs for 24 h. After the treatment, HMVEC were trypsinized and 6.0 x 10^4 HMVEC were plated on 2 mg/mL matrigel (BD Biosciences) in a 24-well plate. The cells were imaged every 30 min for 4 h to measure tube formation. The images were taken on the Spot/retiga at both 4x and 10x. Tube formation was quantified using the 10x images.

Statistics

Experiments were performed in biological triplicates and expressed with the standard error. Images are a representation of n=3. Student's t-test was used to determine significance set at $p< 0.05$.

Results

Physico-chemical properties of collected PEPs

In the two companion papers, we show in detail the characterization of toner powder and PEPs from 11 commonly used laser printers (Pirela et al., 2014a,b). In summary, the ''high emitting'' laser printer used in this study (referred to as Printer B1 in our previous publications)

released up to 1.26 million particles/cm^3 during a one hour, continuous print job. The emitted PM had a unimodal size distribution and aerodynamic diameters that ranged from 39 to 122 nm. STEM/EDX analysis of both the toner powder and PEPs showed presence of ENMs in the toner that became airborne during printing. Further chemical analysis revealed a similar complex chemical fingerprint between the toner and PEPs, with PEPs containing 42% carbon, 1.5% metal (*e.g.*, aluminum, titanium, cerium, zinc and copper) and 56% other (*e.g.*, phosphorus, sulfur, chlorine) (Pirela et al., 2014b).

Sampled PEPs dispersion and characterization in liquid suspensions

Table 4-1 summarizes the particle agglomerate colloidal behavior in both dIH2O and small airway basal medium (SABM), as described by hydrodynamic diameter (d_H), zeta potential (ζ), polydispersity index (PdI) and specific conductance (σ). Observed values of ζ were strongly negative for the $PM_{0.1}$ PEPs size fraction in dIH_2O (-20.6mV) and became positive when dispersed in SABM (9.97 mV). The opposite was observed for the larger PEPs counterpart ($PM_{2.5}$), whose ζ was -16 mV in dIH_2O and remained negative when suspended in SABM (-17.7mV). The WF, used here as a comparator material of known toxicity, were determined to have a d_H of 2197 nm in dIH_2O, which decreased to 1878 nm when dispersed in SABM. Lastly, the d_H of silica increased dramatically from 142.5 nm (in dIH_2O) to 663.8nm (in SABM). The colloidal stability of the particle suspensions was subsequently evaluated 24h post-sonication to DSE_{cr}. The d_H of PEPs ($PM_{0.1}$) suspended in SABM remained stable with an average diameter ranging from 200 to 250 nm (data not shown). Contrasting stability was observed for the bigger size fraction of PEPs ($PM_{2.5}$), whose d_H increased substantially at 10 h post-sonication going from approximately 200 nm to 600 nm (data not shown). SiO_2 and WF also remained as a stable dispersion for up to 24 h. Thus, in order to maintain the most stable particle suspension, the

dispersions were always prepared and sonicated at DSE_{cr} immediately prior to cell treatment.

The VCM measured effective density of the ENMs suspensions and results show that the smallest size fraction of PEPs ($PM_{0.1}$) had an effective density of 2.39 g/cm^3, lower than that of the larger size fraction of PEPs ($PM_{2.5}$) of 3.10g/cm^3. The effective densities of the comparator materials used in the study were 1.2 g/cm^3 for silica and 1.37 g/cm^3 for WF.

Table 4-1. Properties of ENMs dispersions in dIH_2O and SABM. d_H: hydrodynamic diameter; PdI: polydispersity index; ζ: zeta potential; σ: specific conductance and effective density. pH was measured of the SABM media that was used for treatment of cells as well. Values represent the mean (±SD) of a triplicate reading. The average diameters obtained from DLS characterization are derived from the intensity-weighted distributions based on the intensity of light scattered by the particle.

Nanomaterial	Media	dH (nm)	PdI	ζ (mV)	σ (mS / cm)
PEPs $PM_{0.1}$	dIH_2O	178.3 ± 3.5	0.403 ± 0.05	-20.6 ± 1.9	0.185 ± 0
	SABM	381.7 ± 40.2	0.586 ± 0.05	9.97 ± 2.8	2.52 ± 0.0721
PEPs $PM_{2.5}$	dIH_2O	197.8 ± 17.4	0.441 ± 0.06	-16.0 ± 1.01	0.351 ± 0
	SABM	231.1 ± 2.9	0.348 ± 0.005	-17.7 ± 3.6	3.61 ± 0.590
SiO_2	dIH_2O	142.5±2.4	0.207±0.01	33.6±1.70	0.00804±0
	SABM	663.8 ± 124.5	0.277 ± 0.09	28.4 ± 6.0	10.5 ± 0
WF	dIH_2O	2197 ± 118.4	0.561 ± 0.4	8.52 ± 1.2	0.0284 ± 0
	SABM	1526.7 ± 259.6	0.198 ± 0.04	18.8 ± 0.9	10.5 ± 0.462

Dosimetric considerations for *in vitro* testing

In order to ensure that the *in vitro* doses used in this study are equivalent to current consumer exposures to PEPs, the total human lung deposited dose for a corresponding consumer inhalation exposure duration was determined using the MPPD2 model as described in the ‘‘Methods’’ section. The *in vitro* equivalent volumetric dose, $dose_{in\ vitro,\ eq}$, (μg/mL), estimated using the total lung deposition mass flux (1.732 $\mu g/m^2 \bullet min$) was found to be 0.485, 3.88 and 11.65 μg/mL for exposure durations of 1, 8 and 24 h of corresponding inhalation to PEPs, respectively.

Furthermore, the administered dose which is deposited on the cells on the bottom of the well for PEPs $PM_{0.1}$, PEPs $PM_{2.5}$ and comparative materials was calculated as briefly described in the ‘‘Methods’’ section and presented in Supplemental Figure 4-S2. The delivered cell dose at a given exposure time-point is not always the same as the dose administered (Cohen et al., 2013) as it depends on the effective density and size of the formed agglomerates and particokinetics in general in the *in vitro* system, which can have serious implications on toxicological ranking of nanomaterials *in vitro* (Cohen et al., 2014). The estimated fraction of administered particle mass that reaches the bottom of the well in the chosen experimental exposure duration for each particle suspension is summarized in Supplemental Table 4-S2. Results show that it will take less than two hours for all of the administered WF mass to deposit. However, the opposite is observed for SiO_2, as only approximately 40% of the administered dose will actually reach the bottom of the well. Interestingly, for a 24 h *in vitro* exposure duration, both PEPs size fractions, 100% of the administered dose will be deposited to the cells at the bottom of the well (Supplemental Figure 4-S3). It is worth noting that the fate and transport of formed agglomerates in the *in vitro* system is defined by two fundamental parameters, namely the diameter of the

formed agglomerate, as well as, their effective density (Cohen et al., 2014; DeLoid et al., 2014). In this particular PM suspensions, the combinations of diameter and effective density of the formed agglomerates in the media resulted to faster deposition of the $PM_{0.1}$ size fraction compared to the larger PEPs ($PM_{2.5}$) due to higher agglomerate diameter for PEPs $PM_{0.1}$. The corresponding equivalent consumer inhalation exposure duration (hours), and the associated delivered to cell doses used in the study are presented in Supplemental Table 4-S2.

PEPs induce cytotoxicity in SAEC

Supplemental Figure 4-4 illustrates the results from the MTS assay. Results indicate that the $PM_{0.1}$ size fraction of PEPs and WF was toxic to SAEC at the administered dose of 2.5 μg/mL. Although, PEPs ($PM_{2.5}$) and SiO_2 were not toxic at 2.5 μg/mL, they caused an increase in metabolic activity. At the low concentration of 1.0 μg/mL, PEPs ($PM_{0.1}$) or PEPs ($PM_{2.5}$) showed no significant changes in metabolic activity or cytotoxicity. There were also no significant changes seen when SAEC were treated with 0.5 μg/mL of any of the nanoparticles. Therefore, the non-cytotoxic levels of 0.5 μg/mL and 1.0 μg/mL were used for the remaining studies utilizing the co-culture model.

PEPs are engulfed by SAEC but did not reach HMVEC

In this study, the SAEC-HMVEC *in vitro* alveolar-capillary co-culture model was applied to identify cellular effects induced by different size fractions of PEPs. SAEC on the transwell membrane were exposed to PEPs directly, and the underlying HMVEC in the basolateral section were subjected to multiple assays. Therefore, it was of importance to determine the location of the PEPs within the SAEC-HMVEC co-culture model by TEM. As seen in Figure 4-1, SAEC engulfed the PEPs after a 24h treatment. It appears that the PEPs were not able to translocate to

the basolateral chamber, suggesting that the HMVEC did not have direct interaction with PEPs. Therefore, it can be hypothesized that the endothelial cellular effects observed in this co-culture model are mainly due to the cellular communication between the epithelial and endothelial cells caused by PEPs and not direct HMVEC interaction with PEPs.

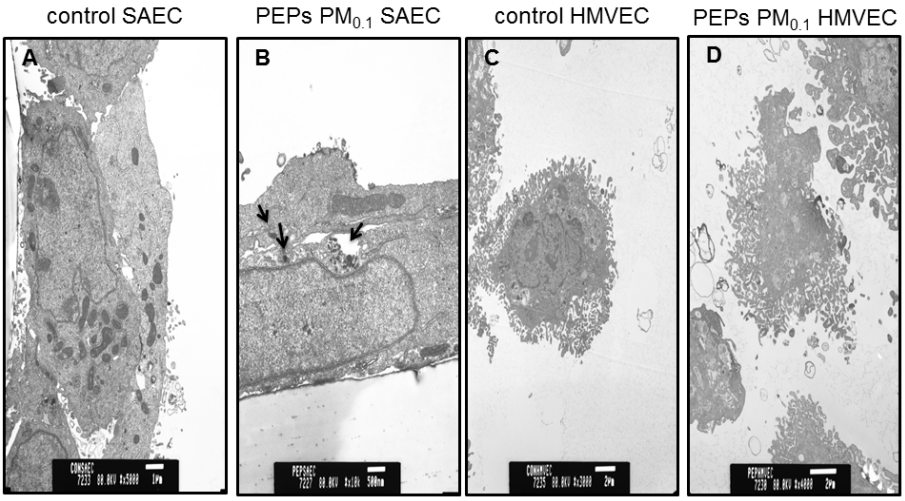

Figure 4-1. TEM images of SAEC and HMVEC after PEPs $PM_{0.1}$ exposure. SAEC were treated with 1.0 μg/mL PEPs $PM_{0.1}$ in the co-culture model for 24 h. Both SAEC and HMVEC were fixed with Karnovsky's fixative, stained with osmium and imaged with a transmission electron microscope. (A) SAEC treated with dIH_2O. (B) SAEC treated with PEPs $PM_{0.1}$, particles are identified with arrows. (C) HMVEC from the basolateral chamber after SAEC treatment with dIH_2O. (D) HMVEC from the basolateral chamber after SAEC treatment with PEPs $PM_{0.1}$. Images represent n=3.

PEPs increase ROS in HMVEC

Nanomaterials have been shown to cause an increase in the production of ROS *in vivo* and *in vitro*, which has been linked to nanoparticle-induced toxic effects (Demokritou et al., 2013; Nel, 2006; Sotiriou et al., 2012). HMVEC were examined to determine their ability to

produce ROS upon co-culture with SAEC exposed to PEPs. As can be seen in Figure 4-2, there was an increase in ROS production in HMVEC when SAEC were treated with PEPs $PM_{0.1}$ 1.0 μg/mL (C), PEPs $PM_{2.5}$ 1.0 μg/mL (D), SiO_2 1.0 μg/mL (E) or WF 1.0 μg/mL (F). Comparison of the intensities among these treatments indicates that exposure to PEPs $PM_{0.1}$ 1.0 μg/mL induced the highest amount of ROS even when compared to cells treated with WF. However, there does not appear to be an increase in ROS with PEPs $PM_{0.1}$ at 0.5 μg/mL compared to the control. To confirm production of ROS, HMVEC were pre-treated with catalase, a ROS scavenger, as illustrated in Figure 4-2 (G–L) resulted in blocking ROS production.

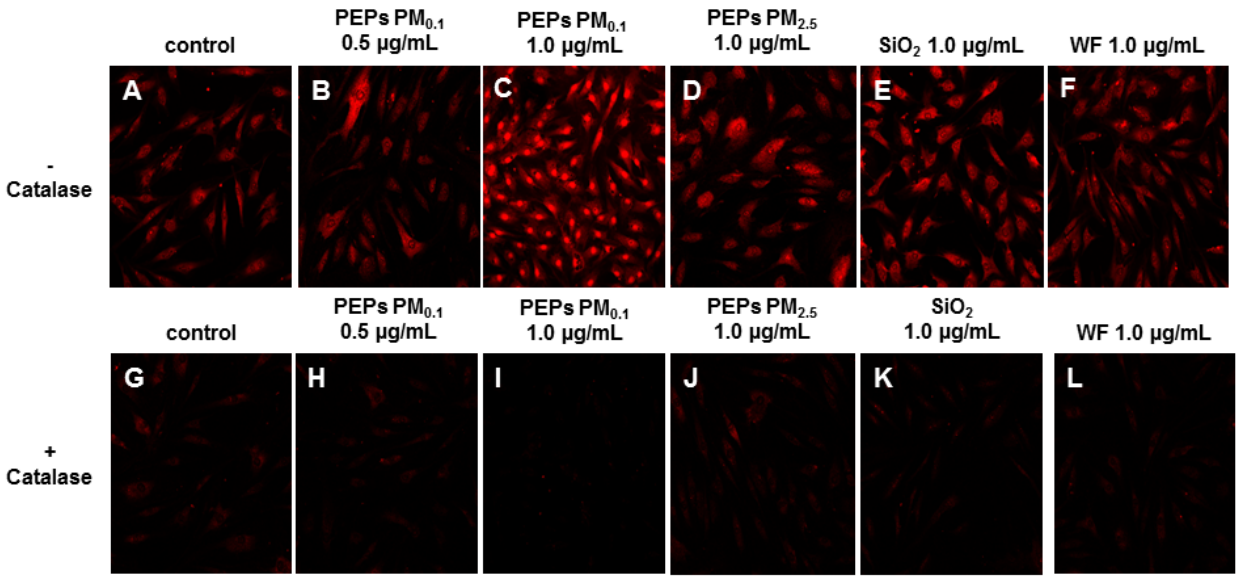

Figure 4-2. Reactive oxygen species are increased in HMVEC when SAEC are treated with PEPs. HMVEC were treated with 5 mM DHE for the last 30 min of 24 h treatment of SAEC with (A) control, (B) PEPs $PM_{0.1}$ 0.5 μg/mL, (C) PEPs $PM_{0.1}$ 1.0 μg/mL, (D) PEPs $PM_{2.5}$ 1.0 μg/mL, (E) SiO_2 1.0 μg/mL, and (F) WF 1.0 μg/mL, (G–L) HMVEC were pre-treated with 2000 U/mL catalase for 1 h. Images were taken using a Zeiss LSM510 microscope. Images represent n=3.

PEPs increase morphological changes in HMVEC

To determine if the treatment of SAEC with PEPs caused morphological changes to the endothelial monolayer, HMVEC were fixed and stained with FITC-phalloidin for actin filaments, as described in the ‘‘Methods’’ section. As seen in Figure 4-3, there is an increase in the remodeling of actin filaments in HMVEC after the treatment of SAEC with PEPs $PM_{0.1}$ at 1.0 μg/mL and PEPs $PM_{2.5}$ at 1.0 μg/mL. Results show that PEPs $PM_{0.1}$ and $PM_{2.5}$ increased cell motile structures in HMVEC, such as stress fibers, filopodia and lamellipodia.

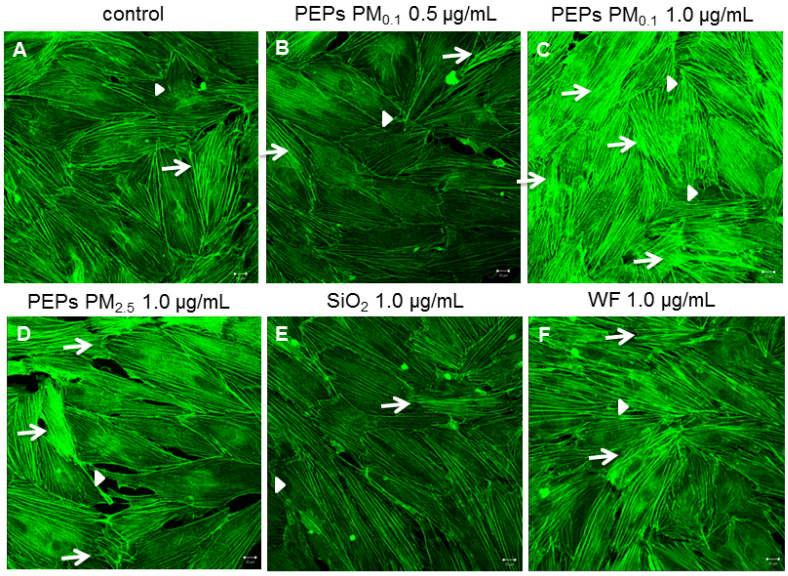

Figure 4-3. SAEC exposure to PEPs increases actin filament remodeling in HMVEC. HMVEC were grown on coverslips in the co-culture model and stained with AlexaFluor 546. (A) Control, (B) PEPs $PM_{0.1}$ 0.5 μg/mL, (C) PEPs $PM_{0.1}$ 1.0 μg/mL, (D) PEPs $PM_{2.5}$ 1.0 μg/mL, (E) SiO_2 1.0 μg/mL, and (F) WF 1.0 μg/mL. Arrows represent increase in actin-filament stress fibers and arrowheads indicate increase in filopodia and lamellipodia. Images were taken using a Zeiss LSM510 microscope. Images represent n=3.

VE-cadherin expression is specific to endothelial cells and is necessary within the adheren junctions to maintain cellular contact within the endothelial monolayer (Mehta & Malik, 2006). To determine the integrity of the endothelium upon co-culturing with PEPs-treated SAEC, HMVEC were fixed and stained with VE-cadherin antibody. PEPs $PM_{0.1}$ 0.5 μg/mL did not change gap formation (Figure 4-4B). There were increased gap junctions in the PEPs $PM_{0.1}$ 1.0 μg/mL (Figure 4-4C) endothelium in comparison to the WF 1.0 μg/mL. PEPs $PM_{2.5}$ 1.0 μg/mL (Figure 4-4D) showed an increase in gap formation; however, it induced less gap formation than PEPs $PM_{0.1}$ 1.0 μg/mL. The SiO_2 did not increase gap formation compared to control while the WF did (Figure 4-4E,F). These results demonstrated that SAEC exposure to PEPs induced morphological changes of HMVEC in the co-culture model.

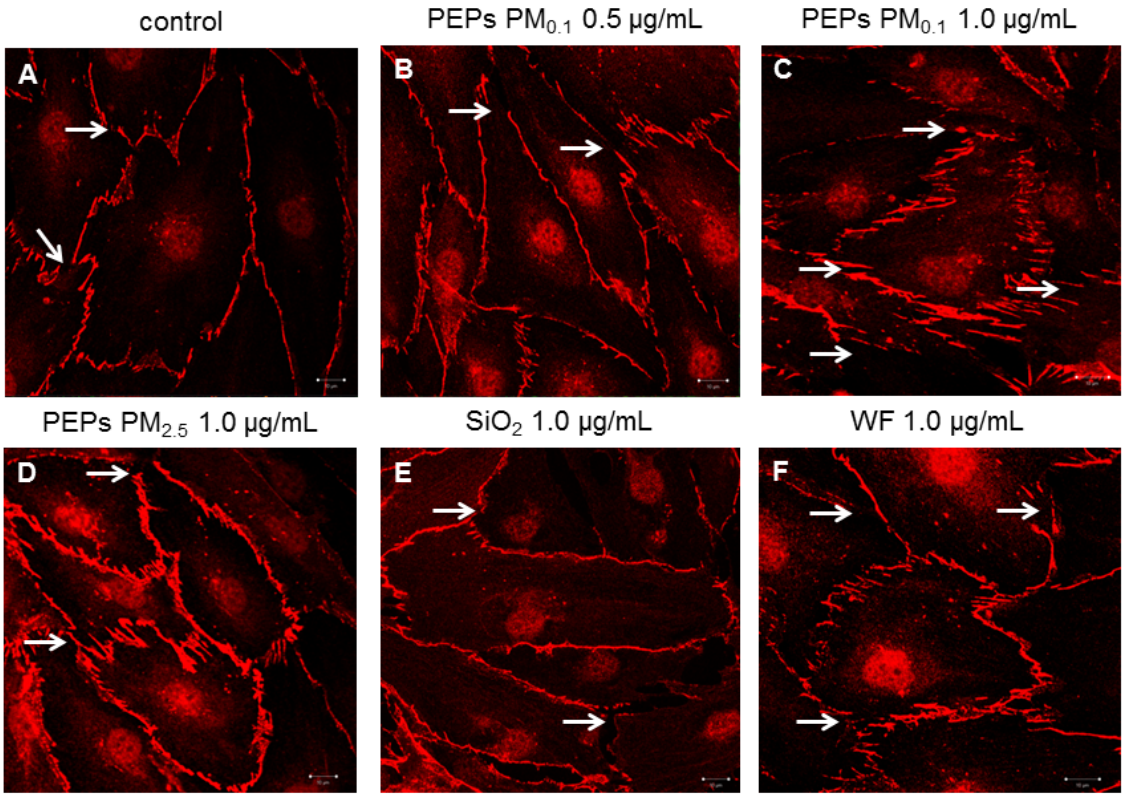

Figure 4-4. SAEC exposure to PEPs causes an increase in gap formations in the endothelial monolayer. HMVEC were grown on coverslips in the co-culture model, stained with rabbit anti-VE Cadherin and secondary anti-rabbit Alexa Fluor 647. (A) Control, (B) PEPs $PM_{0.1}$ 0.5 µg/mL, (C) PEPs $PM_{0.1}$ 1.0 µg/mL, (D) PEPs $PM_{2.5}$ 1.0 µg/mL, (E) SiO_2 1.0 µg/mL, and (F) WF 1.0 µg/mL. Arrows indicate gap formation with the endothelial monolayer. Images were taken using a Zeiss LSM510 microscope. Images represent n=3.

PEPs increase angiogenesis HMVEC

To determine if SAEC exposure to PEPs would increase angiogenesis in HMVEC, an *in vitro* matrigel endothelial tube formation assay was performed. As seen in Figure 4-5 and Supplemental Figure 4-S5, there was an increase in tube formation with PEPs $PM_{0.1}$ 0.5 µg/mL

and 1.0 μg/mL compared to control and PEPs $PM_{2.5}$ 1.0 μg/mL. The 1.0 μg/mL SiO_2 nanoparticles did not increase tube formation in the HMVEC; however, it can be seen that the 1.0 μg/mL WF did increase the number of tubes. These data demonstrate that SAEC exposure to PEPs $PM_{0.1}$ at both 0.5 μg/mL and 1.0 μg/mL has the ability to increase angiogenesis in HMVEC within the co-culture model.

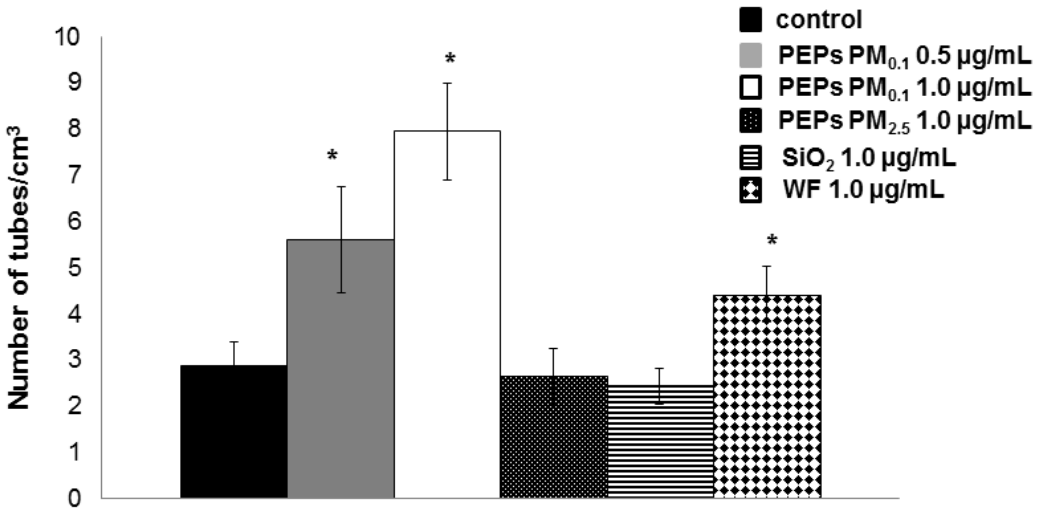

Figure 4-5. HMVEC exhibit increased angiogenesis due to SAEC treatment with PEPs. The quantification of the tube formation in HMVEC within the various treatments at 10x magnification. Pictures represent n=3. *indicates $p < 0.05$ compared to control.

PEPs induce secretion of inflammatory mediators

To determine whether SAEC exposure to PEPs induces cellular communication within the co-culture system, a panel of 27 cytokines and chemokines were measured in both the conditioned media and cellular lysates of each cell type. After a 24 h treatment with PEPs $PM_{0.1}$, SAEC-conditioned media had significantly elevated levels of IL-1b, IL-1ra and IL-6 compared to the control (Figure 4-6A). It can be seen that WF also increased levels of IL-1b and IL-6 but

there was no significant difference between control and SiO_2. As for the SAEC cellular lysates, the following cytokines were all significantly elevated post-exposure to PEPs $PM_{0.1}$ when compared to control (Figure 4-6B): IL-6, IL-8, basic fibroblast growth factors (FGF basic), interferon gamma induced protein 10 (IP-10), monocyte chemotactic protein-1 (MCP-1) and RANTES. The SiO_2-treated SAEC cellular lysates induced an increase in MCP-1 and RANTES when compared to control. As seen in Figure 4-6C, the HMVEC-conditioned media showed significant increase in IL-6, MCP-1 and a decrease in MIP-1b in the PEPs $PM_{0.1}$ group when compared to control. The only significant change that occurred in the conditioned media of the comparative nanomaterial was a decrease in IL-6 with the SiO_2 group. To determine if the HMVEC produced any cytokines or chemokines post-indirect exposure to PEPs $PM_{0.1}$, cellular lysates of the HMVEC were also analyzed using the same 27-member panel. As seen in Figure 4-6D, the only inflammatory mediator that was elevated within the HMVEC cellular lysate was IL-8, which remained unchanged within SiO_2 and WF. These data demonstrate that there is a specific cytokine and chemokine profile that is induced in HMVEC upon SAEC treatment with PEPs $PM_{0.1}$ in the co-culture model. Therefore, it can be concluded that IL-1b, IL-1ra and IL-6 were all elevated in the SAEC conditioned media while IL-6, IL-8, FGF basic, IP-10, MCP-1 and RANTES were significantly elevated in the SAEC cellular lysates. Within the HMVEC conditioned media IL-6, MCP-1 and MIP-1b were all elevated, while only IL-8 was elevated within the HMVEC cellular lysates.

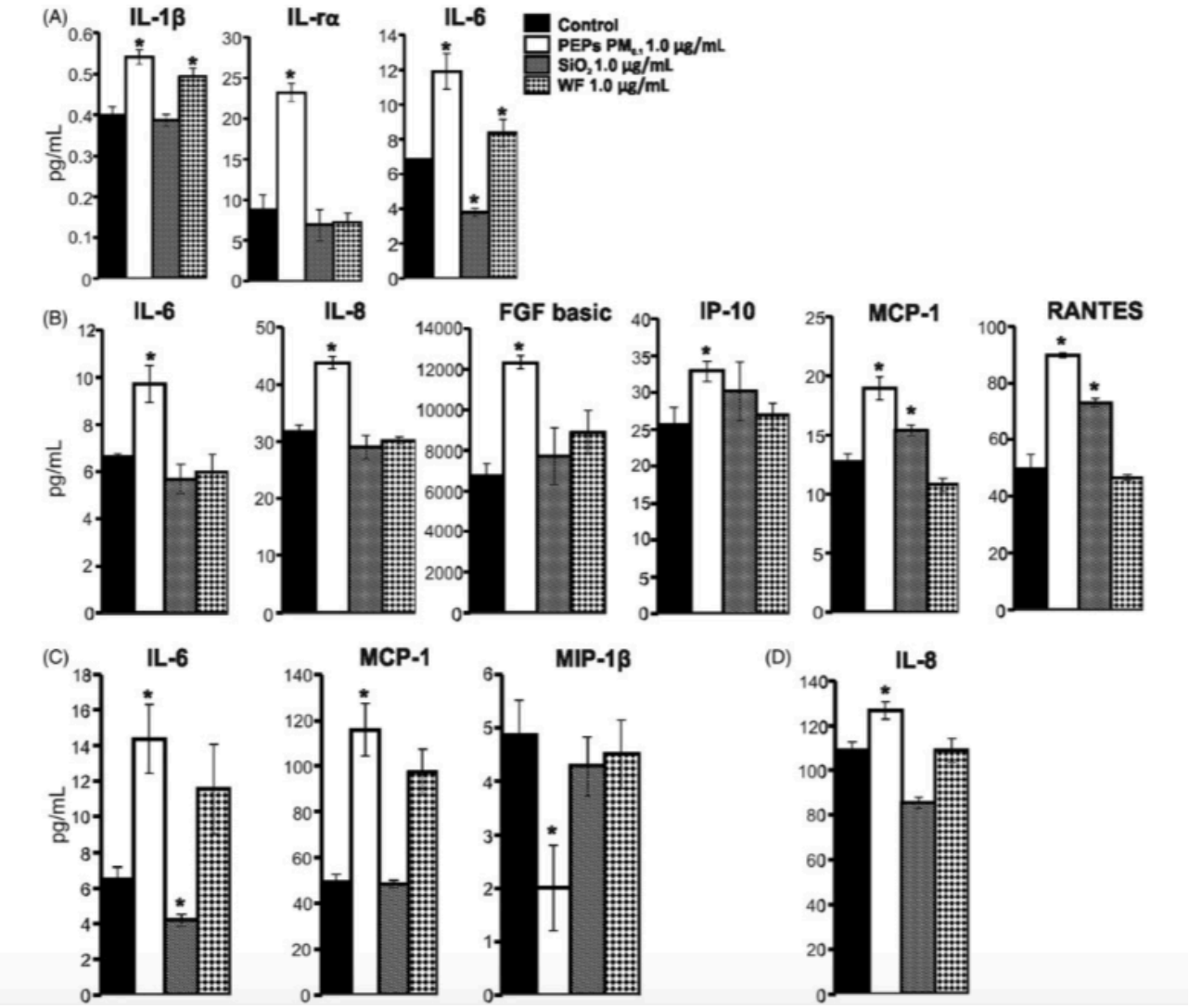

Figure 4-6. Cytokine and chemokine analysis. (A) IL-1 b, IL-1ra, IL-6 levels were measured in SAEC condition media, (B) IL-6, IL-8, FGF basic, IP-10, MCP-1 and RANTES are shown in the cellular lysates of SAEC, (C) IL-6, MCP-1 and MIP-1b are shown within the condition media of HMVEC (D) IL-8 shown in the cellular lysates. Cytokines and chemokines were analyzed after a 24 h treatment of SAEC with PEPs $PM_{0.1}$ 1.0 μg/mL, and SiO_2 1.0 μg/mL and WF 1.0 μg/mL. n=3. * indicates $p < 0.05$ compared to control.

Discussion

The current study provides evidence that PEPs are bioactive and to our knowledge is the first study that has focused on the toxicity of low concentrations (0.5 and 1.0 μg/mL) of real world PEPs instead of the starting bulk toner powder. With the use of the *in vitro* alveolar-capillary unit we were able to demonstrate that PEPs induce cellular communication between the exposed SAEC and the underlying HMVEC. This is an important model to study because it mimics the cellular crosstalk in the alveolar capillary unit upon a nanoparticle inhalation exposure, which is a limitation of monoculture systems. Upon indirect treatment of PEPs, the endothelium was shown to be disrupted through actin remodeling and gap junctions, which has been linked previously to inflammation (Mehta & Malik, 2006). It was also determined that PEPs have the ability to induce ROS in the underlying HMVEC most likely due to the metal content within their complex makeup. Upon further evaluation, PEPs induced an inflammatory response through the activation of cytokines and chemokines, which lead to the crosstalk between SAEC and HMVEC.

Printers have become a standard commodity within offices, homes, schools and many other indoor environments over the past decade. In our two companion papers on the physico-chemical and morphological properties of PEPs and toner formulations, we provide evidence that current toners constitute a NEP and contain ENMs that are subsequently released into the air during consumer use (Pirela et al., 2014b). In particular, the PEPs and toner powder from the printer used in this study shared a complex chemical composition that included a large percentage of organic and elemental carbon, as well as, inorganic elements such as magnesium, aluminum, titanium, iron, cobalt, nickel, copper and zinc, among others. Most of these ENMs released in the air are known to produce negative biological responses in different testing

platforms including lung injury and inflammation, as well as, DNA damage (Demokritou et al., 2013; Watson et al., 2014) and it can be hypothesized based upon this information that the PEPs bioactivity that led to the disruption of the endothelium after epithelial exposure was due to their metal content. To this regard, this study is of paramount importance because it provides evidence that humans are exposed to nanoscale materials released from NEPs during consumer use and those real world exposures may have serious toxicological implications. More importantly, this study illustrates the importance of utilizing the real world exposures across life cycle rather than using the raw material properties for nano-risk assessment studies.

Last but not least, in this study, the *in vitro* alveolar-capillary model of SAEC-HMVEC co-culture was applied to understand the mechanism of PEPs-induced toxicity. It was demonstrated for the first time that PEPs exposure at very low levels altered cellular communication between SAEC and HMVEC. The cellular communication between epithelial and endothelial cells within the lung plays a major role in the pathogenesis of pulmonary inflammation, fibrosis and cancer (Homer et al., 2011; Hoo & Whyte, 2012; Kuebler, 2005; Strieter & Mehrad, 2009; Wallace et al., 2007). This model represents the alveolar-capillary unit, which is the major site of gas exchange within the lung. Damage of this critical pulmonary site due to particle exposure can lead to pulmonary inflammation, fibrosis, decreased gas exchange and other diseases (Strieter & Mehrad, 2009; Wallace et al., 2007). The use of the co-culture model, which allows for the study of epithelial and endothelial cellular communication within the alveolar-capillary unit, offers an advantage over monoculture cell models commonly used in nanotoxicology studies. It is worth noting that a comparative study recently performed by our group showed that the *in vitro* alveolar-capillary co-culture model correlates with *in vivo* results

more closely than a mono-culture model upon treatment with multi-walled carbon nanotubes (MWCNT) (Snyder-Talkington et al., 2014 Unpublished data).

It is worth nothing that SAEC exposure levels were low and equivalent to PEPs inhalation of 1 to 2 h. To our knowledge, this is the first publication that links such a low, non-cytotoxic exposure dose (0.5 and 1.0 μg/mL) to toxicological effects. Additionally, based upon TEM analysis, it was determined that the underlying HMVEC did not have direct contact with PEPs, which is consistent with findings from a MWCNT exposure in co-culture model (Snyder-Talkington, 2013b). In summary, it was clearly demonstrated in this study that the observed biological response seen in the underlying HMVEC in the SAEC-HMVEC co-culture model is independent of cell death signaling.

One possible mechanism for the cellular cross talk is through the expression of cytokines and chemokines. Our results showed that IL-6 was significantly elevated in both the conditioned media of the SAEC and HMVEC, but its expression was only found significantly increased in the cellular lysates of SAEC and not of HMVEC. IL-6 is known to be a pro-inflammatory cytokine that plays a major role in the acute and chronic immune responses by activating pathways that control proliferation, differentiation migration and apoptosis (Maruo et al., 1992; Scheller et al., 2014). It was also noted that MCP-1, also known as CCL2, was elevated within both the cellular lysates of epithelial-exposed PEPs and the conditioned media of the underlying endothelial cells. MCP-1 regulates the migration and infiltration of macro- phages and monocytes during an immune response and has been linked to multiple disease states, such as pulmonary disease (Deshmane et al., 2009). Both IL-6 and MCP-1 have been directly linked to the activation of endothelial cells resulting in increased angiogenesis and membrane permeability (Cromer et al., 2014; Garcia-Roman & Zentella-Dehesa, 2013; Middleton et al., 2014). These

data suggests that the cellular communication is being mediated by both IL-6 and MCP-1. This correlates with findings from a series of *in vivo* and *in vitro* studies evaluating the toxicity of copier-emitted particles (Khatri, 2013a,b; Pirela et al., 2013) and studies that linked the expression of MCP-1 to fibrosis in an *in vivo* MWCNT study (Snyder-Talkington et al., 2013a). It can be concluded here that the alterations seen in the endothelium upon SAEC PEPs exposure is linked to the inflammatory signaling of IL-6 and MCP-1. ICAM-1 and VCAM-1 are adhesion molecules in their soluble form that play a key role within the interaction of leukocytes and endothelial cells (Muller, 2011). It has been previously published that both soluble ICAM-1 and VCAM-1 play a major role in elevated inflammatory response and endothelial dysfunction (Lawson & Wolf, 2009). It is worth noting that both ICAM-1 and VCAM-1 have been shown to be elevated upon particle exposure (Pirela et al., 2013; Snyder-Talkington et al., 2013b). We will also focus on ICAM-1 and VCAM-1 in the next phase of our search, which focuses on *in vivo* mouse exposures.

In this study, it was also demonstrated that PEPs-exposed SAEC induced an up-regulation of ROS production in HMVEC, which is consistent with the results of IL-6 expression since it induces ROS to activate various molecular pathways (Szmitko et al., 2003). It has been well demonstrated that nanoparticle exposure induces the production of ROS (Apopa et al., 2009; Kovacic, 2013; Nel et al., 2006; Roy et al., 2014). The increase in the production of ROS within a cell can lead to damage of DNA, proteins or lipids (Watson et al., 2014). ROS are the terms used for the intermediate forms of aerobic metabolism, which includes superoxide (O_2•), hydrogen peroxide (H_2O_2), hydroxyl radical (•OH) and peroxynitrite (ON_2•) (Rahal et al., 2014). Studies have shown that increased ROS production is related to interruption of the endothelial monolayer and pulmonary hypertension within the lungs (Roberts et al., 2010; Tabima et al.,

2012), indicating that epithelial exposure to PEPs has the ability to increase the ROS production in the underlying endothelial cells, which may lead to a disruption in the endothelial monolayer.

Another interesting finding of this study is the fact that epithelial cell exposure to PEPs induced endothelial cell perm ability and angiogenesis. The vascular endothelial monolayer forms a semi-selective permeability barrier between blood and interstitial space to control the movement of proteins, macromolecules and water across the vessel wall. The preservation of the endothelial monolayer is important to maintain gas exchange function of alveolar-capillary units. Aberrations of the permeability barrier integrity may lead to damage of alveolar-capillary units, which can play a major role in the pathogenesis of fibrosis, angiogenesis, cardiovascular diseases, inflammation and acute lung injury syndromes (Mehta & Malik, 2006). Angiogenesis is the process of new blood vessel formation, which involves vascular permeability, growth factors recruitment, migration, proliferation and tube formation. The process of increasing angiogenesis is associated with cancer, cardiovascular diseases and chronic inflammation (Adams & Alitalo, 2007; Bryan & D'Amore, 2007; Griffioen & Molema, 2000). Results from this study strongly indicate that cellular signaling from epithelial-exposed PEPs induces endothelial angiogenesis through IL-6 and MCP-1 path- ways (Cromer et al., 2014; Garcia-Roman & Zentella-Dehesa, 2013; Middleton et al., 2014). Moreover, the production of IL-6 has been shown to produce cytosolic IL-8 within endothelial cells to increase angiogenesis (Volk et al., 2000). Indeed, our results show that PEPs-exposed SAEC up-regulates the production of IL-8 in the HMVEC cellular lysate. Therefore, it can be concluded that the cytokine and chemokine signaling cascade from PEPs-exposed SAEC is a key step in the cellular alterations seen in the underlying HMVEC.

Conclusion

This study, along with the companion studies on the physico- chemical characteristics of nanoparticles released from toner during consumer use (printing), is the first to demonstrate that the ENMs that are incorporated into the toner are emitted during the use of a laser printer and have bioactive properties. This study provides important findings on the mechanistic pathways of observed bioactivity and demonstrates that exposure of SAEC to different size fractions of PEPs at doses comparable to current inhalation exposures at consumer level induces adverse effects to the underlying HMVEC through cellular communication. The results indicate that the adverse endothelial effects could be due to cellular signals of IL-6 and MCP-1 from the epithelial cells. Demonstration of adverse effects caused by exposure to PEPs in an *in vitro* co-culture model justifies further *in vivo* and *in vitro* toxicological studies of PEPs.

Contributions

Sandra V. Pirela designed and performed the sampling and collection of the size-fractionated PEPs, as well as the preparation of suspension of PEPs and their subsequent characterization before use for the *in vitro* experiments.

Declaration of interest

The authors report no competing financial interests. The findings and conclusion in the report are of the authors and do not necessarily represent the views of the National Institute for Occupational Safety and Health. The authors acknowledge funding for this study from NIEHS (Grant # ES-000002) and NIOSH and CPSC (Grant # 212-2012 -M-51174).

Supplemental Material

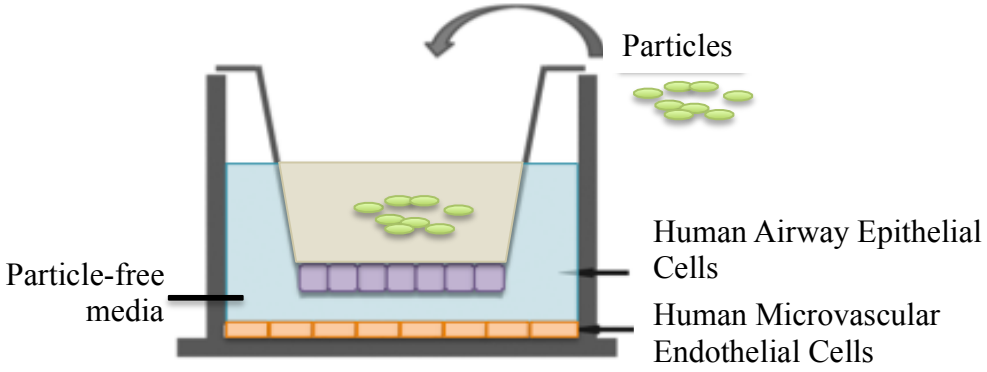

Figure 4-S1. Alveolar-Capillary Unit co-culture *in vitro* model.

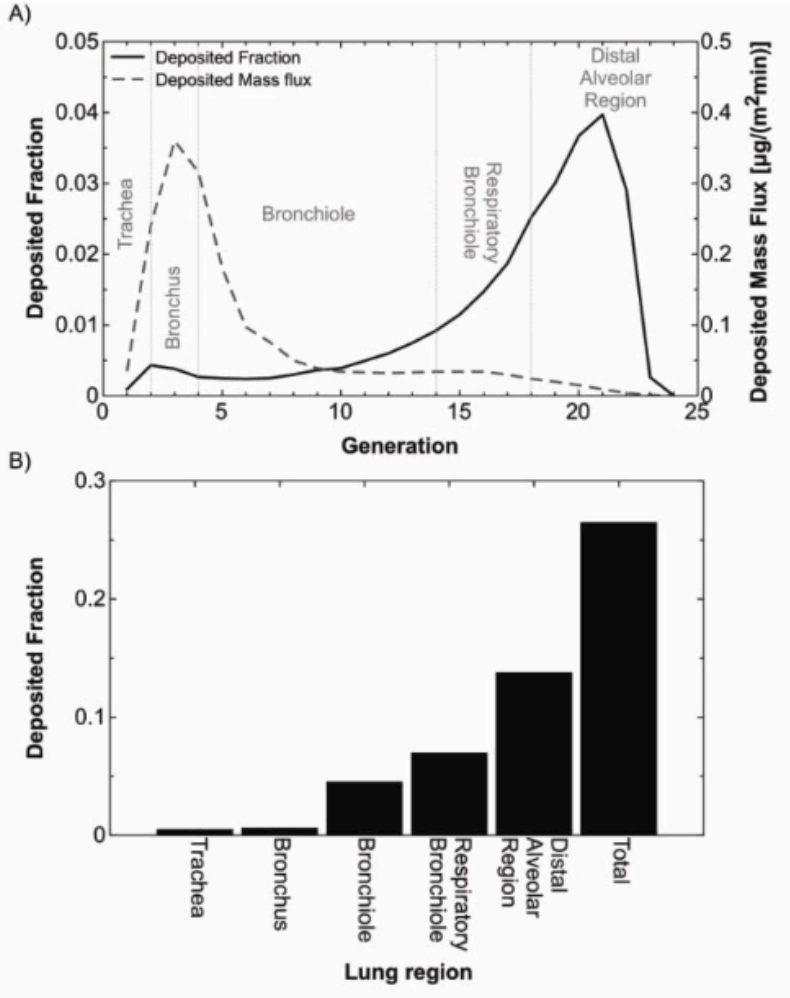

Figure 4-S2. Deposition of PEPs in the human lung. A) Deposition fraction and deposition mass flux as a function of generation number of the human respiratory tree. B) Deposition mass fraction in the total and various sections of the human lung: trachea, bronchus, bronchiole, respiratory bronchioles and distal alveolar region.

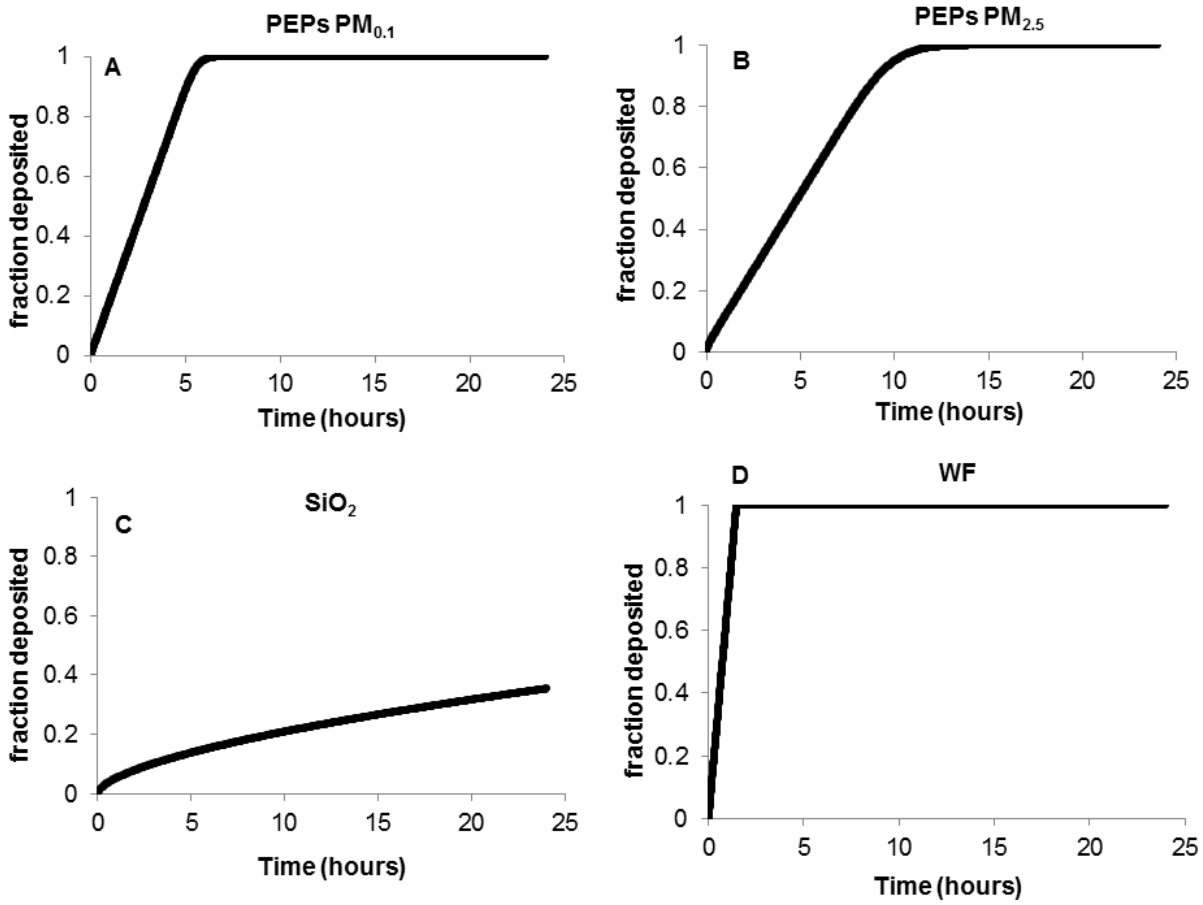

Figure 4-S3. Deposited fraction of the (A) PEPs $PM_{0.1}$, (B) PEPs $PM_{2.5}$, (C) SiO_2 and (D) WF.

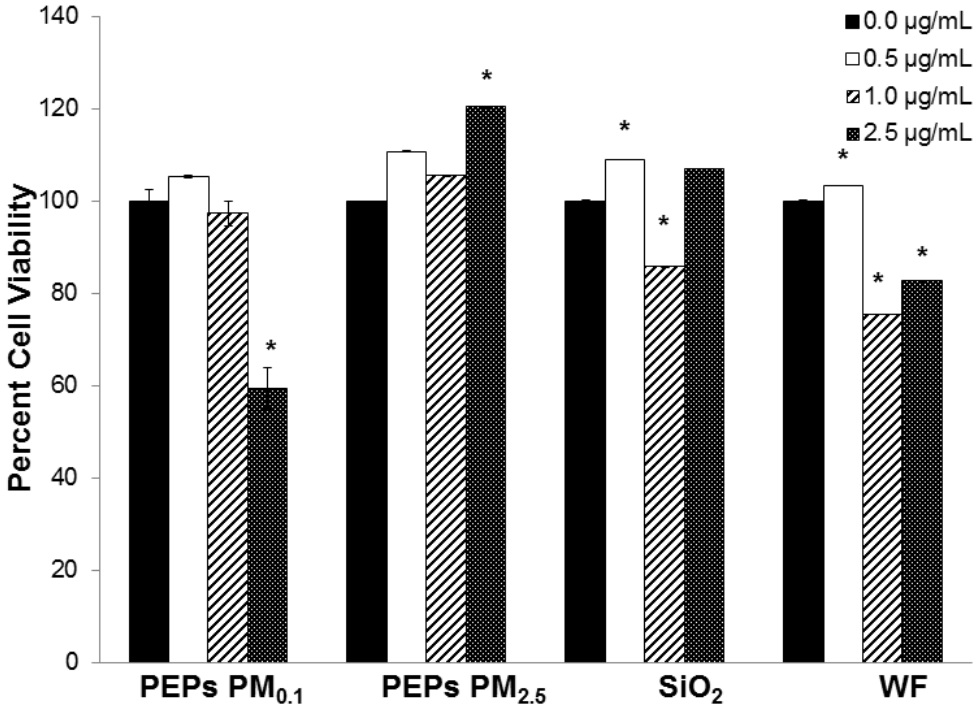

Figure 4-S4. Cytotoxicity of particles in SAEC. SAEC were treated with 0.0 µg/mL, 0.5 µg/mL, 1.0 µg/mL, and 2.5 µg/mL of PEPs $PM_{0.1}$, PEPs $PM_{2.5}$, SiO_2, or WF for 24 h and analyzed by MTT assay. n=3, * indicates $p < 0.05$ compared to relative control.

(A)

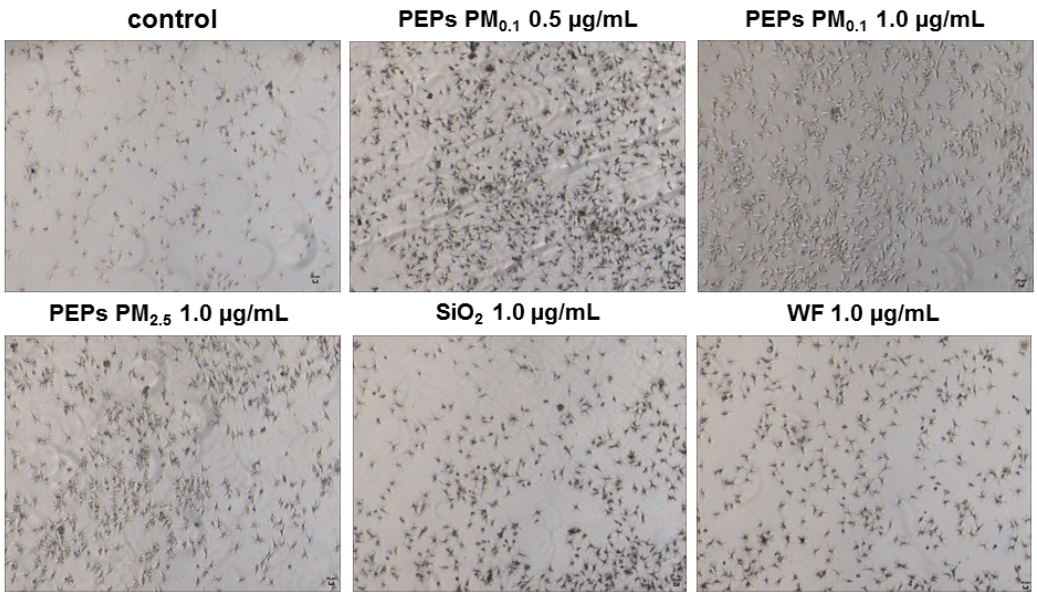

(B)

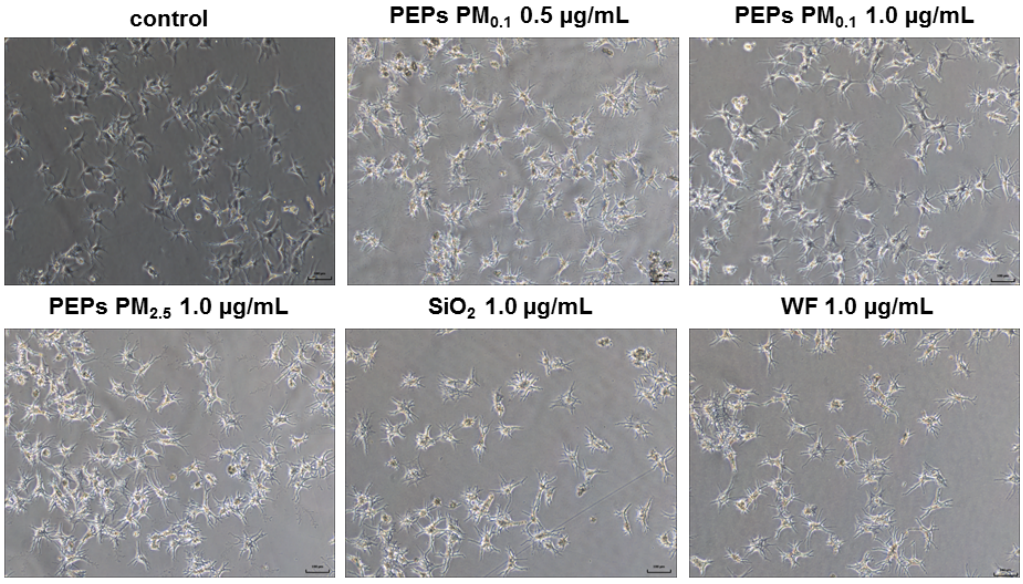

Figure 4-S5. HMVEC exhibit increased angiogenesis due to SAEC treatment with PEPs. HMVEC were grown in the co-culture model and plated on matrigel. (A) HMVEC imaged at 4x and (B) HMVEC imaged 10x to show tube formation with HMVEC after co-culture with SAEC treated with particles. Pictures are a representation of n=3. *indicates $p < 0.05$ compared to control.

Table 4-S1. Summary of parameters used in the *in vivo* lung Multiple Path Particle Deposition model (MPPD2) (Anjilvel and Asgharian 1995). The parameters for airborne nanoparticle distribution (assuming density of aerosolized particles as 2.27 g/cm^3) were derived from real-time monitoring data from Printer B1 as previously published by our group (Pirela, 2014).

Human Model	**Breathing Parameters**	**Airborne Nanoparticle Distribution**
Functional Residual Capacity: 3300 mL	*Tidal Volume*: 625 ml	*Count Mean Diameter:* 57.45 nm
Head Volume: 50 mL	*Breathing Frequency:* 12 breaths/ min	*Geometric Standard Deviation*: 1.67
Breathing Route: Nasal	*Inspiratory Fraction*: 0.5	*Mass Concentration*: 23.86 µg/m^3
	Pause Fraction: 0.0	

Table 4-S2. *In vitro* doses and respective equivalent consumer inhalation exposure to PEPs.

Particle	Cell administered dose[a] (µg/mL)	Cell delivered dose[a] (µg/mL)	Corresponding consumer inhalation exposure duration (hours) to PEPs [b]	
			Conducting, transitional and respiratory zones	Transitional and respiratory zones
PEPs ($PM_{0.1}$, $PM_{2.5}$)	0.5	0.5	1	13
	1.0	1.0	2	26
	2.5	2.5	5	65
SiO_2	0.5	0.177	-	-
	1.0	0.354		
	2.5	0.885		
MS-WF	0.5	0.5	-	-
	1.0	1.0		
	2.5	2.5		

Notes: [a] *In vitro* administered and delivered to cell doses are based on a 24-hour cell exposure. [b] Calculations of the corresponding consumer inhalation exposure duration (hours) to PEPs was based on the added values of deposition mass flux (µg/m^2•min) in the various human airways, excluding head airways: the conducting zone (generations 0 to 16) and the transitional and respiratory zones (generations 17 through 23).

Bibliography

Adams RH, Alitalo K. 2007. Molecular regulation of angiogenesis and lymphangiogenesis. Nat Rev Mol Cell Biol 8:464–78.

Anjilvel S, Asgharian B. 1995. A multiple-path model of particle deposition in the rat lung. Fund Appl Toxicol 28:41–50.

Antonini J, Lawryk N, Murthy G, Brain J. 1999. Effect of welding fume solubility on lung macrophage viability and function in vitro. J Toxicol Environ Health A 58:343–63.

Antonini J, Zeidler-Erdely P, Young S, Roberts J, Erdely A. 2012. Systemic immune cell response in rats after pulmonary exposure to manganese-containing particles collected from welding aerosols. J Immunotoxicol 9:184–92.

Apopa PL, Qian Y, Shao R, Guo NL, Schwegler-Berry D, Pacurari M, et al. 2009. Iron oxide nanoparticles induce human microvascular endothelial cell permability through reactive oxygen species produc- tion and microtubule remodeling. Part Fibre Toxicol 6:1.

Barthel M, Pedan V, Hahn O, Rothhardt M, Bresch H, Jann O, Seeger S. 2011. XRF-analysis of fine and ultrafine particles emitted from laser printing devices. Environ Sci Technol 45:7819–25.

Bello D, Martin J, Santeufemio C, Sun QW, Bunker KL, Shafer M, Demokritou P. 2013. Physico-chemical and morphological character- isation of nanoparticles from photocopiers: implications for environ- mental health. Nanotoxicology 7:989–1003.

Bryan BA, D'Amore PA. 2007. What tangled webs they weave: rho- GTPase control of angiogenesis. Cell Mol Life Sci 64:2053–65.

Byeon JH, Kim J-W. 2012. Particle emission from laser printers with different printing speeds. Atmos Environ 54:272–6.

Chang CL, Demokritou P, Shafer M, Christiani D. 2013. Physico-chemical and toxicological characteristics of welding fume derived particles generated from real time welding processes. Env Sci Process Impact 15:214–24.

Chia-Wei Lee D-JH. 2007. Measurements of fine and ultrafine particles formtion in photocopy centers in Taiwan. Atmos Environ 41:6598–609. Cohen J, Deloid G, Pyrgiotakis G, Demokritou P. 2013. Interactions of engineered nanomaterials in physiological media and implications for

in vitro dosimetry. Nanotoxicology 7:417–31. Cohen JM, Teeguarden JG, Demokritou P. 2014. An integrated approach

for the in vitro dosimetry of engineered nanomaterials. Part Fibre

Toxicol 11:20. Cromer WE, Zawieja SD, Tharakan B, Childs EW, Newell MK,

Zawieja DC. 2014. The effects of inflammatory cytokines on

lymphatic endothelial barrier function. Angiogenesis 17:395–406. DeLoid G, Cohen JM, Darrah T, Derk R, Rojanasakul L, Pyrgiotakis G, et al. 2014. Estimating the effective density of engineered nanomater-

ials for in vitro dosimetry. Nat Commun 5:3514. Demokritou P, Gass S, Pyrgiotakis G, Cohen JM, Goldsmith W,

McKinney W, et al. 2013. An in vivo and *in vitro* toxicological characterisation of realistic nanoscale CeO(2) inhalation exposures. Nanotoxicology 7:1338–50.

Demokritou P, Lee SJ, Ferguson ST, Koutrakis P. 2004. A compact multistage (cascade) impactor for the characterization of atmospheric' aerosols. J Aerosol Sci 35:281–99.

Deshmane SL, Kremlev S, Amini S, Sawaya BE. 2009. Monocyte chemoattractant protein-1 (MCP-1): an overview. J Interferon Cytokine Res 29:313–26.

Furukawa Y, Aizawa Y, Okada M, Watanabe M, Niitsuya M, Kotani M. 2002. Negative effect of photocopier toner on alveolar macrophages determined by in vitro magnetometric evaluation. Ind Health 40: 214–21.

Garcia-Roman J, Zentella-Dehesa A. 2013. Vascular permeability changes involved in tumor metastasis. Cancer Lett 335:259–69.

Gass S, Cohen JM, Pyrgiotakis G, Sotiriou GA, Pratsinis SE, Demokritou P. 2013. A safer formulation concept for flame-generated engineered nanomaterials. ACS Sustain Chem Eng 1:843–57.

Griffioen AW, Molema G. 2000. Angiogenesis: potentials for pharma- cologic intervention in the treatment of cancer, cardiovascular diseases, and chronic inflammation. Pharmacol Rev 52:237–68.

He C, Morawska L, Taplin L. 2007. Particle emission characteristics of office printers. Environ Sci Technol 41:6039–45.

Homer RJ, Elias JA, Lee CG, Herzog E. 2011. Modern concepts on the role of inflammation in pulmonary fibrosis. Arch Pathol Lab Med 135: 780–8.

Hoo ZH, Whyte MK. 2012. Idiopathic pulmonary fibrosis. Thorax 67: 742–6.

Jamieson L. 2012. Ink and toner cartridge use among SMBs in the United States. Photizo Group. Available at: http://photizogroup.-com/ wp-content/uploads/2012/09/8.31.12-U.S.-SMB-Ink-and-Toner- Cartridge-Use.pdf. Accessed on 17 March 2013.

Jiang Ha L. 2010. Measurement of the surface charge of ultrafine particles from laser printers and analysis of their electrostatic force. Atmos Environ 44:3347–51.

Kagi N, Fuji S, Horiba Y, Namiki N, Ohtani Y, Emi H, et al. 2007. Indoor air quality for chemical and ultrafine particle contaminants from printers. Build Environ 42:1949–54.

Khatri M, Bello D, Pal A, Cohen J, Woskie S, Gassert T, et al. 2013a. Evaluation of cytotoxic, genotoxic and inflammatory responses of nanoparticles from photocopiers in three human cell lines. Part Fibre Toxicol 10:42.

Khatri M, Bello D, Pal A, Woskie S, Gassert T, Demokritou P, Gaines P. 2013b. Toxicological effects of PM0.1–2.5 particles collected from a photocopy center in three human cell lines. Inhal Toxicol 25:621–32.

Kovacic PSR. 2013. Nanoparticles: toxicity, radicals, electron transfer, and antioxidants. Methods Mol Biol 1028:15–35.

Kuebler WM. 2005. Inflammatory pathways and microvascular responses in the lung. Pharmacol Rep 57:196–205.

Lawson C, Wolf S. 2009. ICAM-1 signaling in endothelial cells. Pharmacol Rep 61:22–32.

Maruo N, Morita I, Shirao M, Murota S. 1992. IL-6 increases endothelial permeability in vitro. Endocrinology 131:710–14.

McGarry P, Morawska L, He C, Jayaratne R, Falk M, Tran Q, Wang H. 2011. Exposure to particles from laser printers operating within office workplaces. Environ Sci Technol 45:6444–52.

Mehta D, Malik AB. 2006. Signaling mechanisms regulating endothelial permeability. Physiol Rev 86:279–367.

Middleton K, Jones J, Lwin Z, Coward JI. 2014. Interleukin-6: an angiogenic target in solid tumours. Crit Rev Oncol Hematol 89: 129–39.

Mohr U, Ernst H, Roller M, Pott F. 2006. Pulmonary tumor types induced in wistar rats of the co-called ‘‘19-dust study’’. Exp Toxicol Pathol 58: 13–20.

Morawska L, He C, Johnson G, Jayaratne R, Salthammer T, Wang H, et al. 2009. An investigation into the characteristics and formation mechanisms of particles originating from the operation of laser printers. Environ Sci Technol 43:1015–22.

Morimoto Y, Kim H, Oyabu T, Hirohashi M, Nagatomo H, Ogami A, et al. 2005. Negative effect of long-term inhalation of toner on formation of 8-hydroxydeoxyguanosine in DNA in the lungs of rats in vivo. Inhal Toxicol 17:749–53.

Muller WA. 2011. Mechanisms of leukocyte transendothelial migration. Annu Rev Pathol 6:323–44.

Nel A, Xia T, Madler L, Li N. 2006. Toxic potential of material at the nanolevel. Science 311:622–7.

Piao CQ, Liu L, Zhao YL, Balajee AS, Suzuki M, Hei TK. 2005. Immortalization of human

small airway epithelial cells by ectopic expression of telomerase. Carcinogenesis 26:725–31.

Pirela S, Molina R, Watson C, Cohen JM, Bello D, Demokritou P, Brain J. 2013. Effects of copy center particles on the lungs: a toxicological characterization using a Balb/c mouse model. Inhal Toxicol 25:498–508.

Pirela SV, Pyrgiotakis G, Bello D, Thomas T, Castranova V, Demokritou P. 2014a. Development and characterization of an exposure platform suitable for physico-chemical, morphological and toxicological characterization of printer-emitted particles (PEPS). Inhal Toxicol 26:400–8.

Pirela SV, Sotiriou GA, Bello D, Shafer M, Krumeich F, Bunker KL, et al. 2014b. A case study of life-cycle implications from nano-enabled products: consumer exposures to printer-emitted nanoparticles. Nanotoxicology [Epub ahead of print]. doi:10.3109/17435390.2014. 976602.

Rahal A, Kumar A, Singh V, Yadav B, Tiwari R, Chakraborty S, Dhama K. 2014. Oxidative stress, prooxidants, and antioxidants: the interplay. Biomed Res Int 76:1264.

Roberts RA, Smith RA, Safe S, Szabo C, Tjalkens RB, Robertson FM. 2010. Toxicological and pathophysiological roles of reactive oxygen and nitrogen species. Toxicology 276:85–94.

Roy R, Kumar S, Tripathi A, Das M, Dwivedi PD. 2014. Interactive threats of nanoparticles to the biological system. Immunol Lett 158: 79–87.

Scheller J, Garbers C, Rose-John S. 2014. Interleukin-6: from basic biology to selective blockade of pro-inflammatory activities. Semin Immunol 26:2–12.

Schripp T, Wensing M, Uhde E, Salthammer T, He C, Morawska L. 2008. Evaluation of

ultrafine particle emissions from laser printers using emission test chambers. Environ Sci Technol 42:4338–43.

Shao R, Guo X. 2004. Human microvascular endothelial cells immortalized with human telomerase catalytic protein: a model for the study of in vitro angiogenesis. Biochem Biophys Res Commun 321: 788–94.

Slesinski RS, Turnbull D. 2008. Chronic Inhalation exposure of rats for up to 104 weeks to a non-carbon-based magnetite photocopying toner. Int J Toxicol 27:427–39.

Snyder-Talkington BN, Dymacek J, Porter DW, Wolfarth MG, Mercer RR, Pacurari M, et al. 2013a. System-based identification of toxicity pathways associated with multi-walled carbon nanotube- induced pathological responses. Toxicol Appl Pharmacol 272:476–89.

Snyder-Talkington BN, Schwegler-Berry D, Castranova V, Qian Y, Guo NL. 2013b. Multi-walled carbon nanotubes induce human microvascular endothelial cellular effects in an alveolar-capillary co-culture with small airway epithelial cells. Part Fibre Toxicol 10:35.

Sotiriou GA, Diaz E, Long MS, Godleski J, Brain J, Pratsinis SE, Demokritou P. 2012. A novel platform for pulmonary and cardiovas- cular toxicological characterization of inhaled engineered nanomater- ials. Nanotoxicology 6:680–90.

Sriram K, Lin GX, Jefferson AM, Roberts JR, Andrews RN, Kashon ML, Antonini JM. 2012. Manganese accumulation in nail clippings as a biomarker of welding fume exposure and neurotoxicity. Toxicology 291:73–82.

Strieter RM, Mehrad B. 2009. New mechanisms of pulmonary fibrosis. Chest 136:1364–70.

Szmitko PE, Wang CH, Weisel RD, De Almeida JR, Anderson TJ, Verma S. 2003. New markers of inflammation and endothelial cell activation: part I. Circulation 108:1917–23.

Tabima DM, Frizzell S, Gladwin MT. 2012. Reactive oxygen and nitrogen species in pulmonary hypertension. Free Radic Biol Med 52: 1970–86.

Volk T, Hensel M, Schuster H, Kox WJ. 2000. Secretion of MCP-1 and IL-6 by cytokine stimulated production of reactive oxygen species in endothelial cells. Mol Cell Biochem 206:105–12.

Wallace WA, Fitch PM, Simpson AJ, Howie SE. 2007. Inflammation- associated remodelling and fibrosis in the lung – a process and an end point. Int J Exp Pathol 88:103–10.

Wang H, He C, Morawska L, McGarry P, Johnson, G. 2012. Ozone- initiated particle formation, particle aging, and precursors in a laser printer. Environ Sci Technol 46:704–12.

Watson C, Ge J, Cohen J, Pyrgiotakis G, Engelward BP, Demokritou P. 2014. High-throughput screening platform for engineered nanoparticle- mediated genotoxicity using CometChip technology. ACS Nano 8: 2118–33.

Wensing M, Schripp T, Uhde E, Salthammer T. 2008. Ultra-fine particles release from hardcopy devices: sources, real-room measure- ments and efficiency of filter accessories. Sci Total Environ 407: 418–27.

Zeidler-Erdely P, Battelli L, Salmen-Muniz R, Li Z, Erdely A, Kashon M, et al. 2011. Lung tumor production and tissue metal distribution after exposure to manual metal ARC-stainless steel welding fume in A/J and C57BL/6 J mice. J Toxicol Environ Health A 74:728–36.

Appendix B - Chapter 5: Short-term exposure to engineered nanomaterials affects cellular epigenome

Xiaoyan Lu[1], Isabelle R.Miousse[2], Sandra V. Pirela[1], Stepan Melnyk[3], Igor Koturbash[2*], Philip Demokritou[1*]

Nanotoxicology. 2014.

[1]Center for Nanotechnology and Nanotoxicology, Department of Environmental Health, Harvard School of Public Health, Boston, MA, USA

[2]Department of Environmental and Occupational Health, College of Public Health, University of Arkansas for Medical Sciences, Little Rock, AR, USA

[3]Department of Pediatrics, University of Arkansas for Medical Sciences, Little Rock, AR, USA

[*]Corresponding authors:

Abstract

Extensive incorporation of engineered nanomaterials (ENMs) into industrial and biomedical applications increases the risks of exposure to these potentially hazardous materials. While the geno- and cytotoxic effects of ENMs have been investigated, the potential of ENMs to target the cellular epigenome remains largely unknown. Our goal was to determine whether or not industry relevant ENMs can affect the epigenome at low cytotoxic doses. A panel of cells relevant to inhalation exposures such as human and murine macrophages (THP-1 and RAW264.7, respectively) and human small airway epithelial cells (SAEC) were exposed to printer-emitted engineered nanoparticles (PEPs), mild steel welding fumes (MS-WF), copper oxide (CuO), and titanium dioxide (TiO_2) nanoparticles. Toxicological effects, including

cytotoxicity, oxidative stress, and inflammatory responses were assessed, taking into consideration *in vitro* dosimetry. The effects of ENMs on cellular epigenome were determined by addressing the global and transposable elements (TEs)-associated DNA methylation and expression of DNA methylation machinery and TEs. The percentage of ENMs-induced cytotoxicity for all cell lines was in the range of 0-15%. Oxidative stress was evident in SAEC after exposure to PEPs and in THP-1 when exposed to CuO. Additionally, exposure to ENMs resulted in modest alterations in DNA methylation of two most abundant TEs in mammalian genomes, LINE-1 and *Alu*/SINE, their transcriptional reactivation, and decreased expression of DNA methylation machinery in a cell-, dose-, and ENM-dependent manner. These results indicate that exposure to ENMs at environmentally relevant concentrations, aside from the geno- and cytotoxic effects; can also affect the epigenome of target cells.

Introduction

Due to their unique physico-chemical and mechanical properties, ENMs are used extensively in many industrial products and biomedical applications (Pirela et al., 2014b; Pyrgiotakis et al., 2014). While the geno- and cytotoxic effects of ENMs have been investigated in many studies (Cohen et al., 2014a; Setyawatiet al., 2013; Sotiriou et al., 2014; Watson et al., 2014), the potential of ENMs to target the cellular epigenome remains largely unknown. However, it is becoming increasingly recognized that environmental stressors can affect epigenetic mechanisms and that these alterations can play a key role in the development and progression of diseases (Bollati and Baccarelli 2010; Koturbash et al., 2011a).

Epigenetics define somatically heritable changes in gene expression without alterations in DNA sequence. Epigenetic mechanisms of regulation include methylation of DNA, histone modifications, regulation by non-coding RNAs, and nucleosome positioning. DNA methylation,

the most studied epigenetic event, plays a critical role during the development and maintenance of cellular homeostasis. It regulates the expression of genetic information in a sex-, tissue-, and cell type-dependent manner and serves as a key mechanism in silencing of TEs (reviewed in Jones et al., 2012).

Environmental factors have been reported to target the cellular epigenome, indicating TEs as one of the primary targets for alterations in DNA methylation. This is largely due to their abundance: up to two thirds of the genome is estimated to be comprised by TEs (de Koning et al., 2011). A wealth of studies have concluded that ambient particulate matter ($PM_{2.5}$ and PM_{10}) can induce hypomethylation of TEs in blood/buccal cells of exposed humans and in animal and *in vitro* models (Baccarelli et al., 2009; Madrigano et al., 2011; Miousse et al., 2014a; Salam et al., 2012; Stoccoro et al., 2013; Tarantini et al., 2009).

Limited but increasing evidence clearly points to the ability of ENMs to induce epigenetic changes. For instance, cadmium telluride quantum dots (CdTe QDs) have been shown to induce histone hypoacetylation in human breast carcinoma cells (Choi et al., 2008). Other ENMs, such as gold nanoparticles, iron (III) oxide nanoparticles, multi-walled carbon nanotubes, and CdTe QDs induced alterations in miRNA expression (Li et al., 2011; Ng et al., 2011). Similarly, microRNAome was affected in *in vivo* studies (Balansky et al., 2013; Halappanavar et al., 2011). Of particular interest is the study by Gong et al.(2010), which reports that the short-term (24 h) treatment of human keratinocyte cells (HaCaT) with nano-silicon dioxide induced dose-dependent global genomic hypomethylation and alterations in DNA methylation machinery.

Here we hypothesize that ENMs may cause epigenetic changes, exhibited as 1) alterations in global and TEs-associated DNA methylation and 2) the expression of TEs and DNA methylation machinery and that these alterations are both cell- and ENM-dependent. Taking into

account that alveolar epithelial cells and macrophages are directly in contact with inhaled particles and constitute the first line of defense against foreign particles in the lung (Hiraiwa and van Eeden 2013), we exposed these cells to a number of industry related ENMs: PEPs, MS-WF, CuO and TiO_2 nanoparticles at low cytotoxic dose levels. The overall research strategy and experimental design for the study is outlined in Figure 5-1.

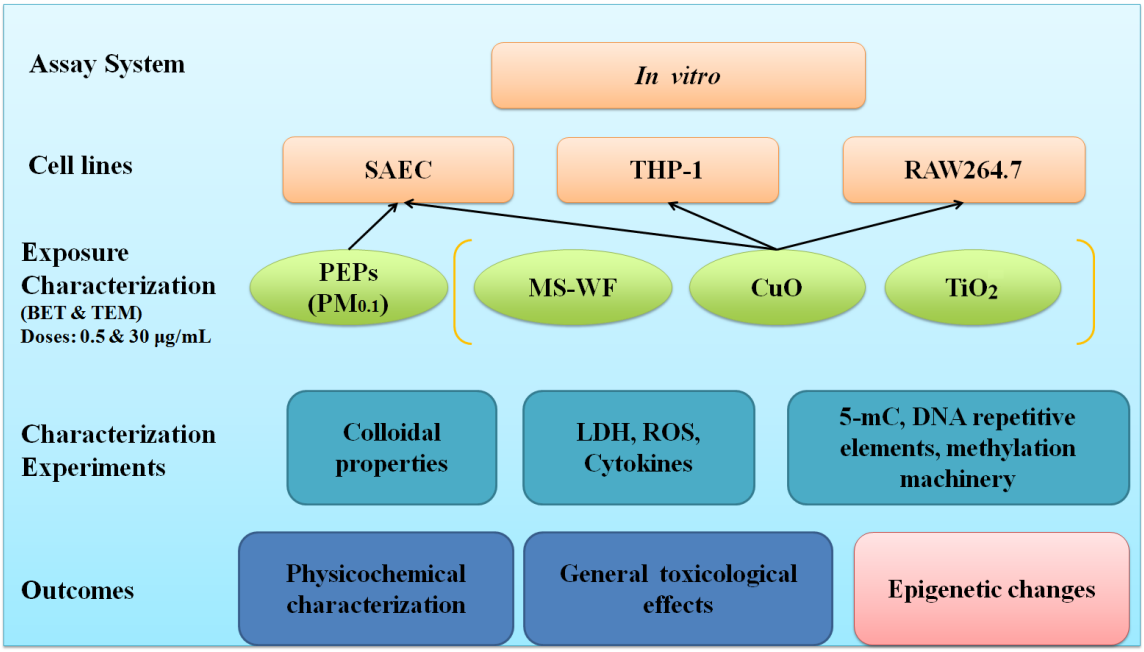

Figure 5-1. Overall experimental design for the epigenetic study of engineered nanomaterials.

Methods

Sources and Characterization of ENMs

A variety of ENMs widely used in commercial applications (TiO_2, CuO) as well as engineered nanoparticles released in the air from nano-enabled products during consumer use (PEPs) and nanoparticles of known toxicological and chemical footprint (MS-WF) were used in the study. The MS-WF particles were a kind gift from Dr. James M Antonini from the National

Institute for Occupational Safety and Health and their physico-chemical properties are described in detail in a previous study (Zeidler-Erdely et al., 2010). The PEPs were sampled using a newly developed printer exposure generation systems described in our previous publication (Pirela et al., 2014a). The TiO_2 and CuO were commercially obtained from EVONIK (EVONIK, Parsippany, NJ) and Sigma Aldrich (Sigma, St. Louis, MO), respectively.

The specific surface area (SSA, m^2/g) of MS-WF, TiO_2, and CuO was measured by the nitrogen adsorption/Brunauer-Emmett-Teller (BET) method using a Micrometrics Tristar 3000 (Micrometrics, Inc., Norcross, GA). The average primary particle diameter d_{BET} of these ENMs was determined from their SSA as d_{BET} (nm) = 6000/(ρ×SSA), where ρ is the material density. Morphological assessment was subsequently performed using transmission electron microscopy (TEM) by a JEOL2100 microscope (JEOL, Peabody, MA) as described in great detail on a previous study (Sotiriou et al., 2012). The detailed chemical composition of PEPs, which were collected from Printer B1, is described in our previous study (Pirela et al., 2014b). Only PEPs with an aerodynamic diameter smaller than 0.1 μm ($PM_{0.1}$) were used in this study.

ENM dispersal and characterization in liquid suspensions

The critical delivered sonication energy (DSE_{cr}) of the ENMs was determined in order to break powder agglomerates in deionized water (DI H_2O) and achieve stable monodispersed agglomerates based on a previously established protocol (Cohen et al., 2013). The DSEcr of MS-WF, TiO_2, CuO, and PEPs was found to be 400, 161, 242, and 514 J/mL, respectively.

The preparation and characterization of particle suspensions for the toxicological studies was performed as follows: a 1 mg/mL stock suspension of each particle suspended in DI H_2O was sonicated to the DSE_{cr} using a Branson Sonifier S-450A (Branson Ultrasonics, Danbury, CT). The DI H_2O-particle suspensions were then diluted to 100 μg/mL level using the

appropriate type of cellular media for the various cell lines used in the study: small airway epithelial cell growth medium with the SAGM bullet kit (SAGM, LONZA, Allendale, NJ) for SAEC, Roswell Park Memorial Institute (RPMI) supplemented with 10% heat-inactivated fetal bovine serum (FBS) and 1×Antibiotic-Antimycotic (RPMI/10%FBS) for THP-1, and Dulbecco's Modified Eagle Medium (DMEM) supplemented with 10% FBS and 100 U/mL penicillin-streptomycin (DMEM/10%FBS) for RAW264.7 (Life Technologies, Grand Island, NY). The pH of all the three media was 7.4. The hydrodynamic diameter (d_H), polydispersity index (PdI), zeta potential (ζ), and specific conductance (σ) of these dispersions at 0 and 24 h exposure time were analyzed by dynamic light scattering (DLS) (ZetasizerNano-ZS, Malvern Instruments, Worcestershire, UK). In addition, the effective density of the formed ENM agglomerates in the culture media was determined using the volumetric centrifugation method (VCM) recently developed by our group (DeLoid et al., 2014). Effective density along with the size of the formed agglomerates are the two most important determinants of the fate and transport and dosimetry *in vitro* (Cohen et al., 2014b). A brief description of the VCM method is presented in Supplementary Materials.

In vitro dosimetric considerations

The actual delivered-to-cell dose of the test particles in specific media as a function of exposure time was determined by the hybrid VCM-*in vitro* sedimentation, diffusion, and dosimetry (VCM-ISDD) method recently developed by our group (Cohen et al., 2014b; Deloid et al., 2014). A brief description is presented in Supplementary Materials.

Cell culture

The RAW264.7 were purchased from ATCC (Manassas, VA) and cultured in DMEM/10% FBS. The SAEC were a present from Jennifer Sisler (NIOSH, Morgantown, WV) and cultured in SAGM. The THP-1 were a gift from Dr. Lester Kobzik (Harvard School of Public Health, Boston, MA) and cultured in RPMI/10% FBS. All cells were cultured at 37°C with 5% carbon dioxide.

The cells were exposed to MS-WF, TiO_2, CuO, and PEPs dispersed in the respective cell culture media at two doses (0.5 and 30 μg/mL) for 24 h. PEPs exposures were only performed on the SAEC and RAW264.7, while the three other particle types were used on all three cell lines. All ENM suspensions were prepared as described above prior to cellular treatment. Cell seeding and harvesting details can found in Supplementary Materials.

Cell viability analysis

The CytoTox-One Homegenous Membrane Integrity Assay (Promega, Madison, WI) was used to estimate the number of non-viable cells present after the exposure to ENMs by measuring the amount of lactate dehydrogenase (LDH) leaked from the cells. The Lysis Solution was used as a positive control, which was included in CytoTox-One Homegenous Membrane Integrity Assay to generate maximum LDH release. Fluorescence intensity was detected by SoftMax Pro 6 GxP Microplate Data Acquisition and Analysis System (Molecular Devices, Sunnyvale, CA) with an excitation/emission wavelength of 560/590 nm. To ensure that the nanoparticles did not interfere with the assay results, particle-only and media-only control groups were used. The particle-only controls were particles in media at 0.5 or 30 μg/ml concentrations (without cells), and media-only controls were only media in the absence of cells. Results indicated that the fluorescence intensity of the particle-only control groups was almost the same

as the media-only group indicative of no autofluorescence effects from particles (data not shown).

Oxidative stress assessment

Dihydroethidium (DHE), a superoxide indicator, is a fluorescent probe used to evaluate the oxidative stress in cells after exposure to ENMs. Fifteen percent hydrogen peroxide (15% H_2O_2, 4.9 mol/L) was used as positive control for 30 min at the end of 24 h exposure. Then, cells were incubated with 5 μM DHE at 37°C for 30 min. The fluorescence intensity was detected by SoftMax Pro 6 GxP Microplate Data Acquisition and Analysis System (Molecular Devices, Sunnyvale, CA) with an excitation/emission wavelength of 518/605 nm. Particle-only control experiments were also included in this assay and compared with media-only control groups. Results indicated that autofluorescence effects were only detected in the particle-only control groups of MS-WF and TiO_2 in SAEC media and TiO_2 in THP-1 media at 30 μg/mL. Thus, the signals for the aforementioned ENM exposures in both cell lines were corrected to take into the account the autofluorescence effects of particle-only controls.

Cytokines analysis

SAEC were treated with 30 μg/mL MS-WF, CuO, and PEPs for 24 h. Cell supernatants were collected and assayed by Eve technologies using a human 41-multiplex assay (Eve Technologies, Calgary, Alberta, Canada). The standard curve matrix, which is the equivalent of a positive control, is used by EVE Technologies with their own specific standard samples for each cytokine (Bedran et al., 2014; Egli et al., 2014).

Nucleic Acids Extraction

RNA and DNA were extracted simultaneously from flash-frozen cells using the AllPrep Mini Kit (Qiagen, Valencia, CA) according to the manufacturer's protocol. DNA concentrations were analyzed by the Nanodrop 2000 (Thermo Scientific, Waltham, MA), and DNA integrity was evaluated on 1% agarose gel.

Analysis of 5-Methylcytosine(5-mC) and 5-hydroxymethylcytosine (5-hmC) levels

RNaseA (Sigma, St. Louis, MO) was added to 1 μg of genomic DNA to a final concentration of 0.02 mg/mL and incubated at 37°C for 15 min. Purified DNA was digested into component nucleotides using Nuclease P1, snake venom phosphodiesterase, and alkaline phosphatase as previously described (James et al., 2010). Methodology has been described in Supplementary Materials.

Analysis of methylation status of TEs

Methylation at the LINE1 and *Alu*/SINE elements was assessed by methylation-sensitive quantitative Real-Time Polymerase Chain Reaction (qRT-PCR). The detail method has been described in Supplementary Materials. Primers are listed in Supplementary Table 5-S1.

Quantitative analysis of gene and TEs expression levels

Complementary DNA (cDNA) was synthesized from 1 μg RNA using random primers and a High Capacity cDNA Reverse Transcription Kit (Applied Biosystems, Foster City, CA) according to the manufacturer's protocol. Quantitative real-time PCR (qRT-PCR) to determine the levels of gene transcripts was performed using 10 ng of cDNA per reaction and the TaqMan Universal PCR Master Mix, no AmpErase® UNG (Life Technologies) on a ViiA 7 instrument (Life Technologies). Assay IDs used in the study are provided in Supplementary Table 5-S2.

Primers for determination of mRNA abundance of LINE-1 and *Alu*/SINE elements are provided in the Supplementary Table 5-S3. The ΔCt values for all genes were determined relative to the control gene *GAPDH* or *RPS13/Rps29* (Supplementary Tables 5-S2 and 5-S3). The ΔΔCt were calculated using each exposed group means relative to control group as described previously (Schmittgen and Livak, 2008). All qRT-PCR reactions were conducted in triplicate and repeated twice.

Copy numbers analysis

LINE-1 copy number was assessed as following: LINE1 ORF2 was amplified by real-time quantitative PCR from 10 ng of gDNA. Relative abundance of the target in gDNA was normalized to 5S ribosomal DNA using the ΔΔCt method. The FAM/ZEN-conjugated primers with the probe sequence are shown in Supplementary Table 5-S4 (Integrated DNA Technologies, Coralville, IA) and were used at a final concentration of 5 μM. Amplification was performed for 40 cycles using conditions for the 2X Taqman Universal Master Mix as recommended by the manufacturer (Life Technologies).

Statistical analysis

The significance was determined by one way ANOVA, followed by Dunnett's or Tukey's test using GraphPad Prism 5.0 software. A $p\text{-}value \leq 0.05$ was considered to be significant.

Results

Physico-chemical and morphological characterization of ENMs

Primary particle size as determined by BET and TEM methods for MS-WF, TiO_2, CuO, or PEPs is shown in Supplementary Figure 5-S1. The BET diameters for MS-WF, TiO_2, and CuO

were 23.8, 21.0, and 58.7 nm, respectively. Similar results were observed by TEM analysis. Moreover, the primary particle size of PEPs was also below 100 nm detected by TEM analysis.

Colloidal properties measured by DLS for all ENMs suspended at 100 μg/mL in either DI H_2O or media are summarized in Supplementary Table 5-S5. First, the d_H and zeta potential were measured at 0 h after sonication by DEScr. Generally, formed ENM agglomerates in SAGM were bigger than other two media. As shown in Supplemental Table 5-S5, for MS-WF, TiO_2, CuO, or PEPs in SAGM, the d_H was found to be 1526.7 ± 259.6, 774.4 ± 59.61, 1367 ± 73.12, and 381.7 ± 40.2 nm, respectively. In RPMI/10%FBS, the d_H for TiO_2, CuO, or PEPs was much smaller than that in SAGM and detected as 307.7 ± 25.22, 907.9 ± 24.81, and 227.3 ± 105.0 nm for these particles, respectively, with little change for MS-WF (1502 ± 96.26 nm). Similarly, the d_H for all ENMs in DMEM/10%FBS was also smaller than that in SAGM. It was observed as 783.0 ± 21.26, 390.4 ± 16.04, 828.3 ± 95.49, and 298.0 ± 5.73 nm for MS-WF, TiO_2, CuO, or PEPs, respectively. Moreover, the zeta potential was found to be negative for TiO_2 and CuO suspended in DI H_2O and the three different media at 0 h. For PEPs and MS-WF in DMEM/10%FBS, zeta potential was found to be negative (-15.9 mV for PEPs, and -12.5 mV for MS-WF) as well as PEPs in DI H_2O (-20.6 mV), and the rest were positive for these two ENMs in different suspensions at 0 h.

The stability of the colloids was also subsequently evaluated 24 h post-sonication to DSE_{cr} (Supplementary Table 5-S5). The d_H at 24 h was found to be similar as those of 0 h for all the ENMs in the three different media. Moreover, the zeta potential at 24 h was also consistent with the results of 0 h for TiO_2 and CuO suspended in DI H_2O and the three different media. For PEPs, the zeta potential at 24 h was similar to those of 0 h in the three different media, except in SAGM which was a little bit lower than that of 0 h (1.22 mV at 24 h versus 9.97 mV at 0 h). For

MS-WF, the zeta potential in SAGM and RPMI/10%FBS was turned to negative at 24 h (-7.56 mV for SAGM, and -7.63 mV for RPMI/10%FBS) and positive at 0 h (18.8 mV for SAGM, and 12.1 mV for RPMI/10%FBS); however, the zeta potential in DMEM/10% FBS was similar between 0 and 24 h. Taken together, the ENM suspensions exhibited stability during the exposure time.

***In vitro* dosimetric considerations**

In order to determine the cell-delivered dose of all ENMs in the three cell culture media as a function of exposure time, the VCM-ISDD method was used. In general, ENMs with greater values of hydrodynamic diameter and effective density in media may deposit faster than those with smaller values. As shown in Supplementary Figures 5-S2 and 5-S3, CuO and MS-WF deposited at a faster rate than TiO_2 and PEPs in the three media for both well plate configurations. This is consistent with their relatively large hydrodynamic diameters (Supplementary Table 5-S5). It will take less than 5 h for all of the administered mass of MS-WF or CuO to deposit on the cells for both the 96-well plate and 100-mm diameter dish configurations. However, the opposite was observed for TiO_2 and PEPs, especially when suspended in RPMI/10%FBS and DMEM/10%FBS. In 96-well plates, only approximately 66% of the administrated dose of PEPs in RPMI/10%FBS will actually reach the bottom of the wells after 24 h exposure, while about 37% of the PEPs in DMEM/10%FBS will reach the bottom; and approximately 93% of the administrated dose of TiO_2 in these two media will actually deposit to the bottom. Although with 100-mm diameter dishes, almost 100% TiO_2 and PEPs deposited to the bottom after 24 h exposure; settling times were longer than those of MS-WF and CuO that also settled 100% at 24 h exposure time.

Cytotoxicity of ENMs

In order to evaluate the potential impact of ENMs on lung tissue, human epithelial cells as well as human and murine macrophages were exposed to MS-WF, TiO_2, CuO, and/or PEPs at 0.5 (low dose) and 30 μg/mL (high dose) for 24 h. LDH analysis provides evidence that all ENMs have a dose-dependent cytotoxic response in all three cell lines, with the exception of CuO on THP-1. The two CuO treatments in this cell line didn't show any cytotoxicity compared with control group, while CuO were the only toxic particles on RAW264.7 among all the ENMs. The percentage of cytotoxicity was in the range of 0-15% for all ENMs in the three cell lines, when compared to the untreated control group (Figure 5-2A).

Oxidative stress induced by ENMs

Levels of ROS were increased in PEPs-treated SAEC and CuO-treated THP-1 at high dose (Figure 5-2B). Although slight increases were observed, no significant difference was evident in total DHE fluorescence between other ENMs and control groups in all three exposed cell lines (Figure 5-2B). Furthermore, an increase in the expression levels of heme oxygenase 1 (*HO-1)* was detected in all three cell lines, indicative of cells conferred cytoprotection innumerous models of oxidative injury (Lee et al., 2014). As shown in Figure 5-2C, CuO at the 30 μg/mL dose significantly increased more than 20-fold of *HO-1* expression in both THP-1 and RAW264.7 compared to the control group. While upregulation was also observed in SAEC for CuO treatment, it did not reach significance. Interestingly, PEPs upregulated *HO-1* expression only in SAEC at the 30 μg/mL dose ($p < 0.01$), whereas MS-WF markedly increased *HO-1* expression in both SAEC and RAW264.7 at same dosage (Figure 5-2C).

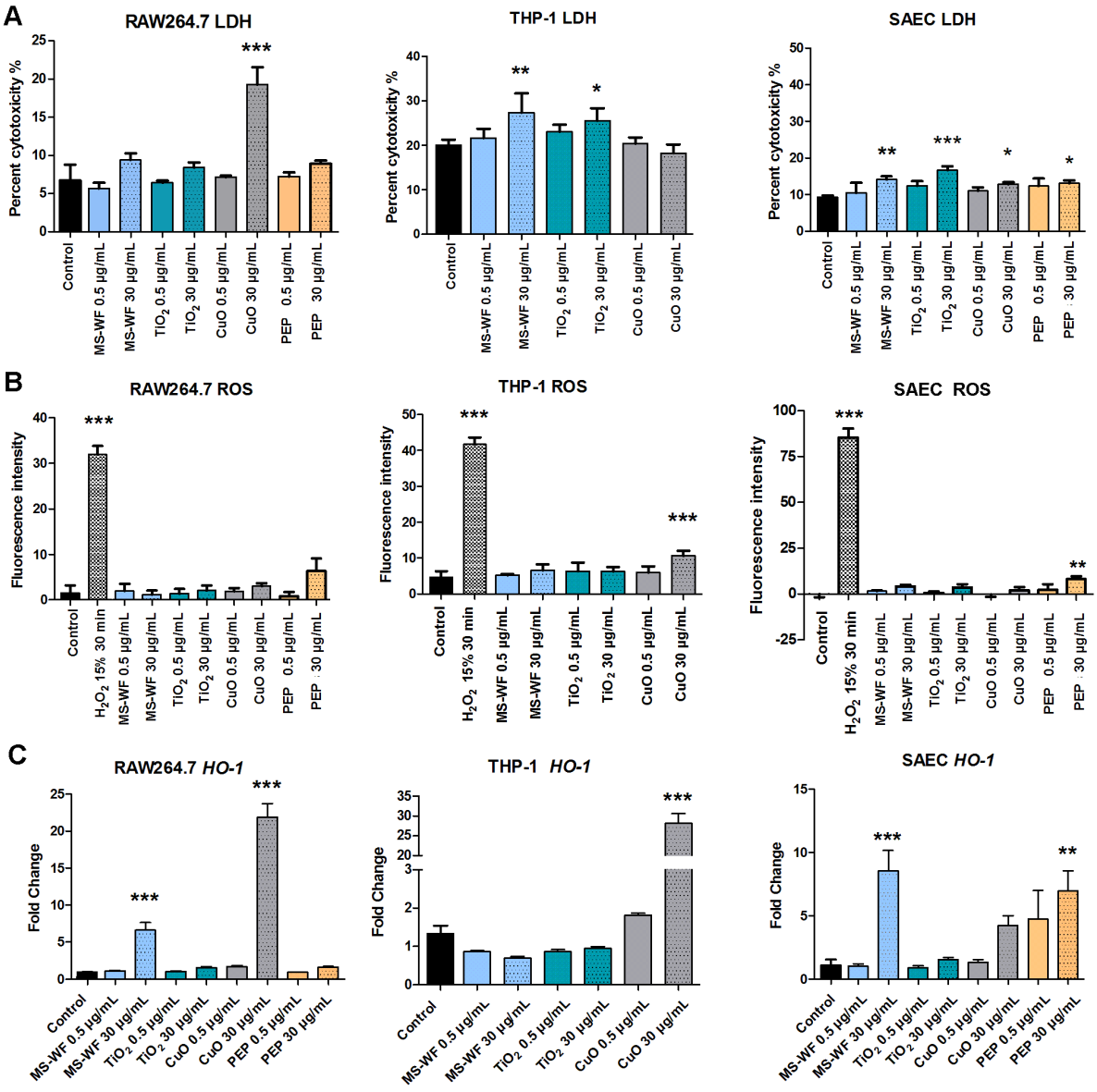

Figure 5-2. Cytotoxicity and oxidative stress induced by ENMs. A. Cytotoxicity of MS-WF, TiO_2, CuO, and PEPs on THP-1, SAECs and RAW264.7 cells. Data obtained from the LDH assay. B. Oxidative stress detection by superoxide-sensitive dihydroethidium in SAEC, THP-1, and RAW264.7 cell lines. C. The expression levels of heme oxygenase-1 *(HO-1*) after these ENMs treatments in the three cell lines. Data are presented as mean±SD. Statistics analysis was determined by one-way ANOVA followed by Dunnett's test. * $p< 0.05$, ** $p< 0.01$. Compared with control group in each cell line.

Effects of ENM exposures on cytokines

Levels of cytokines were measured in SAEC post-exposure to ENMs at high dose. Cytokine release for TiO_2 was not included as TiO_2 was found less toxic compared to other ENMs in the panel (see results above). Exposure to PEPs and MS-WF led to significantly elevated levels of ten cytokines (Supplementary Figure 5-S4). Particularly, granulocyte macrophage colony-stimulating factor (GM-CSF), fractalkine, growth regulated oncogene (GRO), interleukin 6 (IL-6), IL-8, and monocyte Chemoattractant Protein-1 (MCP-1) increased over 88-fold when compared with the control group. CuO exposure had no effects on these cytokines; however, the levels of basic fibroblast growth factor (FGF-2), platelet-derived growth factor-BB (PDGF-BB), and IL-7 increased, while that of epidermal growth factor (EGF) was decreased (Supplementary Figure 5-S5).

Analysis of global DNA methylation

Global DNA methylation was addressed by measuring the levels of 5-mC in control and exposed cells. No significant differences were identified in the levels of 5-mC in response to ENM exposure (Figure 5-3, Panel A). At the same time, some minor differences in 5-mC levels were observed between the cells exposed to various ENMs.

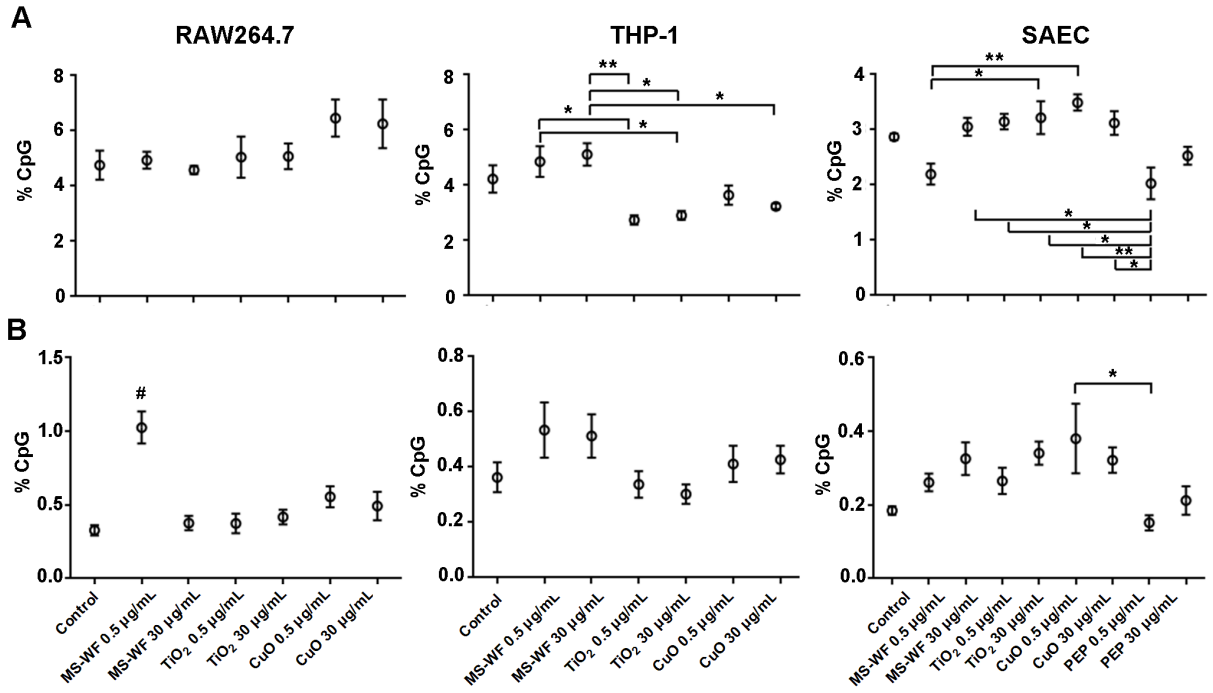

Figure 5-3. Genome wide levels of (A) 5-methylcytosine (5-mC) and (B) 5-hydroxymethylcytosine (5-hmC) in three cell lines after 24 h exposure to ENMs. Data are presented as mean ± SD. Statistics analysis was determined by one way ANOVA followed by Tukey's test. * $p < 0.05$, ** $p < 0.01$. Compared with two groups in each cell line. # indicated that there had significance between 0.5 μg/mL MS-WF treatment and other 6 groups in RAW264.7 cell line, respectively ($p < 0.01$ or $p < 0.001$).

Analysis of methylation status of repetitive elements

Previous studies indicate that analysis of global DNA methylation may mask the redistribution of methylation patterns between the different genomic loci, where the hypomethylation of one and hypermethylation of others may result in cumulatively unchanged levels of DNA methylation (Miousse et al., 2014a). To further investigate whether this

phenomenon can be associated with exposure to ENM, we evaluated the methylation status of two most abundant in human and mouse genomes TEs, LINE-1 (L1), and *Alu* elements that correspond to SINE B1 and SINE B2 in mouse.

First, we addressed the methylation status of L1 element in its four functional units: 5'- and 3'-untraslated regions (UTR) and two open reading frames (ORF1 and ORF2, Figure 5-4). We identified the hypomethylation of ORF1 in SAEC cells after exposure to higher dose of PEPs (30% decrease, *p*-0.04). Interestingly, trends towards modest hypomethylation were also identified in ORF2 and 3'-UTR after exposure of SAEC to 30 μg/mL of PEPs as well as the above mentioned decrease in 5-mC; however, they were statistically insignificant. Some statistically significant, although of very minor magnitude, hypermethylation effects were observed in 5'-UTR, ORF1, and ORF2 of SAEC in response to exposure to CuO. The same effects were detected in ORF2 of THP-1 after exposure to CuO at high dose. Weak hypomethylation was also identified in 5'-UTR and 3'-UTR of RAW264.7 after low dose CuO treatment.

We next addressed the methylation status of SINE B1 and SINE B2 (RAW264.7) and *Alu* elements (THP-1 and SAEC) after exposure to ENMs. Similar to effects observed in L1 5'-UTR, ORF1, and ORF2, significant hypermethylation of *Alu* elements in SAEC after exposure to higher dose of CuO was detected. Interestingly, a similar pattern was observed in THP-1, where exposure to both doses of CuO resulted in *Alu* hypermethylation. However, the most interesting results were found in RAW264.7, where exposure to virtually all ENMs resulted in modest hypermethylation of SINE B1 elements. No significant changes, although, were identified in methylation of SINE B2.

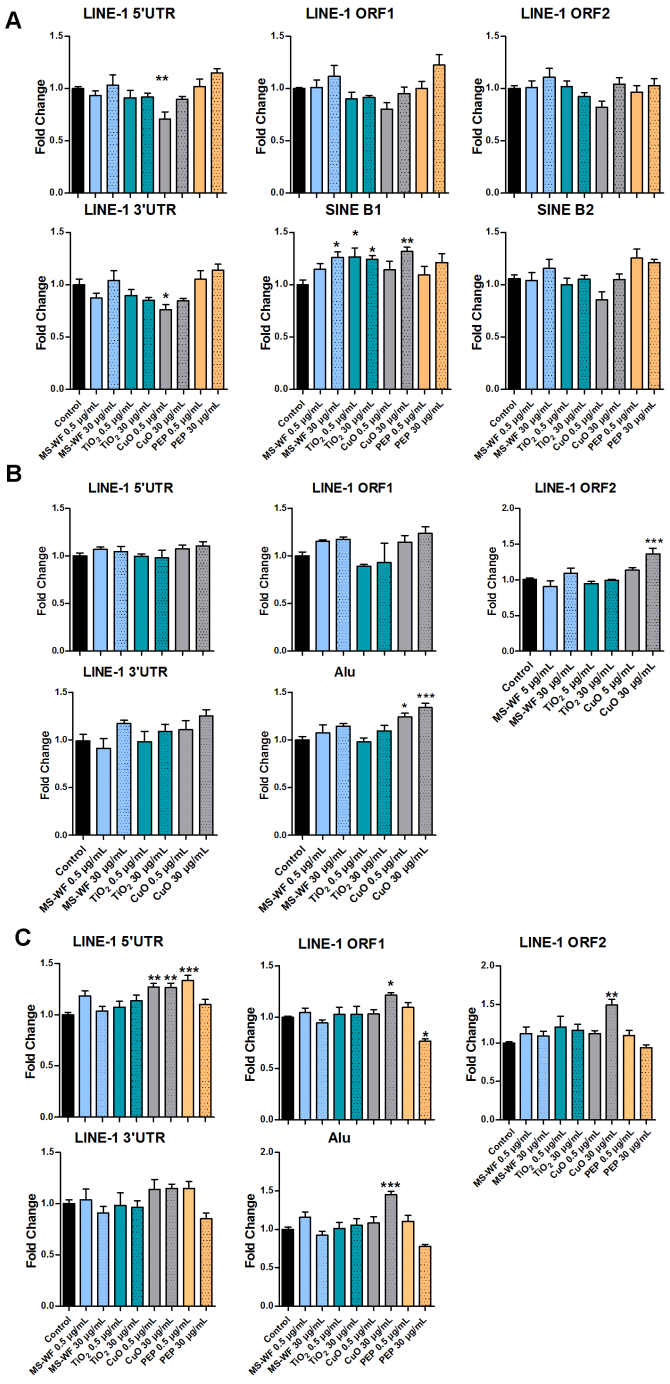

Figure 5-4. Analysis of DNA methylation of LINE-1 and Alu/SINE after exposure to ENMs in (A) RAW264.7, (B) THP-1, (C)SAEC cells. Data are presented as mean ± SD. Statistics analysis was determined by one way ANOVA followed by Dunnett's test. * $p < 0.05$, ** $p < 0.01$, *** $p < 0.001$. Compared with control group in each cell line.

Expression of transposable elements

Exposure to environmental stressors frequently results in transcriptional activation of TEs (Koturbash et al., 2011b; Miousse et al., 2014b; Rudin and Thompson 2001). Therefore, next we sought to evaluate the expression of L1 and *Alu*/SINE in response to exposure to ENMs (Figure 5-5). Exposure to a lower dose of TiO_2 and both doses of CuO resulted in significant and profound reactivation of both L1 ORFs – ORF1 and ORF2 as well as SINE B1 and SINE B2 in RAW264.7. In contrast, exposure to a higher dose of MS-WF led to transcriptional activation of L1 ORF1 and ORF2 and *Alu* (although, the latter two–insignificant) in THP-1, while some weak L1 reactivation was also observed after exposure to a higher dose of TiO_2. Similar to THP-1, effects were detected in SAEC cells, where exposure to high dose of MS-WF and TiO_2 resulted in increased transcripts of L1 ORF2 and *Alu* (although *Alu* in TiO_2 treatment–insignificant). Additionally, exposure to higher dose PEPs also led to increased expression of *Alu* in SAEC.

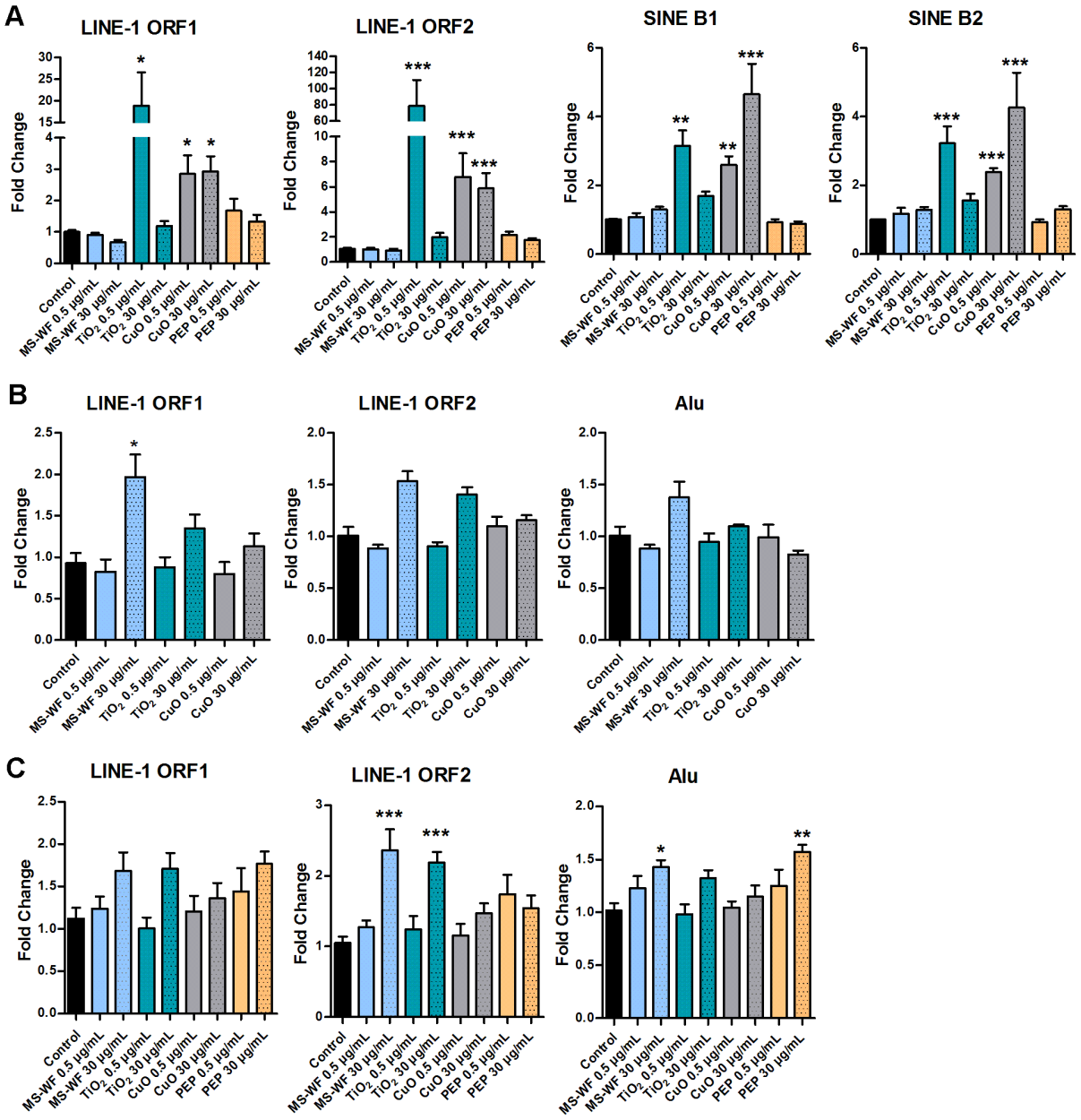

Figure 5-5. Expression of repetitive elements after exposure to ENMs in (A) RAW264.7, (B) THP-1, (C) SAEC cells. Data are presented as mean ± SD. Statistics analysis was determined by one way ANOVA followed by Dunnett's test. *$p < 0.05$, **$p < 0.01$, ***$p < 0.001$. Compared with control group in each cell line.

Analysis of L1 copy numbers

Reactivation of TEs, such as L1 and Alu/SINE, may lead to their retrotransposition and, subsequently, increase in their copy numbers. Taking into account the observed overexpression of L1 ORFs in response to ENMs, we addressed copy numbers of this highly abundant TE 24 h after exposure; however, we did not identify any significant increases in any of the treatment groups (Supplementary Figure 5-S6).

Exposure to ENMs and DNA methylation machinery

Identified changes in expression of genes may predict further alterations within the pathways they control. Therefore, next we addressed the expression of a panel of genes directly involved in establishment and maintenance of methylation marks and, therefore, called DNA methylation machinery. The expression of *DNMT1*, DNA methyltransferase responsible for copying the methylation patterns during the replication on the newly synthesized DNA strand, was found to be negatively affected by exposure to high dose of all ENMs and in all tested cell lines. The only exception was found in SAEC after exposure to high dose of CuO, where a statistically significant (p-0.001) 2-fold increase in the expression of *DNMT1* was observed. Similar patterns, however, less pronounced were observed for both *de novo* methyltransferases *DNMT3A* and *DNMT3B* as well as *UHRF1* (Figure 5-6).

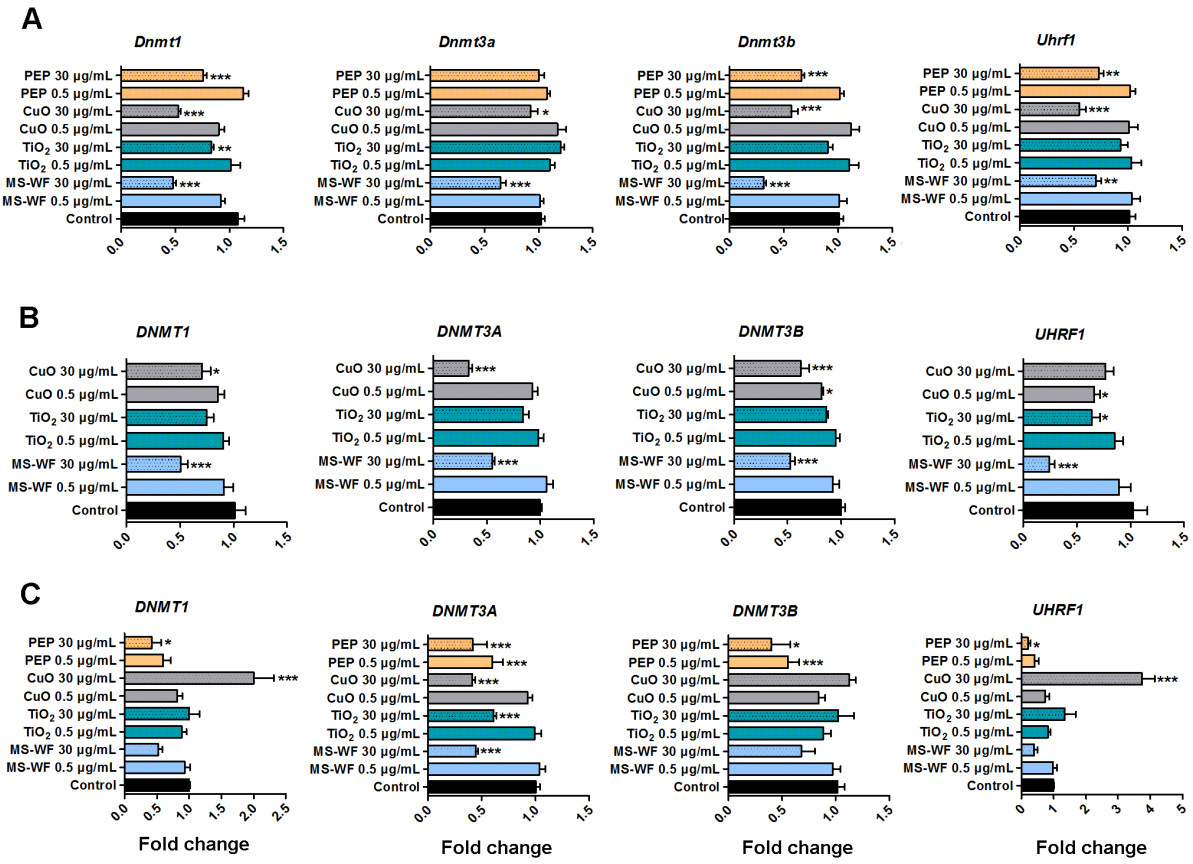

Figure 5-6. Analysis of expression levels of DNA methylation machinery in three cell lines after exposure to ENMs. The expression levels of *DNMT1*, *DNMT3A*, *DNMT3B*, and *UHRF1* in RAW264.7 (A), THP-1 (B), and SAEC (C). Data are presented as mean ± SD. Statistics analysis was determined by one way ANOVA followed by Dunnett's test. *$p < 0.05$, **$p < 0.01$, ***$p < 0.001$. Compared with control group in each cell line.

Effects of exposure to ENMs on DNA hydroxymethylation

Hydroxymethylation of DNA, an epigenetic mechanism discovered several years ago, is considered to be an intermediate chain in the process of DNA demethylation (Kohli and Zhang

2013). The levels of DNA hydroxymethylation in regard to exposure to ENMs were addressed by measuring the 5-hmC. Similar to 5-mC, exposure to ENMs did not greatly affect the levels of 5-hmC in any of the treatment groups, expect the low dose MS-WF exposure in RAW264.7 (Figure 5-3, Panel B). In contrast to DNA methyltransferases, where the congruent response was found for all three genes (*DNMT1*, *DNMT3A,* and *DNMT3B*), *TET1-TET3* genes were differentially regulated, depending on the cell line, ENM, and dose. For instance, exposure to high dose of TiO_2 and PEPs resulted in increased expression of *Tet2* in RAW264.7, while high dose of MS-WF and CuO led to decreased mRNA levels of *Tet3* in the same cell line (Supplementary Figure 5-S7). More simultaneous response was observed in SAEC, where high doses of MS-WF, TiO_2, and CuO and both concentrations of PEPs resulted in decreased expression of all three methyl deoxygenases.

Discussion

In this study, it was demonstrated that ENMs at environmentally relevant concentrations and at low cytotoxicity levels, aside from the inflammatory response and oxidative stress, has also resulted in epigenetic alterations in the target cells – macrophages and lung epithelium. These effects were exhibited as alterations in methylation of two most abundant in mammalian genomes TEs – L1 and Alu/SINE, their reactivation, and down-regulation of DNA methylation machinery.

These epigenetic alterations were associated with minimal cytotoxic effects. The treatment doses of 0.5 and 30 μg/mL used were chosen to cause no more than 20% of cytotoxicity following exposure to the test materials used here. It is worth noting that for the case of PEPs that we have "real world" exposure data, the cell-administered doses of 0.5 and 30 μg/mL correspond to 1 and 60 h of inhalation exposure to PEPs emitted from laser printers (manuscript

in preparation). As the results, the percentage of ENMs-induced cytotoxicity for all three cell lines was below 15%, and no significant changes were detected in cells exposed to 0.5 μg/mL of any of the ENMs. These data are in a good agreement with the previous studies (Badding et al., 2014; Sisler et al., 2014; Xia et al., 2013; Xiong et al., 2013).

Additionally, exposure to ENMs resulted in inflammatory response. Similar effects were observed in mice after exposure to stainless steel welding fumes (Zeidler-Erdely et al., 2011). It is worth noting that the ten cytokines induced by MF-WF or PEPs exposures were most related to asthma and chronic obstructive pulmonary disease (Barnes 2008). A previous study reported that FGF-2 contributes to the progression of pulmonary hypertension in humans and rodents (Izikki et al., 2009). Thus, these results indicated that exposure to ENMs might induce lung diseases, but larger studies are needed to reveal the potential disease risk by the exposure.

Exposure to ENMs also generated oxidative stress, as evidenced from the intracellular generation of ROS and up-regulation of *HO-1* expression (Figure 5-2B and C). This is in agreement with previous studies that reported WF (Antonini et al., 1999), TiO_2 (Shrivastava et al., 2014), and CuO (Wang et al., 2012) capable of generation intracellular ROS. It is worth mentioning that ROS may lead to epigenetic changes that affect the genome by causing alterations in DNA methylation patterns (Gong et al., 2010).

Environmental stressors, independently of their mode of action (geno- or non-genotoxic), have been shown to target the cellular epigenome and DNA methylation, particularly. Exposure to various sources of particulate matter has been frequently associated with alterations in DNA methylation and TEs in particular (Baccarelli et al., 2009; Madrigano et al., 2011; Miousse et al., 2014a; Salam et al., 2012; Stoccoro et al., 2013; Tarantini et al., 2009). Loss of TEs-associated DNA methylation is associated with numerous disease, including cancer (Miousse and

Koturbash, 2015) and has been also reported early after exposure to both physical and chemical carcinogens (Koturbash et al., 2011b; Miousse et al., 2014b). On the other hand, hypermethylation of TEs have been associated with allergen sensitization, suggesting their involvement in the pathogenesis of asthma and allergies (Sordillo et al., 2013). In the current study, levels of global and TE-associated DNA methylation were not greatly affected by ENMs exposure. This can be possibly explained by the short post-exposure time when a sufficient number of cell divisions had not occurred in order to detect potential alterations in DNA methylation. The observed loss of DNA methyltransferases activity, if sustained, will possibly lead to global genomic hypomethylation. Studies, investigating DNA methylation at later time-points after several cell divisions, will address this issue and are currently in progress in our laboratories.

In contrast to methylation, expression of TEs was greatly affected by exposure to ENMs. This well agrees with other studies, reporting reactivation of L1 and *Alu*/SINEs shortly after exposure to environmental toxicants and carcinogens both *in vitro* and *in vivo* (Koturbash et al., 2011b; Rudin and Thompson 2001). Reactivation of TEs may result in their retrotransposition via a "copy-and-paste" mechanism, by which a copy of a newly created TE is being introduced elsewhere in the genome, while the "original" remains at its primary location. Such events may have detrimental effects over genomes, by the mean of genome amplification and mutations within the target-genes of retrotransposition. Growing evidence indicates deleterious effects of retrotransposition in human cancers, including lung cancer (Iskow et al., 2010), and retrotransposition stimulated by exposure to various environmental stressors (Terasaki et al., 2013). Despite the significant increase in L1 and *Alu*/SINEs mRNA transcripts, no increases in TEs copy numbers were detected, suggesting absence of retrotransposition events associated

with exposure to ENMs. It is possible that a 24 h time-point is not sufficient to initiate detectable rates of retrotransposition. Indeed, the most recent study indicates that L1 mobilization may take ~ 120 h after exposure (Terasaki et al., 2013).

Accumulating evidence clearly demonstrates the potential of epigenetic parameters to be introduced into risk and safety assessment (Goodman et al., 2010; Herceg et al., 2013; Koturbash et al., 2011a). This study provides a comprehensive characterization of the short-term effects of *in vitro* exposure of inhaled ENMs on DNA methylation and DNA methylation machinery. We show that such parameters as expression of TEs and DNA methyltransferases can be further utilized in the characterization of ENMs with the potential to be introduced into safety and risk assessment of ENMs. This study also provides a roadmap for future studies on epigenetic effects of ENMs, including evaluation of longer terms of exposure, involvement of histone modifications, and utilization of *in vivo* models, which are ongoing studies in our laboratories. Further delineation of epigenetic alterations caused by ENMs will aid in understanding of the molecular mechanisms of potential health effects associated with exposures.

Conclusions

In this manuscript, we performed an extensive *in vitro* characterization of epigenetic effects associated with DNA methylation by various sources of real world ENMs at low cytotoxic levels. We show that exposure to ENMs modestly affect DNA methylation within the most abundant TEs, but selectively enhance their transcription and suppress the expression of DNA methylation machinery at doses below cytotoxicity. Observed epigenetic alterations are associated with the development of human pathologies, including allergies, asthma, and lung cancer. Further studies are clearly needed in order to investigate short and long-term effects of exposure to ENMs and possible health outcomes of such exposures.

Acknowledgements

We would like to thank Dilpreet Singh for his assistance in TEM analysis, Oleksandra Pavliv for her assistance with DNA methylation analysis, Dr. Andrea Baccarelli and Jia Zhong for their help in reviewing the epigenetic results. We are thankful to Dr. Rebecca Helm for editing the manuscript.

Contributions

Sandra V. Pirela designed and performed the sampling and collection of the size-fractionated PEPs, as well as the preparation of suspension of PEPs and their subsequent characterization before use for the *in vitro* experiments.

Declaration of interest

This work was supported by the funding from NIEHS Center (Grant# ES-000002), NIOSH, CPSC (Grant # 212-2012-M-51174), NIH UL1TR000039 and KL2TR000063, and the Arkansas Biosciences Institute. The authors report no competing financial interests. The authors alone are responsible for the content and writing of the paper.

Supplemental Material

Table 5-S1. The primers for analysis of methylation status of DNA repetitive elements.

Repetitive elements	Forward Primer	Reverse Primer
Mus musculus		
LINE-1 5'UTR	AGTGGATCACAGTGCCTGC	GGGTAGCCTGCTTCCCTATG
LINE-1 ORF1	GAACACAAATGCCAGCCCAG	TGTGAACTTGGTTTTGTCGTGG
LINE-1 ORF2	CTATCTACAAATCCAGCCCTACAG	CTTTTGATTTGCTGGTCTGGG
LINE-1 3'UTR	GGCTTGTACAACCACTCTGGA	TCTGGATATATGCCCAGGAGAG
SINEB1	CGAGATGGCTCAGTGGGTAA	GTGTGTGTGTGTGTGTGCG
SINEB2	GCAAGCATGAGGACCTGAGT	CTGGAGCTCACCAAGTAGGC
rDNA (for normalization of methylation)	CCTGTGAATTCTCTGAACTC	CCTAAACTGCTGACAGGGTG
Homo sapiens		
LINE1 5'UTR	AAAGAAAGGGGTGACGGACG	TACCTAAGCAAGCCTGGGCAA
LINE-1 ORF1	CACCAGGCCTGCCCTAAAA	TCTTCCTAGTCTCGATGGTCT
LINE-1 ORF2	TGGAACCCTTGTGCACTGTT	CCAGAAGTGGAATTGCTGGA
LINE-1 3'UTR	TCAACCTAAGTGTCCATCAACAGA	TCCCAGCCTCTAGTAACCACT
Alu	GCCTGTAATCCCAGCACTTT	TCTCCTGCCTCAGCCTCC

Table 5-S2. Gene-specific primers used for qRT-PCR amplification.

Gene Symbol	Assay Name	RefSeq #	Source
Dnmt1	Mm01151063_m1	NM_001199431.1	Life Technologies
Dnmt3a	Mm00432881	NM_007872.4	Life Technologies
Dnmt3b	Mm01240113_m1	AF068626.2*	Life Technologies
Gapdh (control gene)	Mm99999915_g1	NM_008084.2	Life Technologies
Ho-1	Mm.PT.56a.8600055	NM_010442	Integrated DNA Technologies
Tet2	Mm.PT.56a.30089849	NM_00104040	Integrated DNA Technologies
Tet3	Mm.PT.56a.11954119	NM_183138	Integrated DNA Technologies
Uhrf1	Mm00477868_mH	NM_001111078.1	Life Technologies
DNMT1	Hs.PT.56.28037916	NM_001130823	Integrated DNA Technologies
DNMT3A	Hs01027166_m1	NM_022552.4	Life Technologies
DNMT3B	Hs00171876_m1	NM_001207055.1	Life Technologies
GAPDH(control gene)	Hs.PT.56.589810.g	NM_001256799	Integrated DNA Technologies
HO-1	Hs01110250_m1	NM_002133.2	Life Technologies
TET1	Hs00286756_m1	NM_030625.2	Life Technologies
TET2	Hs00325999_m1	NM_001127208.2	Life Technologies
TET3	Hs00379125_m1	NM_144993.1	Life Technologies
UHRF1	Hs01086727_m1	NM_001048201.1	Life Technologies

*GenBank mRNA

Table 5-S3. TEs expression primers used for qRT-PCR amplification.

Gene Symbol	Forward Primer	Reverse Primer
Musmusculus		
LINE-1 ORF1	GAACCAAGACCACTCACCATCA	CCCTGGACTGGGCGAAGT
LINE-1 ORF2	TTTGGGACACAATGAAAGCA	CTGCCGTCTACTCCTCTTGG
SINEB1	GTGGCGCACGCCTTTAATC	GACAGGGTTTCTCTGTGTAG
SINEB2	GAGATGGCTCAGTGGTTAAG	CTGTCTTCAGACACTCCAG
Rps29 (control gene)	GGAGTCACCCACGGAAGT	TCCATTCAAGGTCGCTTAGTC
Homo sapiens		
LINE-1 ORF1	AGAAGAGCAACTCCAAGACAC	CTTTGAGGGTAACTCGACCTTT
LINE-1 ORF2	AAATGGTGCTGGGAAAACTG	GCCATTGCTTTTGGTGTTTT
Alu	CATGGTGAAACCCCGTCTCTA	GCCTCAGCCTCCCGAGTAG
RPS13 (control gene)	CGAAAGCATCTTGAGAGGAACA	TCGAGCCAAACGGTGAATC

Table 5-S4. The primers for copy number analysis.

Repetitive elements	Forward Primer	Reverse Primer
Mus musculus		
LINE-1 ORF2	GCGGTTCCTCAGAAAATTGG	TGCCCAGGAGAGGTATTGCT
Homo sapiens		
LINE-1 ORF2	TGGAACCCTTGTGCACTGTT	CCAGAAGTGGAATTGCTGGA

Table 5-S5. ENMs characterization and effective density in suspensions. d_H: hydrodynamic diameter, PdI: polydispersity index, ζ: zeta potential, σ: specific conductance, ρ: effective density.

Material	Media	Time (hour)	d_H (nm)*	PdI	ζ (mV)	σ (mS/cm)	ρ (g/cm^3)
TiO_2	SAGM	0	774.4 ± 59.61	0.362 ± 0.030	-9.88 ± 0.710	11.4 ± 0.839	1.521
		24	849.3 ± 29.45	0.325 ± 0.028	-10.4 ± 1.21	11.2 ± 1.35	
	RPMI/ 10%FBS	0	370.7 ± 25.22	0.380 ± 0.008	-10.7 ± 0.802	12.1 ± 0.0577	1.353
		24	350.4 ± 1.422	0.364 ± 0.025	-11.0 ± 0.624	11.7 ± 0.0577	
	DMEM/ 10%FBS	0	390.4 ± 16.04	0.441 ± 0.056	-9.04 ± 0.842	12.8 ± 0.379	1.315
		24	375.9 ± 4.412	0.369 ± 0.025	-10.3 ± 1.06	11.7 ± 0.569	
	DI H_2O	0	359.6 ± 56.75	0.371 ± 0.029	-4.47 ± 0.409	0.00864 ± 0.00102	N/A
CuO	SAGM	0	1367 ± 73.12	0.621 ± 0.052	-27.4 ± 3.61	7.98 ± 0.197	1.599
		24	1208 ± 30.01	0.358 ± 0.067	-29.25 ± 2.76	8.86 ± 0.580	
	RPMI/ 10%FBS	0	907.9 ± 24.81	0.433 ± 0.064	-18.5 ± 10.6	11.3 ± 0.424	1.578
		24	841.2 ± 81.78	0.670 ± 0.036	-10.2 ± 3.65	11.4 ± 1.36	
	DMEM/ 10%FBS	0	828.3 ± 95.49	0.565 ± 0.089	-18.9 ± 5.62	12.7 ± 0.152	1.617
		24	606.8 ± 91.41	0.710 ± 0.040	-29.4 ± 23.1	11.0 ± 0.200	
	DI H_2O	0	887.6 ± 64.56	0.337 ± 0.037	-21.4 ± 1.60	0.0130 ± 0.0002	N/A
PEPs ($PM_{0.1}$)	SAGM	0	381.7 ± 40.2	0.586 ± 0.05	9.97 ± 2.8	2.52 ± 0.0721	2.39
		24	181.3 ± 18.5	0.442 ± 0.02	1.22 ± 2.24	3.99 ± 0.0495	
	RPMI/ 10%FBS	0	227.3 ± 105.0	0.485 ± 0.247	9.55 ± 2.89	7.01 ± 0.960	1.560
		24	227.2 ± 27.01	0.419 ± 0.062	5.48 ± 1.89	10.4 ± 0.321	
	DMEM/ 10%FBS	0	298.0 ± 5.73	0.711 ± 0.078	-15.9 ± 7.65	10.9 ± 0.212	1.899
		24	396.8 ± 31.52	0.522 ± 0.019	-15.4 ± 2.82	11.0 ± 0.153	
	DI H_2O	0	178.3 ± 3.5	0.403 ± 0.05	-20.6 ± 1.9	0.185 ± 0.0	N/A

Table 5-S5 (continued). ENMs characterization and effective density in suspensions. d_H: hydrodynamic diameter, PdI: polydispersity index, ζ: zeta potential, σ: specific conductance, ρ: effective density.

Material	Media	Time (hour)	d_H (nm)*	PdI	ζ (mV)	σ (mS/cm)	ρ (g/cm^3)
MS-WF	SAGM	0	1526.7 ± 259.6	0.198 ± 0.04	18.8 ± 0.9	10.5 ± 0.462	1.372
		24	1532 ± 149.2	0.047 ± 0.029	-7.56 ± 0.64	9.38 ± 0.442	
	RPMI/ 10%FBS	0	1502 ± 96.26	0.236 ± 0.080	12.1 ± 2.66	11.5 ± 1.10	1.563
		24	1384 ± 116.8	0.149 ± 0.037	-7.63 ± 1.92	10.8 ± 1.49	
	DMEM/ 10%FBS	0	783.0 ± 21.26	0.299 ± 0.029	-12.5 ± 4.55	11.7 ± 0.252	1.600
		24	655.8 ± 7.431	0.450 ± 0.050	-13.3 ± 7.98	10.8 ± 0.321	
	DI H_2O	0	2197 ± 118.4	0.561 ± 0.4	8.52 ± 1.2	0.0284 ± 0.0	N/A

N/A: not applicable. Values represent the mean (± SD) of a triplicate reading. *indicated by intensity. The data of MF-WF and PEPs in SAGM or DI H_2O at 0 h were cited in our previous study (Sisler et al. 2014).

Supplemental Methods

Effective density

The effective density of these ENMs was determined using the volumetric centrifugation method (VCM) recently developed by our laboratory (DeLoid et al. 2014). In brief, 1 mL samples of 100 μg/mL suspensions of the ENMs in SAGM, RPMI/10% FBS, or DMEM/10% FBS were dispensed into TPP packed cell volume (PCV) tubes (Techno Plastic Products, Trasadingen, Switzerland) and centrifuged at 2,000 × *g* for 1 h. Agglomerate pellet volumes, V_{pellet}, were measured using a slide rule (Techno Plastic Products, Trasadingen, Switzerland).

Effective agglomerate densities were calculated from V_{pellet} values of triplicate samples for each ENM based on our previous study (DeLoid et al. 2014).

In vitro dosimetric considerations

The actual delivered-to-cell dose of the test particles in specific media was determined by the hybrid VCM-*in vitro* sedimentation, diffusion and dosimetry (VCM-ISDD) model recently developed by our group (Cohen et al., 2014; DeLoid et al., 2014). The model was used to calculate the fraction of administered particles deposited on standard 100-mm diameter dishes or 96-well plates as a function of time *fD(t)* as previously described (Cohen et al., 2014; DeLoid et al., 2014). In summary, the geometric properties of the experimental well used, as well as the particle colloidal properties were used to calculate the cell-delivered dose for the exposure duration used in this study.

Cell seeding and harvesting

RAW264.7 were seeded at 1.25×10^4 per well in a 96-well plate or 2.2×10^6 per dish in 100-mm diameter dishes, allowed to fully attach for 24 h and then exposed to MS-WF, TiO_2, CuO, or PEPs for 24 h. SAEC were plated at 1.5×10^4 per well in a 96-well plate or 2.2×10^6 per dish in 100-mm diameter dishes and also allowed to fully attach for 24 h, followed by media changes to remove any dead cells. At 48 h, SAEC were serum starved for an additional 24 h and then treated with MS-WF, TiO_2, CuO, or PEPs for 24 h. THP-1 were seeded at 6.4×10^4 per well in a 96-well plate or 2.2×10^6 per dish in 100-mm diameter dishes with 200 ng/mL phorbol 12-myristate 13-acetate (PMA) which was used for the differentiation of THP-1 monocytes into macrophages. Differentiation of PMA treated cells was enhanced after the initial 3-day stimulus by removing the PMA-containing media then incubating the cells in fresh RPMI/10% FBS for a further 5 days. Lastly, THP-1 were exposed to MS-WF, TiO_2, or CuO for 24 h. The samples

from 100-mm diameter dishes were used for epigenetic studies, while the samples from 96-well plates were used for general toxicological studies.

Analysis of 5-Methylcytosine(5-mC) and 5-hydroxymethylcytosine (5-hmC) levels

RNaseA (Sigma, St. Louis, MO, USA) was added to 1 μg of genomic DNA to a final concentration of 0.02 mg/mL and incubated at 37°C for 15 minutes. The purified DNA was digested into component nucleotides using Nuclease P1, snake venom phosphodiesterase, and alkaline phosphatase as previously described (James et al. 2010). Briefly, DNA was denatured by heating for 3 minutes at 100°C and rapidly chilled in an iced-water bath. One-tenth volume of 0.1 M ammonium acetate, pH 5.3, was added to 2 units of nuclease P1 (Sigma, St. Louis, MO, USA) for every 0.5 A260 unit of DNA and the mixture incubated at 45°C for 2 h. Subsequently, 1/10 volume of 1 M ammonium bicarbonate and 0.002 units of venom phosphodiesterase I (Sigma, St. Louis, MO, USA) were added and the mixture incubated for 2 h at 37°C. To the mixture, 0.5 units of alkaline phosphatase (Sigma, St. Louis, MO, USA) were then added and the incubation continued for an additional hour. The digested nucleotides were stored at −20°C until liquid chromatography tandem mass spectrometry (LC/MS/MS) analysis. Base separation was performed with a Dionex HPLC system (Thermo Scientific, Waltham, MA, USA) coupled to an electrospray ionization (ESI) tandem mass spectrometer (Thermo-Finnigan LCQ) using a Phenomenex Gemini column (C18, 150 x 2.0 mm, 3 μm particle size) and established methodology (Friso et al. 2002).

Analysis of methylation status of TEs

Methylation at the LINE1 and *Alu*/SINE elements was assessed by methylation-sensitive quantitative Real-Time Polymerase Chain Reaction (qRT-PCR). Genomic DNA was treated with five methylation-sensitive restriction enzymes (New En lacking the specific primers for DNA

amplification, and/or DNA template served as negative control.gland Biolabs, Ipswitch, MA, USA). Briefly, 500 ng of gDNA was treated with 0.5 U of SmaI enzyme in 1X CutSmart buffer and incubated at 25°C for 2 h. 0.5 U of the enzymes HpaII, HhaI, and AciI in 1X CutSmart buffer was added to the mix and incubated at 37°C for 16 h. Finally, 0.5 U of BstUI enzyme in 1X CutSmart buffer was added, and the mix was incubated at 60°C for 4 h. The resulting digested DNA was measured by qRT-PCR using 2 ng digested DNA per reaction and SYBR Select chemistry (Life Technologies, Grand Island, NY, USA). DNA samples 1) not digested with the restriction enzyme mix and 2) RAW 264.7-derived DNA pre-treated with 5-azacytidine, a potent demethylating agent, served as a positive control, while samples lacking the specific primers for DNA amplification, and/or DNA template served as a negative control.

Bibliography

Antonini JM, Lawryk NJ, Murthy GG, Brain JD. 1999. Effect of welding fume solubility on lung macrophage viability and function in vitro. J Toxicol Environ Health A 58:343-363.

Baccarelli A, Wright RO, Bollati V, Tarantini L, Litonjua AA, Suh HH, et al. 2009. Rapid DNA methylation changes after exposure to traffic particles. Am J Respir Crit Care Med 179:572-578.

Badding MA, Fix NR, Antonini JM, Leonard SS. 2014. A comparison of cytotoxicity and oxidative stress from welding fumes generated with a new nickel-, copper-based consumable versus mild and stainless steel-based welding in RAW 264.7 mouse macrophages. PLoS One 9:e101310.

Balansky R, Longobardi M, Ganchev G, Iltcheva M, Nedyalkov N, Atanasov P, et al. 2013. Transplacental clastogenic and epigenetic effects of gold nanoparticles in mice. Mutat Res 751-752:42-48.

Barnes PJ. 2008. The cytokine network in asthma and chronic obstructive pulmonary disease. J Clin Invest 118:3546-3556.

Bedran TB, Mayer MP, Spolidorio DP, Grenier D. 2014. Synergistic anti-inflammatory activity of the antimicrobial peptides human beta-defensin-3 (hBD-3) and cathelicidin (LL-37) in a three-dimensional co-culture model of gingival epithelial cells and fibroblasts. PLoS One 9:e106766.

Bollati V, Baccarelli A. 2010. Environmental epigenetics. Heredity (Edinb) 105: 105-112.

Choi AO, Brown SE, Szyf M, Maysinger D. 2008. Quantum dot-induced epigenetic and genotoxic changes in human breast cancer cells. J Mol Med (Berl) 86:291-302.

Cohen J, Deloid G, Pyrgiotakis G, Demokritou P. 2013. Interactions of engineered nanomaterials in physiological media and implications for in vitro dosimetry. Nanotoxicology 7:417-431.

Cohen JM, Derk R, Wang L, Godleski J, Kobzik L, Brain J, et al. 2014a. Tracking translocation of industrially relevant engineered nanomaterials (ENMs) across alveolar epithelial monolayers in vitro. Nanotoxicology, 8 Suppl 1:216-225.

Cohen JM, Teeguarden JG, Demokritou P. 2014b. An integrated approach for the in vitro dosimetry of engineered nanomaterials. Part Fibre Toxicol 11:20.

de Koning AP, Gu W, Castoe TA, Batzer MA, Pollock DD. 2011. Repetitive elements may comprise over two-thirds of the human genome. PLoS Genet 7:e1002384.

Deloid G, Cohen JM, Darrah T, Derk R, Rojanasakul L, Pyrgiotakis G, et al. 2014. Estimating the effective density of engineered nanomaterials for in vitro dosimetry. Nat Commun 5:3514.

Egli A, Santer DM, O'Shea D, Barakat K, Syedbasha M, Vollmer M, et al. 2014. IL-28B is a Key Regulator of B- and T-Cell Vaccine Responses against Influenza. PLoS Pathog 10:e1004556.

Gong C, Tao G, Yang L, Liu J, Liu Q, Zhuang Z. 2010. SiO(2) nanoparticles induce global genomic hypomethylation in HaCaT cells. Biochem Biophys Res Commun 397: 397-400.

Goodman JI, Augustine KA, Cunnningham ML, Dixon D, Dragan YP, Falls JG, et al. 2010. What do we need to know prior to thinking about incorporating an epigenetic evaluation into safety assessments? Toxicol Sci 116:375-381.

Halappanavar S, Jackson P, Williams A, Jensen KA, Hougaard KS, Vogel U, et al. 2011. Pulmonary response to surface-coated nanotitanium dioxide particles includes induction of acute phase response genes, inflammatory cascades, and changes in microRNAs: a toxicogenomic study. Environ Mol Mutagen 52:425-439.

Herceg Z, Lambert MP, van VK, Demetriou C, Vineis P, Smith MT, et al. 2013. Towards incorporating epigenetic mechanisms into carcinogen identification and evaluation. Carcinogenesis 34:1955-1967.

Hiraiwa K, van Eeden SF. 2013. Contribution of lung macrophages to the inflammatory responses induced by exposure to air pollutants. Mediators Inflamm 2013:619523.

Iskow RC, McCabe MT, Mills RE, Torene S, Pittard WS, Neuwald AF, et al. 2010. Natural mutagenesis of human genomes by endogenous retrotransposons. Cell 141:1253-1261.

Izikki M, Guignabert C, Fadel E, Humbert M, Tu L, Zadigue P, et al. 2009. Endothelial-derived FGF2 contributes to the progression of pulmonary hypertension in humans and rodents. J Clin Invest 119:512-523.

James SJ, Melnyk S, Jernigan S, Pavliv O, Trusty T, Lehman S, et al. 2010. A functional polymorphism in the reduced folate carrier gene and DNA hypomethylation in mothers of children with autism. Am J Med Genet B Neuropsychiatr Genet 153B:1209-1220.

Jones PA. 2012. Functions of DNA methylation: islands, start sites, gene bodies and beyond. Nat Rev Genet 13:484-492.

Kohli RM, Zhang Y. 2013. TET enzymes, TDG and the dynamics of DNA demethylation. Nature 502:472-479.

Koturbash I, Beland FA, Pogribny IP. 2011a. Role of epigenetic events in chemical carcinogenesis--a justification for incorporating epigenetic evaluations in cancer risk assessment. Toxicol Mech Methods 21:289-297.

Koturbash I, Scherhag A, Sorrentino J, Sexton K, Bodnar W, Tryndyak V, et al. 2011b. Epigenetic alterations in liver of C57BL/6J mice after short-term inhalational exposure to 1,3-butadiene. Environ Health Perspect 119:635-640.

Lee YH, Cheng FY, Chiu HW, Tsai JC, Fang CY, Chen CW, et al. 2014. Cytotoxicity, oxidative stress, apoptosis and the autophagic effects of silver nanoparticles in mouse embryonic fibroblasts. Biomaterials 35:4706-4715.

Li S, Wang H, Qi Y, Tu J, Bai Y, Tian T, et al. 2011. Assessment of nanomaterial cytotoxicity with SOLiD sequencing-based microRNA expression profiling. Biomaterials 32:9021-9030.

Madrigano J, Baccarelli A, Mittleman MA, Wright RO, Sparrow D, Vokonas PS, et al. 2011. Prolonged exposure to particulate pollution, genes associated with glutathione pathways, and DNA methylation in a cohort of older men. Environ Health Perspect 119:977-982.

Miousse IR, Chalbot MC, Aykin-Burns N, Wang X, Basnakian A, Kavouras IG, et al. 2014a. Epigenetic alterations induced by ambient particulate matter in mouse macrophages. Environ Mol Mutagen 55:428-435.

Miousse IR, Shao L, Chang J, Feng W, Wang Y, Allen AR, et al. 2014b. Exposure to low-dose (56)Fe-ion radiation induces long-term epigenetic alterations in mouse bone marrow hematopoietic progenitor and stem cells. Radiat Res 182:92-101.

Miousse IR, Koturbash I. 2015. The fine LINE: methylation drawing the cancer landscape. Biomed Res Int In Press.

Ng CT, Dheen ST, Yip WC, Ong CN, Bay BH, Lanry Yung LY. 2011. The induction of epigenetic regulation of PROS1 gene in lung fibroblasts by gold nanoparticles and implications for potential lung injury. Biomaterials 32:7609-7615.

Pirela SV, Pyrgiotakis G, Bello D, Thomas T, Castranova V, Demokritou P. 2014a. Development and characterization of an exposure platform suitable for physico-chemical, morphological and toxicological characterization of printer-emitted particles (PEPs). Inhal Toxicol 26:400-408.

Pirela SV, Sotiriou GA, Bello D, Shafer M, Bunker KL, Castranova V, et al. 2014b. Consumer exposures to laser printer-emitted engineered nanoparticles: A case study of life-cycle implications from nano-enabled products. Nanotoxicology Nov 11:1-9. [Epub ahead of print]

Pyrgiotakis G, McDevitt J, Gao Y, Branco A, Eleftheriadou M, Lemos B, et al. 2014. Mycobacteria inactivation using Engineered Water Nanostructures (EWNS). Nanomedicine, 10:1175-1183.

Rudin CM, Thompson CB. 2001. Transcriptional activation of short interspersed elements by DNA-damaging agents. Genes Chromosomes Cancer 30:64-71.

Salam MT, Byun HM, Lurmann F, Breton CV, Wang X, Eckel SP, et al. 2012. Genetic and epigenetic variations in inducible nitric oxide synthase promoter, particulate pollution, and exhaled nitric oxide levels in children. J Allergy Clin Immunol 129:232-239.

Schmittgen TD, Livak KJ. 2008. Analyzing real-time PCR data by the comparative C(T) method. Nat Protoc 3:1101-1108.

Setyawati MI, Tay CY, Chia SL, Goh SL, Fang W, Neo MJ, et al. 2013. Titanium dioxide nanomaterials cause endothelial cell leakiness by disrupting the homophilic interaction of VE-cadherin.Nat Commun 4:1673.

Shrivastava R, Raza S, Yadav A, Kushwaha P, Flora SJ. 2014. Effects of sub-acute exposure to TiO2, ZnO and Al2O3 nanoparticles on oxidative stress and histological changes in mouse liver and brain. Drug Chem Toxicol 37:336-347.

Sisler JD, Pirela SV, Friend S, Farcas M, Schwegler-Berry D, Shvedova A, et al. 2014. Small airway epithelial cells exposure to printer-emitted engineered nanoparticles induces cellular effects on human microvascular endothelial cells in an alveolar-capillary co-culture model. Nanotoxicology Nov 1:1-11. [Epub ahead of print]

Sordillo JE, Lange NE, Tarantini L, Bollati V, Zanobetti A, Sparrow D, et al. 2013. Allergen sensitization is associated with increased DNA methylation in older men. Int Arch Allergy Immunol 161:37-43.

Sotiriou GA, Diaz E, Long MS, Godleski J, Brain J, Pratsinis SE, et al. 2012. A novel platform for pulmonary and cardiovascular toxicological characterization of inhaled engineered nanomaterials. Nanotoxicology 6:680-690.

Sotiriou GA, Watson C, Murdaugh KM, Darrah TH, Pyrgiotakis G, Elder A, et al. 2014. Engineering safer-by-design, transparent, silica-coated ZnO nanorods with reduced DNA damage potential. Environ Sci Nano 1:144-153.

Stoccoro A, Karlsson HL, Coppede F, Migliore L. 2013. Epigenetic effects of nano-sized materials. Toxicology 313:3-14.

Tarantini L, Bonzini M, Apostoli P, Pegoraro V, Bollati V, Marinelli B, et al. 2009. Effects of particulate matter on genomic DNA methylation content and iNOS promoter methylation. Environ Health Perspect 117:217-222.

Terasaki N, Goodier JL, Cheung LE, Wang YJ, Kajikawa M, Kazazian HH, Jr., et al. 2013. In vitro screening for compounds that enhance human L1 mobilization. PLoS One 8:e74629.

Wang Z, Li N, Zhao J, White JC, Qu P, Xing B. 2012. CuO nanoparticle interaction with human epithelial cells: cellular uptake, location, export, and genotoxicity. Chem Res Toxicol 25:1512-1521.

Watson C, Ge J, Cohen J, Pyrgiotakis G, Engelward BP, Demokritou P. 2014. High-throughput screening platform for engineered nanoparticle-mediated genotoxicity using CometChip technology. ACS Nano 8:2118-2133.

Xia T, Hamilton RF, Bonner JC, Crandall ED, Elder A, Fazlollahi F, et al. 2013. Interlaboratory evaluation of in vitro cytotoxicity and inflammatory responses to engineered nanomaterials: the NIEHS Nano GO Consortium. Environ Health Perspect 121:683-690.

Xiong S, Tang Y, Ng HS, Zhao X, Jiang Z, Chen Z, et al. 2013. Specific surface area of titanium dioxide (TiO2) particles influences cyto- and photo-toxicity. Toxicology 304:132-140.

Zeidler-Erdely PC, Kashon ML, Li S, Antonini JM. 2010. Response of the mouse lung transcriptome to welding fume: effects of stainless and mild steel fumes on lung gene expression in A/J and C57BL/6J mice. Respir Res 11:70.

Zeidler-Erdely PC, Battelli LA, Stone S, Chen BT, Frazer DG, Young SH, et al. 2011. Short-term inhalation of stainless steel welding fume causes sustained lung toxicity but no tumorigenesis in lung tumor susceptible A/J mice. Inhal Toxicol 23:112-120.

Summary and Conclusions

An integrated platform that enables researchers to assess the health implications of exposures to emissions from nano-enabled products, at the different stages of their lifecycle, is required in order to perform a proper risk assessment. More importantly, this comprehensive methodology highlights the importance of understanding the life-cycle nano-environmental health and safety implications of NEPs and assessing real world exposures, as well as their associated toxicological properties rather than merely focusing on the materials used in the synthesis of an NEP.

In this dissertation, we provided such multi-tiered approach that allows for the association between exposure scenario and the respective toxicological outcome while focusing on the consumer use stage of a nano-enabled product (NEP). Particularly, the methodology shown here was created with the case study of laser printers since these instruments are quickly becoming a staple in our home and business environments. As such, there are studies showing evidence of the pollutants released by laser printers. However, the toxicological assessments have focused on using the raw or pristine toner powder instead of the emissions released by the laser printer.

One of the novelties of this dissertation is the development of a printer exposure generation system (PEGS) to perform real time and time-integrated monitoring and collection of the particles emitted by laser printers. Additionally, the inhalation exposure component for exposure of animals to freshly generated printer-emitted particles (PEPs) allowed for the proper assessment of real world laser printer emissions rather than the materials used in the synthesis of the toner powder. It is worth noting, that the features of the PEGS allow for adjustments in the air exchange rate and air flow in the chamber to simulate current exposure scenarios. Most

importantly, this is a versatile platform that can be modified and be used to study pollutants released by any NEP.

In this project, the PEGS was used for a thorough physico-chemical, morphological and toxicological analysis of the collected PEPs. It was demonstrated that the toner used by laser printers is a nano-enabled product, as it contains a complex chemical mixture of nanoparticles (*e.g.*, ceria, titania, silica, zinc oxide, nickel oxide). Moreover, after analyzing the printer emission profile of various printers from different models and manufacturers, it was found that during a print job there is a release of engineered nanomaterials -of similar chemical composition as the toner- in concentrations as high as 1.3 million particles/cm^3 as well as volatile organic compounds (VOCs). The presence of metal and metal oxides on the PM in addition to the high concentration of VOCs are concerning since it is known that metal/metal oxides and such gaseous pollutants can trigger a toxic response in the lungs.

As mentioned before, the *in vitro* toxicological assessments done so far to study emissions from printers have used the toner powder rather than the PM emitted by printers. Thus, the collected size-fractionated PM released by the printer was used to study the cellular response following exposure at a range of doses using both a mono- and co-culture experimental model. It was found that PEPs could elicit a myriad of biological responses that included, but were not limited to: decreased cell viability, compromised cellular membrane integrity, elevated production of reactive oxygen species, cytoskeletal rearrangement, angiogenesis and increased cellular motile structures (filopodia), among others. A dose-dependent alteration in the DNA methylation machinery was also detected following exposure to PEPs, which highlights the need to understand the mechanism of action of these particles and search for long-term effects after exposure. Lastly, an animal model was used to further investigate the biological reactivity of

PEPs and to validate the results observed *in vitro*. After exposure to PEPs *via* intratracheal instillation or whole-body inhalation, mice exhibited no lung injury observed. However, there was an increase in neutrophil degranulation markers, lavaged neutrophils and secreted levels of a cytokine involved in lung repair, in addition to changes in gene expression and epigenetic mechanisms.

It is worth noting that the results presented in this dissertation for the *in vivo* toxicological analysis are preliminary and due to the low sample size, no definitive conclusions can be made of this primary data set. However, the data from this primary analysis has led for the creation of a number of hypotheses as to the particular interaction occurring between the organism and the PEPs. Thus, future studies need to be performed to understand the details of the mechanisms of toxicity of printer-emitted nanoparticles in the direct site of injury (*i.e.*, respiratory system) as well as indirect sites, such as the cardiovascular and nervous system. Additionally, it is worth assessing the damage various doses and exposure durations of PEPs can have on the cellular level as it pertains to modulations in gene expression and mechanisms of DNA methylation (*i.e.*, epigenetics). Particularly, the expression of genes controlling lung function as well as those whose mutations will increase significantly the incidence of respiratory diseases must be further researched. In addition to effects of PM, the response to the VOCs emitted by the printers need to be evaluated by exposing animals to PEPs, gaseous pollutants emitted by the printer, both PEPs and gaseous pollutants and a room air control. Such experiment would be helpful in determining the effect on toxicity, if any, exists when an individual is exposed to both the particulate matter and VOCs emitted by a laser printer during a print job. The adverse effects of VOCs remain a topic of interest, however, the absorption of VOCs onto the surface of inorganic

nanoparticles and the interactions of the organic and the metal components of PEPs continue to be poorly understood in the context of this particular exposure scenario.

The furthering of the study should also be done to evaluate the effect PEPs can have on the health of those individuals constantly exposed to laser printer emissions. It may be possible to evaluate the immediate human response following inhalation to PEPs in a consumer or business scenario, perhaps by performing nasal lavage and quantify white blood cell population and cytokine expression to assess if an immune response is taking place. If so, a detailed comparison should be done on responses in both predisposed and healthy individuals, as these can vary greatly in their impact on health.

While it is critical to obtain a larger data set on the adverse effects PEPs can have on human health and have a stronger assessment of the risk, it is imperative to come up with control solutions to reduce, or eliminate, the risk of exposure to such emissions. In my opinion this can be achieved in different ways. Policy makers may require setting a limit (*e.g.*, NOAEL, LOAEL) on the dose and duration of the exposure to emission from laser printers. Manufacturing companies could develop control technologies in the printer itself that may reduce or even prevent exposure to printer-emitted pollutants. For example, adding high-efficiency particulate air filters to more areas in the casing of the printer may reduce particulate matter release. Another possibility could be installing cooling fans that would reduce the internal printer temperature and thus, decrease emission of gaseous pollutant. The individual exposed could also modify the workspace by placing the printer in a well-ventilated area and ensure the equipment has been serviced and maintained following the manufacturer's recommendation. These are just a few of the recommendations that can be done in order to decrease exposure to laser printer emissions at the consumer level. I believe that as the technology improves, we will acquire more

knowledge to develop suitable solutions to mitigate our risk of exposure to environmental stressors that may be present in both our place of work and our home. Thus, making the risk assessment process an imperative one.